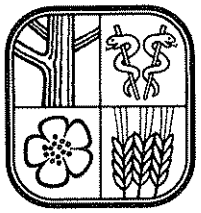

SVERIGES
LANTBRUKSUNIVERSITET

Modelling and Optimization of Passive and Adaptively controlled Active Cab Suspensions on Terrain Vehicles, especially Agricultural Tractors

Per-Anders Hansson

Dissertation

Institutionen för lantbruksteknik

Swedish University of Agricultural Sciences
Department of Agricultural Engineering

Rapport 164
Report
Uppsala 1993
ISSN 0283-0086
ISRN SLU-LT-R--164--SE

DOKUMENTDATABLAD för rapportering till SLU:s lantbruksdatabas LANTDOK, Svensk lantbruksbibliografi och AGRIS (FAO:s lantbruksdatabas)

Institution/motsvarande	Dokumenttyp	
Department of Agricultural Engineering Swedish University of Agricultural Sciences P.O. Box 7033 S-750 07 Uppsala Sweden	Dissertation, Department Report	
	Utgivningsår 1993	Målgrupp F

Författare/upphov

Hansson, Per-Anders

Dokumentets titel

Modelling and Optimization of Passive and Adaptively controlled Active Cab Suspensions on Terrain Vehicles, especially Agricultural Tractors

Ämnesord (svenska och /eller engelska)

Hyttfjädring, helkroppsvibrationer, terräng-fordon, lantbrukstraktorer, simulering, optimering, modellering, validering, passiv fjädring, aktiv fjädring, adaptiv aktiv fjädring, linjärkvadratisk optimering, malvern-filtrering

Cab suspension, whole body vibrations, tractors, terrain vehicles, vehicle dynamics, nonlinear elements, modelling, simulation, optimization, validation, passive suspension, active suspension, adaptive active suspension, suspension systems, optimal control, optimal estimation

Projektnamn (endast SLU-projekt)

Serie-/tidskriftstitel och volym/nr	ISBN/ISRN
Swedish University of Agricultural Sciences Department of Agricultural Engineering Report	SLU-LT-R--164--SE
	ISSN 0283-0086

Språk	Smf-språk	Omfång	Antal ref.
English	English	218 pages + encl.	63

Postadress	Besöksadress	Telefonnummer	Telefax
SVERIGES LANTBRUKSUNIVERSITET Ultunabiblioteket, Förvärvsavdelningen/LANTDOK Box 7071 S- 750 07 UPPSALA	Centrala Ultuna 22 Uppsala	018-67 10 00 vx 018-671103	018-3010 06

ABSTRACT

The main purpose of this work was to study the possibilities of using the cab suspension technique to improve the driver's environment on an agricultural tractor.

Two simulation models describing the frame-suspension-cab system were developed: A nonlinear model for studying the characteristics for suspensions with only small constrictions on the geometry and on the working principles of the elements, and a linear model which is a simplified description of the same system including more constraints, but more applicable when designing and studying performance particularly for active suspensions. The simulation models were validated against measurements made on a full-scale cab suspension.

The influence of different passive suspension parameters on vibration damping capacity and the requirement for free space in the construction were investigated. Particular emphasis was placed on the effects of passive non-linear suspension elements and varying locations of the elements.

An optimization model, based on an evolution algorithm, was developed and used to optimize parameters in a passive suspension with different types of generally defined constraints.

The development and analysis of LQG based active cab suspensions are described. The vibration damping characteristics of the suspensions are studied. The change in characteristics when the suspension's configuration or design variables are changed is also studied.

The results show that an active cab suspension based on linear state feedback must have time variant adaptive characteristics to be really useful. An adaptive active suspension controller based on LQG technique has been developed and studied. The principle for the adaptation is based on the parameters in the penalty matrices being varied so that the resulting controller always strives to make optimum use of the available travel space.

CONTENTS

1 INTRODUCTION

The driver's environment in a modern off-road vehicle has numerous drawbacks. High vibration loads, poor working postures, etc., place stresses on the driver's health and cause, in the longer term, incurable damage to exposed parts of the driver's body.

The stress also decreases the driver's capacity to register complex information, and to use the information to give the vehicle a better and more effective adjustment. The work is therefore performed with a lower degree of efficiency.

The research striving to reduce the driver's vibration load has mainly concerned different types of seat suspensions. The possibilities to reduce vibration load in more than one direction are, however, small using this technique. Relative differences in movement also arise between the driver and his immediate surroundings, which is why a seat suspension never can present satisfactory vibration protection.

Better vibration protection can be obtained if the whole cab is mounted with a suspension in relation to the rest of the vehicle. The cab suspension's potential to damp vibrations also in the horizontal and rotational directions makes it highly suitable for use on agricultural tractors where this type of vibration is particularly common.

The suspension elements used can be passive or supplied with different types of active functions. Passive suspensions do not require a supply of power, which makes them simple, inexpensive and reliable. Their potential to reduce vibrations is, on the other hand, fundamentally limited. Active supensions may use continuous or intermittent power supply from an external source and permit the use of more general control forces than are available from passive elements. The vibration damping capacity is better with active elements, but the complexity and the expense are also increasing. Active suspensions can also be simplified to varying degrees to provide suspensions containing most of the advantages of fully active suspensions but with reduced complexity and production costs.

A cab suspension with springs and dampers is a complex construction with numerous parameters influencing the vibration damping capacity. Developing an analytic simulation model describing the system, offers possibilities to investigate the influence of different suspension principles and variables in a scientific way. The simulation model has to be designed so that the influence of all the interesting parameters can be examined, and so that agreement with the real system is sufficiently correct.

A soft suspension with low natural frequencies normally offers better vibration damping capacity than a stiffer one, but needs more travel space to avoid over-travel. The restricted space is therefore one of the basic constraints when designing effective supensions.

A characteristic of agricultural tractor driving is the extremely varying vibration loads resulting when performing different types of working operations. It is therefore very important that a suspension works well when driving over all types of surfaces with all

possible speeds. These characteristics can be improved in a passive suspension by using nonlinear elements, but an adaptively controlled active suspension has an even bigger potential.

The main purpose of this work has been to study the possibilities of the cab suspension technique to improve the driver's environment on an agricultural tractor.

A study of all possible types of suspension techniques would be too comprehensive for a work of this type. This study has therefore mainly been directed to the two extremes, namely the totally passive suspension without any possibilities to adjust parameters, and the fully active supension with total control of the controller parameters and the actuator forces.

Two simulation models describing the frame-suspension-cab system have been developed: A nonlinear model which can be used to study the characteristics for suspensions with only small constrictions on the geometry and on the elements' working principles, and a linear model which is a simplified description of the same system including more constraints, but is more usable when designing and studying performance for specially active suspensions.

The simulation models have been validated against measurements made on a full scale cab suspension. The models have also been compared with each other.

Earlier cab suspension studies, together with the result of this study, have shown that it is possible to design a suspension that works well for a well-defined normal vibration load. The possibilities to design a suspension with attractive characteristics in all types of circumstances have been very little studied. Consequently, a major part of this work has been directed towards different possibilities to achieve these favourable characteristics.

2 BACKGROUND

The vibration load on the driver of an agricultural tractor has several negative effects. Besides contributing to physiological changes in the back and joints, the vibrations also cause other types of discomfort. Further consequences are a lower quality of the performed job and a lower degree of utilization for the machine.

Physiological changes, as for example changes to the lumbar region, are hard to relate to the vibrations because of the other factors that may cause an influence. As early as 1960, Rosegger & Rosegger presented a study where drivers of agricultural vehicles showed an substantially increased frequency of changes in the back and stomach problems. The reasons reported were vibrations and shocks in combination with the twisted working postures common in tractor driving. In a later study (Thelin, 1980), tractor drivers were compared with farmers who had not driven tractors. The tractor drivers ran a five-fold increased risk to be affected with lumbar disorders as well as hip joint disorders.

The more short range effects on driver health and well-being are easier to study and a great number of studies have also been published, dealing with, for example tiredness, nausea and deteriorated power of observation. Wuolijoki (1981) gives a good survey.

The vibrations also affect the driver's capacity to steer and control the vehicle. McLeod & Griffin (1988) studied the effects of different vibration exposures on a person's capacity to perform precision work. The capacity was significantly lowered when the surroundings were vibrating. The influence was particularly large at vibration frequencies of 4 Hz and higher. The ability to read information from a digital display was also found to decrease at increased vibration levels.

In many practical situations the driving speed is limited by the vibrations that reach the driver, whose capacity is then decreased. In some cases, the vibrations also affect the quality of the work and the degree of vehicle utilization (Matthews, 1973).

One reason for the vibrations in an agricultural tractor being assumed to be particularly dangerous are the interactive effects which probably arise when the vibrations are combined with twisted and leaning working postures (Bottoms, 1975). The transmission of vibrations from the seat through the body to the head have shown a significant increase when the body is twisted (Bjurwald et al., 1973). This result supports the statement above.

Most of the working equipment is situated behind the tractor, which results in the drivers being forced to assume an extremely twisted posture when controlling the equipment. When ploughing, the cab also leans sideways, which makes the situation even worse.

In most vehicles, the vibrations in one direction, normally the vertical, dominate the total vibration load. The driver of an agricultural tractor is loaded by vibrations with high levels in most directions, also the rotational directions, which may be another reason for a worsening situation (Matthews, 1973).

3 OBJECTIVES

The main objective of this study is to reduce the vibration load on the driver of an agricultural tractor, to protect his health and to increase the quality and the quantity of the performed work.

More specifically, the objective is to study the characteristics for different passive and active cab suspensions when used on agricultural tractors. In particular the vibration damping potentials and needs for free available travel space of the suspensions will be studied.

A further objective is to develop methods, for the different types of suspensions, to optimize the function with respect to the vibration damping potential, dependent on the constraints defined.

4 LITERATURE

The survey begins with a description of the positive and negative effects of cab suspension when used on a terrain vehicle (Ch. 4.1). The theoretical and practical work performed to study terrain vehicle cab suspensions are then discussed (Ch. 4.2).

A terrain vehicle suspension must be effective when driving both on very smooth and on very rough surfaces. The principle problems that arise, and the attempts to solve the problems, are described in Ch. 4.3.

Some types of simulation models involve major constraints when different types of suspension elements and principles are studied. The possibilities for different types of simulation models to describe the real system in an exact and realistic way are discussed in Ch. 4.4.

The primary goal for the work is to reduce the vibration load on the driver. The principles for relating vibration loads in different directions to a measure of the total load on the driver are described in Ch. 4.5.

The coordinate axes in this study are directed and denoted as shown in Figure 1, with x positive in the normal driving direction, y positive to the left and z positive upwards. The axes are mutually perpendicular. The rotational degrees of freedom are denoted xr (roll), yr (pitch) and zr (yaw).

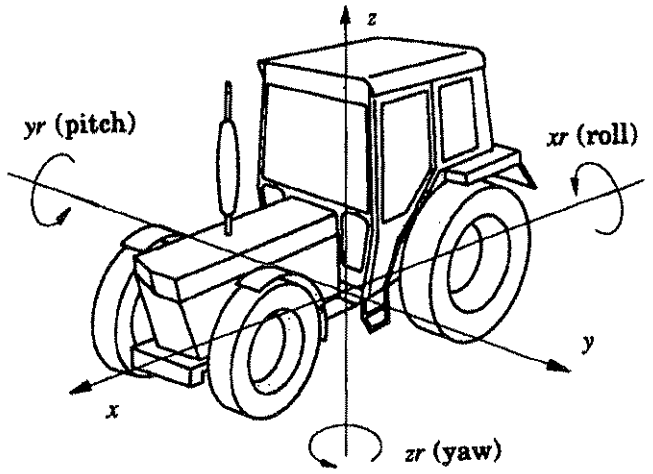

Fig. 1. Directions and notations for the coordinate axes.

4.1 Benefits for cab suspension

The benefits obtained by using cab suspensions have been discussed in many studies. Hilton & Moran (1975) point out the possibilities for damping in 6 d.o.f., elimination of relative motions between the driver and the cab, and the increased possibilities to reduce the noise levels. Decreasing levels for the high frequency vibrations at the steering wheel and the controls when using a suspended cab are also mentioned. Disadvantages described are the higher costs and the reduced driver awareness in some circumstances.

The use of a cab suspension also offers possibilities to design a suspension, striving to keep the cab horizontal, which is very positive, for example when ploughing (Weigelt & Göhlich, 1985). These authors also discuss the need for better vibration damping on a future tractor constructed for higher velocities.

4.2 Practical and theoretical studies

A very early cab suspension study was performed by Suggs & Huang (1969), with a model in scale 1:3/8. The suspension used had one d.o.f. (z) with the natural frequency 2.25 Hz. The results indicated that a lower natural frequency would have been preferable with regard to the vibration damping but that the travel space did not allow it.

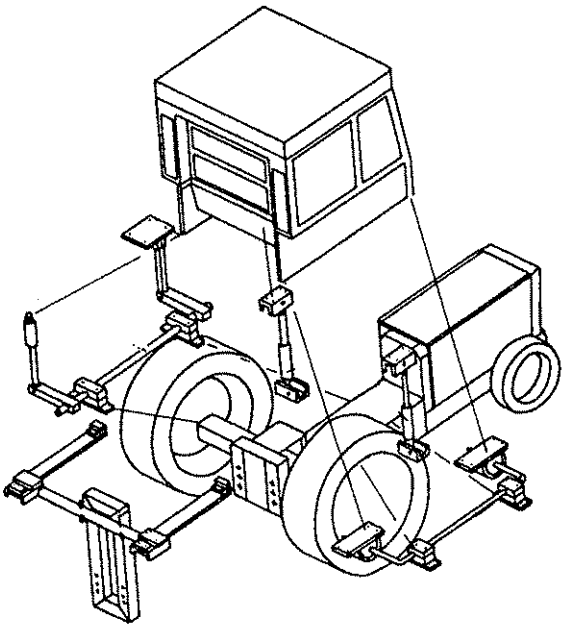

Fig. 2. Cab suspension (Göhlich, 1984).

A more comprehensive study of cab suspensions was performed by Hilton & Moran (1975), who built a passive experiment suspension with 3 d.o.f. (z, roll and pitch) and possibilities to change the natural frequency in each direction. The cab was mounted on an ordinary agricultural tractor. The performance of different linear suspension characteristics was studied when driving on different test tracks and in ordinary driving situations. Substantially decreased vibration levels were reached in all three free directions, with best results on smoother surfaces.

A suspension with 5 d.o.f. was developed in The Netherlands ('t Hart, 1977). A passive suspension which was assumed to be linear was designed to give natural frequencies lower than 1.1 Hz in all directions. Large travel space was needed to avoid over-travel but good vibration damping capacity was provided, especially in the z direction.

Cab suspensions have also been studied in Berlin (Kauss & Weigelt, 1980). The authors describe an experimental suspension based on vertical gas hydraulic spring elements and another based on leaf springs, both with three d.o.f. One of these suspensions was also tested with active elements (Kauss, 1981). The controller was based on traditional velocity feedback with constant feedback gains and the elements were powered from the tractor's standard hydraulic system. Kauss also theoretically studied the characteristics for active suspensions based on feedback of different parameters.

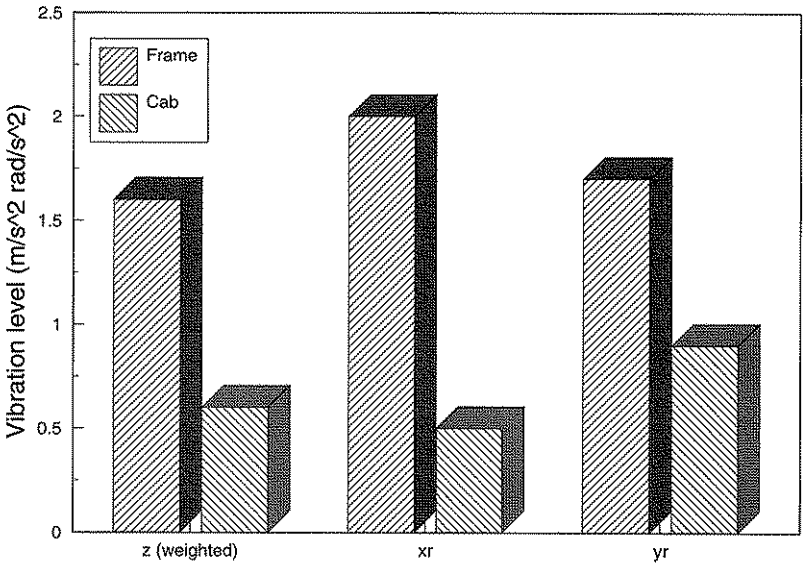

Fig. 3. Vibration levels with and without cab suspension when driving on the smooth test track (SS-ISO 5008) at 12 km/h (after Kauss & Weigelt, 1980).

The vibration damping potential for a passive cab suspension on a forestry machine (a forwarder) was tested in a Swedish study (Zylberstein, 1981). Both the measured vibration load and the driver's subjective estimate of the load decreased when the cab was suspended. The drivers, on the other hand, also reported a feeling of decreased interaction with the vehicle in some driving sequences.

On some larger vehicles, such as mining trucks and heavy-duty truck tractors, the principle has been accepted and has also resulted in improvements for the driver at reasonable cost (Rova, 1990).

A variant of passive cab suspension is introduced by Renault in their bigger agricultural tractor models (Robert, 1988), but the technique is still waiting for the break-through in the agricultural sector.

Only a few models describing the dynamical system vehicle-suspension-cab are reported for agricultural vehicles. Other models describing the same system for trucks are reported. However, because of the small horizontal vibration levels in these vehicles, the models are normally only two-dimensional and therefore only have limited applicability to terrain vehicles.

Roley (1975) reports on a simulation model for movements in 4 d.o.f. used to compare the vibration damping capacity for passive linear, semi-active and active cab suspensions on agricultural tractors (Figure 4). The passive elements studied were simplified to give the same characteristics in all directions. As expected, the active suspension was the most

effective one, but little consideration was paid to the requirement of the different suspensions need for free travel space. A similar simulation model, but with 5 d.o.f., was developed by Rakheja & Sankhar (1984). This model dealt only with linear simplified elements.

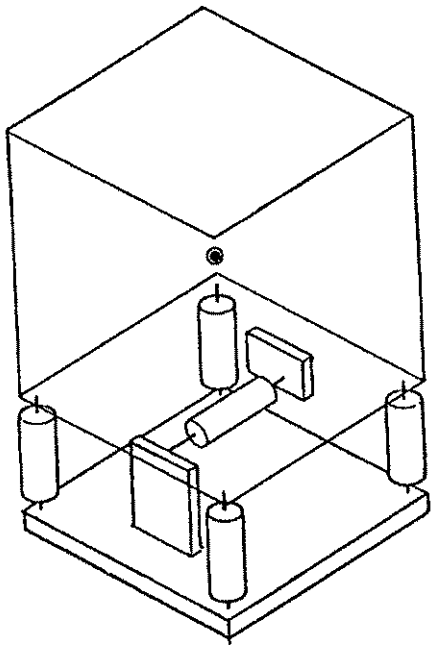

Fig. 4. Schematic description of a cab suspension (Roley, 1975).

El Madany (1987), after studying a model describing a truck cab suspension, recognized that the main constraint for the design is the limited space available for suspension travel. El Madany studied the demands for free available travel space in the z direction for different linear suspensions. Results from studies without any discussion of the different suspensions' need for available travel space have been criticized for their limited practical use (Sharp & Crolla, 1987).

The normal way, when designing cab suspensions, is to reduce the suspension's natural frequencies. Besides the need for large available travel space, natural frequencies below 1.0 Hz also result in large static travel when the vertical payload is varied or when driving on side-slopes. It is then possible, and in some cases probably necessary, to include a self levelling system, which typically involves time constants of many seconds, to compensate for static load variations (Sharp & Crolla, 1987). A slowly reacting load leveller can be built with fairly simple components and with low energy consumption.

4.3 Suspensions with adaptive and nonlinear characteristics

Most terrain vehicles are designed both for driving on relatively smooth surfaces, and for driving in the terrain with, in some cases, very high vibration levels. Agricultural tractors are, for example, both used with trailers as transport vehicles and for driving on very rough surfaces such as the first tillage operation after ploughing.

Different types of trailers and implements also influence the vibration levels on the tractor, partly by providing vibrations themselves and partly by affecting the vehicle's dynamic properties (Crolla, 1980; Claar & Sheth, 1982). The conclusion must be the importance of having a suspension system with good vibration damping capacity for all types of driving and implements.

To avoid over-travel when driving over very rough surfaces, a passive linear suspension must be very heavily damped. For more normal driving on smoother surfaces, this suspension is too stiff to be optimal, and the vibration damping capacity is reduced (Karnopp & Margolis, 1984). Also for an active suspension, the control setting usable on rough surfaces is excessively adjusted to counteract for major travel to be effective on smoother conditions.

It seems that a suspension must have time variant characteristics to be optimal when the conditions change. In automatic control terms, such a principle is denoted as "adaptive". The cab suspension studies described have not discussed possibilities to use adaptively controlled suspension. In the literature on automobile suspensions, however, there are some papers discussing adaptive suspension systems.

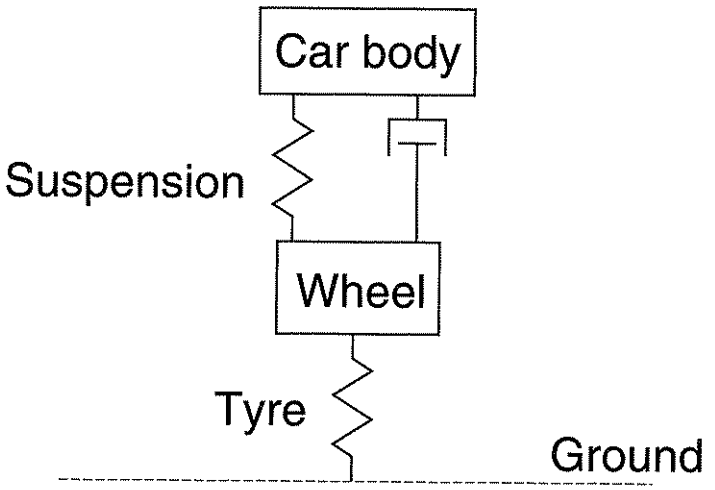

Fig. 5. Automobile quarter car suspension model frequently used in suspension studies.

Relatively simple systems with adaptation of the dampers and in some cases also the springs with respect to velocity, steering angle, etc., are already in production for some cars. An adaptive system where the springs and dampers in an otherwise passive system can be regulated depending on velocity, steering angle and braking forces was theoretically studied by Karnopp & Margolis (1984).

At the Royal Institute of Technology in Stockholm, Sweden, a system with high practical potential was developed (Lizell, 1990). A slowly acting active system compensating for body motion was combined with adaptively controlled damping for each wheel. The adaptation of the control gains was based on the frequency content and the amplitude of the suspension velocity.

Hac (1987) describes theoretically an adaptive control for a fully active automobile suspension. The control is based on LQG-theory and is described for an quarter car model. The feedback gains were assumed to be precalculated and stored in the controller's memory. The choice of gains was decided from the velocity and the characteristics of the surface. The adaptive system can be defined as a Gain Scheduling controller without feedback. The identification of the variables deciding the gain is not described. A similar system applied to heavy commercial and military vehicles is described by Sachs (1979).

Adaptive suspension systems can be sensitive to extreme input from, for example, potholes in an otherwise smooth surface. The adaptation must, in that case, be rapid but not so fast that the system becomes instable (Sharp & Crolla, 1987). This characteristic is normal for most types of adaptive control systems.

The problems appearing when steering large vessels affected by wind and wave disturbances have a lot in common with the suspension problems discussed earlier (Byrne & Katebi, 1988). Similar control strategies can be used.

Another way to develop a suspension with good function on most surfaces is to use nonlinear passive elements. These elements contribute to the suspension being soft in the normal working range but harder damped for extreme strokes, in order to reduce the maximum travel and thereby also the risk for over-travel. The effectiveness of a passive nonlinear suspension could never be as good as an adaptively controlled active one but the costs and the reliability problems become smaller.

It is not possible to analyse the characteristics for nonlinear elements with the normal tools used for linear systems. The systems have to be analysed in the time domain.

The effects of nonlinear elements with different characteristics in a car suspension were studied by Mitschke (1969). Both nonlinear springs and dampers were tested.

Nonlinear damping elements were also tested in a one-dimensional cab suspension for an agricultural tractor designed for commercial use (Lines et al., 1989). A relatively soft suspension was used to reach good vibration damping capacity, but resulted in over-travel under rough conditions. The over-travel contributes to very high peak vibration

values and was experienced as very unpleasant for the test drivers. Better results were reached when the damping was made progressive with quadratic damping characteristics (Figure 6). This nonlinear arrangement gave good vibration isolation at normal driving and completely removed the high peak acceleration loads.

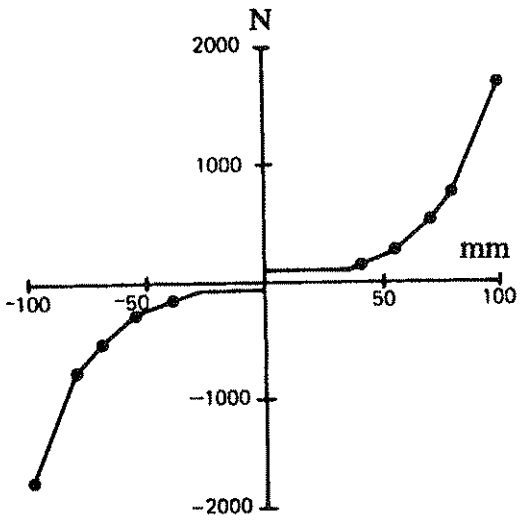

Fig. 6. Damping force vs displacement at constant velocity (0.05 m/s) for a nonlinear suspension element (Lines et al., 1989).

4.4 Agreement between theoretical models and practical measurements

The reported simulation models describing the vehicle-suspension-cab system are mainly linear models. Simplifications must normally be performed when describing a mechanical system as linear, and results in constraints for i.e. nonlinear elements, non-symmetric elements and co-operating elements.

With a correctly designed simulation model taking care of the nonlinear relations is it possible to break the described constraints.

Nonlinear models have to be, with few exceptions, analysed in the time domain. The output is then totally dependent on the defined input, and not some kind of average as for linear models analysed in the frequency domain. This can be a restriction or a favour dependent on the application.

The models used for simulation of the influence of different suspension parameters on the vibration load in the cab, either describe the total system made up of ground-tyre-frame-suspension-cab or just the frame-suspension-cab system. With few exceptions, the models are not validated against practical measurements (Stayner et al., 1984). The experience is that the models describing the total system, including the ground-tyre interaction, shows rather poor agreement with practical measurements. One reason

reported is the linear spring and damping characteristics used, despite the fact that the characteristics, especially for the tyres, should be nonlinear and more complex. Also Deltentre & Destain (1990) report that the linear models are able to predict trends in the results but no absolute levels.

4.5 Effects of whole body vibrations

Important variables involved in the measurement of vibration exposures are magnitude, frequency, direction and duration. These variables do not, however, always adequately define the severity of the vibrations. There may be differences in susceptibility within individuals (intra subject variability) and differences between individuals (inter subject variability). Many studies have been performed to study the influence of the variables, one at a time or two or more combined.

The result of the studies was an International standard for evaluation of human exposure to whole body vibrations (ISO 2631, 1974). The standard includes exposure time limits for humans in vibrating environments. The first edition was subjected to criticism, and has also been reviewed. Even the reviewed version has been criticized, especially the evaluation of the time factor (Kjellberg & Wikström, 1985).

The British standard (BS 6841, 1987) evaluates the vibration load in a more complete approach and, in contrast to ISO 2631, includes outlines for evaluation of vibrations in the rotational dimensions. ISO 2631 evaluates the vibrations measured at the driver's seat, while BS 6841 evaluates vibration exposures also on the driver's feet and at the back support (Figure 7). BS 6841 has not been accepted as International standard and the vibration exposures have therefore been evaluated according to the latest Swedish version of ISO 2631, SS-ISO 2631 (1982), in this study. This standard is called ISO 2631 throughout the present study.

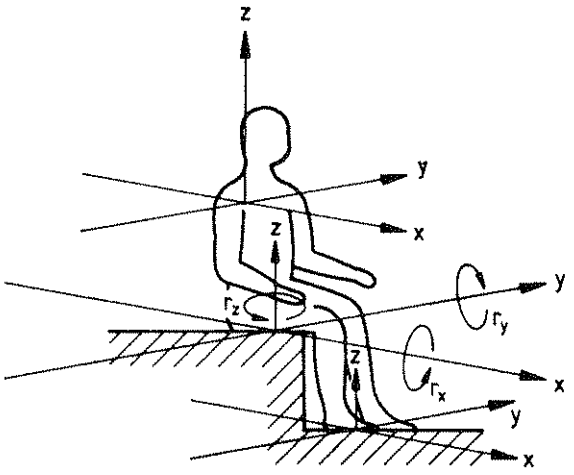

Fig. 7. Coordinate system and vibration measurement positions according to BS 6841 (1987).

4.5.1 Measurements and analysis

ISO 2631 evaluates the effects of whole body vibrations with the frequencies 1.0-80 Hz in the x, y and z directions. The standard is valid for vibrations with Crest factors (the size of the extreme value in relation to the RMS value) not exceeding 6. The effects when relative movements appear between the driver's upper body and feet, as is the case when using a suspended seat, are not considered.

The vibrations should be measured at the point where they are transmitted to the body, in an agricultural tractor between the seat cushion and the body. Typical driving situations should be selected, and the measurement time should not be below 60 s to get correct values for vibration levels and Crest factors.

The human body shows different sensitivity for vibrations depending on direction and frequency content. In the vertical direction, the body's most sensitive range is 4-8 Hz, while sensitivity in horizontal directions is highest between 1 and 2 Hz. In general, the body is also more sensitive in the x and y directions compared to the z direction.

ISO 2631 defines weighting filters (Figure 8) to be connected between the transducer and the data acquisition unit. The filters reduce signal components outside the areas with highest human sensitivity. The RMS value of the filtered signal then gives a direct value for the effects on the human body.

Evaluation of the effects of vibration loads with one dominating frequency can be performed in a slightly different way, but since vibrations of this type hardly occur in a terrain vehicle, the method will not be further discussed.

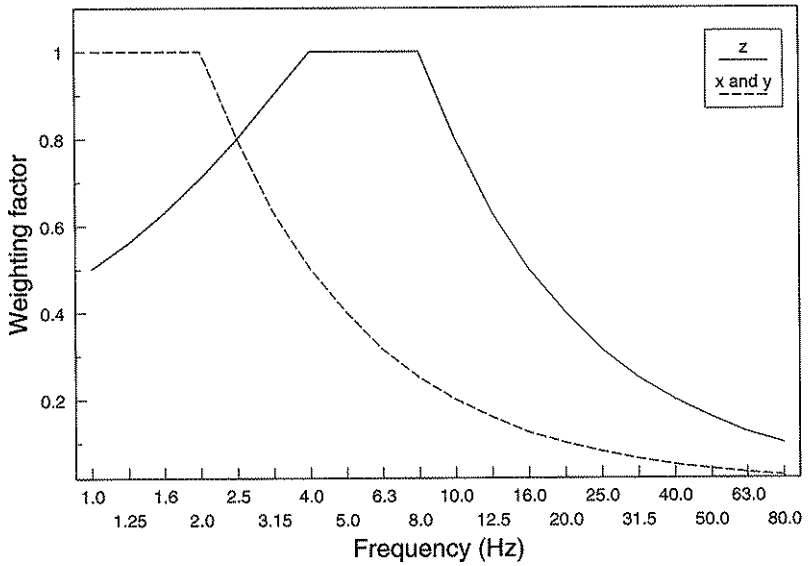

Fig. 8. Frequency weighting for vibrations in the x, y and z directions (ISO 2631).

For vibration loads with substantial effects in more than one direction the effects of the total load may be bigger than the effects of the components evaluated one at a time. To make an evaluation of the total load possible, ISO 2631 defines a vector sum (a_{tot}) as the weighted sum of the vibration loads in the three linear directions.

$$a_{tot} = \sqrt{(1,4a_{xw})^2 + (1,4a_{yw})^2 + (a_{zw})^2} \tag{1}$$

where

a_{iw} = weighted acceleration level in the i direction ($i = x, y, z$).

The factor 1.4 ($\sqrt{2}$) depends on the human body's greater sensitivity to vibrations in the x and y directions.

4.5.2 Main criteria for evaluation of vibration effects

The consequences of the vibration load are estimated according to three main human criteria. These are:

- preservation of working efficiency
- preservation of health and safety
- preservation of comfort.

The exposure times for varying loads are defined in Figure 9 for the z direction. The figure also shows the decreasing sensitivity for frequencies outside the 4-8 Hz domain. For vibration loads in the x and y directions, curves are defined with the most sensitive area between 1 and 2 Hz. Weighted values for one individual dimension should be compared to the horizontal part of the curves.

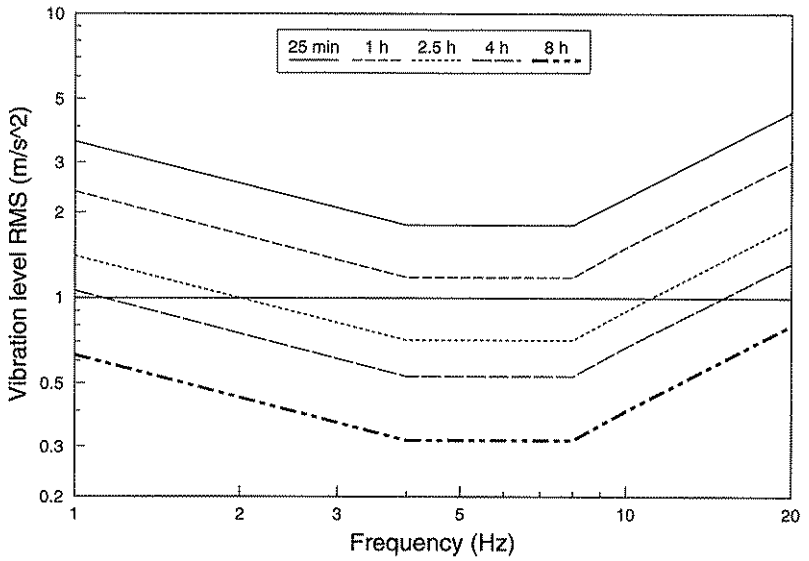

Fig. 9. Exposure limits for decreased working efficiency in the z direction (ISO 2631).

Figure 9 shows the limits for decreased working efficiency. For decreased comfort, the curves are lowered 10 dB. For health and safety, the curves are raised 6 dB. The curves in the figure are defined for one third-octave band analysis with analog bandpass filters and have to be raised 4-8 dB for digital broad band analysis.

The vector-sum values should firstly be compared to values measured with the same technique at other working places. According to the standard, it is also possible to evaluate the values against the horizontal range of the curves for vibrations in the z direction. The curves then have to be raised 4-8 dB.

The big interval in the recommendations for the changing of the limits when the measurement technique is varied, makes it hard to safely relate a measured vibration value to a defined exposure time limit. The logarithmic base for the limits, however, makes it possible to estimate the relative relation between two loads, without calculation of exact exposure time values.

5 METHODOLOGY

This chapter describes two simulation models for the frame-suspension-cab system. The nonlinear model can be used to study the characteristics for suspensions with only small constrictions on the geometry and on the working principles of the elements. The linear model is a simplified description of the same system but is of greater applicability when designing and studying the performance for particularly active suspensions.

5.1 Nonlinear time domain simulation model

5.1.1 Demands at the model

A simple model, described for simulation in the frequency domain, may be sufficient for a study of basic cab suspension principles. A more complete study of the characteristics and possibilities requires a more detailed model, based on as few simplifications and restrictions as possible.

Among the demands for a simulation model to study the influence of important factors, special mention can be made of the following:

- possibilities to simulate movements in 6 d.o.f. for each solid body
- possibilities to study the effects of passive, semi-active and active suspension elements
- possibilities to simulate suspensions including digital controllers
- no constraints included for elements relating to locations and directions
- possibilities to analyse time histories and extreme values for the variables involved
- possibilities to use input signals measured during real driving situations
- possibilities to combine the model with an optimization algorithm.

5.1.2 The simulated system

A model for studying different types of cab suspensions can describe the whole vehicle including the ground-tyre interplay or just the frame-cab interplay.

The possibilities to describe, with reasonable precision, the transmission of ground irregularities through the rubber tyres to the frame are small. Incomplete knowledge of the tyres' dynamic properties and of the ground-tyre interaction are contributory causes (Stayner et al., 1984; Crolla, 1981). More recent work on tyre dynamics have resulted in the errors decreasing, but even better tyre dynamic descriptions are required (Lines et al., 1992).

The simulation model is defined only to describe the frame-cab system. Accelerations measured at the vehicle frame when driving over representative surfaces can then be used as input to the model. A linear model describing this system is also directly suited for implementation in an active cab suspension controller, which hardly is the case for a

model also describing the ground-tyre interplay. The cab's mass is then assumed to be so small, in relation to the rest of the vehicle, that cab movement does not affect the movements of the rest of the vehicle.

A free body in space may move in 6 d.o.f.; three linear directions and three rotational. Measurements have shown that the tractor's and the cab's angular vibrations around the z axis can be negligible. Nonetheless, this dimension is included in the model, since it only slightly increases the complexity. Some of the tested suspension configurations may also induce vibrations in the sixth dimension.

5.1.3 Simulation program principle

To meet the defined demands, the simulation model has to be designed for time domain simulation.

The algorithm is based on differential equations, describing the cab's movements when influenced by defined forces and moments. The cab and the frame are assumed to be solid bodies without elasticity. The principle for the algorithm is schematically described in Figure 10.

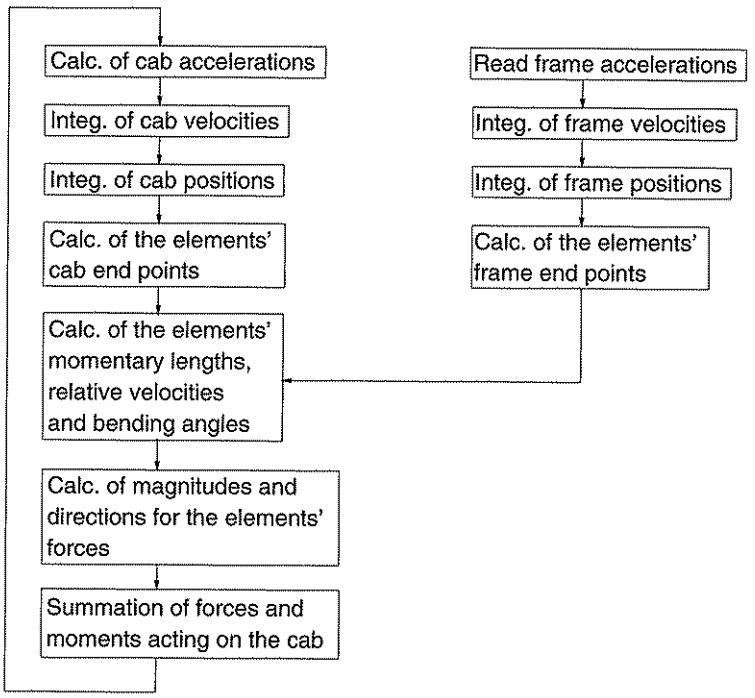

Fig. 10. Simulation model description.

Assume that $t=t_0$ and that the sums of the forces and moments influencing the cab are known. For the motion of the cab's c.o.g., the following is valid:

$$\ddot{x}_{cg}^{c} = \frac{\Sigma F_x}{m} \tag{2}$$

$$\ddot{y}_{cg}^{c} = \frac{\Sigma F_y}{m} \tag{3}$$

$$\ddot{z}_{cg}^{c} = \frac{\Sigma F_z}{m} \tag{4}$$

where

i_{cg}^{c} = c.o.g coordinate in the i direction $(i = x, y, z)$

ΣF_i = total force in the i direction $(i = x, y, z)$

m = cab mass.

The cab is assumed to be symmetric in relation to the coordinate axes through the c.o.g. with the products of inertia (I_{xy}, I_{xz}, ...) = 0. Euler's simplified formulas for the angular movements of a solid non-elastic body can be used if the deviations from the balanced position are assumed to be small:

$$\dot{xr} = \frac{\Sigma M_x - (I_{zz} - I_{yy}) \cdot \dot{yr} \cdot \dot{zr}}{I_{xx}} \tag{5}$$

$$\dot{yr} = \frac{\Sigma M_y - (I_{xx} - I_{zz}) \cdot \dot{xr} \cdot \dot{zr}}{I_{yy}} \tag{6}$$

$$\dot{zr} = \frac{\Sigma M_z - (I_{yy} - I_{xx}) \cdot \dot{yr} \cdot \dot{xr}}{I_{zz}} \tag{7}$$

where

ir = angle of rotation in relation to the i axis $(i = x, y, z)$

ΣM_i = total torque around the i axis $(i = x, y, z)$

I_{ii} = cab moment of inertia $(i = x, y, z)$.

Integration then gives the cab velocities in relation to a coordinate system fixed in space, for $t=t_0+\Delta t$ where Δt=the integration time step.

The coordinates at $t=t_0$ for the endpoints of the elements must be defined as inputs to the model. For a point located in the cab moving in space, the following are valid:

$$\dot{x}^c = \dot{x}_{cg}^{c} - (y^c - y_{cg}^{c})\dot{zr} + (z^c - z_{cg}^{c})\dot{yr} \tag{8}$$

$$\dot{y}^c = \dot{y}_{cg}^{c} - (z^c - z_{cg}^{c})\dot{xr} + (x^c - x_{cg}^{c})\dot{zr} \tag{9}$$

$$\dot{z}^c = \dot{z}^c_{cg} - (x^c - x^c_{cg})\dot{y}r + (y^c - y^c_{cg})\dot{x}r \tag{10}$$

where

i^c = the coordinate in the i direction for the point $(i = x, y, z)$ (Symon,1971).

The frame accelerations in 5 d.o.f. are read from an input file. The same integration technique as for the cab's movements is then used to calculate the position of the frame and the frame endpoints of the suspension elements at $t=t_0+\Delta t$. The cab movements are, as mentioned earlier, assumed not to influence the frame movements.

With the coordinates for the suspension elements' cab and frame endpoints calculated for $t=t_0+\Delta t$, the formulas in Chs. 5.1.5.1.2 and 5.1.5.2.2 are used to calculate the magnitudes of the forces from each element. More complex relations for the force magnitudes, when using active elements, are described in Ch. 9. The calculations to decide the forces' directions are described in Chs. 5.1.5.1.1 and 5.1.5.2.1 for the element types simulated.

The components for one force are:

$$F_x = F_A \cdot D_x \tag{11}$$

$$F_y = F_A \cdot D_y \tag{12}$$

$$F_z = F_A \cdot D_z \tag{13}$$

where

F_A = axial force from one element (positive for pressure)

F_i = force component in the i direction $(i = x, y, z)$

D_i = component in the i direction for the normalized direction vector (direction cosines) $(i = x, y, z)$.

For the torque the following are valid:

$$M_x = F_y(z^c_{cg} - z^c_c) + F_z(y^c_c - y^c_{cg}) \tag{14}$$

$$M_y = F_z(x^c_{cg} - x^c_c) + F_x(z^c_c - z^c_{cg}) \tag{15}$$

$$M_z = F_x(y^c_{cg} - y^c_c) + F_y(x^c_c - x^c_{cg}) \tag{16}$$

where

M_i = torque in relation to the i axis through the cab's c.o.g. $(i = x, y, z)$

i_c^c = coordinate for the cab end point of the element ($i = x, y, z$).

The total force and torque at $t=t_0+\Delta t$ are calculated by summing the components from each element. The results are used to calculate the parameter values for $t=t_0+2\Delta t$ and the simulation continues.

The simulation program is based on 5 parts (Figure 11).

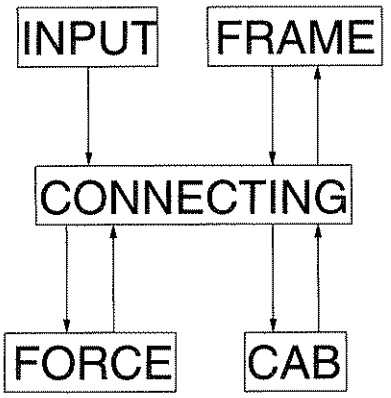

Fig. 11. The simulation program.

The INPUT part deals with the connection with the input file containing the frame acceleration values. The FRAME part handles the calculations of the parameters included in the frame movement, and the CAB part handles the cab movements.

The FORCE part calculates the forces from the different elements. For a passive suspension this part is very simple and included in the CAB part. When a digitally controlled active suspension is used, the FORCE part is more complex. To manage the cooperation between the different parts, a CONNECTING part is used.

5.1.4 Integration algorithms

The Simnon software package has been used to solve the differential equations describing the cab's movements (Elmqvist et al., 1986). Simnon is especially designed for simulation in the time domain, with several integration algorithms implemented. A Runge-Kutta algorithm of order 4/5 gave acceptable execution times with small errors.

One part of the simulation model was also programmed in a program language without any built-in integration algorithms (Matlab). The integrations were then performed with a predictor method started up with a simple Euler algorithm (Gustavsson, 1989). The calculation errors became about the same compared to the Simnon algorithm, but the execution times were greatly increased, which is why this technique was not used further.

The choice of integration time step, together with the choice of algorithm, has a major influence on the accuracy of the calculation. Depending on the approximations of the parameter values between the calculation time instants, large time steps may give unacceptable error levels. Too large time steps may also cause a stable system to become unstable in simulation.

The accumulated round up errors, depending on the computer's finite word length, increases when using small time steps. The local contributions in each step are independent of the time step. The total error then increases with the number of steps and therefore with decreasing time steps. The round-up errors are normally not critical, so the time step choice is a question of priorities between calculation time and accurateness.

The input signals describing the frame motion were recorded with 200 Hz sample frequency. A time step bigger than 0.005 s would not use the total information in these signals. When no frequencies above 6-10 Hz were present in the signals, a maximum time step of 0.005 s was considered as quite sufficient, and has been used for the reported simulations.

Simnon has a built-in step length adjustment, decreasing the time steps when too large errors are indicated. The small value for the defined maximum time step relative to the frequency contents in the input made this function inactive in the simulations shown. The value defined as maximum time step was therefore also the one used.

5.1.5 Operation principles for suspension elements

The types of element used make it possible to construct a 6 d.o.f. suspension with approximate linear characteristics in the horizontal and vertical directions. The results from the study can then be converted to all types of suspension configurations and also much easier to understand.

Two principally different types of suspension elements are used in the simulations. The first type has its two end points constructed as frictionless ball joints. The reaction forces from these elements are directed in the axial directions. The characteristics can be passive or with some type of active control.

The other type of element is mounted elastically in the frame with a torque transferring bushing or spring. The connection between the element and the cab is defined as a frictionless ball joint. The torque from the elastic mounting results in a force influencing the cab in the radial direction of the element.

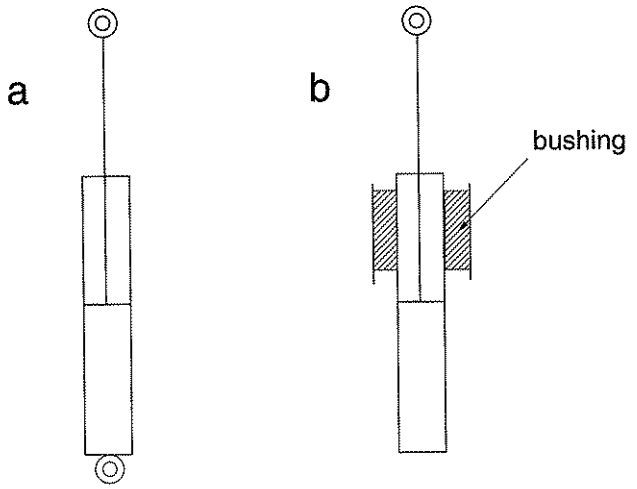

Fig. 12. Suspension element with a: axial and b: axial and radial working principles.

5.1.5.1 Axially working elements

A suspension element with end points constructed as frictionless ball joints is shown in Figure 12. A characteristic of this element is that the reacting force is directed exactly in the length direction of the elements. The force can be a function of many factors:

$$F = f(l_{e0} \quad l_e \quad \dot{l}_e \quad \ddot{l}_e \quad T_K \quad m_e \quad q_h \quad \ldots) \tag{17}$$

where

l_e = suspension element length

l_{e0} = element length in balanced position

T_K = temperature

m_e = element mass

q_h = hydraulic flow from external source.

5.1.5.1.1 Calculation of force components

The direction of the force from an element with axial working principle acting on the cab is defined by the positions of the element's end points.

The direction cosines are calculated from:

$$D_x = \frac{x_c^c - x_b^c}{l_e} \tag{18}$$

$$D_y = \frac{y_c^c - y_b^c}{l_e} \tag{19}$$

$$D_z = \frac{z_c^c - z_b^c}{l_e} \tag{20}$$

where

$$l_e = \left((x_c^c - x_b^c)^2 + (y_c^c - y_b^c)^2 + (z_c^c - z_b^c)^2\right)^{0.5} \tag{21}$$

$$\left(\left(\frac{x_c^c - x_b^c}{l_e}\right)^2 + \left(\frac{y_c^c - y_b^c}{l_e}\right)^2 + \left(\frac{z_c^c - z_b^c}{l_e}\right)^2\right)^{0.5} = 1 \tag{22}$$

i_b^c = coordinate for the element's frame endpoint $(i = x, y, z)$

5.1.5.1.2 Linear and nonlinear passive elements

For an ideal linear spring, the following is valid:

$$F = k \cdot (l_{e0} - l_e) \tag{23}$$

and for a linear damper:

$$F = -c \cdot \dot{l}_e \tag{24}$$

where

k = spring constant

c = damping constant.

Perfectly linear elements are not common in practice but allow the use of analytical methods for the analysis of suspension characteristics.

A nonlinear element has a characteristic that in any way differs from the linear one. Besides nonlinearities planned in the construction, other factors such as slip stick and hysteresis also give nonlinear effects. Elements with oil and gas normally also have temperature dependent characteristics.

The working principle for the nonlinear dampers used in the simulations can be described by:

$$F = -c(l_e) \cdot \dot{l}_e \tag{25}$$

where the damping constant is time variant:

$$c(l_e) = c_0\left(1 + \left|\frac{l_e - l_{e0}}{PK1_c}\right|^{PK2_c}\right) \tag{26}$$

$$R_0 = c_0/c_c \tag{27}$$

c_0 = damping constant in the balanced position ($l_e = l_{e0}$)

R_0 = degree of damping in the balanced position

c_c = damping constant at critical damping (see Ch. 5.1.5.1.3)

$PK1_c$ = progressivity constant 1

$PK2_c$ = progressivity constant 2.

$PK1_c$ can be defined as the deviation from the balanced position where c is twice as high as for $l_e = l_{e0}$. $PK2_c$ describes the shape of the curve. $PK2_c = 2$ defines a quadratic curve, etc. (Figure 13). In the report, $PK1_{cV}$, $PK2_{cV}$ and R_{0V} have been used to describe the characteristics for vertically working elements and $PK1_{cH}$, $PK2_{cH}$ and R_{0H} for horizontally working elements.

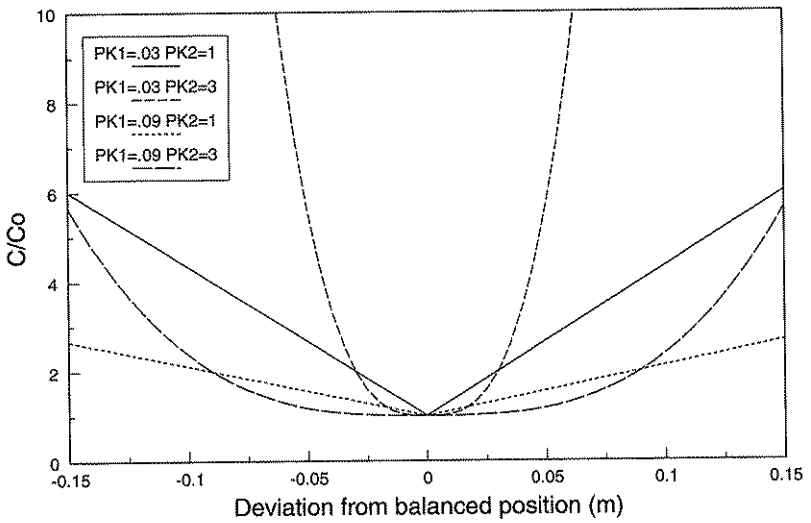

Fig. 13. The damping constant c for different $PK1_c$ and $PK2_c$.

5.1.5.1.3 Frequency characteristics

A suspension with a linear element with one degree of freedom can be described as in Figure 14 where m = the mass of the suspended cab. The suspension element is assumed to be a combined spring and damper.

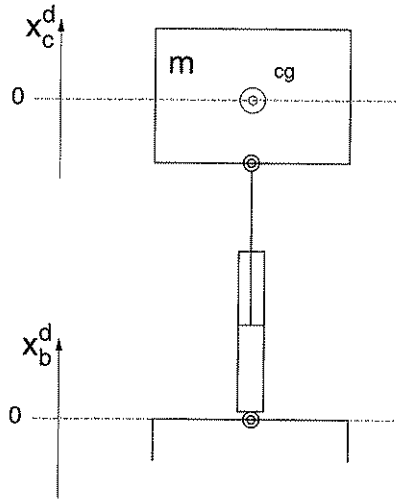

Fig. 14. Linear suspension with one d.o.f.

Assume that the body is moved from the balanced position. The differential equation describing the body's return to the balanced position ($x_c^d = 0$) becomes (Harris, 1988):

$$m\ddot{x}_c^d + c\dot{x}_c^d + kx_c^d = 0 \tag{28}$$

where

x_c^d = deviation from the balanced position.

The solution is dependent on the size of the damping constant c relative to the critical damping constant c_c:

$$c_c = 2\sqrt{k \cdot m} \tag{29}$$

defining the damping degree R:

$$R = c/c_c \tag{30}$$

For $R = 0$ the body will oscillate with unchanged amplitude with the frequency f_n, the undamped natural frequency:

$$f_n = \frac{1}{2\pi}\sqrt{\frac{k}{m}} \tag{31}$$

If $0 < R < 1,0$ the solution becomes:

$$x_c^d = e^{-ct/2m}(A \sin(\omega_D t) + B \cos(\omega_D t)) \tag{32}$$

where

$$A = \dot{x}_c^d/\omega_n \text{ when } t = 0 \tag{33}$$

$$B = x_c^d \text{ when } t = 0 \tag{34}$$

$$\omega_D=\omega_n\sqrt{1-R^2} = \text{ damped natural frequency.} \tag{35}$$

The damping is so small that the mass will oscillate around the balanced position before returning to equilibrium.

The solution can also be written:

$$x_c^d = Ce^{-ct/2m}\sin(\omega_D t + \theta) \tag{36}$$

where

$$C = \sqrt{A^2+B^2} \tag{37}$$

$$\theta = tan^{-1}(B/A) \tag{38}$$

When $c = c_c$ and thereby $R = 1$ the solution becomes:

$$x_c^d = (A + Bt)e^{-ct/2m} \tag{39}$$

which means that the mass is reaching the balanced position in the fastest way possible, without any oscillations occurring.

When $c > c_c$ and $R > 1$ the solution becomes:

$$x_c^d = e^{-ct/2m}\left(Ae^{\omega_n\sqrt{R^2-1}t} + Be^{-\omega_n\sqrt{R^2-1}t}\right) \tag{40}$$

which means that the body is moving, without oscillations, asymptotically closer to the balanced position.

Assume instead that, for the system in Figure 14, the foundation b is oscillating with the angular velocity ω and the amplitude A_b:

$$x_b^d = A_b\sin(\omega t) \tag{41}$$

When the oscillations dependent on the initial conditions have been damped out, the body's motion can be described by:

$$x_c^d = \mathrm{T}A_b\sin(\omega t - \phi) \tag{42}$$

where

$$T = \left(\frac{1 + (2R\omega/\omega_n)^2}{\left(1 - \frac{\omega^2}{\omega_n^2}\right)^2 + (2R\omega/\omega_n)^2} \right)^{0.5} \tag{43}$$

$$\phi = \mathrm{Tan}^{-1}\left(\frac{2R(\omega/\omega_n)^3}{1 - \frac{\omega^2}{\omega_n^2} + 4R^2\omega^2/\omega_n^2} \right) \tag{44}$$

where

T = transmissibility

ϕ = phase shift.

The transmissibility T defines the relation between the body's and the foundation's movements, but the curves are valid also for the transmission of velocities and accelerations.

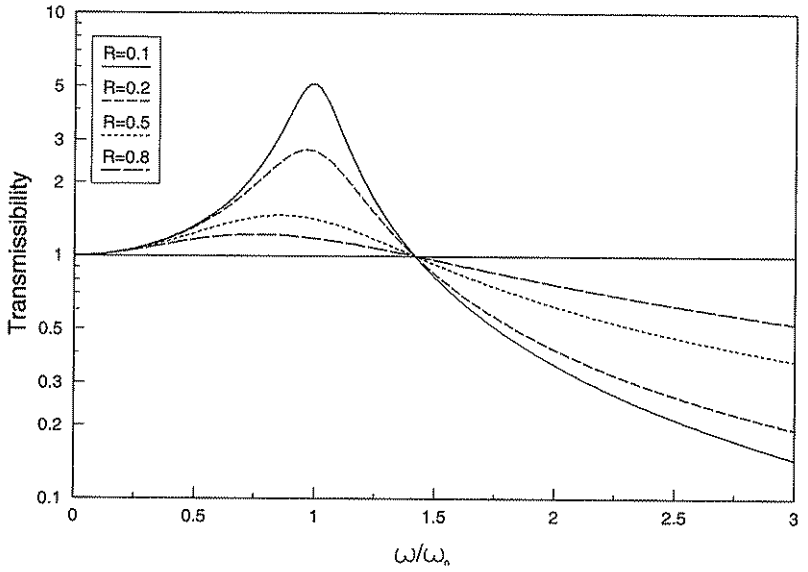

Fig. 15. Transmissibility vs ω/ω_n

Figure 15 shows the transmissibility as a function of ω/ω_n for different degrees of damping. This type of curve is further described as the amplitude characteristic for a system. The figure shows that foundation vibrations with frequencies close to the suspension's natural frequency become highly amplified, particularly for low damped systems. The transmissibility is higher than one for frequencies lower than $\sqrt{2} \cdot f_n$.

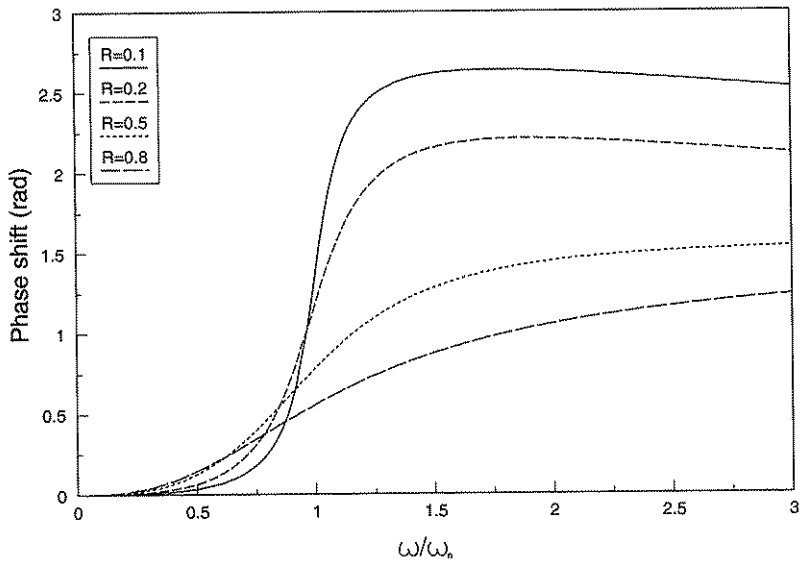

Fig. 16. Phase shift vs ω/ω_n

ϕ represents the phase shift in the system (Figure 16). This type of curve is further described as the phase characteristics of a system.

The theory described above is valid not only for a signal including one single frequency, but also for signals with a broad frequency content. Each frequency component is then amplified and phase shifted according to the described formulas.

It is not possible to obtain formulas such as the ones described above for the amplitude and phase characteristics of nonlinear systems. The response from the system is amplitude dependent and the differential equations cannot be solved analytically. Approximative solutions can be found by stepwise linearisation for some of the simpler nonlinear systems. In general, however, time domain simulation is the best tool when investigating nonlinear system characteristics.

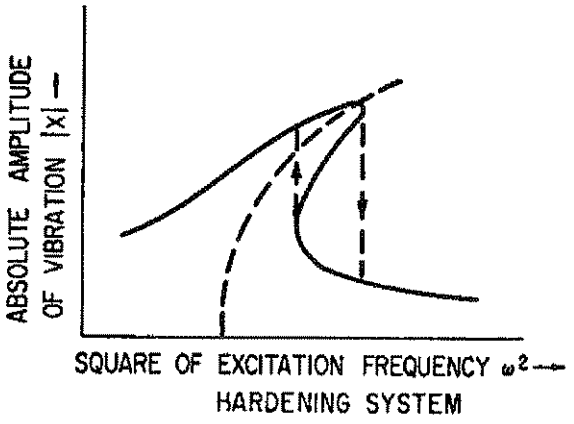

Fig. 17. Amplitude characteristics for a suspension with nonlinear spring characteristics (Harris, 1988).

Figure 17 shows the amplitude characteristics of a system with a nonlinear spring becoming stiffer against the end positions. The natural frequency and its amplitude dependency is marked with a dashed line. In one area, three different transmissibility values are possible for the same frequency, which further accentuates that no exact solution can be found.

5.1.5.2 Radially working elements

The radially working elements (Figure 12) are mounted elastically in the frame. The elastic mounting contributes to a torque being needed to bend the element from the balanced position. The torque affects the cab with a force in the element's radial direction. The connection between an element and the cab is defined as a frictionless ball joint.

The radially working elements used in the simulations normally also have a spring and damping function in the axial direction. The influence from the element at the cab then becomes the resultant of the radial and axial force. The forces are assumed to be independent of each other and can then also be calculated separately. The characteristics for elements which are rigid in the axial direction, with a suspension working only in the radial direction, are studied in the following parts.

The relation between the bending angle and the resulting torque depends on the design of the elastic bushing. A robust rubber bushing, a coil spring, etc., can be used.

The resulting torque is normally independent of the bending direction. In the calculations below, and in the simulation model, the bushings are assumed to be indefinitely stiff in the axial direction. It is also assumed that the torque produced in the bushing is frequency independent, and that the bushings work without energy dissipation.

The position of the element's mounting point in the frame is defined to be in the middle of the bushing, at the element's rotation centre when radially loaded.

5.1.5.2.1 Calculation of force components

A radially working element influences the cab with a force perpendicular to the element and towards the unloaded position.

A help point P_{H1} is defined to be located 1.00 m from the element's frame end point, in the unloaded direction of the element. This point follows the frame movements and shows therefore momentarily the element's unloaded direction (Figure 18).

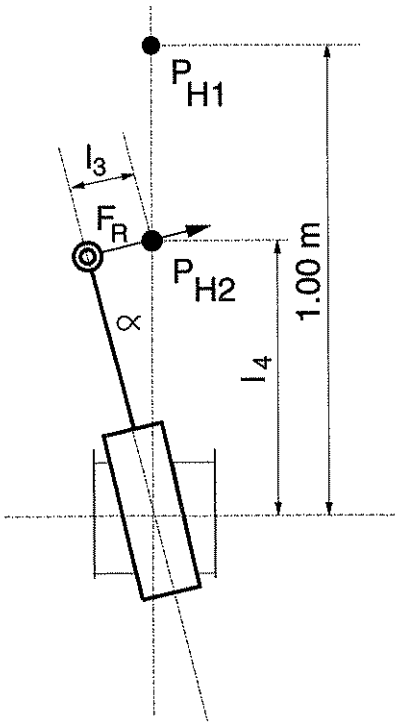

Fig. 18. Radially working element with the bending angle α relative to the unloaded position.

The vector **H** is directed from the element's frame mounting point to P_{H1}. **H**'s direction cosines can be calculated from:

$$D_{xH} = x^c_{H1} - x^c_b \tag{45}$$

$$D_{yH} = y^c_{H1} - y^c_b \tag{46}$$

$$D_{zH} = z^c_{H1} - z^c_b \tag{47}$$

where

i_{H1}^{c} = help point coordinate in the i direction $(i = x, y, z)$

For the element's angle α in relation to the vector **H** the following is valid (Spiegel, 1968):

$$\alpha = \cos^{-1}(D_x \cdot D_{xH} + D_y \cdot D_{yH} + D_z \cdot D_{zH}) \tag{48}$$

The magnitude of the force influencing the cab is:

$$F_R = \frac{q \cdot \alpha}{l_e} \tag{49}$$

where

q = bending constant

The lengths l_3 and l_4 (Figure 18) can be calculated from :

$$l_3 = l_e \cdot \tan\alpha \tag{50}$$

$$l_4 = \frac{l_e}{\cos\alpha} \tag{51}$$

The element's radial force is directed against P_{H2}, whose coordinates are:

$$x_{H2}^{c} = x_b^c + l_4 \cdot D_{xH} \tag{52}$$

$$y_{H2}^{c} = y_b^c + l_4 \cdot D_{yH} \tag{53}$$

$$z_{H2}^{c} = z_b^c + l_4 \cdot D_{zH} \tag{54}$$

F_R's direction cosines can now be calculated from:

$$D_{xR} = \frac{x_{H2}^{c} - x_c^c}{l_3} \tag{55}$$

$$D_{yR} = \frac{y_{H2}^{c} - y_c^c}{l_3} \tag{56}$$

$$D_{zR} = \frac{z_{H2}^{c} - z_c^c}{l_3} \tag{57}$$

When the directions and the magnitudes of the radial forces are calculated, the resulting forces and torque influencing the cab can be calculated with the same formulas as for axially working elements.

5.1.5.2.2 Linear and nonlinear passive elements

For the relation between the bending angle α and the torque M_α the following is valid:

$$M_\alpha = \alpha \cdot q \tag{58}$$

The value of q is constant for a linear suspension.

The torque can also be described by a nonlinear function. The nonlinearities can be described in many different ways. The nonlinearities used in the simulations are based on the same principle as for the axially working elements described earlier. The bending constant q is defined by:

$$q(\alpha) = q_0\left(1 + \left|\frac{\alpha}{PK1_\alpha}\right|^{PK2_\alpha}\right) \tag{59}$$

where

q_0 = bending constant in the unloaded position.

5.1.5.2.3 Frequency characteristics

A schematic suspension with two radially working elements is shown in Figure 19.

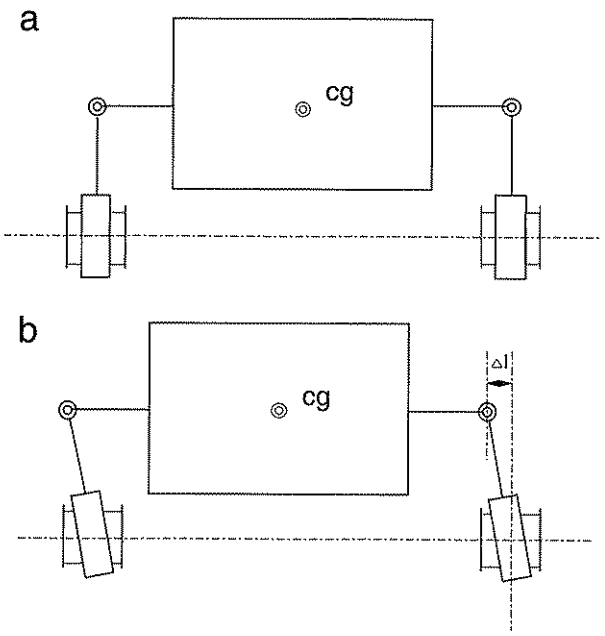

Fig. 19. Body suspended with two radially working elements. In b the body is moved Δl sideways from the balanced position.

To study the frequency characteristics for a suspension of this type, assume that the body is moved Δl sideways, so that the elements are bent at the angle α from the balanced position. A radial force from each element then strives to return the body to the original location:

$$F_R = \frac{M_\alpha}{l_e} = \frac{\alpha \cdot q}{l_e} \tag{60}$$

For small angles α can be approximated as $\Delta l / l_e$ and the forces of inertia depending on the body's vertical movements be neglected.

F_R's components then become:

$$F_{RH} = F_R \cdot \cos\alpha = \frac{\Delta l \cdot q}{(l_e)^2} \cdot \cos\alpha \tag{61}$$

$$F_{RV} = F_R \cdot \sin\alpha = \frac{\Delta l \cdot q}{(l_e)^2} \cdot \sin\alpha \tag{62}$$

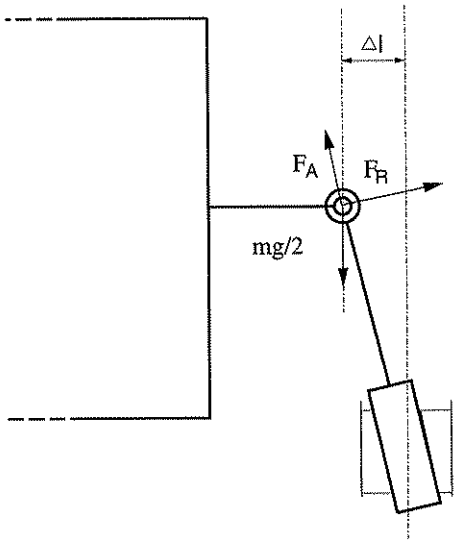

Fig. 20. Forces at each element.

For the forces, the following is valid:

$$F_{AV} - \frac{mg}{2} + F_{RV} = 0 \tag{63}$$

$$F_{RH} - F_{AH} = F_{HC} \tag{64}$$

where

$F_{AH} = F_A$'s horizontal component

$F_{AV} = F_A$'s vertical component

F_{HC} = horizontal resultant force on the cab

$$F_{AV} = \frac{mg}{2} - \frac{\Delta l \cdot q}{(l_e)^2} \cdot \sin\alpha \tag{65}$$

$$F_{AH} = F_{AV} \cdot \tan\alpha \tag{66}$$

$$F_{HC} = F_{RH} - F_{AH} = \frac{\Delta l \cdot q}{(l_e)^2} \cdot \cos\alpha - \left(\frac{mg}{2} - \frac{\Delta l \cdot q}{(l_e)^2} \cdot \sin\alpha \right) \tan\alpha \tag{67}$$

For small angles:

$$\cos\alpha \approx 1 \text{ and } \sin\alpha \approx \alpha \approx \Delta l / l_e \tag{68}$$

and thus

$$F_{HC} \approx \frac{\Delta l \cdot q}{(l_e)^2} - \frac{m \cdot g \cdot \Delta l}{2 \cdot l_e} + \frac{(\Delta l)^3 \cdot q}{(l_e)^4} \tag{69}$$

If α is small, $\frac{\Delta l}{l_e}$ is also small and $\frac{(\Delta l)^3}{l_e^4} \approx 0$

and thus

$$F_{HC} \approx \frac{\Delta l \cdot q}{(l_e)^2} - \frac{m \cdot g \cdot \Delta l}{2 \cdot l_e} \tag{70}$$

In the terminology used for the elements with axial working principle, the force striving to return the body to the balanced position is described by:

$$F = k \cdot \Delta l \tag{71}$$

which results in:

$$2\left(\frac{\Delta l \cdot q}{(l_e)^2} - \frac{m \cdot g \cdot \Delta l}{2 \cdot l_e}\right) \approx k \cdot \Delta l \tag{72}$$

or

$$k \approx \frac{2q}{(l_e)^2} - \frac{m \cdot g}{l_e} \tag{73}$$

The k value can be used in the formulas describing the characteristics for a system with one d.o.f (Ch. 5.1.5.1.3) to calculate the suspension system's horizontal natural frequency:

$$f_{nH} = \frac{1}{2\pi}\left(\frac{k}{m}\right)^{0.5} \approx \frac{1}{2\pi}\left(\frac{2q}{m(l_e)^2} - \frac{g}{l_e}\right)^{0.5} \tag{74}$$

The same calculation technique can, of course, also be used when more than two suspension elements are used.

Shock absorbers can be used to damp the horizontal movements. If the dampers are linear with known damping constants and symmetrically located, the approximate frequency characteristics can be calculated with the formulas in Ch. 5.1.5.1.3.

The simplifications necessary to make the formulas linear contribute to the phase shift and transmissibility curves only showing approximative solutions. The approximation errors also increase when the suspension travel and angle deviations are increased.

Up to now the discussion has only dealt with motions in one horizontal d.o.f. If the elastic bushings or springs are symmetrical, the above described formulas are valid for motions in both the x and y directions.

The calculations above are valid when the suspension elements are vertical in the balanced position and symmetrically mounted. The simulation model also provides an opportunity to study the effects of nonsymmetrically mounted elements. The calculations of the suspension's frequency characteristics then become very complex and in most cases impossible to perform.

5.2 Linear model

A linear model of the frame-cab-suspension offers better possibilities to design and study the performance and stability of different active suspension techniques. A linear model also makes it possible to analyse frequency characteristics for different suspension principles, even passive ones, in a more effective way.

The construction of a linear model is normally based on some simplifications and constraints relating to the real system. It is very important that the errors introduced when making the model linear are as small as possible and, in addition, it is important that the constraints introduced should not prevent study of an important parameter.

5.2.1 Equations of motion

Consider a completely rigid body, elastically supported on n points by linear springs that have three mutually perpendicular stiffnesses k_{xi}, k_{yi} and k_{zi}, for $i = 1, \ldots, n$. The springs are mounted at the coordinates x_{ci}^c, y_{ci}^c and z_{ci}^c. The coordinate axes are fixed in the body parallel to these directions, through an origin at the cab's c.o.g. The equations of motion for small free vibrations can be placed in the form:

$$\mathbf{M}\ddot{\mathbf{x}}_c^d + \mathbf{K}\mathbf{x}_c^d = \mathbf{0} \tag{75}$$

where $\mathbf{x}_c^d$ is the body displacement vector:

$$\mathbf{x}_c^d = \begin{pmatrix} x_c^d \\ y_c^d \\ z_c^d \\ xr_c^d \\ yr_c^d \\ zr_c^d \end{pmatrix} \tag{76}$$

The first three elements describe the linear displacements and the second three describe the angular displacements (Harris, 1988).

The matrices **K** and **M** are symmetric square time invariant matrices:

K = (77)

$$\begin{pmatrix}
\sum_{i=1}^{n} k_{xi} & 0 & 0 & 0 & \sum_{i=1}^{n} k_{xi} z_{ci}^{c} & -\sum_{i=1}^{n} k_{xi} y_{ci}^{c} \\
0 & \sum_{i=1}^{n} k_{yi} & 0 & -\sum_{i=1}^{n} k_{yi} z_{ci}^{c} & 0 & \sum_{i=1}^{n} k_{yi} x_{ci}^{c} \\
0 & 0 & \sum_{i=1}^{n} k_{zi} & \sum_{i=1}^{n} k_{zi} y_{ci}^{c} & -\sum_{i=1}^{n} k_{zi} x_{ci}^{c} & 0 \\
0 & -\sum_{i=1}^{n} k_{yi} z_{ci}^{c} & \sum_{i=1}^{n} k_{zi} y_{ci}^{c} & \sum_{i=1}^{n} \left(k_{yi} z_{ci}^{c^2} + k_{zi} y_{ci}^{c^2} \right) & -\sum_{i=1}^{n} k_{zi} x_{ci}^{c} y_{ci}^{c} & -\sum_{i=1}^{n} k_{yi} x_{ci}^{c} z_{ci}^{c} \\
\sum_{i=1}^{n} k_{xi} z_{ci}^{c} & 0 & -\sum_{i=1}^{n} k_{zi} x_{ci}^{c} & -\sum_{i=1}^{n} k_{zi} x_{ci}^{c} y_{ci}^{c} & \sum_{i=1}^{n} \left(k_{zi} x_{ci}^{c^2} + k_{xi} z_{ci}^{c^2} \right) & -\sum_{i=1}^{n} k_{xi} y_{ci}^{c} z_{ci}^{c} \\
-\sum_{i=1}^{n} k_{xi} y_{ci}^{c} & \sum_{i=1}^{n} k_{yi} x_{ci}^{c} & 0 & -\sum_{i=1}^{n} k_{yi} z_{ci}^{c} x_{ci}^{c} & -\sum_{i=1}^{n} k_{xi} y_{ci}^{c} z_{ci}^{c} & \sum_{i=1}^{n} \left(k_{xi} y_{ci}^{c^2} + k_{yi} x_{ci}^{c^2} \right)
\end{pmatrix}$$

M = (78)

$$\begin{pmatrix}
m & 0 & 0 & 0 & 0 & 0 \\
0 & m & 0 & 0 & 0 & 0 \\
0 & 0 & m & 0 & 0 & 0 \\
0 & 0 & 0 & I_{xx} & -I_{xy} & -I_{xz} \\
0 & 0 & 0 & -I_{xy} & I_{yy} & -I_{yz} \\
0 & 0 & 0 & -I_{xz} & -I_{yz} & I_{zz}
\end{pmatrix}$$

If the axes are the principle axes of inertia, the products of inertia terms vanish and no inertia coupling is present.

Then assume that n external forces are influencing the body with the components F_{xj}, F_{yj} and F_{zj} $(j = 1, \ldots, n)$ at the coordinates x_{fj}^c, y_{fj}^c and z_{fj}^c.

The equation then becomes:

$$\mathbf{M}\ddot{\mathbf{x}}_c^d + \mathbf{K}\mathbf{x}_c^d = \mathbf{F} \tag{79}$$

where $\mathbf{F}$ = (80)

$$\begin{pmatrix} \sum_{j=1}^{n} F_{xj} \\ \sum_{j=1}^{n} F_{yj} \\ \sum_{j=1}^{n} F_{zj} \\ \sum_{j=1}^{n} (F_{yj} z_{fj}^c + F_{zj} y_{fj}^c) \\ \sum_{j=1}^{n} (F_{zj} x_{fj}^c + F_{xj} z_{fj}^c) \\ \sum_{j=1}^{n} (F_{xj} y_{fj}^c + F_{yj} x_{fj}^c) \end{pmatrix}$$

Observe that $\mathbf{F}$ normally is time variant while both $\mathbf{M}$ and $\mathbf{K}$ are approximately time invariant.

5.2.2 Equations of motion for the suspended cab

The formulas in the previous chapter might perhaps seem rather complicated, but become easier to understand when used in an application.

Assume a schematic cab suspension such as that in Figure 21

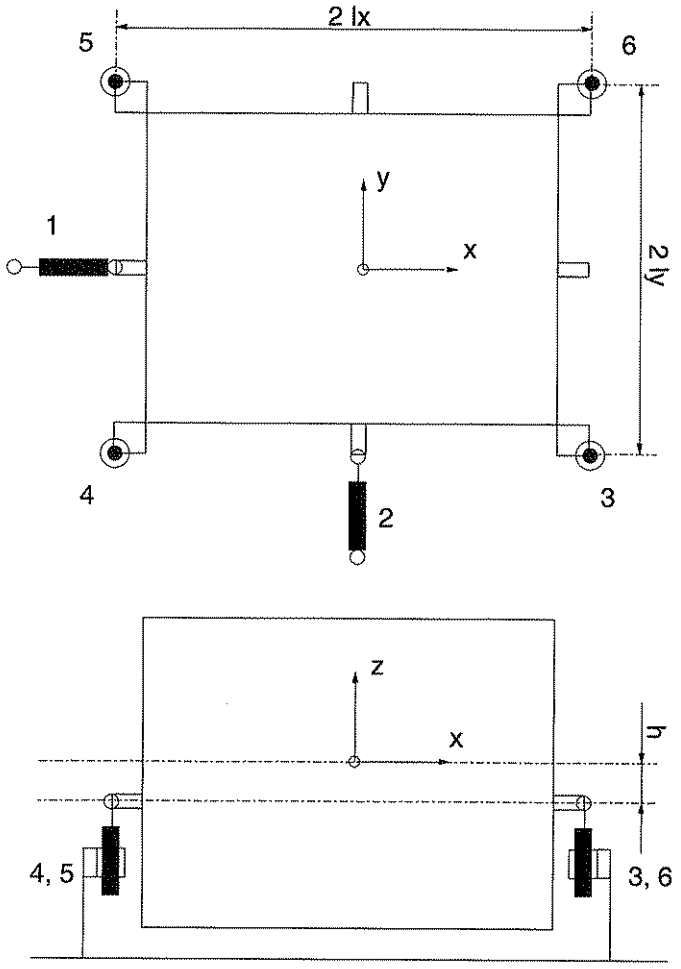

Fig. 21. Schematic cab suspension.

As described earlier, the cab's angular motion around the z axis can be neglected, which decreases the order of **K**, **M** and **F** to five.

In a real suspension are there more than one horizontal element mounted to dampen the motions in the x and y directions (see for example Figure 33 or Figure 50). With no motion around the z axis, however, the total force in the x direction from the horizontal elements can be summed up in one single element (element 1). The same can be done for the y direction (element 2).

The cab is standing on four elements with combined radial and axial working principles (elements 3-6). The axial function then mainly influences the vibrations in the z direction and the angular vibrations around the x and y axes. The radial function of elements 3-6

influences together with elements 1-2 the transmission of vibrations in the x and y directions. With $h \neq 0$, the angular motions around the x and y axes are also influenced by elements 1-2 and the radial forces of element 3-6.

Elements 1-2 are located in the cab's symmetrical plane, which is why $y_{c1}^c = x_{c2}^c = 0$, $x_{c1}^c = -l_x$ and $y_{c2}^c = -l_y$. Assume that the vertical elements 3-6 are symmetrically located. Then $x_{c3}^c = -x_{c4}^c = -x_{c5}^c = x_{c6}^c = l_x$ and $-y_{c3}^c = -y_{c4}^c = y_{c5}^c = y_{c6}^c = l_y$. Assume also that all the elements' cab end points are located at the same height, thus $z_{c1}^c = z_{c2}^c = z_{c3}^c = z_{c4}^c = z_{c5}^c = z_{c6}^c = -h$

Elements 1-2 only influence the cab in one dimension each and thus $k_{x2} = k_{y1} = k_{z1} = k_{z2} = 0$. The axial function of elements 3-6 decides k_{z3}, k_{z4}, k_{z5} and k_{z6}, when k_{x3}, k_{x4}, k_{x5}, k_{x6}, k_{y3}, k_{y4}, k_{y5} and k_{y6} are decided by the radial function (see Ch. 5.1.5.2.3). The springs are assumed to be linear.

The suspension elements are influencing the cab with forces additional to the spring forces. These forces can be dependent on the elements' damping characteristics or perhaps by an active suspension controller. In a practical application these forces are normally only able to apply in the element's axial directions. Still calculating with small amplitude vibrations, it is then valid that the only force components separated from zero can be F_{x1}, F_{y2}, F_{z3}, F_{z4}, F_{z5} and F_{z6}. The external forces influence the cab at the same points as the other forces from the suspension elements, and thus $x_{f1}^c = x_{c1}^c$, $y_{f1}^c = y_{c1}^c$, etc.

5.2.3 State space description

5.2.3.1 System dynamics model

The frame-suspension-cab system studied above can be described in the standard form for linear time invariant differential equations, the state space representation:

$$\dot{\mathbf{x}}_o^s = \mathbf{A}_o \mathbf{x}_o^s + \mathbf{B}_o^u \mathbf{u}_o + \mathbf{B}_o^v \mathbf{v}_o \tag{81}$$

where

$\mathbf{x}_o^s$ = the state vector

$\mathbf{u}_o$ = the control input vector

$\mathbf{v}_o$ = the disturbance input vector

$$(\mathbf{x}_o^s)^T = \tag{82}$$

$$(x_1^s \;\; x_2^s \;\; x_3^s \;\; x_4^s \;\; x_5^s \;\; x_6^s \;\; x_7^s \;\; x_8^s \;\; x_9^s \;\; x_{10}^s \;\; x_{11}^s \;\; x_{12}^s \;\; x_{13}^s \;\; x_{14}^s \;\; x_{15}^s) =$$

$$(x_c^d \;\; \dot{x}_c^d \;\; y_c^d \;\; \dot{y}_c^d \;\; z_c^d \;\; \dot{z}_c^d \;\; xr_c^d \;\; \dot{xr}_c^d \;\; yr_c^d \;\; \dot{yr}_c^d \;\; x_b^d \;\; y_b^d \;\; z_b^d \;\; xr_b^d \;\; yr_b^d)$$

The foundation displacement vector $\mathbf{x}_b^d$ describes the three linear and two angular displacements of the frame. $\mathbf{x}_b^d$ is measured relative to the same system as the cab displacement vector $\mathbf{x}_c^d$.

$$\mathbf{x}_b^d = \begin{pmatrix} x_b^d \\ y_b^d \\ z_b^d \\ xr_b^d \\ yr_b^d \end{pmatrix} \tag{83}$$

$$\mathbf{A}_o = \tag{84}$$

$$\begin{pmatrix}
0 & 1 & 0 & 0 & 0 & 0 & 0 & 0 & 0 & 0 & 0 & 0 & 0 & 0 & 0 \\
\frac{-4k_x}{m} & 0 & 0 & 0 & 0 & 0 & 0 & 0 & \frac{4k_x h}{m} & 0 & \frac{4k_x}{m} & 0 & 0 & 0 & g - \frac{4k_x h}{m} \\
0 & 0 & 0 & 1 & 0 & 0 & 0 & 0 & 0 & 0 & 0 & 0 & 0 & 0 & 0 \\
0 & 0 & \frac{-4k_y}{m} & 0 & 0 & 0 & \frac{-4k_y h}{m} & 0 & 0 & 0 & 0 & \frac{4k_y}{m} & 0 & -g + \frac{4k_y h}{m} & 0 \\
0 & 0 & 0 & 0 & 0 & 1 & 0 & 0 & 0 & 0 & 0 & 0 & 0 & 0 & 0 \\
0 & 0 & 0 & 0 & \frac{-4k_z}{m} & 0 & 0 & 0 & 0 & 0 & 0 & 0 & \frac{4k_z}{m} & 0 & 0 \\
0 & 0 & 0 & 0 & 0 & 0 & 0 & 1 & 0 & 0 & 0 & 0 & 0 & 0 & 0 \\
0 & 0 & \frac{-4k_y h}{I_{xx}} & 0 & 0 & 0 & \frac{-4k_z l_y^2}{I_{xx}} - \frac{4k_y h^2}{I_{xx}} & 0 & 0 & 0 & 0 & \frac{4k_y h}{I_{xx}} & 0 & \frac{4k_z l_y^2}{I_{xx}} + \frac{4k_y h^2}{I_{xx}} & 0 \\
0 & 0 & 0 & 0 & 0 & 0 & 0 & 0 & 0 & 1 & 0 & 0 & 0 & 0 & 0 \\
\frac{4k_x h}{I_{yy}} & 0 & 0 & 0 & 0 & 0 & 0 & 0 & \frac{-4k_z l_x^2}{I_{yy}} - \frac{4k_x h^2}{I_{yy}} & 0 & \frac{-4k_x h}{I_{yy}} & 0 & 0 & 0 & \frac{4k_z l_x^2}{I_{yy}} + \frac{4k_x h^2}{I_{yy}} \\
0 & 0 & 0 & 0 & 0 & 0 & 0 & 0 & 0 & 0 & 0 & 0 & 0 & 0 & 0 \\
0 & 0 & 0 & 0 & 0 & 0 & 0 & 0 & 0 & 0 & 0 & 0 & 0 & 0 & 0 \\
0 & 0 & 0 & 0 & 0 & 0 & 0 & 0 & 0 & 0 & 0 & 0 & 0 & 0 & 0 \\
0 & 0 & 0 & 0 & 0 & 0 & 0 & 0 & 0 & 0 & 0 & 0 & 0 & 0 & 0 \\
0 & 0 & 0 & 0 & 0 & 0 & 0 & 0 & 0 & 0 & 0 & 0 & 0 & 0 & 0
\end{pmatrix}$$

$$\mathbf{B}_o^u = \begin{pmatrix} 0 & 0 & 0 & 0 & 0 & 0 \\ \frac{1}{m} & 0 & 0 & 0 & 0 & 0 \\ 0 & 0 & 0 & 0 & 0 & 0 \\ 0 & \frac{1}{m} & 0 & 0 & 0 & 0 \\ 0 & 0 & 0 & 0 & 0 & 0 \\ 0 & 0 & \frac{1}{m} & \frac{1}{m} & \frac{1}{m} & \frac{1}{m} \\ 0 & 0 & 0 & 0 & 0 & 0 \\ 0 & \frac{h}{I_{xx}} & -\frac{l_y}{I_{xx}} & -\frac{l_y}{I_{xx}} & \frac{l_y}{I_{xx}} & \frac{l_y}{I_{xx}} \\ 0 & 0 & 0 & 0 & 0 & 0 \\ -\frac{h}{I_{yy}} & 0 & -\frac{l_x}{I_{yy}} & \frac{l_x}{I_{yy}} & \frac{l_x}{I_{yy}} & -\frac{l_x}{I_{yy}} \\ 0 & 0 & 0 & 0 & 0 & 0 \\ 0 & 0 & 0 & 0 & 0 & 0 \\ 0 & 0 & 0 & 0 & 0 & 0 \\ 0 & 0 & 0 & 0 & 0 & 0 \\ 0 & 0 & 0 & 0 & 0 & 0 \end{pmatrix} \tag{85}$$

$$(\mathbf{u}_o)^T = (F_1 \quad F_2 \quad F_3 \quad F_4 \quad F_5 \quad F_6) = (F_{x1} \quad F_{y2} \quad F_{z3} \quad F_{z4} \quad F_{z5} \quad F_{z6}) \tag{86}$$

$$\mathbf{B}_o^v = \begin{pmatrix} 0 & 0 & 0 & 0 & 0 \\ 0 & 0 & 0 & 0 & 0 \\ 0 & 0 & 0 & 0 & 0 \\ 0 & 0 & 0 & 0 & 0 \\ 0 & 0 & 0 & 0 & 0 \\ 0 & 0 & 0 & 0 & 0 \\ 0 & 0 & 0 & 0 & 0 \\ 0 & 0 & 0 & 0 & 0 \\ 0 & 0 & 0 & 0 & 0 \\ 0 & 0 & 0 & 0 & 0 \\ 0 & 0 & 0 & 0 & 0 \\ 1 & 0 & 0 & 0 & 0 \\ 0 & 1 & 0 & 0 & 0 \\ 0 & 0 & 1 & 0 & 0 \\ 0 & 0 & 0 & 1 & 0 \\ 0 & 0 & 0 & 0 & 1 \end{pmatrix} \tag{87}$$

$$(\mathbf{v}_0)^T = (x_b^d \quad y_b^d \quad z_b^d \quad x\dot{r}_b^d \quad y\dot{r}_b^d) \tag{88}$$

where (89)

$k_x = k_{x3} = k_{x4} = k_{x5} = k_{x6}$

$$k_y = k_{y3} = k_{y4} = k_{y5} = k_{y6} \tag{90}$$

$$k_z = k_{z3} = k_{z4} = k_{z5} = k_{z6} \tag{91}$$

The first parts in $\mathbf{A}_o(2,15)$ and $\mathbf{A}_o(4,14)$ depend on the components of the cab's weight striving to move the cab in the direction it is leaning when the cab and frame are inclined (Figure 22). All the other expressions in the system matrices can be derived from the formulas in Ch. 5.2.1.

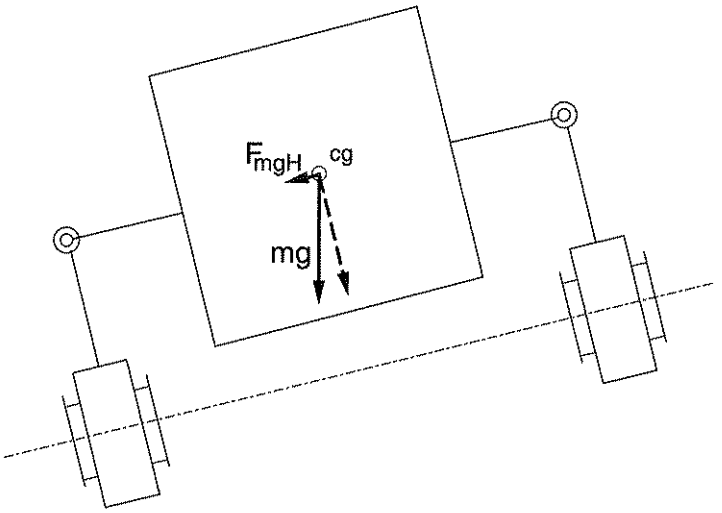

Fig. 22. Forces when the cab and frame are inclined.

When using the system states in a state feedback controller, they must be able to measure or be possible to estimate by an observer. The system description above contains states describing the cab's and the frame's absolute levels. These states were found to be very difficult to measure or to estimate with an observer.

To avoid the difficulties, the system can be described slightly differently. Three new states for $x_c^d - x_b^d$, $y_c^d - y_b^d$ and $z_c^d - z_b^d$ are introduced. These states are very easy to measure with length transducers at the suspension elements.

The system then becomes

$$\dot{\mathbf{x}}_e^s = \mathbf{A}_e\mathbf{x}_e^s + \mathbf{B}_e^u\mathbf{u}_e + \mathbf{B}_e^v\mathbf{v}_e \text{ with:} \tag{92}$$

$$(\mathbf{x}_e^s)^T = (x_c^d - x_b^d \quad y_c^d - y_b^d \quad z_c^d - z_b^d \quad \dot{x}_c^d \quad \dot{y}_c^d \quad \dot{z}_c^d \quad xr_c^d \quad \dot{xr}_c^d \quad yr_c^d \quad \dot{yr}_c^d \quad \dot{x}_b^d \quad \dot{y}_b^d \quad \dot{z}_b^d \quad xr_b^d \quad yr_b^d) \tag{93}$$

$$\mathbf{A}_e = \tag{94}$$

$$\begin{pmatrix}
0 & 0 & 0 & 1 & 0 & 0 & 0 & 0 & 0 & 0 & -1 & 0 & 0 & 0 & 0 \\
0 & 0 & 0 & 0 & 1 & 0 & 0 & 0 & 0 & 0 & 0 & -1 & 0 & 0 & 0 \\
0 & 0 & 0 & 0 & 0 & 1 & 0 & 0 & 0 & 0 & 0 & 0 & -1 & 0 & 0 \\
\frac{-4k_x}{m} & 0 & 0 & 0 & 0 & 0 & 0 & 0 & \frac{4k_x h}{m} & 0 & 0 & 0 & 0 & 0 & g - \frac{4k_x h}{m} \\
0 & \frac{-4k_y}{m} & 0 & 0 & 0 & 0 & \frac{-4k_y h}{m} & 0 & 0 & 0 & 0 & 0 & 0 & -g + \frac{4k_y h}{m} & 0 \\
0 & 0 & \frac{-4k_z}{m} & 0 & 0 & 0 & 0 & 0 & 0 & 0 & 0 & 0 & 0 & 0 & 0 \\
0 & 0 & 0 & 0 & 0 & 0 & 0 & 1 & 0 & 0 & 0 & 0 & 0 & 0 & 0 \\
0 & \frac{-4k_y h}{I_{xx}} & 0 & 0 & 0 & 0 & \frac{-4k_z l_y^2}{I_{xx}} - \frac{4k_y h^2}{I_{xx}} & 0 & 0 & 0 & 0 & 0 & 0 & \frac{4k_z l_y^2}{I_{xx}} + \frac{4k_y h^2}{I_{xx}} & 0 \\
0 & 0 & 0 & 0 & 0 & 0 & 0 & 0 & 0 & 1 & 0 & 0 & 0 & 0 & 0 \\
\frac{4k_x h}{I_{yy}} & 0 & 0 & 0 & 0 & 0 & 0 & 0 & \frac{-4k_z l_x^2}{I_{yy}} - \frac{4k_x h^2}{I_{yy}} & 0 & 0 & 0 & 0 & 0 & \frac{4k_z l_x^2}{I_{yy}} + \frac{4k_x h^2}{I_{yy}} \\
0 & 0 & 0 & 0 & 0 & 0 & 0 & 0 & 0 & 0 & 0 & 0 & 0 & 0 & 0 \\
0 & 0 & 0 & 0 & 0 & 0 & 0 & 0 & 0 & 0 & 0 & 0 & 0 & 0 & 0 \\
0 & 0 & 0 & 0 & 0 & 0 & 0 & 0 & 0 & 0 & 0 & 0 & 0 & 0 & 0 \\
0 & 0 & 0 & 0 & 0 & 0 & 0 & 0 & 0 & 0 & 0 & 0 & 0 & 0 & 0 \\
0 & 0 & 0 & 0 & 0 & 0 & 0 & 0 & 0 & 0 & 0 & 0 & 0 & 0 & 0
\end{pmatrix}$$

$$\mathbf{B}_e^u = \begin{pmatrix}
0 & 0 & 0 & 0 & 0 & 0 \\
0 & 0 & 0 & 0 & 0 & 0 \\
0 & 0 & 0 & 0 & 0 & 0 \\
\frac{1}{m} & 0 & 0 & 0 & 0 & 0 \\
0 & \frac{1}{m} & 0 & 0 & 0 & 0 \\
0 & 0 & \frac{1}{m} & \frac{1}{m} & \frac{1}{m} & \frac{1}{m} \\
0 & 0 & 0 & 0 & 0 & 0 \\
0 & \frac{h}{I_{xx}} & -\frac{l_y}{I_{xx}} & -\frac{l_y}{I_{xx}} & \frac{l_y}{I_{xx}} & \frac{l_y}{I_{xx}} \\
0 & 0 & 0 & 0 & 0 & 0 \\
-\frac{h}{I_{yy}} & 0 & -\frac{l_x}{I_{yy}} & \frac{l_x}{I_{yy}} & \frac{l_x}{I_{yy}} & -\frac{l_x}{I_{yy}} \\
0 & 0 & 0 & 0 & 0 & 0 \\
0 & 0 & 0 & 0 & 0 & 0 \\
0 & 0 & 0 & 0 & 0 & 0 \\
0 & 0 & 0 & 0 & 0 & 0 \\
0 & 0 & 0 & 0 & 0 & 0
\end{pmatrix} \tag{95}$$

$$\mathbf{u}_e = \mathbf{u}_o \tag{96}$$

$$\mathbf{B}_e^v = \mathbf{B}_o^v \tag{97}$$

$$(\mathbf{v}_e)^T = (\ddot{x}_b^d \quad \ddot{y}_b^d \quad \ddot{z}_b^d \quad \dot{xr}_b^d \quad \dot{yr}_b^d) \tag{98}$$

Note that the disturbance input vector now contains the frame accelerations in the x, y and z directions.

From the state space model, the accelerations (vibrations) in the cab can be defined as outputs. For the vector including the accelerations at the cab's c.o.g. ($\ddot{\mathbf{x}}_c^d$) the following is valid:

$$\ddot{\mathbf{x}}_c^d = \mathbf{C}_e \mathbf{x}_e^s + \mathbf{D}_e \mathbf{u}_e \tag{99}$$

where

$$(\ddot{\mathbf{x}}_c^d)^T = (\ddot{x}_c^d \quad \ddot{y}_c^d \quad \ddot{z}_c^d \quad \ddot{x}\ddot{r}_c^d \quad \ddot{y}\ddot{r}_c^d) \tag{100}$$

$$\mathbf{C}_e = \tag{101}$$

$$\begin{pmatrix}
\frac{-4k_x}{m} & 0 & 0 & 0 & 0 & 0 & 0 & 0 & \frac{4k_x h}{m} & 0 & 0 & 0 & 0 & 0 & g - \frac{4k_z h}{m} \\
0 & \frac{-4k_y}{m} & 0 & 0 & 0 & 0 & \frac{-4k_y h}{m} & 0 & 0 & 0 & 0 & 0 & 0 & -g + \frac{4k_y h}{m} & 0 \\
0 & 0 & \frac{-4k_z}{m} & 0 & 0 & 0 & 0 & 0 & 0 & 0 & 0 & 0 & 0 & 0 & 0 \\
0 & \frac{-4k_y h}{I_{xx}} & 0 & 0 & 0 & 0 & \frac{-4k_z l_y^2}{I_{xx}} - \frac{4k_y h^2}{I_{xx}} & 0 & 0 & 0 & 0 & 0 & 0 & \frac{4k_z l_y^2}{I_{xx}} + \frac{4k_y h^2}{I_{xx}} & 0 \\
\frac{4k_x h}{I_{yy}} & 0 & 0 & 0 & 0 & 0 & 0 & 0 & \frac{-4k_z l_x^2}{I_{yy}} - \frac{4k_x h^2}{I_{yy}} & 0 & 0 & 0 & 0 & 0 & \frac{4k_z l_x^2}{I_{yy}} + \frac{4k_x h^2}{I_{yy}}
\end{pmatrix}$$

$$\mathbf{D}_e = \tag{102}$$

$$\begin{pmatrix}
\frac{1}{m} & 0 & 0 & 0 & 0 & 0 \\
0 & \frac{1}{m} & 0 & 0 & 0 & 0 \\
0 & 0 & \frac{1}{m} & \frac{1}{m} & \frac{1}{m} & \frac{1}{m} \\
0 & \frac{h}{I_{xx}} & -\frac{l_y}{I_{xx}} & -\frac{l_y}{I_{xx}} & \frac{l_y}{I_{xx}} & \frac{l_y}{I_{xx}} \\
-\frac{h}{I_{yy}} & 0 & -\frac{l_x}{I_{yy}} & \frac{l_x}{I_{yy}} & \frac{l_x}{I_{yy}} & -\frac{l_x}{I_{yy}}
\end{pmatrix}$$

The accelerations at other locations in the cab can easily be calculated from $\ddot{\mathbf{x}}_c^d$.

5.2.3.2 Model with frequency weighted outputs

ISO 2631 shows that the human body is variably sensitive to vibrations dependent on the direction and the frequency content. In the BS 6841 standard, the transfer functions for the weighting filters defined in ISO 2631 are described in a format that can be converted to state space format. The second order transfer functions are very good approximations

of the curves defined in the ISO standard (Figure 23). The approximations are non-unique, and in view of the subjective nature of the the weighting factors, any reasonable approximation will be acceptable.

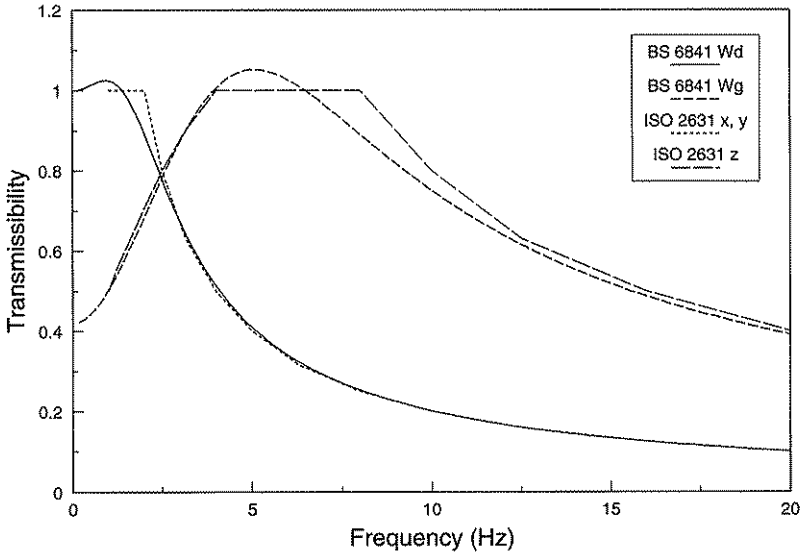

Fig. 23. Frequency weighting filters defined in ISO 2631 and BS 6841.

The filters in the x direction are described by (Wd in BS 6841):

$$\begin{pmatrix} \dot{x}^s_{H1} \\ \dot{x}^s_{H2} \end{pmatrix} = \begin{pmatrix} -19.9 & 1 \\ -157.9 & 0 \end{pmatrix} \begin{pmatrix} x^s_{H1} \\ x^s_{H2} \end{pmatrix} + \begin{pmatrix} 12.57 \\ 157.9 \end{pmatrix} \ddot{x}^d_c \tag{103}$$

$$\ddot{x}^d_w = (1 \quad 0) \begin{pmatrix} x^s_{H1} \\ x^s_{H2} \end{pmatrix} \tag{104}$$

where

$\ddot{x}^d_w$ = weighted acceleration value in the x direction

x^s_{H1}, x^s_{H2} = help states.

The filter transfer functions are identical in the x and y directions:

$$\begin{pmatrix} \dot{y}^s_{H1} \\ \dot{y}^s_{H2} \end{pmatrix} = \begin{pmatrix} -19.9 & 1 \\ -157.9 & 0 \end{pmatrix} \begin{pmatrix} y^s_{H1} \\ y^s_{H2} \end{pmatrix} + \begin{pmatrix} 12.57 \\ 157.9 \end{pmatrix} \ddot{y}^d_c \tag{105}$$

$$\ddot{y}_w^d = (1 \quad 0)\begin{pmatrix} y_{H1}^s \\ y_{H2}^s \end{pmatrix} \tag{106}$$

For vibrations in the z direction, the filter can be described (Wg in BS 6841):

$$\begin{pmatrix} \dot{z}_{H1}^s \\ \dot{z}_{H2}^s \end{pmatrix} = \begin{pmatrix} -48.93 & 1 \\ -1108 & 0 \end{pmatrix}\begin{pmatrix} z_{H1}^s \\ z_{H2}^s \end{pmatrix} + \begin{pmatrix} 49.42 \\ 465.8 \end{pmatrix}\ddot{z}_c^d \tag{107}$$

$$\ddot{z}_w^d = (1 \quad 0)\begin{pmatrix} z_{H1}^s \\ z_{H2}^s \end{pmatrix} \tag{108}$$

The frequency weighting filters from the standard can be included in the model to get outputs directly describing the effects on the human body.

$$\dot{\mathbf{x}}_w^s = \mathbf{A}_w\mathbf{x}_w^s + \mathbf{B}_w^u\mathbf{u}_w + \mathbf{B}_w^v\mathbf{v}_w \tag{109}$$

where

$$(\mathbf{x}_w^s)^T = \left((\mathbf{x}_e^s)^T \quad x_{H1}^s \quad x_{H2}^s \quad y_{H1}^s \quad y_{H2}^s \quad z_{H1}^s \quad z_{H2}^s\right) \tag{110}$$

$$\mathbf{A}_w = \begin{pmatrix} \mathbf{A}_e & \mathbf{0} \\ \mathbf{A}_{wp1} & \mathbf{A}_{wp2} \end{pmatrix} \tag{111}$$

$\mathbf{A}_{wp1} =$ (112)

$$\begin{pmatrix} \frac{-4k_x \cdot 12.57}{m} & 0 & 0 & 0 & 0 & 0 & 0 & \frac{4k_x h \cdot 12.57}{m} & 0 & 0 & 0 & 0 & 0 & g \cdot 12.57 - \frac{4k_x h \cdot 12.57}{m} \\ \frac{-4k_x \cdot 157.9}{m} & 0 & 0 & 0 & 0 & 0 & 0 & \frac{4k_x h \cdot 157.9}{m} & 0 & 0 & 0 & 0 & 0 & g \cdot 157.9 - \frac{4k_x h \cdot 157.9}{m} \\ 0 & \frac{-4k_y \cdot 12.57}{m} & 0 & 0 & 0 & 0 & \frac{-4k_y h \cdot 12.57}{m} & 0 & 0 & 0 & 0 & 0 & -g \cdot 12.57 + \frac{4k_y h \cdot 12.57}{m} & 0 \\ 0 & \frac{-4k_y \cdot 157.9}{m} & 0 & 0 & 0 & 0 & \frac{-4k_y h \cdot 157.9}{m} & 0 & 0 & 0 & 0 & 0 & -g \cdot 157.9 + \frac{4k_y h \cdot 157.9}{m} & 0 \\ 0 & 0 & \frac{-4k_z \cdot 49.42}{m} & 0 & 0 & 0 & 0 & 0 & 0 & 0 & 0 & 0 & 0 & 0 \\ 0 & 0 & \frac{-4k_z \cdot 465.8}{m} & 0 & 0 & 0 & 0 & 0 & 0 & 0 & 0 & 0 & 0 & 0 \end{pmatrix}$$

$$\mathbf{A}_{wp2} = \begin{pmatrix} -19.90 & 1 & 0 & 0 & 0 & 0 \\ -157.9 & 0 & 0 & 0 & 0 & 0 \\ 0 & 0 & -19.90 & 1 & 0 & 0 \\ 0 & 0 & -157.9 & 0 & 0 & 0 \\ 0 & 0 & 0 & 0 & -48.93 & 1 \\ 0 & 0 & 0 & 0 & -1108 & 0 \end{pmatrix} \tag{113}$$

$$\mathbf{B}_w^u = \begin{pmatrix} \mathbf{B}_e^u \\ \mathbf{B}_{wp}^u \end{pmatrix} \tag{114}$$

$$\mathbf{B}_{wp}^u = \begin{pmatrix} \frac{12.57}{m} & 0 & 0 & 0 & 0 & 0 \\ \frac{157.9}{m} & 0 & 0 & 0 & 0 & 0 \\ 0 & \frac{12.57}{m} & 0 & 0 & 0 & 0 \\ 0 & \frac{157.9}{m} & 0 & 0 & 0 & 0 \\ 0 & 0 & \frac{49.42}{m} & \frac{49.42}{m} & \frac{49.42}{m} & \frac{49.42}{m} \\ 0 & 0 & \frac{465.8}{m} & \frac{465.8}{m} & \frac{465.8}{m} & \frac{465.8}{m} \end{pmatrix} \tag{115}$$

$$\mathbf{u}_w = \mathbf{u}_e \tag{116}$$

$$\mathbf{B}_w^v = \begin{pmatrix} \mathbf{B}_e^v \\ \mathbf{0}^{6*5} \end{pmatrix} \tag{117}$$

$$\mathbf{v}_w = \mathbf{v}_e \tag{118}$$

The vector with weighted vibrations $\ddot{\mathbf{x}}_w^d$ can be calculated from:

$$\ddot{\mathbf{x}}_w^d = \mathbf{C}_w \mathbf{x}_w^s \tag{119}$$

where

$$(\ddot{\mathbf{x}}_w^d)^T = (\ddot{x}_w^d \quad \ddot{y}_w^d \quad \ddot{z}_w^d) \tag{120}$$

$\mathbf{C}_w =$

$$\begin{pmatrix} 0 & 0 & 0 & 0 & 0 & 0 & 0 & 0 & 0 & 0 & 0 & 0 & 0 & 0 & 0 & 1 & 0 & 0 & 0 & 0 & 0 \\ 0 & 0 & 0 & 0 & 0 & 0 & 0 & 0 & 0 & 0 & 0 & 0 & 0 & 0 & 0 & 0 & 0 & 1 & 0 & 0 & 0 \\ 0 & 0 & 0 & 0 & 0 & 0 & 0 & 0 & 0 & 0 & 0 & 0 & 0 & 0 & 0 & 0 & 0 & 0 & 0 & 1 & 0 \end{pmatrix} \tag{121}$$

No filters are defined for the angular vibrations so this output can be calculated directly from $\ddot{\mathbf{x}}_c^d$.

5.2.3.3 Partition into uncoupled models

The dynamic models above describe the movements of the frame and the cab in 5 d.o.f. The models become rather complex and result in complex active suspension controllers.

By assuming some constraints for the suspension geometry, it is possible to uncouple the movements in the different dimensions, which enables the model to be partitioned into 5 smaller models. The theory can then also be used for a suspension with free motion just in one or a few d.o.f., which is very valuable for the practical application of the results.

The cab's movements in the z dimension can be described in the state space model:

$$\dot{\mathbf{x}}_{zp}^{s} = \begin{pmatrix} 0 & 1 & -1 & 0 & 0 \\ \frac{-4k_z}{m} & 0 & 0 & 0 & 0 \\ 0 & 0 & 0 & 0 & 0 \\ \frac{-4k_z \cdot 49.42}{m} & 0 & 0 & -48.93 & 1 \\ \frac{-4k_z \cdot 465.8}{m} & 0 & 0 & -1108 & 0 \end{pmatrix} \mathbf{x}_{zp}^{s} + \begin{pmatrix} 0 \\ \frac{1}{m} \\ 0 \\ \frac{49.42}{m} \\ \frac{465.8}{m} \end{pmatrix} F_{zp} + \begin{pmatrix} 0 \\ 0 \\ 1 \\ 0 \\ 0 \end{pmatrix} \dot{z}_b^d \tag{122}$$

where

$$(\mathbf{x}_{zp}^{s})^T = (z_c^d - z_b^d \quad \dot{z}_c^d \quad \dot{z}_b^d \quad z_{H1}^s \quad z_{H2}^s) \tag{123}$$

$$F_{zp} = F_3 + F_4 + F_5 + F_6 \tag{124}$$

$$\dot{z}_w^d = (0 \quad 0 \quad 0 \quad 1 \quad 0)\mathbf{x}_{zp}^{s} \tag{125}$$

If the suspension elements' cab end points are located at the same height as the cab's c.o.g. ($h = 0$), also the movements in the other dimensions can be described in smaller models.

For the x dimension motion the following is valid:

$$\dot{\mathbf{x}}_{xp}^{s} = \begin{pmatrix} 0 & 1 & -1 & 0 & 0 & 0 \\ \frac{-4k_x}{m} & 0 & 0 & g & 0 & 0 \\ 0 & 0 & 0 & 0 & 0 & 0 \\ 0 & 0 & 0 & 0 & 0 & 0 \\ \frac{-4k_x \cdot 12.57}{m} & 0 & 0 & 12.57 \cdot g & -19.90 & 1 \\ \frac{-4k_x \cdot 157.9}{m} & 0 & 0 & 157.9 \cdot g & -157.9 & 0 \end{pmatrix} \mathbf{x}_{xp}^{s} + \begin{pmatrix} 0 \\ \frac{1}{m} \\ 0 \\ 0 \\ \frac{12.57}{m} \\ \frac{157.9}{m} \end{pmatrix} F_1 + \begin{pmatrix} 0 & 0 \\ 0 & 0 \\ 1 & 0 \\ 0 & 1 \\ 0 & 0 \\ 0 & 0 \end{pmatrix} \begin{pmatrix} \dot{x}_b^d \\ yr_b^d \end{pmatrix} \tag{126}$$

where

$$(\mathbf{x}_{xp}^{s})^T = (x_c^d - x_b^d \quad \dot{x}_c^d \quad \dot{x}_b^d \quad yr_b^d \quad x_{H1}^s \quad x_{H2}^s) \tag{127}$$

$$\ddot{x}_w^d = (0 \quad 0 \quad 0 \quad 0 \quad 1 \quad 0)\mathbf{x}_{xp}^s \tag{128}$$

For the y dimension motion the following is valid:

$$\dot{\mathbf{x}}_{yp}^s = \begin{pmatrix} 0 & 1 & -1 & 0 & 0 & 0 \\ \frac{-4k_y}{m} & 0 & 0 & -g & 0 & 0 \\ 0 & 0 & 0 & 0 & 0 & 0 \\ 0 & 0 & 0 & 0 & 0 & 0 \\ \frac{-4k_y \cdot 12.57}{m} & 0 & 0 & -12.57 \cdot g & -19.90 & 1 \\ \frac{-4k_y \cdot 157.9}{m} & 0 & 0 & -157.9 \cdot g & -157.9 & 0 \end{pmatrix} \mathbf{x}_{yp}^s + \begin{pmatrix} 0 \\ \frac{1}{m} \\ 0 \\ 0 \\ \frac{12.57}{m} \\ \frac{157.9}{m} \end{pmatrix} F_2 + \begin{pmatrix} 0 & 0 \\ 0 & 0 \\ 1 & 0 \\ 0 & 1 \\ 0 & 0 \\ 0 & 0 \end{pmatrix} \begin{pmatrix} \ddot{y}_b^d \\ \dot{xr}_b^d \end{pmatrix} \tag{129}$$

where

$$(\mathbf{x}_{yp}^s)^T = (y_c^d - y_b^d \quad \dot{y}_c^d \quad \dot{y}_b^d \quad xr_b^d \quad y_{H1}^s \quad y_{H2}^s) \tag{130}$$

$$\ddot{y}_w^d = (0 \quad 0 \quad 0 \quad 0 \quad 1 \quad 0)\mathbf{x}_{yp}^s \tag{131}$$

For the angular motions around the x axis the following is valid:

$$\dot{\mathbf{x}}_{xrp}^s = \begin{pmatrix} 0 & 1 & 0 \\ \frac{-4k_z l_y^2}{I_{xx}} & 0 & \frac{4k_z l_y^2}{I_{xx}} \\ 0 & 0 & 0 \end{pmatrix} \mathbf{x}_{xrp}^s + \begin{pmatrix} 0 & 0 & 0 & 0 \\ \frac{-l_y}{I_{xx}} & \frac{-l_y}{I_{xx}} & \frac{l_y}{I_{xx}} & \frac{l_y}{I_{xx}} \\ 0 & 0 & 0 & 0 \end{pmatrix} \begin{pmatrix} F_3 \\ F_4 \\ F_5 \\ F_6 \end{pmatrix} + \begin{pmatrix} 0 \\ 0 \\ 1 \end{pmatrix} \dot{xr}_b^d \tag{132}$$

where

$$(\mathbf{x}_{xrp}^s)^T = (xr_c^d \quad \dot{xr}_c^d \quad xr_b^d) \tag{133}$$

$$\ddot{xr}_c^d = \begin{pmatrix} \frac{-4k_z l_y^2}{I_{xx}} & 0 & \frac{4k_z l_y^2}{I_{xx}} \end{pmatrix} \mathbf{x}_{xrp}^s + \begin{pmatrix} \frac{-l_y}{I_{xx}} & \frac{-l_y}{I_{xx}} & \frac{l_y}{I_{xx}} & \frac{l_y}{I_{xx}} \end{pmatrix} \begin{pmatrix} F_3 \\ F_4 \\ F_5 \\ F_6 \end{pmatrix} \tag{134}$$

For the angular motions around the y axis the following is valid:

$$\dot{\mathbf{x}}_{yrp}^s = \begin{pmatrix} 0 & 1 & 0 \\ \frac{-4k_z l_x^2}{I_{yy}} & 0 & \frac{4k_z l_x^2}{I_{yy}} \\ 0 & 0 & 0 \end{pmatrix} \mathbf{x}_{yrp}^s + \begin{pmatrix} 0 & 0 & 0 & 0 \\ \frac{-l_x}{I_{yy}} & \frac{l_x}{I_{yy}} & \frac{l_x}{I_{yy}} & \frac{-l_x}{I_{yy}} \\ 0 & 0 & 0 & 0 \end{pmatrix} \begin{pmatrix} F_3 \\ F_4 \\ F_5 \\ F_6 \end{pmatrix} + \begin{pmatrix} 0 \\ 0 \\ 1 \end{pmatrix} \dot{yr}_b^d \tag{135}$$

where

$$(\mathbf{x}^s_{yrp})^T = (yr^d_c \quad \dot{yr}^d_c \quad yr^d_b) \tag{136}$$

$$\ddot{yr}^d_c = \begin{pmatrix} \frac{-4k_z l_x^2}{I_{yy}} & 0 & \frac{4k_z l_x^2}{I_{yy}} \end{pmatrix} \mathbf{x}^s_{yrp} + \begin{pmatrix} \frac{-l_x}{I_{yy}} & \frac{l_x}{I_{yy}} & \frac{l_x}{I_{yy}} & \frac{-l_x}{I_{yy}} \end{pmatrix} \begin{pmatrix} F_3 \\ F_4 \\ F_5 \\ F_6 \end{pmatrix} \tag{137}$$

5.3 The input to the models

The simulation models need an input describing the tractor frame movements when driving on surfaces representative of normal working operations.

The research to find out standardized surfaces for vibration testing of agricultural tractors resulted in two different test tracks being developed at NIAE in the United Kingdom (SS-ISO 5008, 1981). The tracks were designed to correspond to surfaces commonly found in agricultural tractor work. Analysis of whether these tracks are also representative under Swedish circumstances, or how to make a more representative track, is an very comprehensive task and impossible to include in the present study. Consequently, the tracks were used because they are well known, reproducible, and because no important criticism has been raised against them.

Measurements have to be made in 6 d.o.f. to get a complete description of the frame movements. Premeasurements showed that the angular vibrations around the z axis were very small and could be neglected. The movements were therefore measured in 5 d.o.f.

Five accelerometers were used to measure the frame movements. One triaxial transducer measured linear vibrations in the x, y and z dimensions. An accelerometer measuring in the z direction was mounted immediately laterally of the triaxial transducer. The difference between the two signals was divided by the distance between the transducers to get the angular accelerations around the x axis in rad/s^2. The angular vibrations around the y axis were measured and calculated in the same way, using a fifth accelerometer signal.

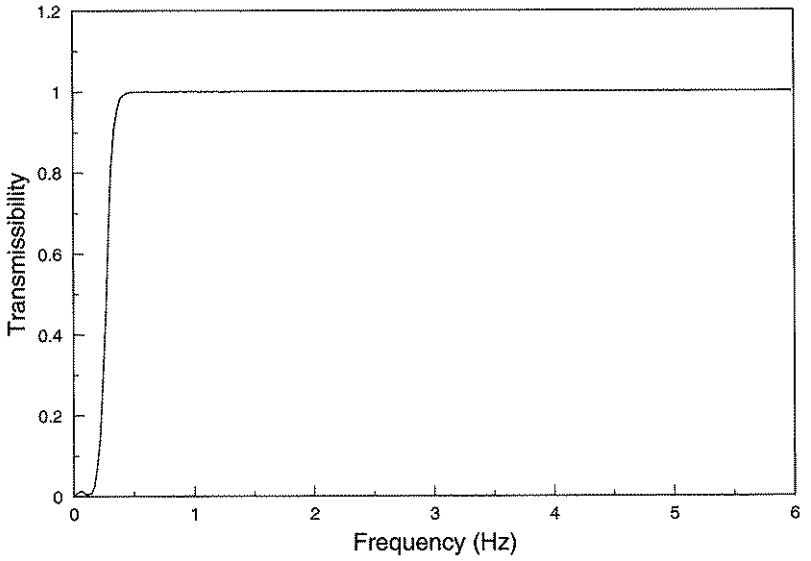

Fig. 24. Transmissibility for a sixth order Butterworth highpass filter with a cutting frequency of 0.3 Hz.

The measured acceleration time series were integrated to get the frame's momentary velocities and positions. The integation also amplified very small measurement and calibration errors which made it necessary to filter the signals with a sixth order Butterworth highpass filter with a cutting frequency of 0.3 Hz (Figure 24). When filtering the signals twice, with changed direction the second time, the phase was not changed. The signal's power contents under 0.5 Hz were very small, so the filtering had insignificant effects on the real movements.

6 VALIDATION

It is of course very important that the developed simulation models can calculate the movements in a real frame-suspension-cab system as correctly as possible. This chapter describes some studies performed to study the correctness of the simulation models.

In the first part, the vibration transmissibility curves obtained with the nonlinear simulation model have been compared with the theoretical curves. In the second part of this chapter, results from the nonlinear simulation model are compared with the results obtained from measurements on a full-scale suspended cab. In the last part, results calculated with the linear and the nonlinear simulation model are compared in order to study the agreement between the two theoretical models.

6.1 Theoretical investigation of amplitude characteristics and coherence

For a linear suspension with one degree of freedom, the frequency characteristic for the transmission of accelerations between the cab and the frame can be determined if the suspension's natural frequencies and damping degrees are known. Ch. 5 describes how this can be carried out in a suspension shaped like the basic suspension described earlier.

In a suspension with more than one degree of freedom the transmission of vibrations in one direction is normally affected by the movements in other directions. The calculations therefore become more complex and no analytical solutions can normally be found. Neither is it normally possible to get an analytical solution in a suspension with one or more nonlinearities.

The vibration transmission can thus be determined analytically for some simplified cases. By defining such a case for the simulation program and comparing the amplitude characteristics carried out with the theoretical one, the program's algorithm can be controlled and verified.

By also studying the amplitude characteristics when the suspension and frame movements are three-dimensional, it is possible to get a measure of the influence of movement in other directions on the vibration transmission in the primarily studied dimension. The defined suspension elements must still have linear characteristics in order to prevent the influence of further nonlinearities.

The coherence between the input and output from the model has also been analyzed to get a measure of how well the studied system interacts with the perfect linear one and at which frequencies the results differ.

6.1.1 Vertical movements

6.1.1.1 Assumptions

The amplitude characteristics for vertical movements in a suspension like the one described in Ch. 7.1 have been studied. The vertical suspension elements have been defined to have linear characteristics with a natural frequency of 2.0 Hz and the degree of damping = 0.2.

In the one-dimensional studies, the accelerations of the frame in the vertical direction have been defined as the vertical accelerations immediately below the cab's c.o.g. when driving on track 1 at a speed of 12 km/h.

Acceleration values in the vertical direction for the frame and for the cab's c.o.g. were then used to calculate the amplitude characteristics and coherence for frequencies between 0-5 Hz. The simulated driving time was limited to 20 s and gave data records with approximately 4 000 values. To obtain good accuracy with the FFT-algorithm, with many points in the interesting range, four data records were combined into one with a length of approx. 16 000 values. When combining the records, a Hanning window was used to minimize the edge effects.

The parameters required were then calculated with assistance of the Matlab software package's Spectrum function, set to use a 8 192 points window with 4 000 points overlap in the calculations.

The same analysis was also performed on a simulation with three-dimensional frame movements from track 1 with a driving speed of 12 km/h. The vertical natural frequency was unchanged at 2.0 Hz and the damping degree at 0.2. The horizontal natural frequency was 1.0 Hz with a damping degree of 0.5. As a measure of the frame's movements in this study, the imagined movements of the cab's c.o.g. if all suspensions were locked was used.

6.1.1.2 Results

Figure 25 shows the transmissibility of the suspension when the foundation was only vibrating in the vertical direction. The coherence for the same simulation is shown in Figure 26. The results of the simulations with the frame's movements in three dimensions are shown in the same figures.

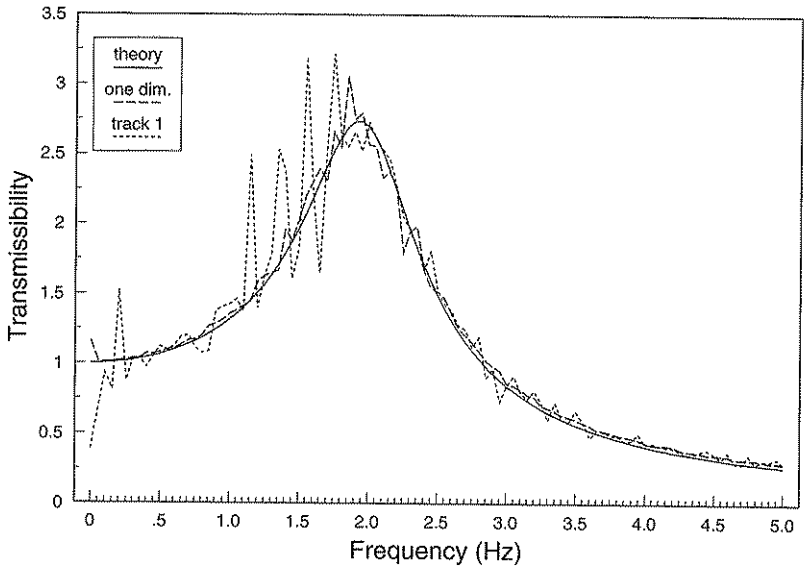

Fig. 25. Transmissibility for the transmission of vibrations in the z dimension for a suspension with a vertical natural frequency of 2.0 Hz and a damping degree of 0.2.

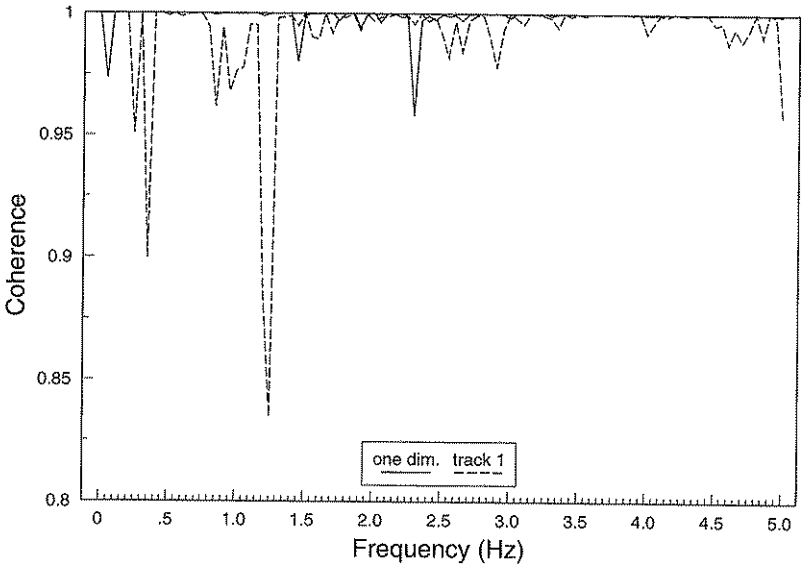

Fig. 26. Coherence for the transmission of vibrations in the z dimension for a suspension with a vertical natural frequency of 2.0 Hz and a damping degree of 0.2.

6.1.1.3 Conclusions

The transmissibility corresponds very well to the theoretical curve and the coherence shows only small differences from the optimal value of 1.0 when the frame only vibrates in one direction.

As expected, the curves show larger differences when the foundation moves in three dimensions, depending on the movements in other directions introducing more nonlinear effects. The differences can also be observed at the coherence curves. Compared to the one-dimensional curves, these curves have lower values, especially below 1.5 Hz.

An area with lower coherence is found around 1.0 Hz, possibly resulting from interaction with the vertical suspension, which has a natural frequency of 1.0 Hz.

6.1.2 Horizontal movements

6.1.2.1 Assumptions

A study similar to the one for vertical movements was also performed for horizontal movements. The parameters influencing the horizontal characteristics were defined to give a horizontal natural frequency of 2.0 Hz and a damping degree of 0.2.

The movements of the foundation were defined as the movements in the y dimension for a point placed as high as the cab's c.o.g. when driving on track 1 at the speed of 12 km/h. The movements in the other directions were defined to 0. The analysis of the results was done in the same way as for the one-dimensional vertical movements.

The same simulation was also performed with the three-dimensional movements measured on track 1 at a driving speed of 12 km/h as input. The horizontal natural frequency was unchanged = 2.0 Hz. The vertical suspension was defined to have a characteristic with a natural frequency of 1.0 Hz and a damping degree of 0.5.

6.1.2.2 Results

Figure 27 shows the transmissibility for simulations with frame vibrations only in the y dimension together with the theoretical curve.

The coherence for the same data are shown in Figure 28. The results for the simulations with three-dimensional foundation movements are found in the same diagrams.

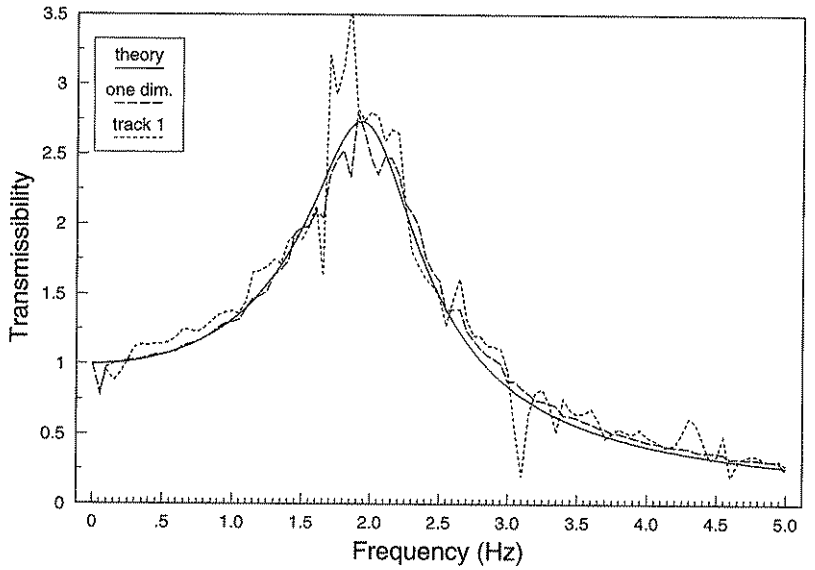

Fig. 27. Transmissibility of vibrations in the y dimension for a suspension with a horizontal natural frequency of 2.0 Hz and a damping degree of 0.2.

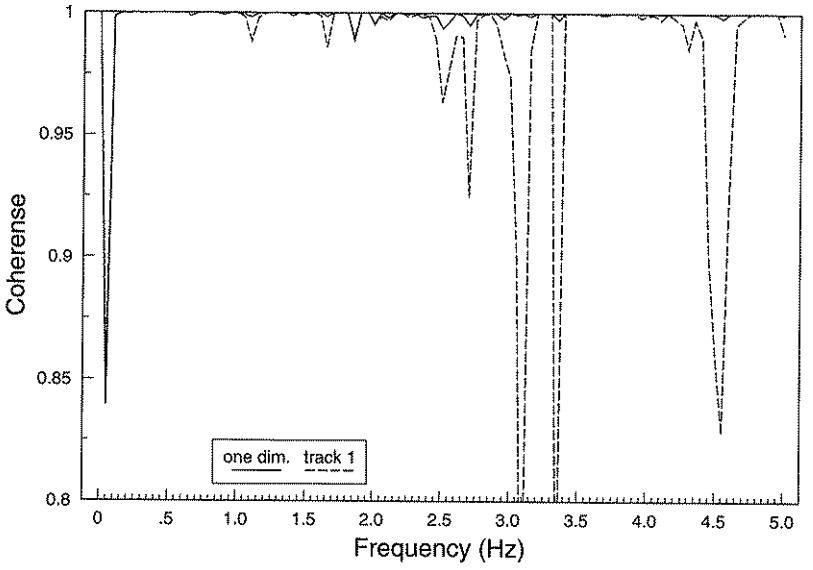

Fig. 28. Coherence for the transmission of vibrations in the y dimension for a suspension with a horizontal natural frequency of 2.0 Hz and a damping degree of 0.2.

6.1.2.3 Conclusions

The transmissibility and coherence correspond very well to the theoretical curves when simulating only one-dimensional movement. The differences, however, are somewhat

larger compared to the study of vertical movements, probably because the formulas for calculation of the suspension's horizontal natural frequency are based on the assumption on small deviations from the balanced position, and are therefore not exact.

The transmissibility and coherence show, just as for the vertical study, larger differences when the frame's movements are three-dimensional, but still correspond relatively well to the theoretical curves.

6.2 Validation against practical measurements

In order to examine the cab suspension principle described earlier, a full-scale model of the cab and the suspension was built. The full-scale model was also used in the validation of the simulation model. The cab model was built as a shell construction loaded with lead weights located so that the cab's mass and moments of inertia correspond to the same values for a normal tractor cab. The cab was mounted with a suspension in a surrounding foundation analogous to a vehicle frame (Figure 29).

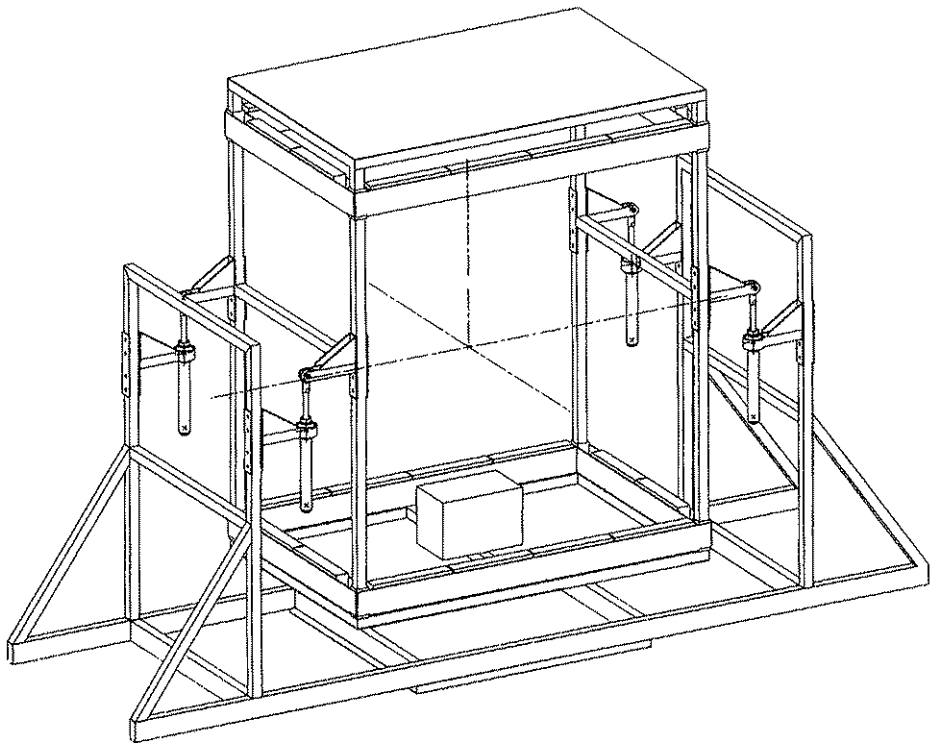

Fig. 29. Model of the cab and the suspension used for the validation measurements. The horizontal dampers are not set out.

The cab and the suspension were placed on a hydraulically operated vibrating platform with possibilities to control the movements in the x, y and z directions and the rotational movements around the x and y axes.

The connection between the cab and the "frame" was constructed so that most of the parameters could be varied. The majority of the cab parameters were also adjustable, since the positions of the lead weights could be changed.

The vibrations at the cab and at the "frame" were recorded during a time period when the system was placed on the vibrating platform. Afterwards, all the parameters in the suspension were measured and described for the simulation program.

The movements of the frame together with the measured parameters were used as inputs to the simulation model. The model was then programmed to calculate the vibrations transmitted to the cab. Comparing the measured vibrations in the cab with the corresponding results from the simulation model, offered a possibility to examine the correctness of the simulation program.

The object of the measurements was to validate the simulation model. Therefore, the suspension parameter choice was not optimized when the measurements were performed.

6.2.1 Measurements of cab characteristics

The cab used for the validations was constructed with the CAD program CATIA. The program also estimated the mass and the moments of inertia. Since some changes in the original construction were made, and as a control, the cab's mass, c.o.g. position and moments of inertia were measured after the validation measurements had been carried out.

The cab's mass was measured with a potentiometer. Because of the symmetry, the locations of the c.o.g. in the x and y dimensions were exactly in the middle of the cab. The moments of inertia (I_{xx}, I_{yy} and I_{zz}) were measured by suspending the cab as a pendulum and recording the oscillation time (Figure 30) (Harris, 1988).

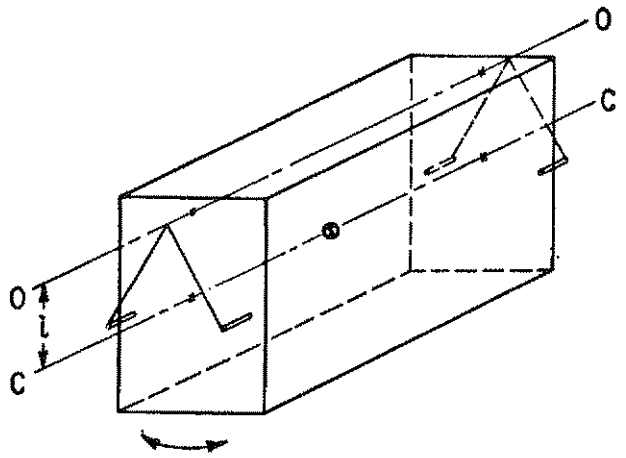

Fig. 30. Measuring of the moment of inertia in relation to an axis through the c.o.g.

The moments of inertia in relation to an axle C-C through the body's c.o.g. is described by:

$$I_{cc} = ml^2\left[\left(\frac{\tau_0}{2\pi}\right)^2\left(\frac{g}{l}\right)-1\right] \tag{138}$$

where

τ_0 = oscillation time

l = distance between 0-0 and C-C

The accuracy depends on the precision in the measurement of l. Performing a second experiment with another support axle 0' – 0' with $l' = l + \Delta l$ and the period τ'_0 makes it possible to describe l as a function of Δl:

$$l = \Delta l\left[\frac{\left(\tau_0'^2/4\pi^2\right)(g/\Delta l)-1}{\left(\left(\tau_0^2-\tau_0'^2\right)/4\pi^2\right)(g/\Delta l)-1}\right] \tag{139}$$

The calculated l value is then used in the first formula. The value can also be used to determine the z coordinate for the cab's c.o.g.

The moments of inertia became:

$I_{xx} = 392\ kgm^2$

$I_{yy} = 469\ kgm^2$

$I_{zz} = 274\ kgm^2$

and the mass

$m = 640\ kg$.

6.2.2 Suspension principle and geometry

The experimental suspension used in the performed measurements was mainly constructed according to the principles examined in the theoretical part.

6.2.2.1 Characteristics of vertical springs and dampers

The cab's vertical suspension was carried out with four vertically positioned elements connected in pairs to two gas accumulators (Figure 31).

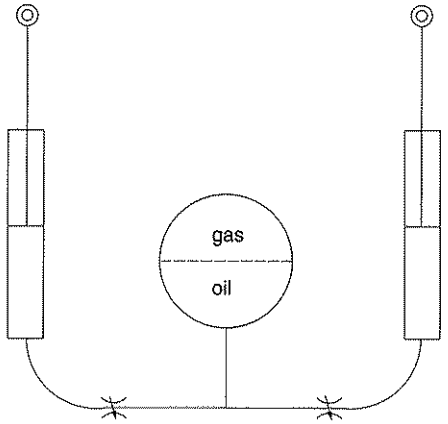

Fig. 31. Principle for two connected vertical suspension elements.

The two front elements were connected to one accumulator and the two rear elements to another. If the cab's c.o.g. is located lower than a plane through the cab end points of the vertical elements, the cab strives to keep itself horizontal according to rotations around the frame's x axis. The suspension is unusable if the c.o.g. is located above the described plane.

Since two elements are connected to a common accumulator, the spring force from each element depends on the total length of the two elements. Depending on the gas compression, the function becomes nonlinear. The gas and oil volumes could be changed to give the elements changed characteristics.

The damping in the vertical elements was decided by a restriction in each element's hydraulic connection to the accumulator and with an inner restriction.

6.2.2.2 Characteristics of horizontal springs and dampers

When the validation measurements were performed, the vertical elements were mounted in the frame with rubber bushings allowing the elements to change the angle against the foundation (Figure 32). When the elements are moved from their balanced positions they influence the cab with radial forces. The force amplitudes depend on the angles of the elements in relation to the balanced positions.

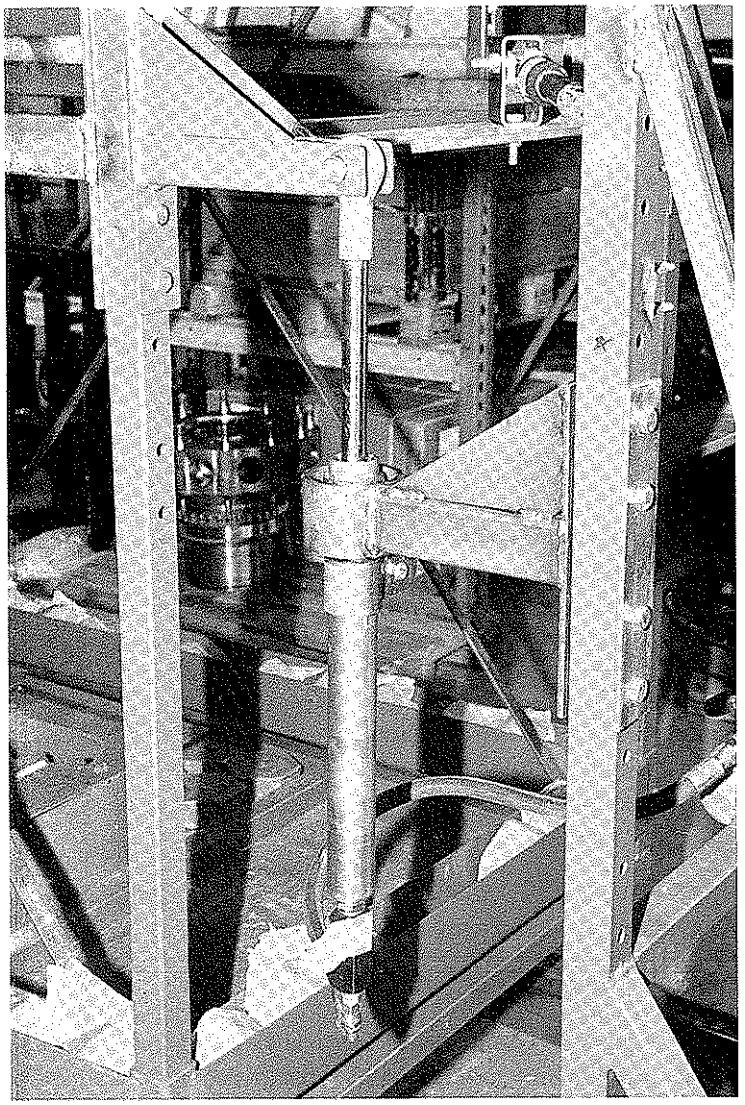

Fig. 32. Vertical suspension element.

To damp the movements in the x and y directions, four standard shock absorbers were mounted horizontally approximately at the same level as the cab end points of the vertical elements. Two absorbers were mounted at the front and two at the rear, with an angle of 45° towards the driving direction, to get symmetrical damping (Figure 33).

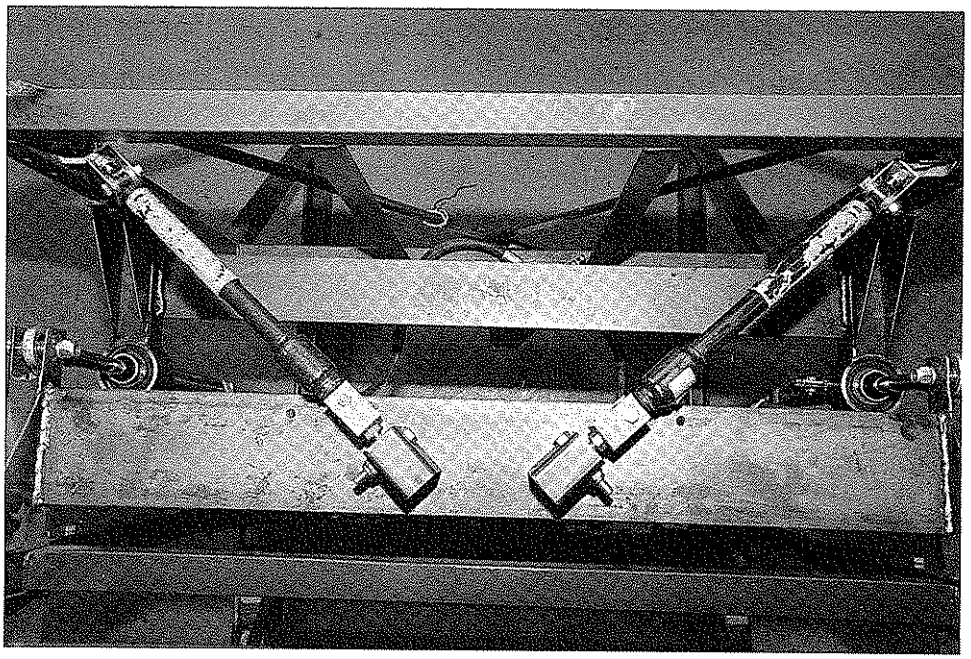

Fig. 33. Horizontally acting shock absorbers (seen from above).

6.2.3 Element end point coordinates

The coordinates for the elements' end points measured in relation to the cab's c.o.g. are shown in Table A. The measurements were performed with the cab in a balanced position. More than one setting of the elements was tested but the reported values describe the setting when the validation was performed.

Table A. The coordinates for the cab and frame end points of the suspension elements

Element	Cab			Frame		
	x (m)	y (m)	z (m)	x (m)	y (m)	z (m)
1	-0.95	0.48	0.45	-0.95	0.48	0.18
2	0.95	0.48	0.45	0.95	0.48	0.18
3	0.95	-0.48	0.45	0.95	-0.48	0.18
4	-0.95	-0.48	0.45	-0.95	-0.48	0.18
5	-0.85	0.11	0.53	-1.17	0.43	0.46
6	0.85	0.11	0.53	1.17	0.43	0.46
7	0.85	-0.11	0.53	1.17	-0.43	0.46
8	-0.85	-0.11	0.53	-1.17	-0.43	0.46

6.2.4 Measurements of spring and damper characteristics

The simulation model needed a complete description of all parameters in the suspension used, to be able to calculate the transmission of vibrations from the frame to the cab.

6.2.4.1 Vertical elements

The vertical elements were connected in pairs to a common gas volume, and thus the static force was dependent on the total length of the two elements. The damping in one element was, on the other hand, approximately independent of the position and movement of the other.

A measurement arrangement as shown in Figure 34 was used. The element tested was connected to a hydraulic piston pushing and pulling the element depending on the oil flow to the piston. The hydraulic flow was controlled by an electrically controlled proportional valve mounted at a hydraulic power unit (Hansson, 1989). Between the piston and the tested element a force transducer was mounted to momentarily measure the force between the piston and the element. A potentiometer was also mounted to measure piston displacement.

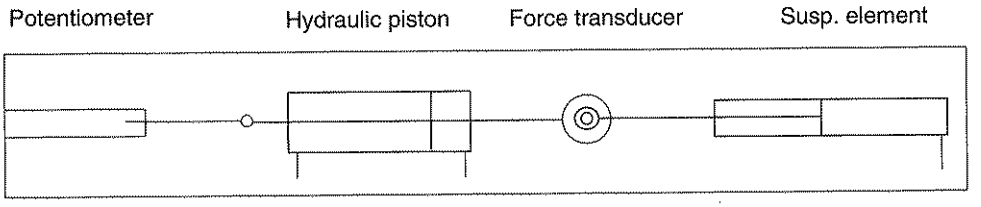

Fig. 34. Arrangement to measure spring and damper characteristics.

The force transducer and the potentiometer were connected to a computer for data acquisition. When performing the dynamic measurements, the computer controlled the voltage to the proportional valve and and thereby the oil flow to the piston. The piston was controlled to have a reciprocating movement. It was also possible to adjust the oil flow manually.

The spring characteristic for the element was measured by placing the piston in different positions and recording the force as a function of the total length of the two elements (Figure 35).

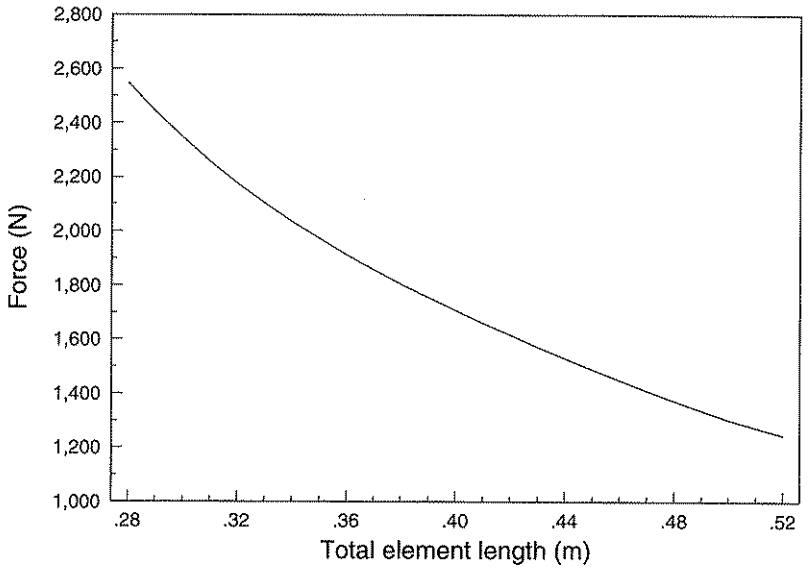

Fig. 35. Static force vs total length of two connected elements.

The dynamic force was calculated by reducing the total force when the piston was moving with the static component calculated as described above. The potentiometer signal enabled measurements to be made of the element velocities and the relations between the damping forces and the velocities (Figure 36). The shock absorbers used were designed to be linear in the normal working range but with progressive damping towards the end points. When performing the validation measurements, however, only the linear area was used.

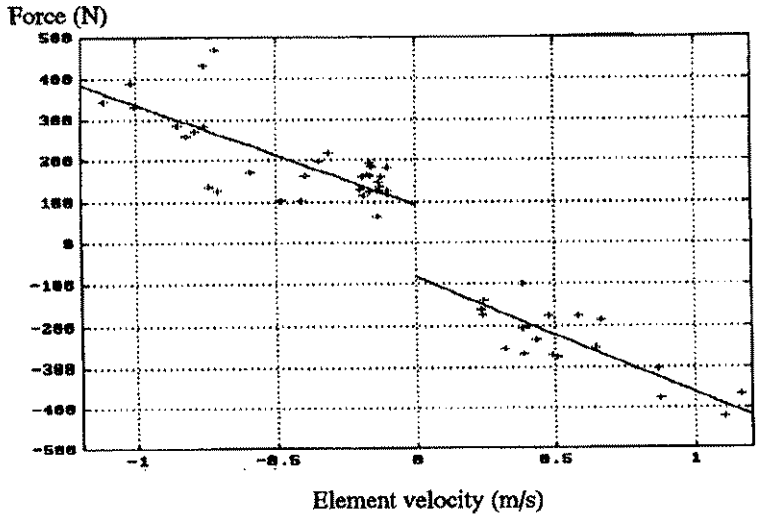

Fig. 36. Damping force vs velocity for tested element (single measurements and regression lines).

For negative velocities the equation became:

$$F = 92.2 - 242,6 \quad \dot{l}_e \tag{140}$$

and for positive velocities

$$F = -80.8 - 281.9 \quad \dot{l}_e \tag{141}$$

when pushing forces are defined as positive and $\dot{l}_e$ = the time derivative of the element's length.

The relatively large spread of the measurement points together with the fact that the damping diverges from zero for low velocities, indicates that some uncontrollable friction and so-called "slip stick" occurs in the elements.

6.2.4.2 Horizontally working elements

The bending constant for the rubber bushings deciding the elasticity in the horizontal directions was measured according to the principle shown in Figure 37. The bushing was loaded with different bending moments and the divergencies from the balanced position were measured. It can be assumed that the bending characteristics change when an axial load is present. The bushing was therefore loaded with 25 % of the cab's weight (m1) straight downwards. The extra load was hung up in the centre of the bushing so as not to influence the results in other aspects.

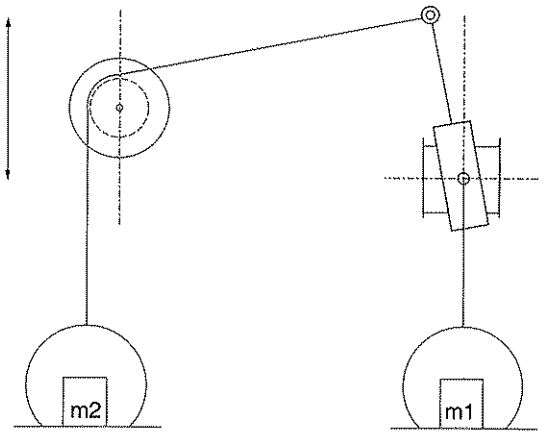

Fig. 37. Outline of the arrangement to measure the bending constant of the rubber bushings.

After each measurement the rubber was unloaded for 60 s, to avoid the influence of any creep tendencies in the bushings. The bending angle as a function of the loading torque is shown in Figure 38.

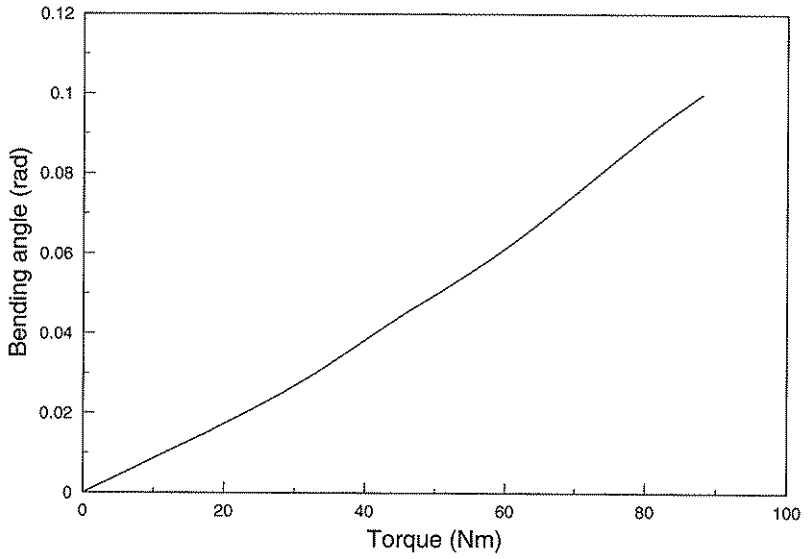

Fig. 38. Bending angle vs bending torque for the tested rubber bushings.

The shock absorbers used for the horizontal damping were normally standard elements from a car manufacturer. The characteristics of the absorbers were measured by a manufacturer and the result is shown in Figure 39.

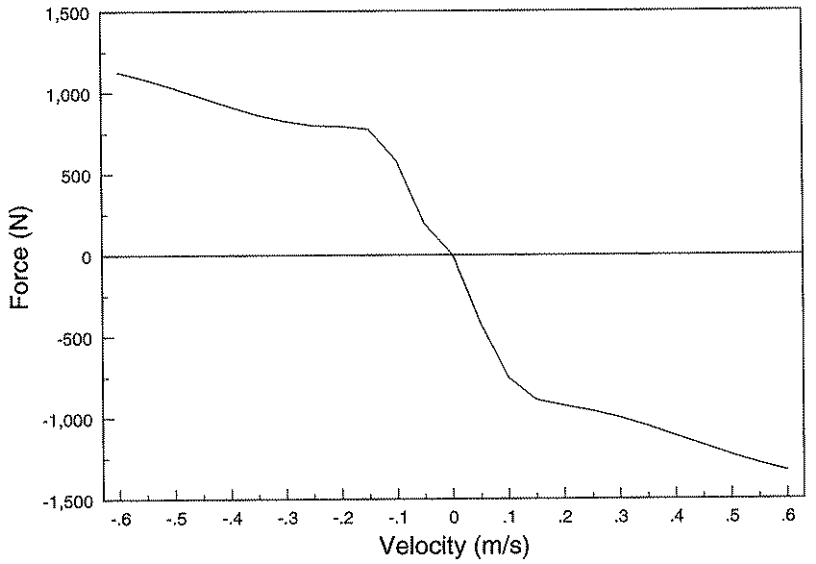

Fig. 39. Damping characteristics for horizontal shock absorbers.

6.2.5 The vibrating platform

The foundation with the suspension and the cab was placed on a vibrating platform (Figure 40). Five powerful hydraulic pistons were used to move the platform in five d.o.f. The oil flows to the pistons were controlled by a Nord-100 computer.

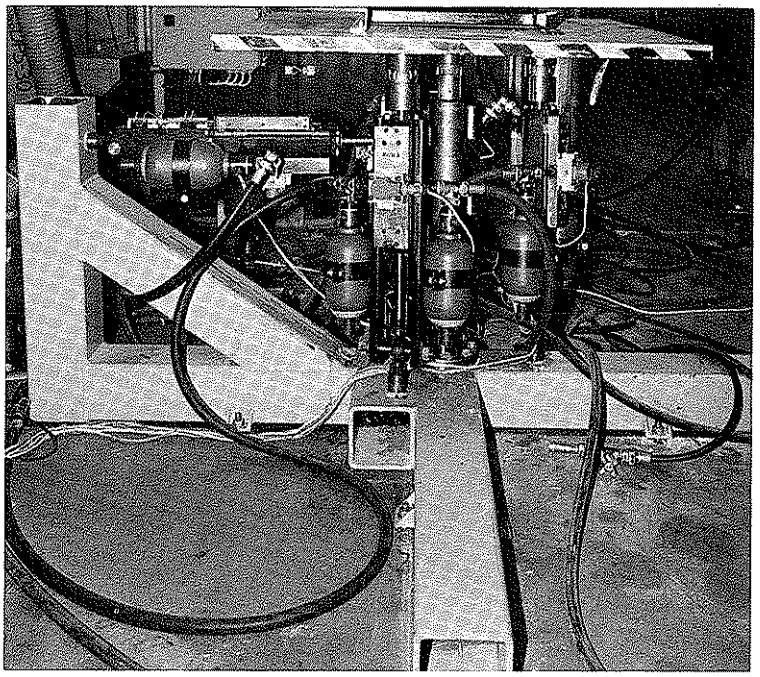

Fig. 40. The vibrating platform.

The platform movements could be programmed in each degree of freedom for different synthetic signals, for example sinus vibrations, frequency sweeps and ramps. It was also possible to simulate driving sequences with a defined vehicle driving on a defined surface. In this case, the computer used recorded accelerometer signals from the driving sequence, together with the accelerometer's coordinates, to calculate the platform movements.

Potentiometers were placed on the five hydraulic pistons. The potentiometer signals were used as feedback by the control computer. The signals were also used to momentarily calculate the positions for a defined point at the platform together with the platform angle in relation to the x and y plane. A D-A card in the computer gave as output analog signals proportional to the computed values. These signals were used to describe the foundation movements for the simulation program.

The total mass of the cab and the foundation was about 900 kg, which was also the vibrating platform's approximate capacity. Therefore the possibilities to present high vibration loads at higher frequencies than 3-4 Hz were limited. The signals used to describe the movements of the platform for the simulation model were based on the real values and not the desired values and thus that restraint has no effect on the results of the validation.

The vibrating platform has characteristics that made it very suitable for the performed measurements and also most suitable for further product development.

6.2.6 Data acquisition

The validation required signals describing the movements of the cab and the foundation in five d.o.f. each. The description of the platform's movements in the x, y and z directions were available from the controlling computers D-A card as described earlier. The foundation's inclination in relation to the x and y axes were measured by a two axial airplane gyro transducer. The signals described distances and angles and have to be derived twice to get acceleration values. Treating the foundation as a solid body gave possibilities to compute the movements for points located anywhere at the foundation.

Five accelerometers were used to measure the cab's motions, one measuring in the z direction, two in the x direction and two in the y direction. The signals from the transducers gave possibilities to calculate the accelerations in the x, y and z directions, and the angular accelerations around the x and y axes, for every point in the cab.

After amplification, the ten signals were connected to a computer with a 12 bits A-D card. The computer sampled the signals with 200 Hz sample frequency and stored the time series in its memory. Before the signals were sampled they were filtered with a 10 Hz anti-aliasing low pass filter.

6.2.7 Changes of the measurement system

If the foundation is assumed to be a non-elastic body, it is possible to calculate the motions for any point on the body from the signals measured at the vibrating platform. The first preliminary studies showed that the construction was too weak. The elasticity in the foundation affected the vibration transmission from the platform to the points where the suspension elements were mounted. The elasticity was most marked for fast movements in the y direction, which resulted in torsion in the foundation.

The cab and the foundation were therefore strengthened with extra stabilising steel beams. The strengthening improved the stability considerably, but it was not possible to get rid of all the elasticity in the y direction.

An extra transducer, measuring in the y direction, was placed near the points where the suspension elements were mounted onto the foundation, in order to get an almost exact and nondistorted input to the simulation model (Figure 41). The signal from the extra accelerometer was connected to an extra D-A computer input channel. The measurements then included eleven signals.

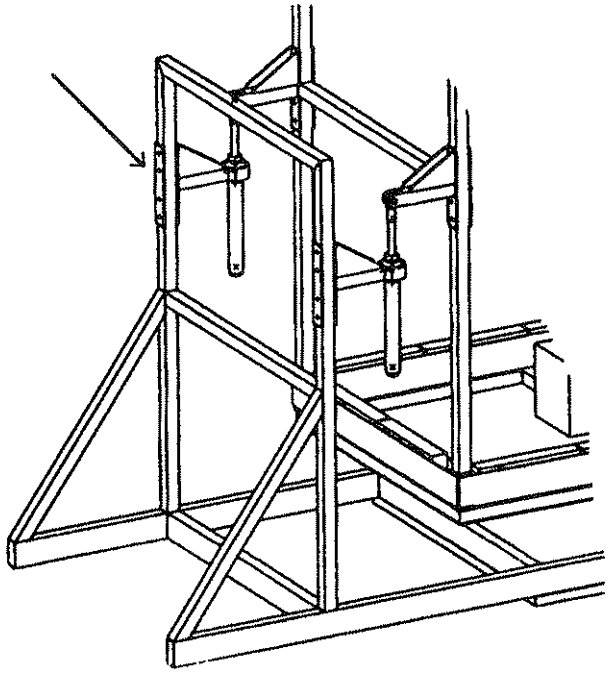

Fig. 41. The location of the extra transducer.

6.2.8 Experiments and analysis

The described measurements system was used for experiments using different simulated platform movements. Initially, the control computer was programmed for platform movements in only one d.o.f. The motions simulated were sinus waves, sinus with sweeping frequency and randomized noise with defined band width. Then the option to simulate earlier recorded driving sequences with five d.o.f. motions was used. Even some of the signals used in the theoretical simulations performed in this study were tested. Finally, also synthetic signals combined to give a 5 d.o.f. synthetic movement were tested.

Each experiment lasted for approximately 35 s and resulted in records with about 7000 values for each channel.

After the experiments, the values describing the foundation's displacement were converted to acceleration values and defined as input signal for the simulation program. The signal from the extra accelerometer measuring in the y direction was used to describe the foundation's y acceleration. This signal was also used, together with the signal describing the platform's displacement in the y direction, to calculate the foundation's angular movements around the x axis. That value was estimated to be more exact than the value from the gyro transducer, because the gyro was mounted on the platform with no possibilities to correct for any torsion in the foundation.

When the suspension elements' characteristics were measured and programmed in the simulation model, the model was able to calculate the vibration transmission from the foundation to the cab. The calculated vibrations could then be compared with the vibrations measured in the cab.

6.2.9 Results

The agreement between the measured acceleration values and the values calculated by the simulation model was studied for the linear dimensions x, y and z.

Figures 42-44 show the calculated curves together with the measured ones, calculated for a point 1.10 m over the cab's floor, for an experiment where the foundation motion was collected from a real driving sequence. The 10 s shown in the figures was chosen because they include both driving on a smooth surface with low vibration levels, and at a rougher surface with higher levels. The same tendencies as in the figures were characteristic for most of the analysed measurements.

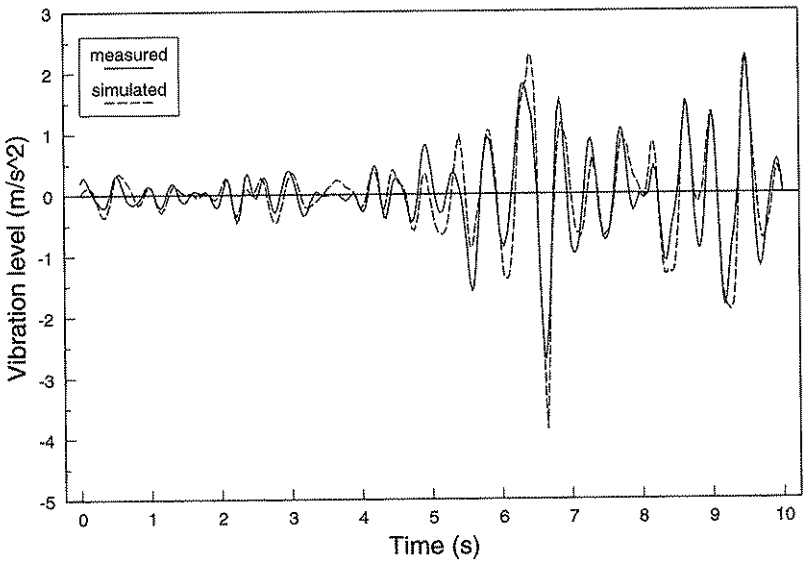

Fig. 42. Measured and simulated acceleration in the x direction for a point located vertically above the cab's c.o.g. at 1.10 m above the cab floor.

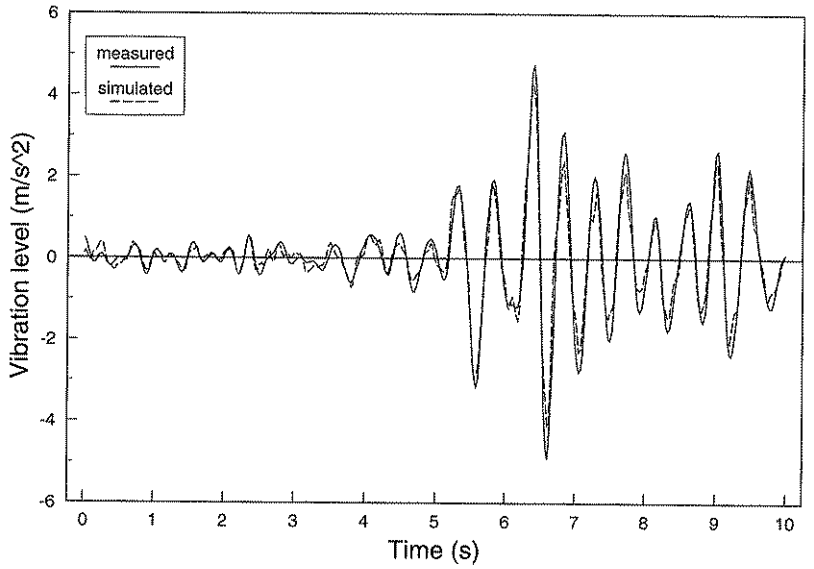

Fig. 43. Measured and simulated acceleration in the y direction for a point located vertically above the cab's c.o.g. at 1.10 m above the cab floor.

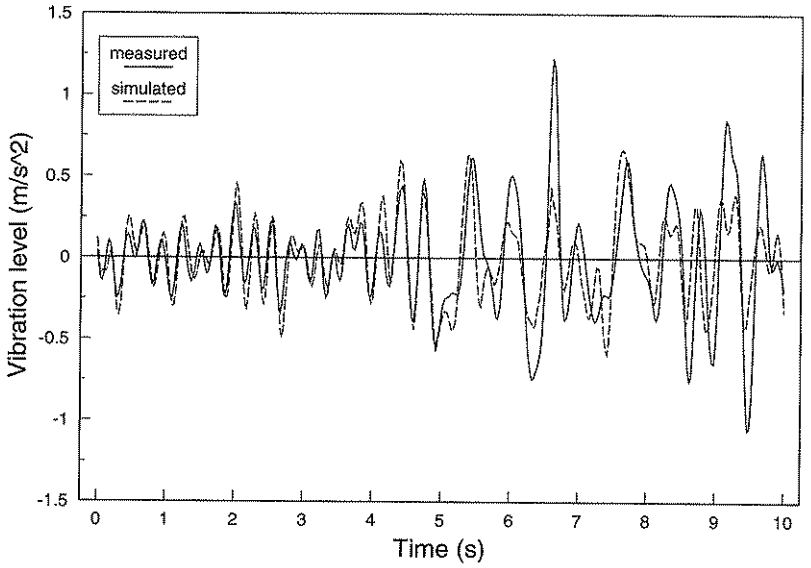

Fig. 44. Measured and simulated acceleration in the z direction for a point located vertically above the cab's c.o.g. at 1.10 m above the cab floor.

The signals' frequency contents were also analysed to get a deeper understanding of how well the simulated signals were correlated to the measured ones. The whole 35 s data record from the measurement where the 10 s shown in Figures 42-44 were collected was used to get better accuracy.

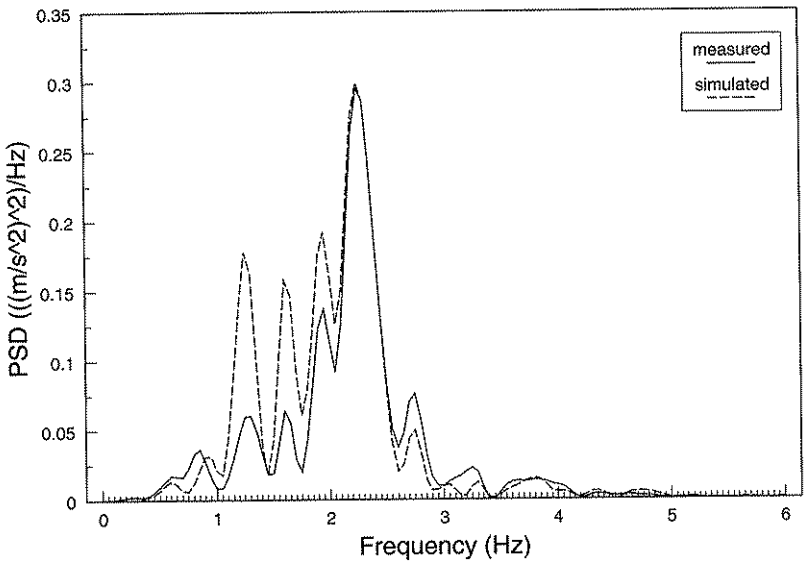

Fig. 45. PSD for measured and simulated acceleration in the x direction for a point located vertically above the cab's c.o.g. at 1.10 m above the cab floor.

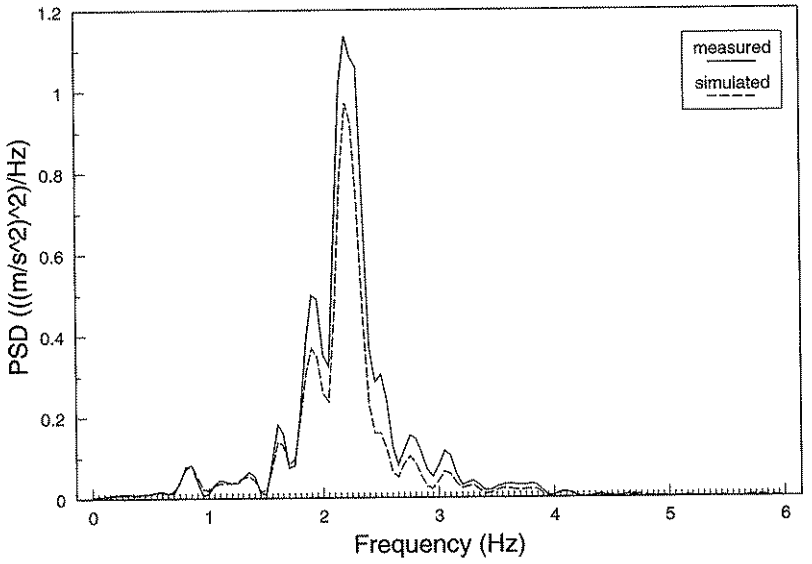

Fig. 46. PSD for measured and simulated acceleration in the y direction for a point located vertically above the cab's c.o.g. at 1.10 m above the cab floor.

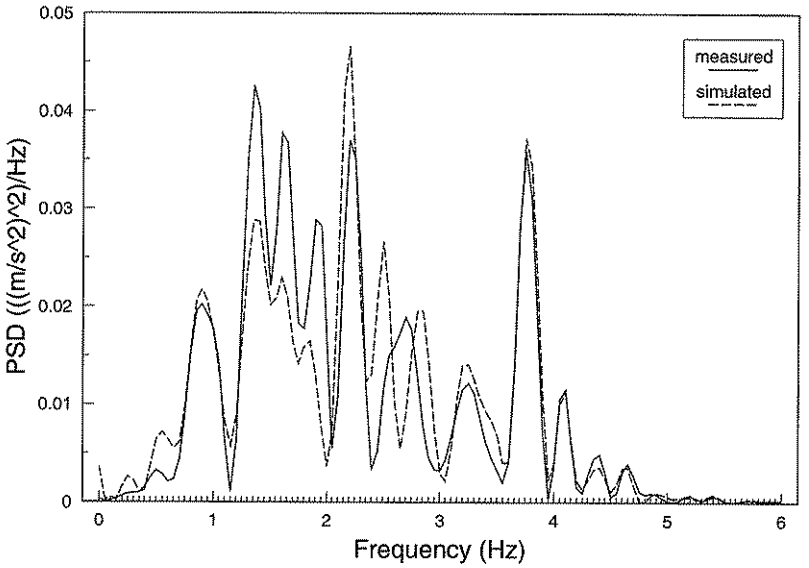

Fig. 47. PSD for measured and simulated acceleration in the z direction for a point located vertically above the cab's c.o.g. at 1.10 m above the cab floor.

6.2.10 Conclusions

The possibilities of the simulation model to accurately calculate the vibration transmission are, of course, dependent on the input signal being correct.

In the y direction, the extra accelerometer located as in Figure 41 contributed to the input probably being fairly correct. The agreement between calculated and measured values is also good, which indicates that the model is able to calculate the vibration transmission in that direction well and that the measurements of the influencing suspension parameters were performed with small errors.

The same suspension parameters and algorithms in the simulation program were used to calculate the vibration transmission in both the x and y dimensions. The calculations of the transmission in these two directions would therefore logically have the same accuracy.

The input signals in the x dimension were, however, measured at the platform, with no possibilities to correct for undesirable torsion in the foundation. The agreement in the x dimension was not as good as in the y dimension, which indicates that some undesired elasticity was, in fact, present.

Figure 44 shows that the model calculates the transmission of vibrations in the z direction relatively well for low vibration levels, but that the agreement decreases when the loads

get higher. A probable reason is that the foundation can not exactly transmit the vibrations from the platform to the mounting places of the suspension elements on the upper part of the foundation. Slip stick effects in the elements, as indicated in Figure 36, are also possible reasons for the difference.

Figure 47 shows that the measured vibrations in the z dimension are smaller than those simulated in the 1.0-2.0 Hz frequency range but bigger around 2.0-3.5 Hz. A possible reason is that the measurements of the vertical elements' damping characteristics gave too low values, and therefore influenced the vibration transmission. However , the small differences in the curves above 3.5 Hz do not support that hypothesis. An increased damping should have influenced the curves also in this frequency area. A more probable reason is that the elasticity in the foundation also has an influence in that direction.

The results indicate that the simulation model is able to calculate the transmission of vibrations fairly accurately when the input can be exactly measured and described. It must, however, be stated that the measurement accuracy was not so good that a smaller error in the simulation model would be possible to detect. If the measurements were to be repeated it would probably be possible to get better results if the foundation's movements were measured closer to the mounting locations of the suspension elements. Another possibility to get more accurate results would be to use a small scale model of the cab and the suspension, whereby it would be possible to make the construction less elastic, and also easier for the vibrating platform to handle.

6.3 Comparison between the linear and the nonlinear model

The linear simulation model described in Ch. 5.2 is a simplified description of the nonlinear one described in Ch. 5.1. The effects of the simplifications can be studied if the same suspension geometry, element characteristics and frame movements are used in a simulation with each model, and the results compared.

6.3.1 Assumptions

A linear passive suspension with a natural frequency of 1.0 Hz and a degree of damping of 0.5 in the x, y and z dimensions is defined both in the linear and the nonlinear model. The spring and damping constants of the elements are calculated with the formulas in Ch 5.

The passive linear suspension was simulated in the linear model by using the feedback matrix **K**:

$$\mathbf{K}=\begin{pmatrix} 0 & 0 & 0 & 0 & 0 & 0 \\ 0 & 0 & 0 & 0 & 0 & 0 \\ 0 & 0 & 0 & 0 & 0 & 0 \\ 4c & 0 & 0 & 0 & 0 & 0 \\ 0 & 4c & 0 & 0 & 0 & 0 \\ 0 & 0 & c & c & c & c \\ 0 & 0 & 0 & 0 & 0 & 0 \\ 0 & h\cdot 4c & -l_y\cdot c & -l_y\cdot c & l_y\cdot c & l_y\cdot c \\ 0 & 0 & 0 & 0 & 0 & 0 \\ -h\cdot 4c & 0 & -l_x\cdot c & l_x\cdot c & l_x\cdot c & -l_x\cdot c \\ -4c & 0 & 0 & 0 & 0 & 0 \\ 0 & -4c & 0 & 0 & 0 & 0 \\ 0 & 0 & -c & -c & -c & -c \\ & & \mathbf{0}^{8*6} & & & \\ 0 & -h\cdot 4c & l_y\cdot c & l_y\cdot c & -l_y\cdot c & -l_y\cdot c \\ h\cdot 4c & 0 & l_x\cdot c & -l_x\cdot c & -l_x\cdot c & l_x\cdot c \end{pmatrix} \quad (142)$$

where

$$c=\frac{4\pi R f_n m}{4} \quad (143)$$

The system is then described with the angular velocities around the x and y axes instead being added as states 22-23 to the continuous time model described in Ch. 5.2.3.2. The fact that states 22-23 are the derivatives of states 14-15 is used for the connection between these states in the model matrix.

The nonlinear model was integrated with Simnon's Runge Kutta algorithm of order 4-5 while Matlab's "LSIM" function was used for the linear model. Also a Runge-Kutta algorithm of order 2-3 was used in Simnon, but the results were very similar and are therefore not shown in the diagrams.

The suspension geometry used in the nonlinear model is the same as described in Ch. 7.1. The geometry used in the linear model was the simplified version (described in Ch. 5.2.2) of the same suspension with l_x = 1.00 m and l_y = 0.60 m. Simulations were performed both with all elements mounted on the cab at the same height as the cab's c.o.g. (h=0.00) and with the elements mounted 0.40 m under the cab's c.o.g. (h=0.40).

The input used is measured when driving on track 1 with the speed of 12 km/h and is further described in Ch. 9.7.

6.3.2 Results

The weighted accelerations in the x, y and z dimensions measured at the cab's c.o.g. simulated with the linear and the nonlinear model with the assumptions described above are shown in Figure 48 for h=0.00 m. Figure 49 shows the same values but for h=0.40 m.

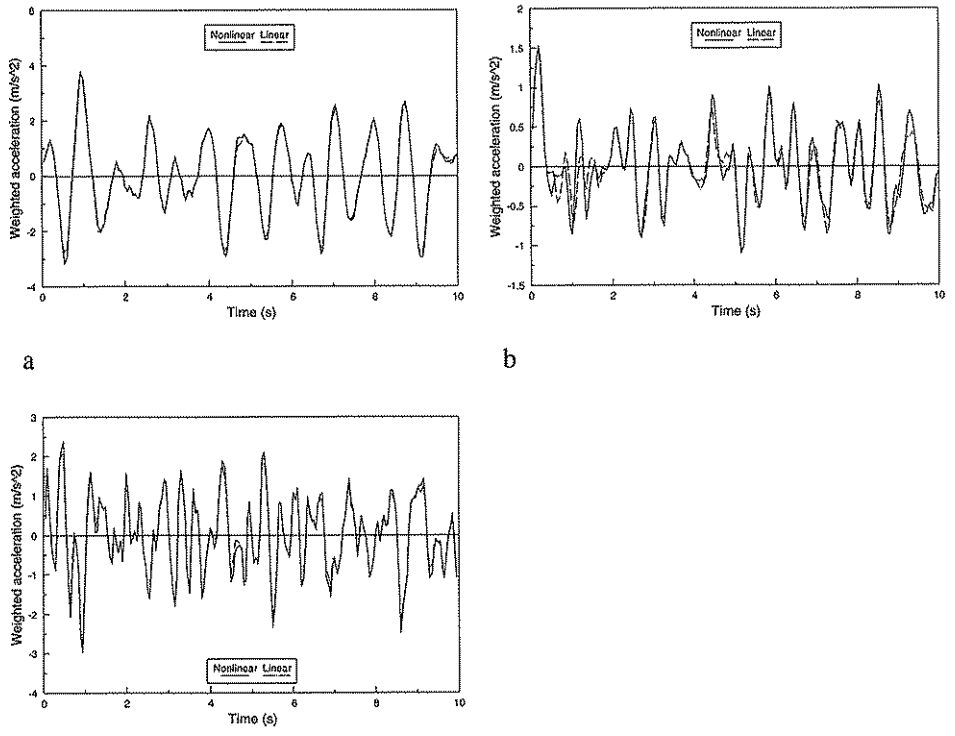

Fig. 48. Weighted accelerations in the x (Fig. a), y (Fig. b) and z (Fig. c) dimension using the same passive linear suspension characteristics and other assumptions calculated with the linear and nonlinear simulation models (h=0.00 m).

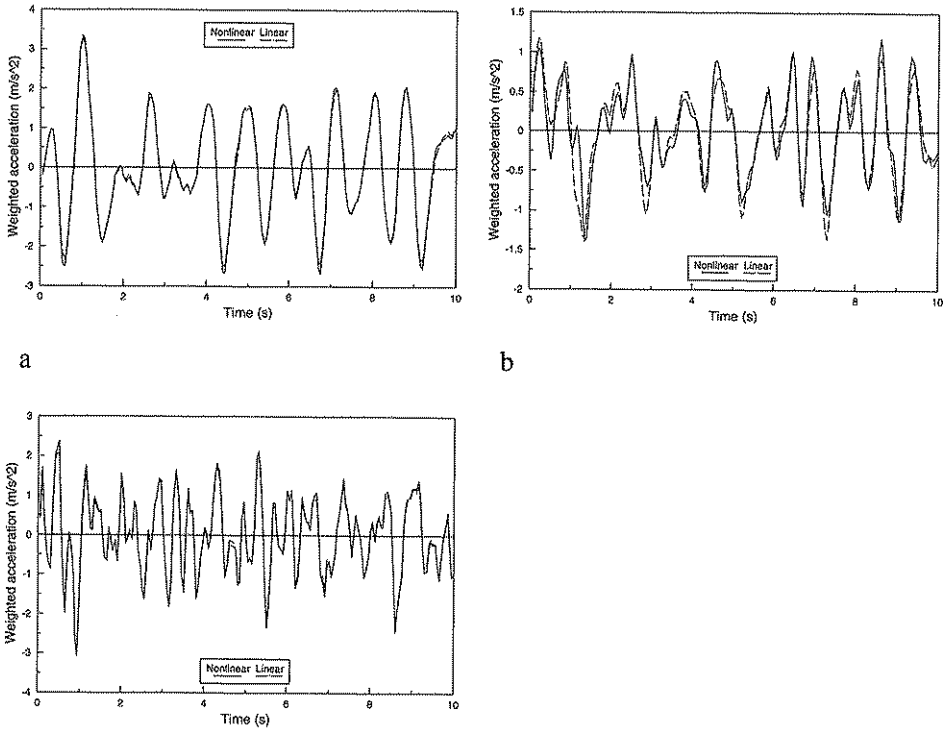

Fig. 49. Weighted accelerations in the x (Fig. a), y (Fig. b) and z (Fig. c) dimension using the same passive linear suspension characteristics and other assumptions calculated with the linear and nonlinear simulation models (h=0.40 m).

6.3.3 Conclusions

The figures show that the curves calculated with the linear model differ very little from the ones calculated with the nonlinear model. The differences are somewhat larger with h=0.40 m, specially in the y dimension, but are still small, showing that the linear model is a good description of the nonlinear one, and that the assumptions necessary for the linearization have little effect on the results.

7 SUSPENSIONS WITH PASSIVE ELEMENTS

The characteristics for different types of passive suspensions with linear and nonlinear elements are studied. The nonlinear time domain model is used for the simulations.

The geometry for the suspension used in the studies is first described, followed by the characteristics for the input signals used. The following chapters contain the assumptions and the results for each study.

7.1 The suspension's geometry and basic characteristics

The characteristics of a suspension are influenced by many factors. If the influence of one or more of the factors (parameters) is to be studied, it is important that none of the others are changed. The results then become much easier to interpret and understand. The described simulations are performed using the approach that, from a basic suspension configuration, different parameters are varied and the effects of the variations are then studied.

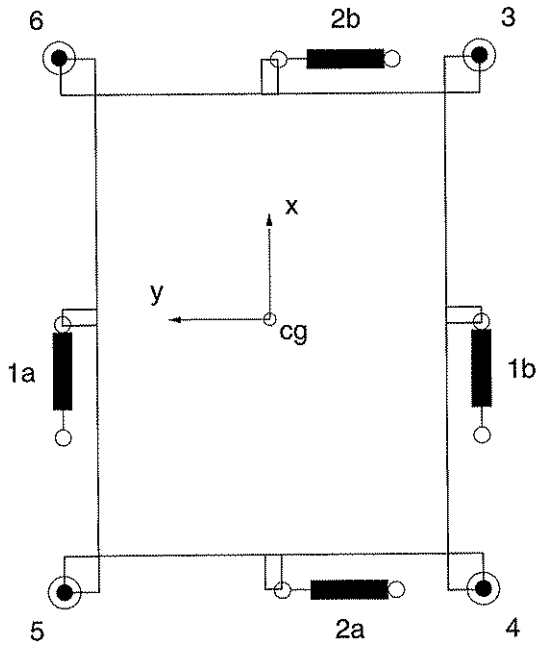

Fig. 50. Schematic view of the basic suspension seen from above.

The basic suspension is described in Figure 50. In principle the geometry is the same as for the suspension described in linear state space format in Ch. 5.2 (Figure 21). The cab is standing on four elements with combined radial and axial working principles (elements 3-6). The axial functions then mainly influence the vibrations in the z dimension and the rotational movements around the x and y axes. Horizontal damping elements (elements 1a, 1b, 2a and 2b in Figure 50) are used, together with the radial functions of elements 3-6, for the suspension in the horizontal directions.

All the suspension elements have a length of 0.40 meter in the balanced position. The coordinates for the suspension elements' cab and frame end points in the balanced position are found in Table B. As can be seen in the table, all the cab end points of the elements are located at the same height as the cab's c.o.g.

Table B. The coordinates for the cab and frame end points of the elements in the basic suspension measured relative to the cab's c.o.g.

Element	Cab			Frame		
	x (m)	y (m)	z (m)	x (m)	y (m)	z (m)
1a	0	0.60	0	-0.40	0.60	0
1b	0	-0.60	0	-0.40	-0.60	0
2a	-1.00	0	0	-1.00	0.40	0
2b	1.00	0	0	1.00	0.40	0
3	1.00	-0.60	0	1.00	-0.60	-.40
4	-1.00	-0.60	0	-1.00	-0.60	-.40
5	-1.00	0.60	0	-1.00	0.60	-.40
6	1.00	0.60	0	1.00	0.60	-.40

The relatively symmetric suspension geometry is used because it offers possibilities to calculate approximate natural frequencies and degrees of damping in the different dimensions. As mentioned above, the results obtained may then also be useful when designing suspensions based on other types of suspension element principles, which is very important.

The axial function of elements 3-6 is defined to reach a vertical natural frequency of 1.0 Hz and a nonlinear damping with $R_{0V} = 0.4$, $PK1_{cV} = 0.06$ m and $PK2_{cV} = 2$ (quadratic damping progressivity). The elastic mountings of elements 3-6 in the frame are worked out for a natural frequency of 0.75 Hz in the x and y dimensions. The horizontal dampers (elements 1a, 1b, 2a and 2b) are defined as linear and with the damping constants calculated for a damping degree of 0.8.

The characteristics for the cab used were:

$I_{xx} = 444\ kgm^2$

$I_{yy} = 506\ kgm^2$

$I_{zz} = 213\ kgm^2$

m = 580 kg

The cab's c.o.g. position was:

x: 0.60 m in front of the rear axle

y: at the tractor's symmetry line

z: 1.50 m above the ground.

The cab's characteristics are adjusted for the influence of the driver. It is assumed that the driver follows the cab's movements.

7.2 The simulation model inputs

The input signals used to describe the frame's movements are measured as described in Ch. 5.3.

Two input signals are used. The first signal is measured when driving along the smoother test track (track 1) described in SS-ISO 5008 at the prescribed velocity of 12 km/h. This track can be described as the average tractor driving surface. The second input used is measured when driving along the rough test track (track 2) described in the same standard. To get extreme vibration values, the speed was increased from the prescribed 5 km/h to 6 km/h. The resulting vibration load was defined as the highest that the suspension should be able to manage without over-travel. The vibration load was so high that the driver was almost losing control over the vehicle on the test track.

The tractor used in the measurements was a Volvo BM T-650, a 75 hp tractor with 2 WD (more tractor data in Table C). Measurements have to be made in 6 d.o.f. to get a complete description of the tractor's frame movements. Premeasurements showed that the angular vibrations around the z axis were very small and could be neglected. The movements were therefore measured in 5 d.o.f.

The RMS values for the input signals used are described in Table D. The vibrations are calculated for a point located in the tractor's symmetry line, 1.50 m above the ground and 0.60 m in front of the tractor's rear axle.

Table C. Tractor data

Model	Volvo BM T-650
Mass	3900 kg
Length	3.680 m
Height	2.580 m
Wheel base	2.440 m
Track width front	1.570 m
Track width rear	1.745 m
Tyres front	10.00-16/8
Tyres rear	18.4-34/8
Inflation pressure front	0.25 MPa
Inflation pressure rear	0.14 MPa

Table D. The input signals RMS values calculated for a point located in the tractor's symmetry line, 1.50 m above the ground and 0.60 m in front of the tractor's rear axle

	Vibration level RMS (m/s^2 rad/s^2)			
	Track 1		Track 2	
Direction	ISO 2631	Not weighted	ISO 2631	Not weighted
x	0.79	1.11	1.87	2.02
y	1.03	1.68	1.34	1.92
z	1.76	2.16	3.06	4.07
xr	-	1.92	-	2.33
yr	-	1.47	-	1.88
vector sum	2.52	-	4.44	-

The frequency contents are shown in Figures 84-85 for similar signals measured when a more modern 4 WD tractor was driven on the same tracks.

7.3 Parameters influencing the vertical suspension

7.3.1 Linear springs and linear dampers

The purpose was to study in what way different vertical linear spring and damping characteristics influence the suspension's vibration damping potential.

7.3.1.1 Assumptions

The spring constants for elements 3-6 was defined so that the vertical natural frequencies 0.75-1.50 Hz were reached. Each natural frequency was simulated with the damping constants defined for the degrees of damping 0.2, 0.5, 0.8 and 1.0. The suspension geometry and the other suspension parameters were defined as described in Ch. 7.1. Simulations were performed with inputs measured when driving on track 1 at a speed of 12 km/h and on track 2 at a speed of 6 km/h.

7.3.1.2 Results

The weighted acceleration values in the x, y and z directions, the angular accelerations around the x and y axes, the ISO 2631 vector sum and the maximum travel for the cab's c.o.g. in the x, y and z directions were analysed. The results are shown in Appendix 15.1.

The diagrams in Figures 51-55 show the weighted acceleration levels and the maximum travel in the z direction for the two tracks. The angular vibrations around the x axis are also shown. The angular vibrations around the y axis show approximately the same tendencies as those around the x axis and are therefore not described in the diagrams.

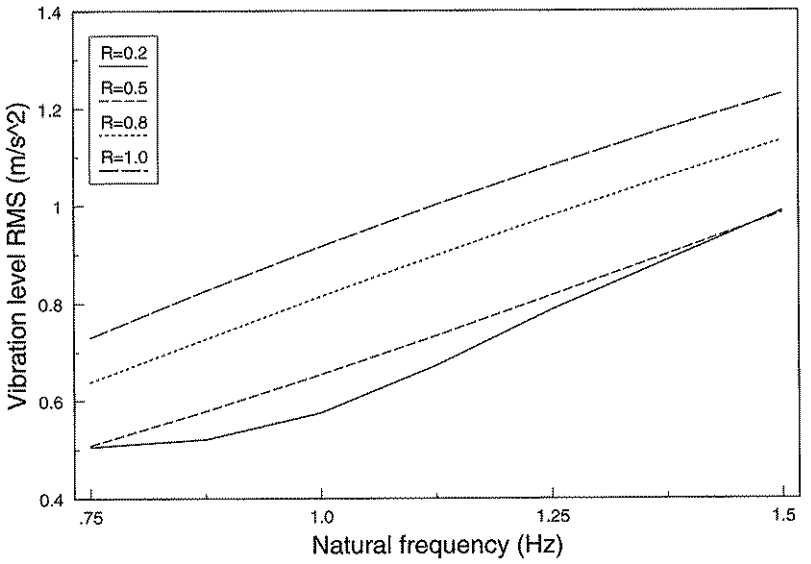

Fig. 51. Weighted vibration levels in the z direction for different vertical natural frequencies and degrees of damping when driving on track 1 at 12 km/h.

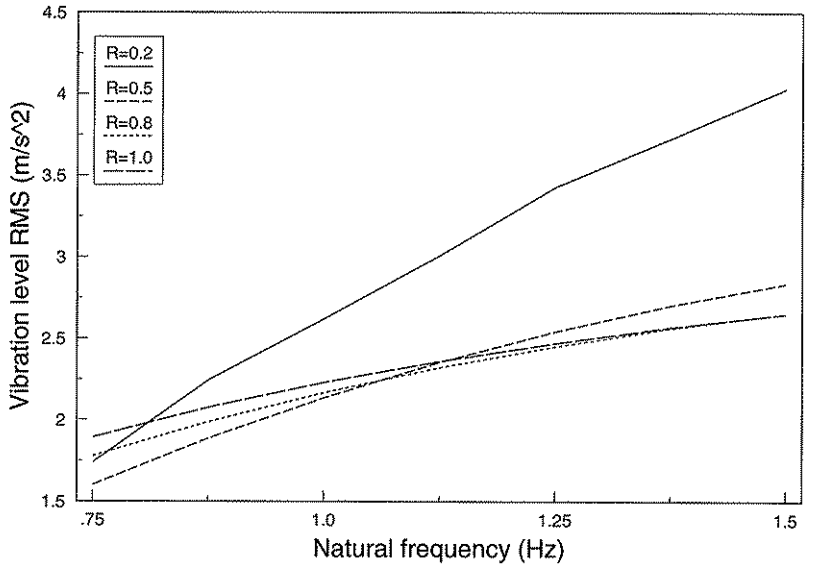

Fig. 52. Weighted vibration levels in the z direction for different vertical natural frequencies and degrees of damping when driving on track 2 at 6 km/h.

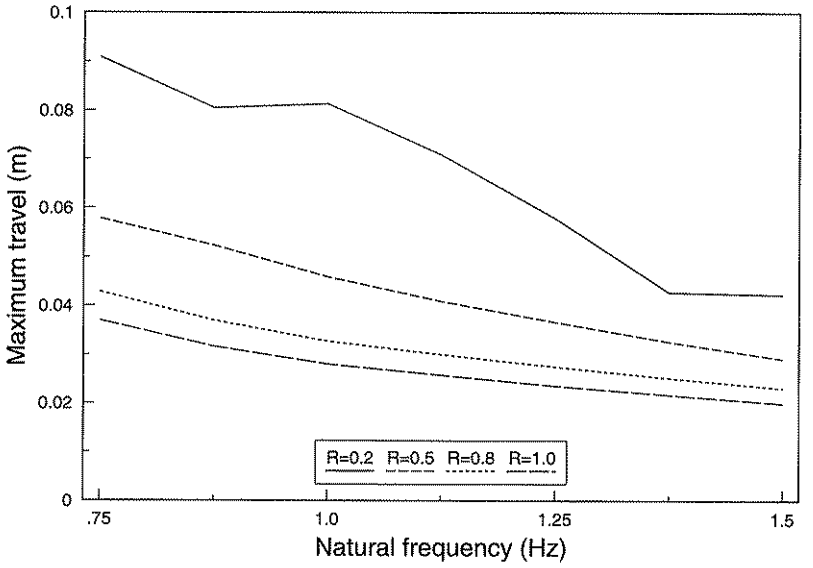

Fig. 53. Maximum travel for the cab's c.o.g. from the balanced position in the z direction for different vertical natural frequencies and degrees of damping when driving on track 1 at 12 km/h.

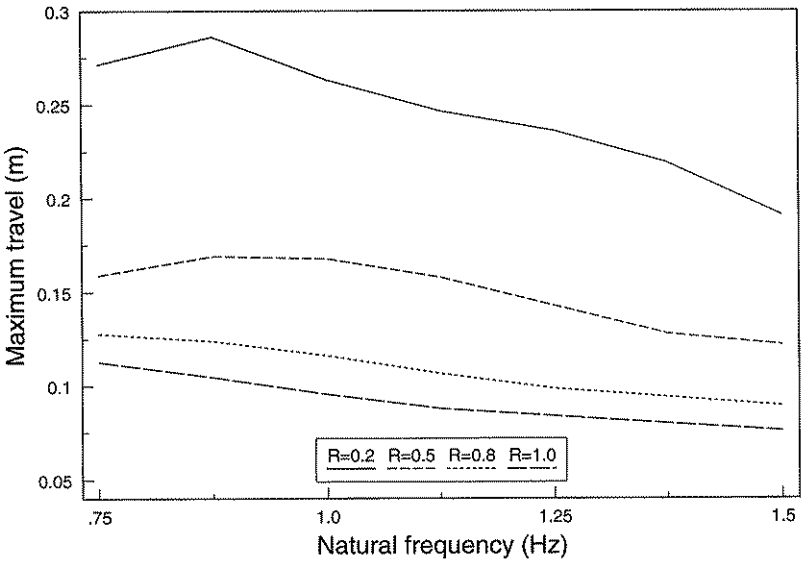

Fig. 54. Maximum travel for the cab's c.o.g. from the balanced position in the z direction for different vertical natural frequencies and degrees of damping when driving on track 2 at 6 km/h.

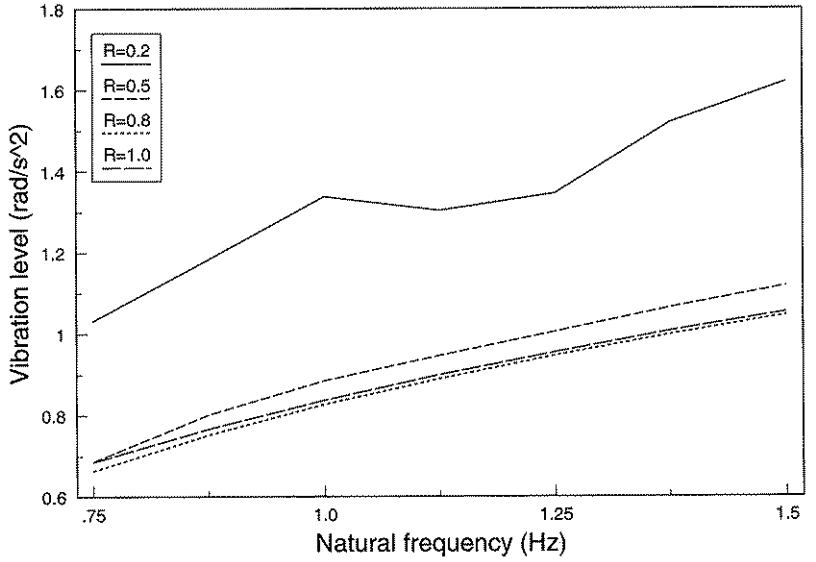

Fig. 55. Levels for angular vibrations around the x axis for different vertical natural frequencies and degrees of damping when driving on track 1 at 12 km/h.

7.3.1.3 Conclusions

The simulations show, as expected, that the suspensions with lower vertical natural frequencies offer a better vibration damping potential in the z direction when driving both on smooth and rough surfaces.

On the smooth track, suspensions with a damping degree of 0.2 offer the best vibration protection. The best damping potential on the very rough track 2 is reached with the more damped suspensions.

Also the angular vibrations around the x and y axes decrease when using softer spring elements. These vibration levels become much lower for damping degrees of 0.5-1.0 than for a damping degree of 0.2.

The cab's maximum travel from the balanced position in the z dimension increases when the suspension's natural frequency and degree of damping are decreased. Also the maximum travel in the x and y dimensions are influenced for the softest suspensions.

The simulations show that it is necessary to have a vertical natural frequency as low as 0.75-1.0 Hz in order to reach a good potential for vibration damping in the z dimension. Such a suspension must be damped very hard to avoid the travel becoming too large when driving on very rough surfaces. A high degree of damping decreases the vibration damping potential and thus the choice of linear suspension characteristics must be a compromise. To avoid too large static deviations when the static load is varied, is it also probably necessary to include a slowly reacting self levelling system, at least with the natural frequency as low as 0.75 Hz.

7.3.2 Linear springs and nonlinear dampers

The purpose of the simulations was to study how different nonlinear damping elements affected the suspension's vibration damping characteristics.

7.3.2.1 Assumptions

The characteristics of the vertical dampers were defined as in Ch. 5.1.5.1.2. The parameters describing the dampers' hardness as a function of the strokes from the balanced position are the vertical natural frequency (f_{nV}), the damping degree in the balanced position (R_{0V}) and the progressivity constants ($PK1_{cV}$ and $PK2_{cV}$). To get soft suspensions with high vibration damping potentials, f_{nV} was chosen to be 0.75. The damping degree in the balanced position was chosen to be 0.4 while $PK1_{cV}$ and $PK2_{cV}$ were varied in order to study the effects of different types of progressivity. $PK1_{cV}$ was varied between 0.03 and 0.09 m and $PK2_{cV}$ between 1 and 3. The other parameters were defined as in the basic suspension in Ch. 7.1. Simulations were performed with inputs measured when driving on track 1 at 12 km/h and on track 2 at 6 km/h.

7.3.2.2 Results

The same parameters as in Ch. 7.3.1 have been analysed and the results are shown in Appendix 15.2.

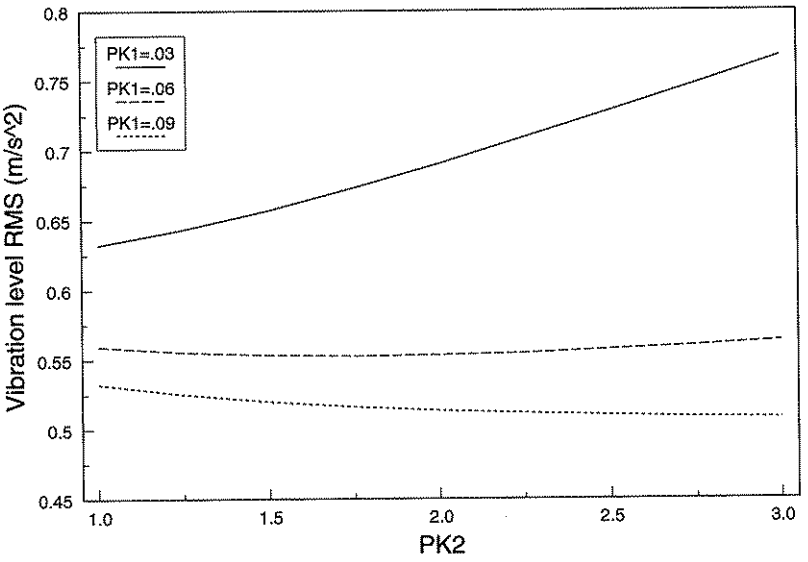

Fig. 56. Weighted vibration levels in the z dimension for suspensions with varying vertical nonlinear damping characteristics when driving on track 1 at 12 km/h.

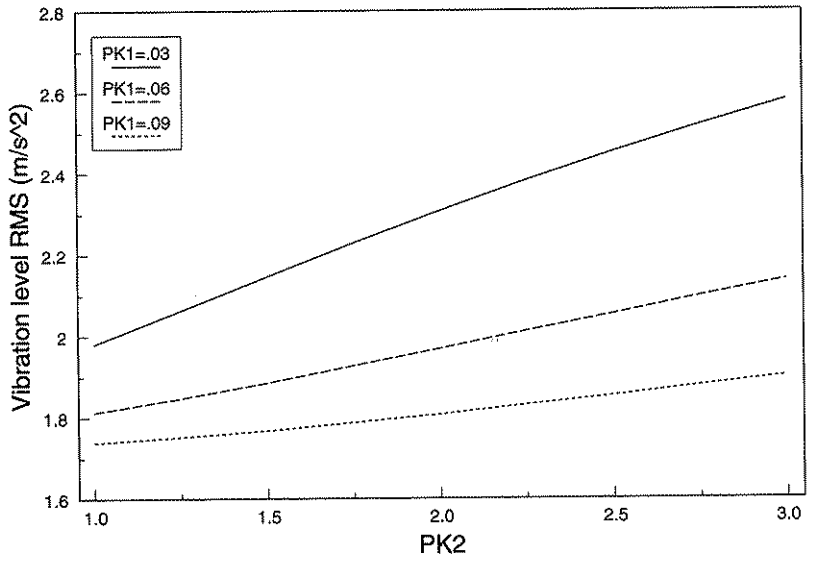

Fig. 57. Weighted vibration levels in the z dimension for suspensions with varying vertical nonlinear damping characteristics when driving on track 2 at 6 km/h.

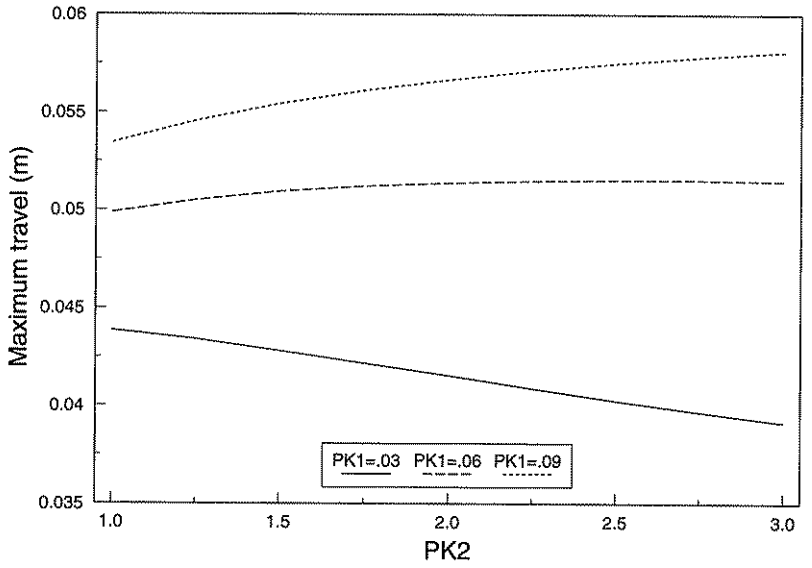

Fig. 58. Maximum travel from the balanced position in the z dimension for suspensions with varying vertical nonlinear damping characteristics when driving on track 1 at 12 km/h.

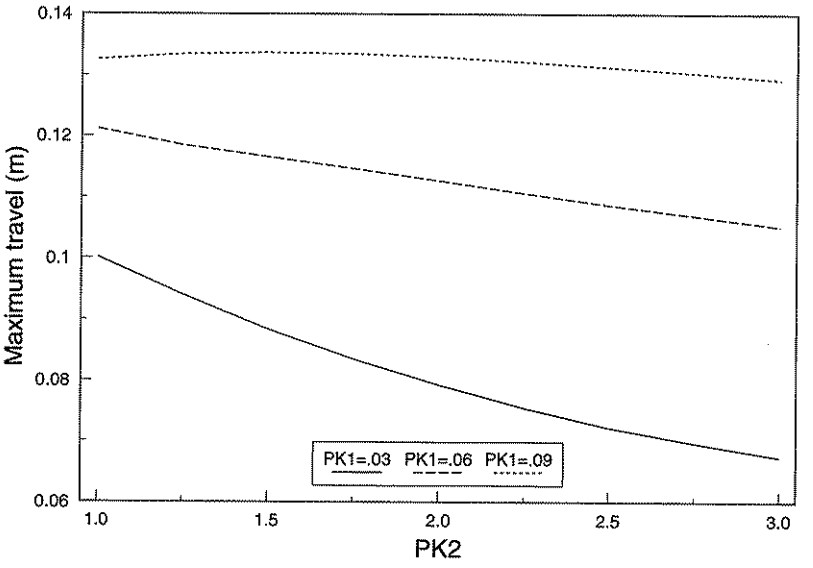

Fig. 59. Maximum travel from the balanced position in the z dimension for suspensions with varying vertical nonlinear damping characteristics when driving on track 2 at 6 km/h.

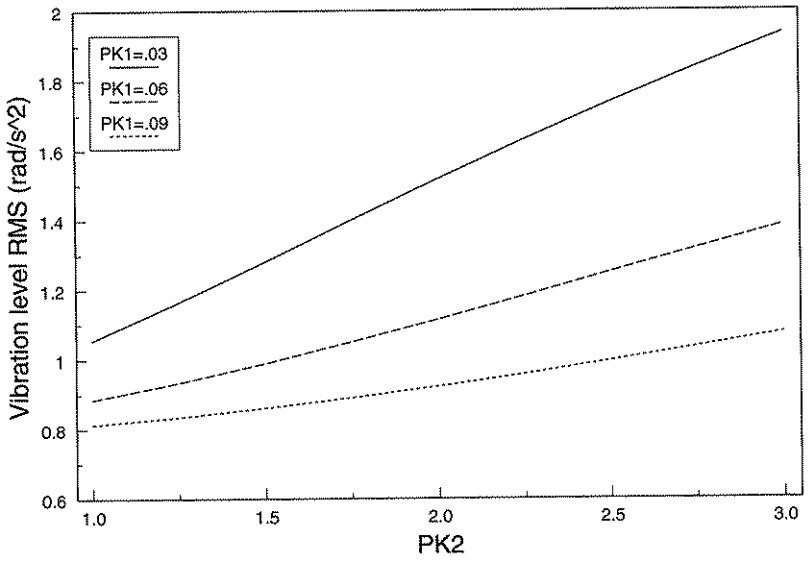

Fig. 60. Levels for angular vibrations around the x axis for suspensions with varying vertical nonlinear damping characteristics when driving on track 2 at 6 km/h.

7.3.2.3 Conclusions

The results show, in general, that nonlinear vertical damping elements can be used to reach a good vibration damping potential, without unreasonable demands on travel space, in a vertical suspension with low natural frequency.

The effects of the progressivity constants $PK1_{cV}$ and $PK2_{cV}$ on the travel and the vibration transmission in the z direction depend on the level of the input signal. On track 1, where the mean suspension travel is relatively small, a big $PK2_{cV}$ results in lower vibration levels in the z dimension than a small $PK2_{cV}$, which depends on lower average damping. On track 2, where the travel often exceeds $PK1_{cV}$, a big $PK2_{cV}$ results in harder average damping and higher vibration levels in the cab.

The vibration levels for the angular vibrations around the x and y axes show approximately the same tendencies when $PK1_{cV}$ and $PK2_{cV}$ vary as the z dimension vibrations do on the same track.

One property for suspensions with high progressivity is that the safety against over-travel becomes higher at vibration loads higher than those used in the rating calculations. A further increase of the input vibration level increases the maximum travel much less when using nonlinear progressive dampers, because they are much harder than the linear elements when travel is large. This contributes also to the possibility to decrease the safety margin in the design work.

7.4 Parameters influencing the horizontal suspension

The simulations were performed to study how different suspension parameters influence the horizontal vibration transmission in the basic suspension described in Ch. 7.1. The spring function in the horizontal dimension is mainly decided by the bending constant (q) for the vertical elements (elements 3-6 in Figure 50). The damping characteristics in the x and y directions are mainly influenced by the horizontally directed damping elements 1a, 1b, 2a and 2b in Figure 50.

The parameter values corresponding to the approximate natural frequencies and degrees of damping in the horizontal directions have been calculated with the formulas in Ch. 5. The other parameters have been defined as in the basic suspension and kept constant.

7.4.1 Linear springs and linear dampers

The purpose was to study how different types of linear horizontal suspension characteristics influence the vibration damping capacity.

7.4.1.1 Assumptions

Simulations were performed as previously, with inputs measured when driving on track 1 at 12 km/h and on track 2 at 6 km/h. The same parameters were analysed as in the previous studies. All values were measured at the cab's c.o.g. An analysis of values measured at other points than the c.o.g. would have been interesting in some cases. The simulation model output also included such values, but a further increase in the already large amount of analysed variables was considered only to complicate the work.

7.4.1.2 Results

The detailed results are described in Appendix 15.3. The diagrams in Figures 61-64 show the weighted acceleration levels and the maximum travel in the x dimension for the two tracks. The vibrations and travel in the y dimension show with few exceptions the same tendencies as in the x dimension and are therefore only described in the Appendix.

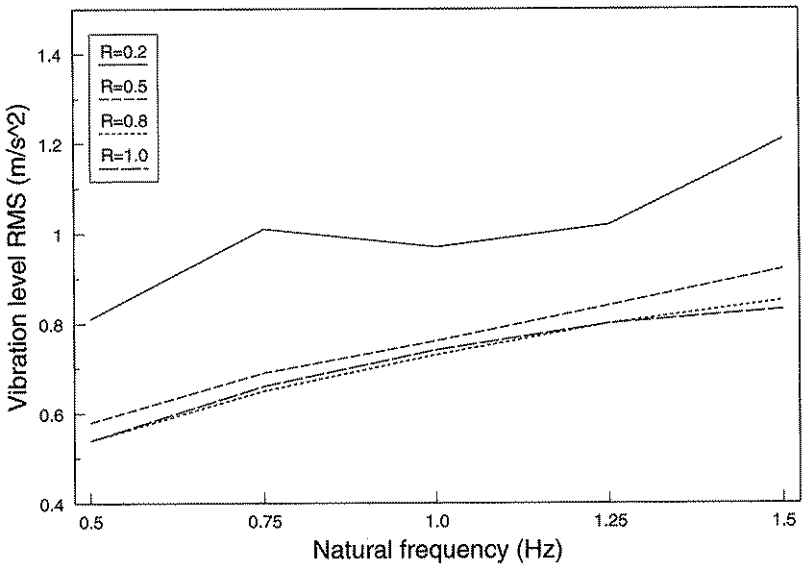

Fig. 61. Weighted vibration levels in the x direction for different horizontal natural frequencies and degrees of damping when driving on track 1 at 12 km/h.

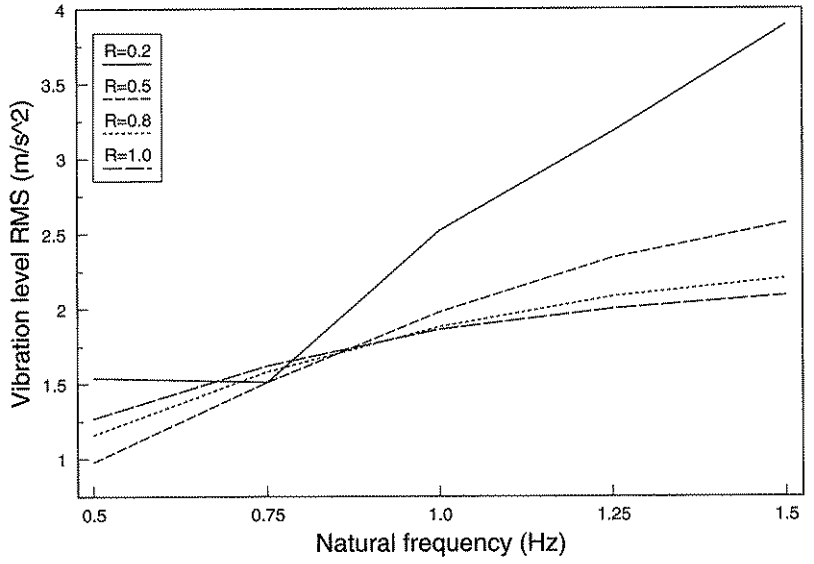

Fig. 62. Weighted vibration levels in the x direction for different horizontal natural frequencies and degrees of damping when driving on track 2 at 6 km/h.

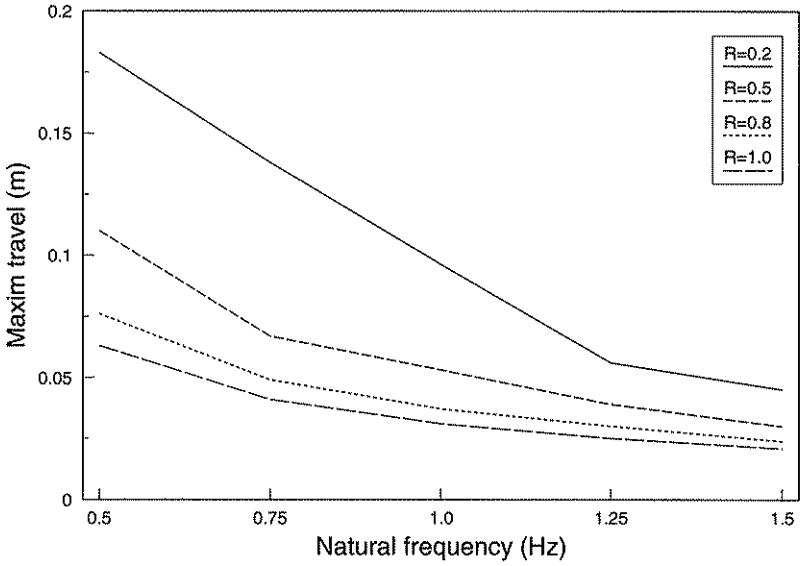

Fig. 63. Maximum travel for the cab's c.o.g. from the balanced position in the x direction for different horizontal natural frequencies and degrees of damping when driving on track 1 at 12 km/h.

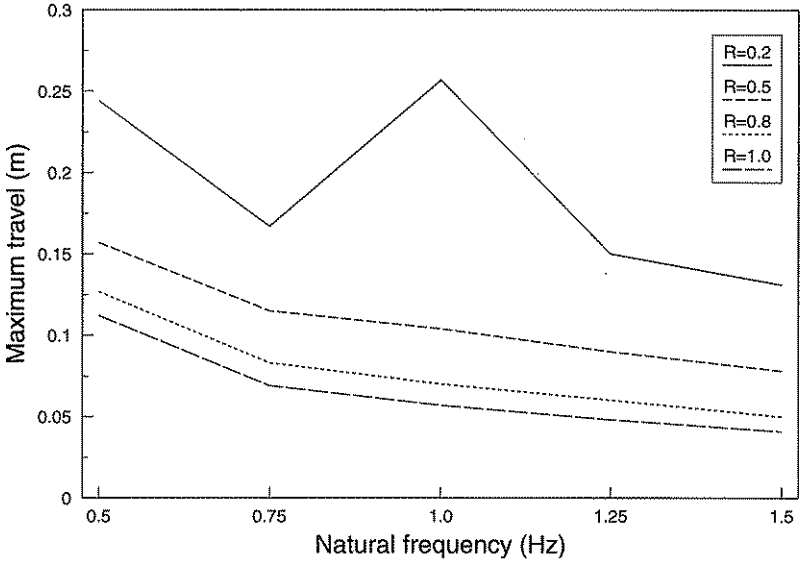

Fig. 64. Maximum travel for the cab's c.o.g. from the balanced position in the x direction for different horizontal natural frequencies and degrees of damping when driving on track 2 at 6 km/h.

7.4.1.3 Conclusions

The acceleration levels in the x and y directions decrease, as expected, when the horizontal natural frequencies are decreased. The maximum travel increases at the same time.

The suspension's vertical degrees of damping have a large influence on the cab's maximum travel and the vibration levels. At natural frequencies over 1.0 Hz the best vibration damping potential is reached with damping degrees as high as 0.8-1.0. These degrees of damping also result in the smallest maximum travel from the balanced position.

The low ISO 2631 weighted vibration levels for the relatively high degrees of damping in the x and y dimensions can partly be explained by the frequency weighting factors in these directions being highest for signals with frequencies below 2.0 Hz. At the low natural frequencies studied, a high damping degree decreases mainly the transmission of vibrations with frequencies in the most sensitive domain for humans. At the same time, a higher damping degree increases the transmission of higher frequencies. The ISO weighting, however, results in the total load not being particularly influenced.

Suspensions with horizontal natural frequencies of 0.5 and 0.75 Hz offer good vibration damping potentials on both smoother and rougher surfaces. The maximum travel with a suspension of that kind becomes, however, relatively high, but is decreased when the damping degrees are increased. To avoid too large static deviations when driving on slopes, horizontal suspensions with such low natural frequencies must probably also include a slow reacting self levelling system.

In most studies, the vibrations in the z direction and the angular vibrations around the x and y axes are very little influenced by the suspension's horizontal natural frequencies and degrees of damping. The suspensions with low degrees of damping become, however, jerky and unstable, which results in increased vibration loads also in the dimensions normally not influenced.

7.4.2 Linear springs and nonlinear dampers

The purpose of the described simulations was to study how different nonlinear horizontal damping characteristics influence the suspension's vibration damping potential.

7.4.2.1 Assumptions

The results from the simulations in the previous chapter show that a horizontal natural frequency as low as 0.5-0.75 Hz is needed to reach a good vibration damping potential. Such suspensions result in large suspension element strokes and a need for large available travel spaces to avoid over-travel. Elements with nonlinear characteristics can be used to reduce the maximum travel.

Simulations have been performed with $PK1_{cH}$ for the horizontal dampers = 0.03, 0.06 and 0.09 m and with $PK2_{cH}$ =1, 2 and 3. R_{0H} was placed at 0.4 to get soft damping around the balanced position. The bending constants q for the vertically standing elements were chosen to be constant in order to reach a linear spring function in horizontal directions.

q is defined so that the natural frequencies in the x and y directions are 0.5 Hz according to the formulas in Ch. 5. The vertically working suspension is defined as in the previous study.

7.4.2.2 Results

The detailed results are described in Appendix 15.4. Figures 65-68 describe the influence of varying $PK1_{cH}$ and $PK2_{cH}$ at the weighted vibration levels and the maximum travel in the x dimension when driving on the two tracks. The corresponding values for the y dimension show approximately the same tendencies and are therefore not shown in diagrams.

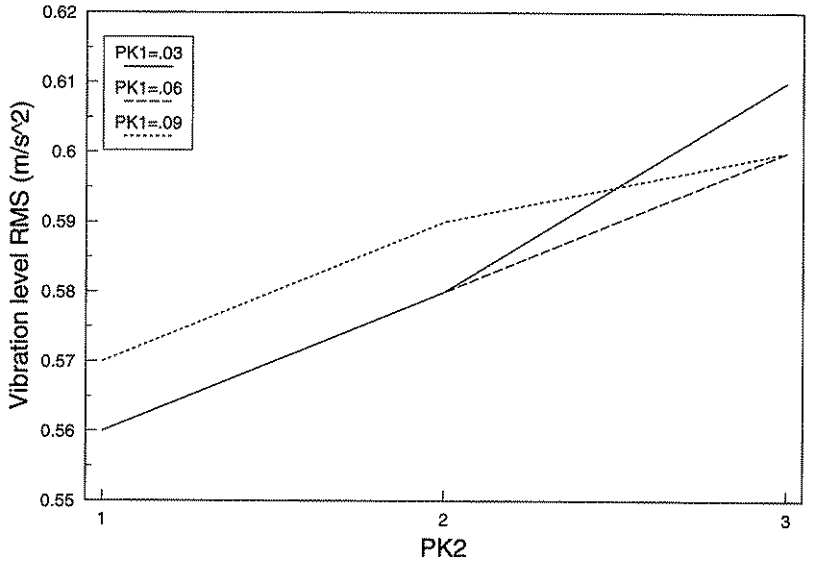

Fig. 65. Weighted vibration levels in the x dimension for suspensions with varying horizontal nonlinear damping characteristics when driving on track 1 at 12 km/h.

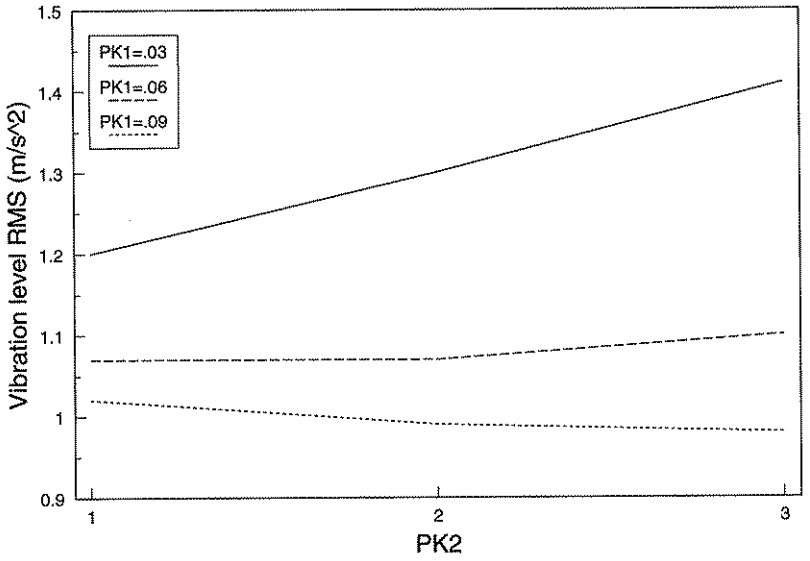

Fig. 66. Weighted vibration levels in the x dimension for suspensions with varying horizontal nonlinear damping characteristics when driving on track 2 at 6 km/h.

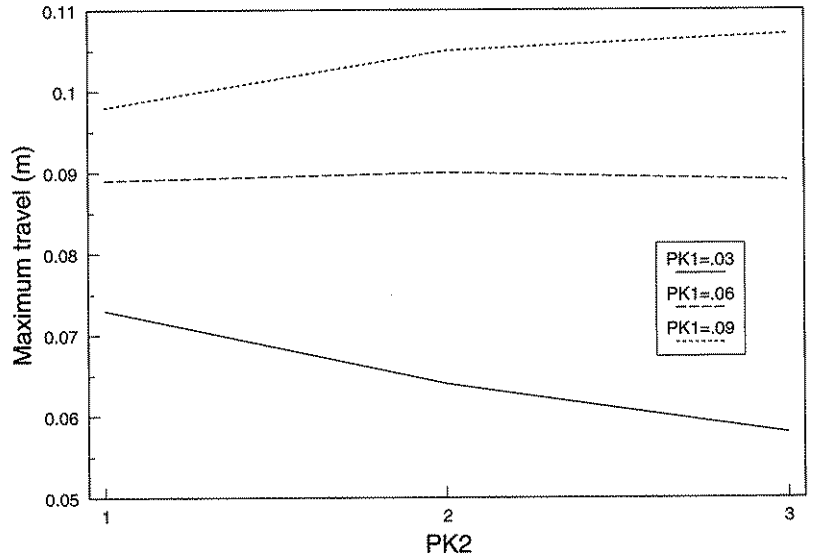

Fig. 67. Maximum travel from the balanced position in the x dimension for suspensions with varying horizontal nonlinear damping characteristics when driving on track 1 at 12 km/h.

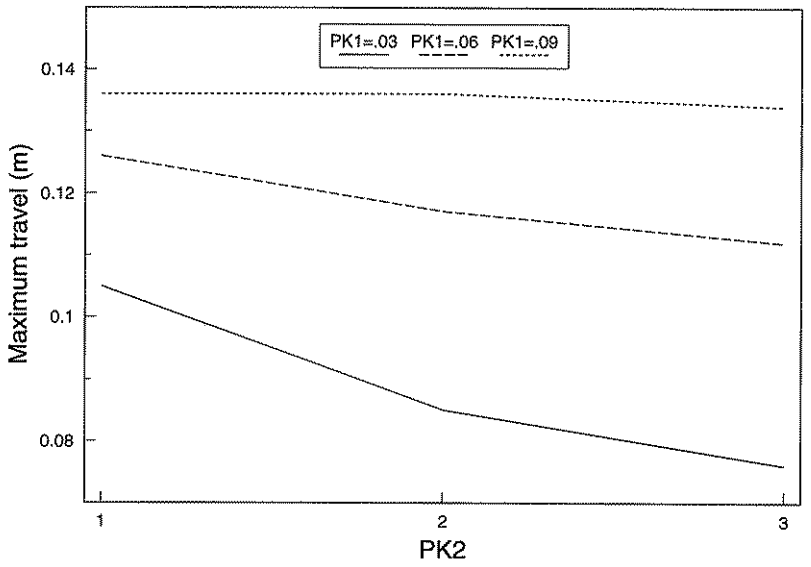

Fig. 68. Maximum travel from the balanced position in the x dimension for suspensions with varying horizontal nonlinear damping characteristics when driving on track 2 at 6 km/h.

7.4.2.3 Conclusions

The results show that it is possible to reduce the demands for available travel space also in the horizontal directions by using damping elements with nonlinear characteristics.

A suspension with high progressivity increases the vibration levels more on the rougher surface where the elements more often work with strokes in the area with higher damping. The increase of the vibration loads is very small on the smoother surface when damper progressivity is increased.

The vibration loads in the other dimensions are very little influenced when the characteristics of the horizontal dampers are changed.

7.4.3 Nonlinear springs and linear dampers

The purpose of the simulations was to study the effects of different horizontal nonlinear spring characteristics.

7.4.3.1 Assumptions

The characteristics of the horizontal spring function are decided by the elastic mounting in the frame of the vertical elements (q for elements 3-6 in Figure 50). The elastic mountings have been defined to be relatively soft (with small q_0) for small deviations and then exponentially stiffer for increased deviations.

q_0 was defined to give the horizontal natural frequency of 0.5 Hz in the balanced position, calculated with the formulas in Ch. 5. The damping degree in the horizontal directions has been defined to 1.0 referring to q_0. When the elements are bent from the balanced position, q increases, and thus the damping degrees decrease. This is because the dampers are linear and the damping constants therefore do not increase with increasing strokes.

Simulations were performed with $PK1_\alpha$ = 0.075-0.225 rad which correspond to q being doubled for the horizontal deviations 0.03-0.09 m if the elements are 0.40 m long. $PK2_\alpha$ has been varied between 1, 2 and 3 corresponding to linear, quadratic and cubic progressivity. The parameters not mentioned have been defined as in the basic suspension configuration described in Ch. 7.1.

7.4.3.2 Results

The same parameters as in the previous study were analysed. The detailed results are described in Appendix 15.5. The influence of varying $PK1_\alpha$ and $PK2_\alpha$ on the weighted acceleration levels and at the maximum travel for the cab's c.o.g. in the x dimension are shown in Figures 69-72.

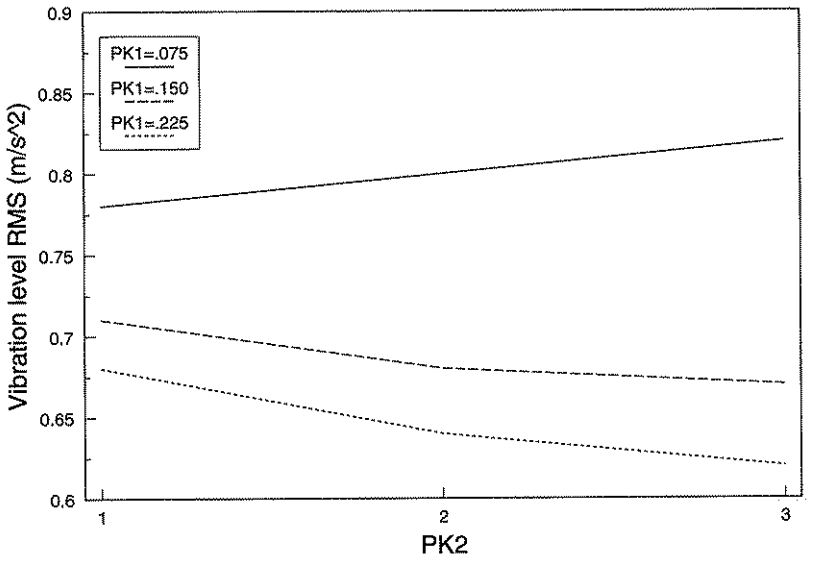

Fig. 69. Weighted vibration levels in the x direction for suspensions with varying non-linear mountings of the vertical elements when driving on track 1 at 12 km/h.

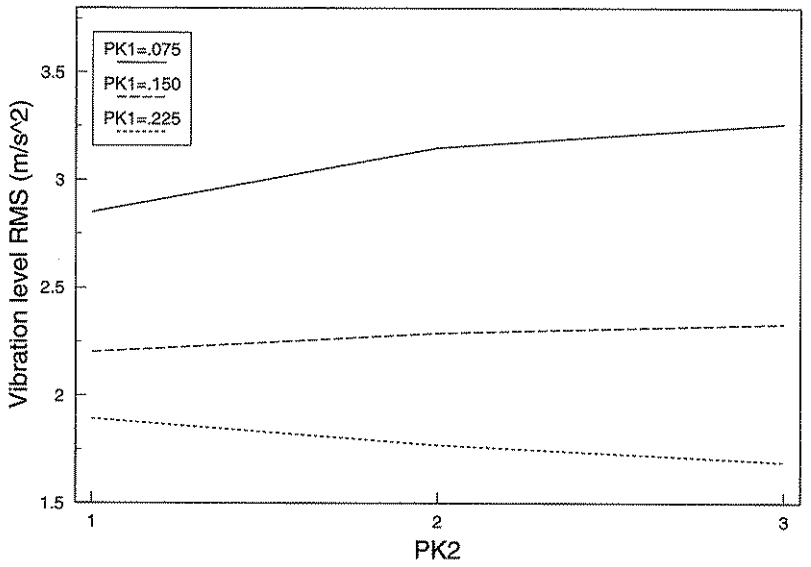

Fig. 70. Weighted vibration levels in the x direction for suspensions with varying non-linear mountings of the vertical elements when driving on track 2 at 6 km/h.

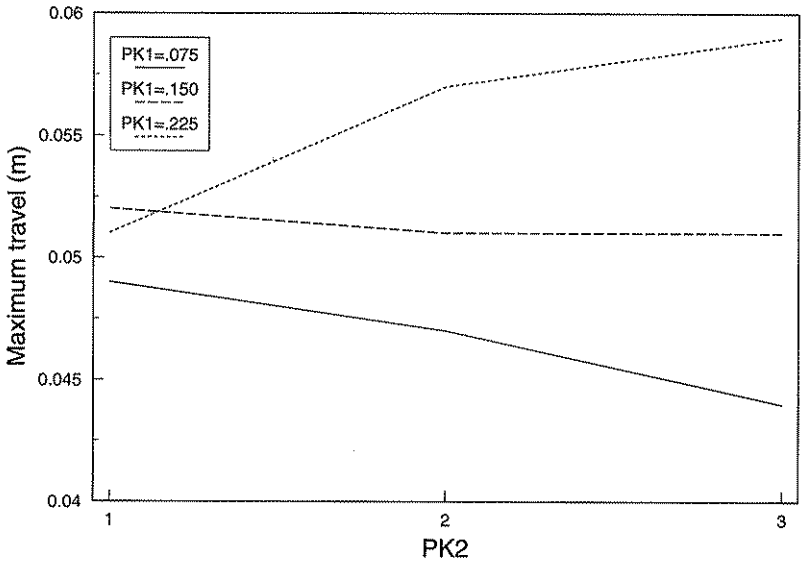

Fig. 71. Maximum travel for the cab's c.o.g. in the x direction for suspensions with varying nonlinear mountings of the vertical elements when driving on track 1 at 12 km/h.

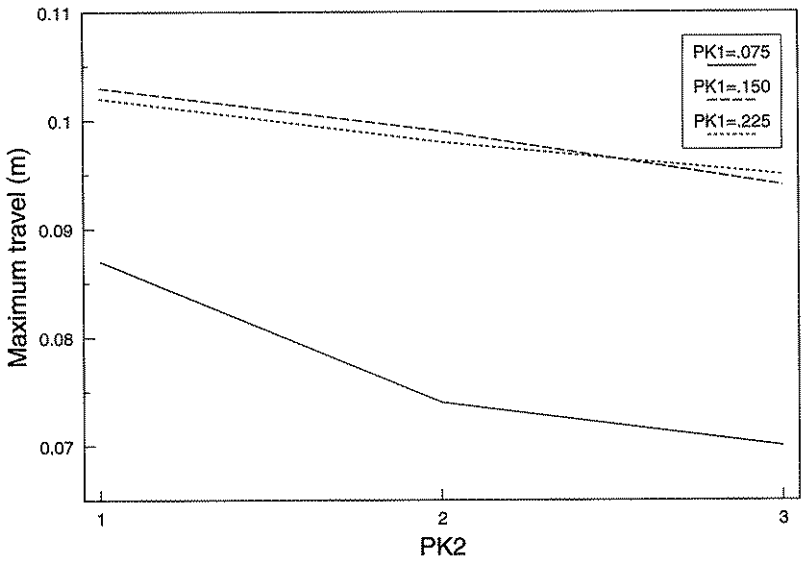

Fig. 72. Maximum travel for the cab's c.o.g. in the x direction for suspensions with varying nonlinear mountings of the vertical elements when driving on track 2 at 6 km/h.

7.4.3.3 Conclusions

The simulations show that it is possible to decrease the horizontal travel by using suspensions with nonlinear horizontal spring functions.

Figures 69 and 70 show, however, that highly nonlinear spring characteristics result in a substantial increase in the vibration load, especially when driving on the very rough surface. The decrease for the maximal deviations is obtained at the expense of a high vibration load increase. The previous study showed that it is possible to get the same decrease in maximum travel with a smaller increase of the vibration loads if nonlinear horizontal dampers were used.

7.5 Effects of the vertical locations of the suspension elements

An important factor in the design of a cab suspension is the locations of the suspension elements. The purpose of the study was to show the influence of the vertical positions of the suspension elements on the vibration damping characteristics.

7.5.1 Assumptions

All the cab end points of the elements are assumed to be located at the same vertical height in the balanced position. This height has been varied between 1.0 m below and 1.0 m above the cab's c.o.g. All other parameters have been defined as in the basic suspension (Ch. 7.1). As in previous simulations, the inputs have been from the two test tracks and the analysed parameters are also the same as before.

7.5.2 Results

The complete results are shown in Appendix 15.6. The results from the simulations with input from track 1 are also shown in Figures 73-75. The results for the very rough track 2 show about the same trends and are therefore only shown in the Appendix. The vibration levels and deviations from the balanced position are measured at the cab's c.o.g.

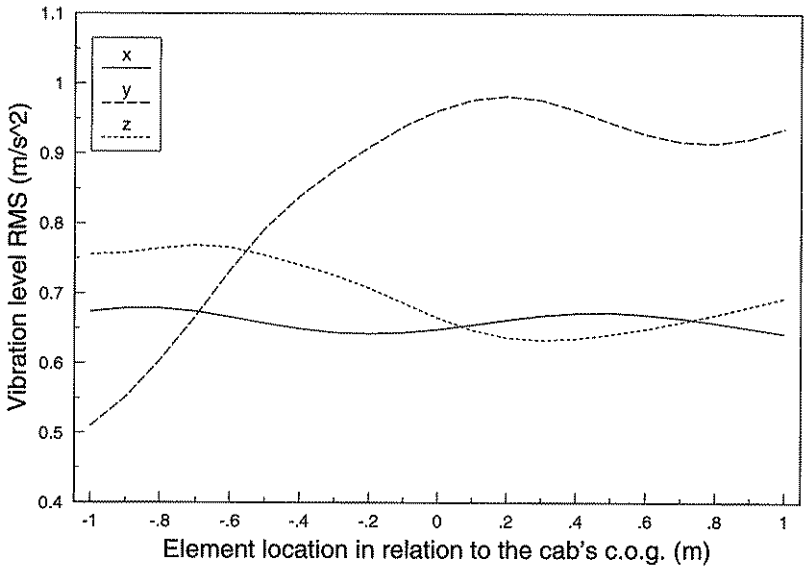

Fig. 73. Weighted vibration levels in the x, y and z directions for suspensions with elements located at varying heights when driving on track 1 at 12 km/h.

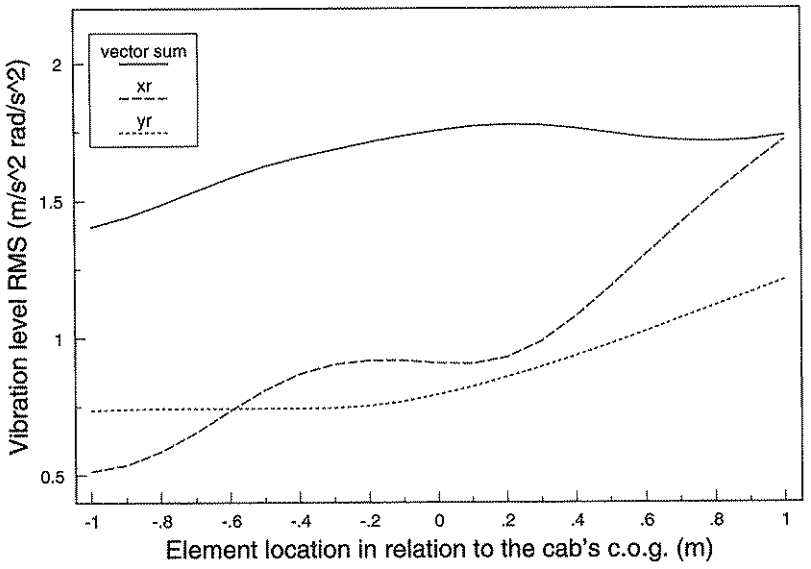

Fig. 74. Weighted vibration levels (ISO 2631 vector sum) and angular vibrations around the x and y axes for suspensions with elements located at varying heights when driving on track 1 at 12 km/h.

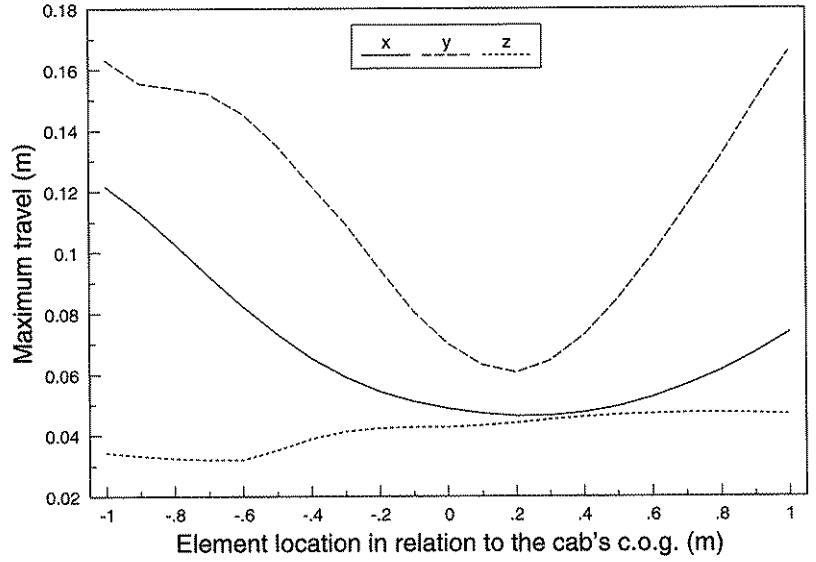

Fig. 75. Maximum travel, measured at the cab's c.o.g., in the x, y and z directions for suspensions with elements located at varying heights when driving on track 1 at 12 km/h.

7.5.3 Conclusions

The mounting heights of the suspension elements have significant effects on the suspension's vibration damping characteristics.

The angular vibrations are increased when the mounting heights of the elements are increased above the cab's c.o.g. The reason is probably that the suspension becomes unstable with pendulum tendencies. The oscillation centre is then located approximately at the same height as the cab mounting heights of the elements. The angular vibrations around the x axis increase more than the vibrations around the y axis. This can be explained by the distance between the elements only being 1.2 m in the y dimension while the distance in the x dimension is 2.0 m and thereby results in greater stability for angular movements around the y axis.

The accelerations in the z dimension are very little influenced by the mounting heights of the elements. The acceleration levels in the x dimension are relatively unaffected by mounting heights when driving on the smoother track. The levels on the rougher track show the same tendencies as the y dimension vibrations with decreasing values when the distance between the mounting plane of the elements and the cab's c.o.g. is increased. The results using the two different input signals otherwise show the same trends but at different levels.

A low element mounting height results in an decreased total vibration load measured at the cab's c.o.g. The maximum deviations from the balanced position, and thereby the demands on travel space in the design, are increasing at the same time. The lowest maximum travel is reached with the elements mounted slightly above the cab's c.o.g.

7.6 Effects of the horizontal locations of the suspension elements

The characteristics of a suspension with springs and dampers such as the one described in Ch. 7.1 are dependent on the locations of the vertically working elements in the x and y dimensions. The main reason is that the natural frequencies for angular movements around the x and y axes are directly affected by the distance of the elements from the cab's c.o.g.

7.6.1 Assumptions

Simulations have been performed to study how the parameters mentioned affect the weighted vibration levels in the x, y and z dimensions, the angular vibrations around the x and y axes and the maximum angular deviations between the cab and the frame when driving over the test tracks. Since the parameters varied mainly influenced the angular movement, the angular deviations were considered to be more interesting to analyse than the linear deviations.

The distance between the vertical elements, which were placed symmetrically and mounted on the cab at the height of the cab's c.o.g., has been varied in the x dimension between 0.6-3.0 m and in the y dimension between 0.6 and 2.0 m (Figure 76). When the distance in the x dimension was varied, the distance in the y dimension was kept constant

= 1.20 m. When the distance in the y dimension was varied, the distance in the x dimension was kept constant = 2.0 m. These values were chosen because they are reasonable to use in a real application.

The four horizontal shock absorbers were also moved corresponding to the movements of the vertical elements, but the locations of these elements influence the characteristics of the suspension very little as long as they are symmetrically mounted.

The characteristics of the suspension elements have been defined in the same way as for the basic suspension described in Ch. 7.1. In the same way as in earlier simulations, the two input signals measured on test tracks 1 and 2 have been used.

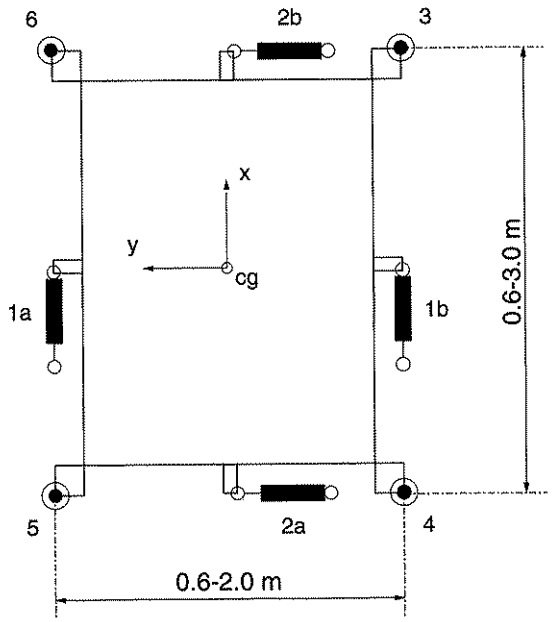

Fig. 76. The cab, seen from above, with the studied vertical suspension element positions shown.

7.6.2 Results

The complete results are shown in Appendix 15.7. The angular vibration levels and the maximum angular suspension deviations when driving on track 1 at 12 km/h are shown in Figures 77-80.

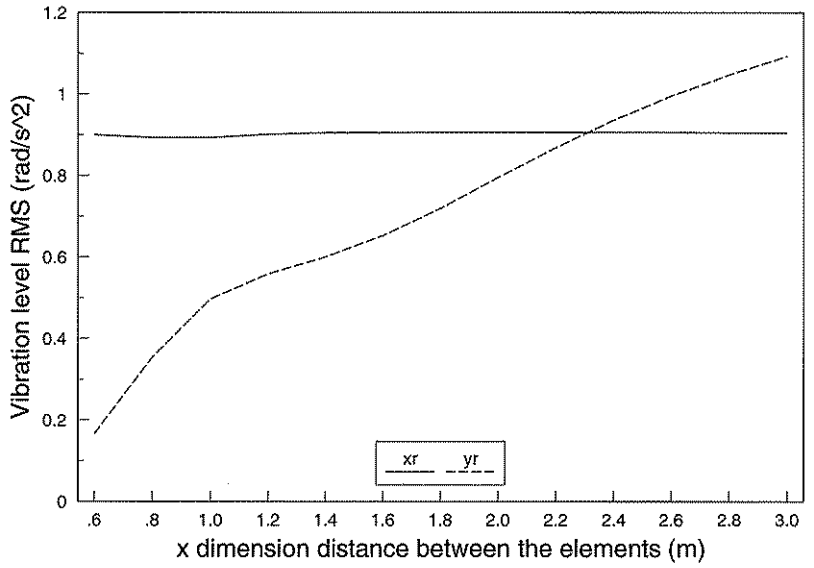

Fig. 77. Angular vibration levels around the x and y axes for a suspension with varying distance in the x dimension between the vertical suspension elements when driving on track 1 at 12 km/h.

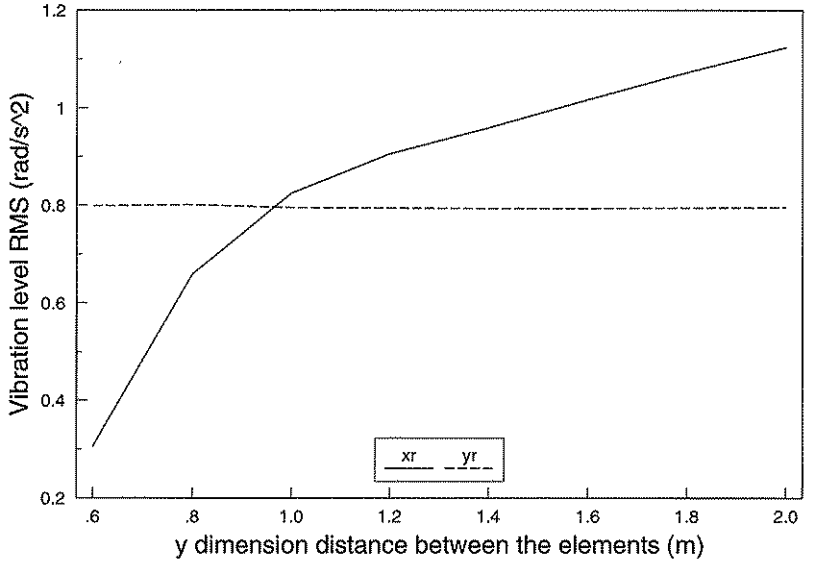

Fig. 78. Angular vibration levels around the x and y axes for a suspension with varying distance in the y dimension between the vertical suspension elements when driving on track 1 at 12 km/h.

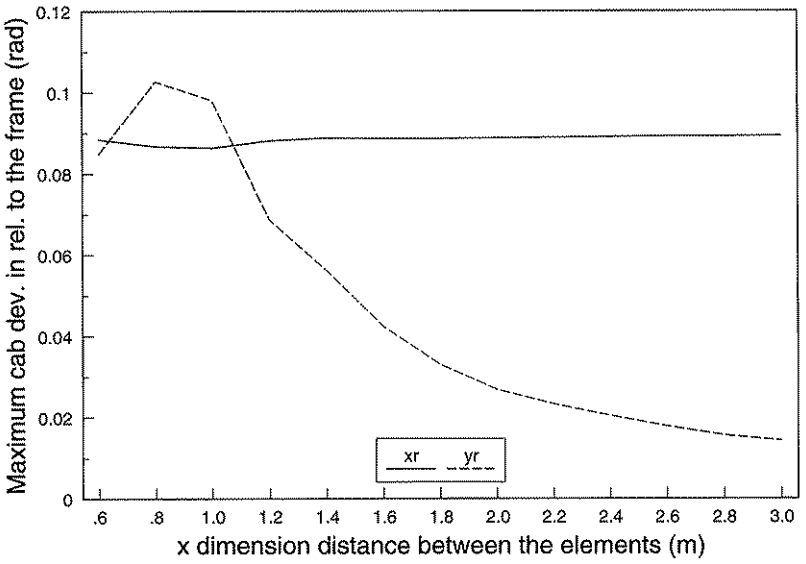

Fig. 79. Maximum angular deviations between the cab and the frame for a suspension with varying distance in the x dimension between the vertical suspension elements when driving on track 1 at 12 km/h.

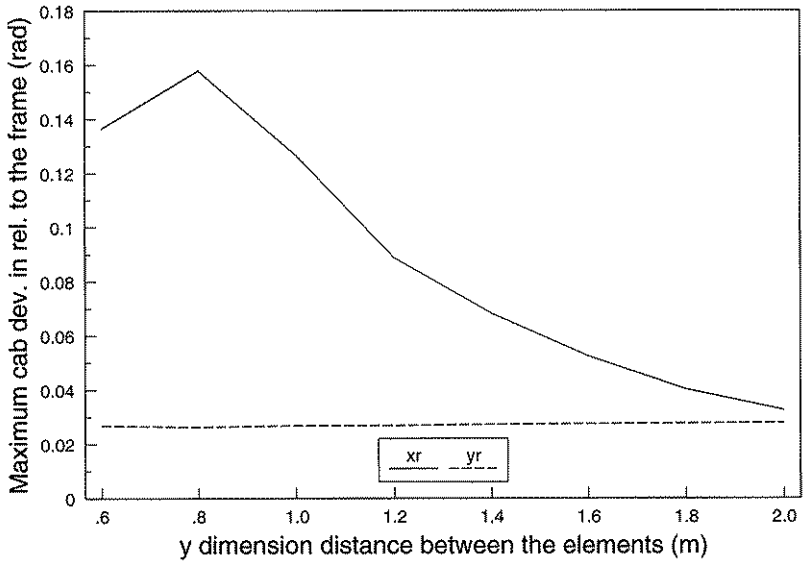

Fig. 80. Maximum angular deviations between the cab and the frame for a suspension with varying distance in the y dimension between the vertical suspension elements when driving on track 1 at 12 km/h.

7.6.3 Conclusions

When the distance in the x dimension between the elements is varied while the distance in the y dimension is held constant, only the transmission of angular vibrations around the y axis is influenced. The transmission of movements in the other degrees of freedom becomes almost constant.

A small x dimension distance between the elements decreases the natural frequencies for angular movements around the y axis, which gives softer suspensions and decreasing vibration levels. In the studied suspension geometry, with all elements mounted at the same height as the cab's c.o.g., the natural frequency becomes proportional to the distance between the elements. The distance 0.60 m corresponds to a natural frequency below 0.5 Hz, which may explain the low levels for angular vibrations around the y axis for such a suspension.

When the angular vibration levels decrease with decreasing distance between the elements, the maximum angular deviation between the cab and the frame is increasing at the same time. The big angular deviations give rise to big demands for travel space and can also be assumed to reduce the driver's feeling of security.

The changed characteristics of the suspension when the horizontal distance between the elements in the y dimension follows the same trends as when the x dimension distance is varied but with the angular vibrations around the x axis as the variable influenced.

A comparison between the results on the two different test tracks shows that the tendencies are about the same but with higher levels for the angular vibrations on the rougher track. The maximum travel is surprisingly not much larger on the rougher track, probably because the nonlinear damping characteristic of the vertical elements limits the angular suspension deviation.

Simulations were also performed where the distances both in the x and y dimensions are varied at the same time. The results show, just as for the simulations shown above, that the transmission of angular vibrations around the x axis is almost only dependent on the y dimension distance, and the reverse.

8 OPTIMIZATION OF PASSIVE SUSPENSIONS

An optimization model has been developed to optimize suspension parameters with respect to specially defined conditions and constraints. Examples of constraints may, for example, be the maximum amount of free space at different places and restrictions on the locations of the elements. The vector sum (ISO 2631) measuring the total vibration load at the driver has been used as objective function.

The optimization model is based on an evolution algorithm. The strategy, as the name indicates, is based on the biological evolution with mutations and selections.

8.1 Evolution strategy

Let μ individuals be parents to λ children. Choose the μ best individuals among the children and let them be parents to the next generation of λ children. The number of children must be more numerous than the number of parents. The best individuals can be selected among both parents and children or just among the children. To select the next generation among both children and parents may cause the evolution to reach a standstill.

A special case adaptable to technical optimization is obtained if the best individual becomes the only parent for the next generation. This strategy can be used as a search algorithm in an optimization problem when deciding a vector $\mathbf{P} = [p_1 \quad p_2 \quad \dots \quad p_n]$ minimizing $f(\mathbf{P})$ under defined constraints.

The evolution is started by stating an initial estimate $\mathbf{P}_0$. Then a new generation of estimates $\mathbf{P}_x$ is built up from

$$\mathbf{P}_x = \mathbf{P}_0 + \mathbf{Z} \quad x = 1, 2, 3, \dots, \lambda \tag{144}$$

where

$$\mathbf{Z} = (z_1 \quad z_2 \quad \dots \quad z_n) \quad \text{n = number of parameters} \tag{145}$$

$$z_i = N(0, s^2) \tag{146}$$

The estimate $\mathbf{P}_x$ giving the best value for the function is selected as $\mathbf{P}_0$ for a new generation of estimates. The procedure is repeated until $f(\mathbf{P})$ has been optimized with necessary precision (Rechenberg, 1973).

Choosing the standard deviation s may cause problems. A small s can cause the algorithm to stop at a local minimum and a big s may increase the convergence time. It is logical to assume that the optimum solution is getting closer after some evolution generations and therefore s should decrease when the optimum is assumed to be closer.

An appropriate measure of the algorithm's effectiveness is a value describing how fast the estimates are getting closer to the optimum. Rechenberg defines $\phi_{1,\lambda}$ as the expected value for the local advance in the direction of the gradient for each generation.

The expected value ($\phi_{1,\lambda}$) is naturally dependent on how $f(\mathbf{P})$ is defined. In the following, is it assumed that the values for the optimized function are equal for all points in the parameter space having the same distance to the optimum. In a multi-dimensional function, that assumption can normally be a sufficiently good approximation (Muth, 1982). The calculations will be different for other types of functions but the values for $\phi_{1,\lambda}$ correspond relatively well (Rechenberg, 1973).

$$\phi_{1,\lambda} = C_{1,\lambda} \cdot s - \frac{ns^2}{2 \cdot R_E} \tag{147}$$

$R_E = |\mathbf{P}_i - \mathbf{P}_{opt}|$ the estimate's distance to the optimum. (148)

$$C_{1,\lambda} = \sqrt{\frac{2}{\pi}} \cdot \frac{\lambda}{2^{\lambda-1}} \int_{-\infty}^{+\infty} z e^{-z^2} (1 - erf(z))^{\lambda-1} dz \tag{149}$$

where

$$erf(z) = \frac{2}{\sqrt{\pi}} \int_0^z e^{-t^2} dt \tag{150}$$

R_E is not known and must be estimated.

Numerical values for $C_{1,\lambda}$ with $\lambda = 1 - 32$ are found in Table E.

Table E. $C_{1,\lambda}$ vs λ for $\lambda = 1 - 32$

λ	$C_{1,\lambda}$	λ	$C_{1,\lambda}$	λ	$C_{1,\lambda}$	λ	$C_{1,\lambda}$
1	0	9	1.485	17	1.794	25	1.965
2	0.564	10	1.539	18	1.820	26	1.982
3	0.846	11	1.586	19	1.844	27	1.998
4	1.029	12	1.629	20	1.867	28	2.014
5	1.163	13	1.668	21	1.889	29	2.029
6	1.267	14	1.703	22	1.910	30	2.043
7	1.352	15	1.736	23	1.929	31	2.056
8	1.423	16	1.766	24	1.948	32	2.070

With normed quantities:

$$\phi^* = \frac{\phi \cdot n}{R_E} \tag{151}$$

$$s^* = \frac{s \cdot n}{R_E} \tag{152}$$

$$\phi^*_{1,\lambda} = C_{1,\lambda} \cdot s^* - \frac{1}{2} s^{*2} \tag{153}$$

$\phi^*_{1,\lambda}/\lambda$ describes the relation between the convergence speed and the number of calculations in each evolution step. Figure 81 shows $\phi^*_{1,\lambda}/\lambda$ as a function of s^*.

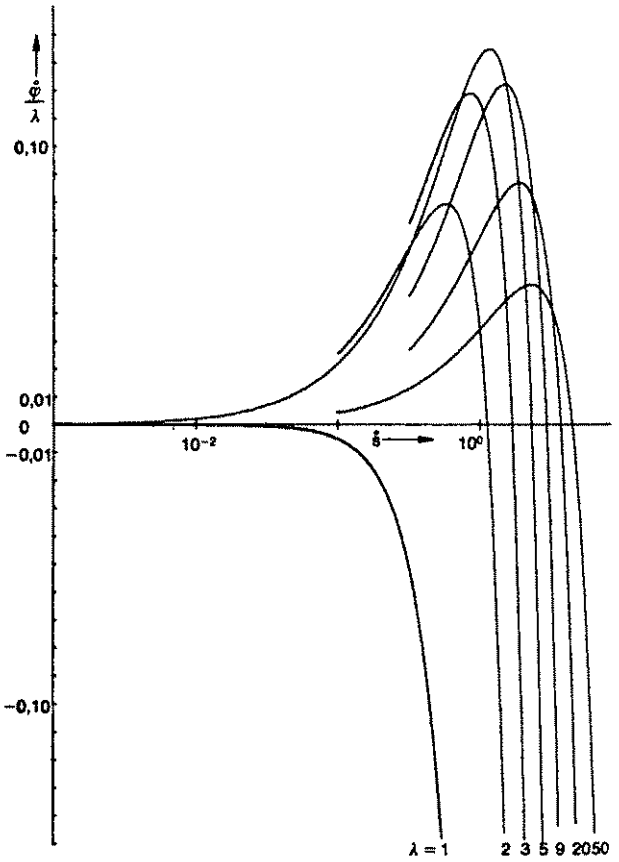

Fig. 81. $\phi^*_{1,\lambda}/\lambda$ as a function of s^* for different λ (Muth, 1982).

Figure 81 shows that for $\lambda > 1$ an area can be found where new estimates, on average, are getting closer to the optimum ($\phi^*_{1,\lambda} > 0$). This area is called the evolution window. The figure also shows that the optimum convergence speed is reached for $\lambda = 3 - 9$.

The optimum evolution step varies and therefore s has to be variable. One usable approach is to create 1/3 of the new generation with $s_{i+1} = \alpha \cdot s_i$, 1/3 with $s_{i+1} = s_i$ and 1/3 with $s_{i+1} = s_i/\alpha$. The value for s_{i+1} giving the best estimate is then chosen as s_i for the next generation. This theory is not theoretically supported but has shown good practical qualities. For α, values between 1.1 and 2.0 can be suitable.

The convergence speed is highly dependent on the choice of the standard deviation for the first generation (s_0). According to Muth, pre-experiments may be appropriate to find an optimum s_0. A value useful in practice is:

$$s_0 = M \cdot \frac{C_{1,\lambda}}{\sqrt{6 \cdot n}} \tag{154}$$

where

M = the assumed median value of the deviation of the system parameters from the optimum value.

8.1.1 Adaptation of the algorithm

The evolution method has shown good convergence behaviour, particularly for multi-dimensional optimizations, and has also been reported as easy to describe in computer software (Rechenberg, 1973, Muth, 1982, and Ahlén et al., 1982). Also other optimization methods, for example the gradient method, should have been possible to use. The evolution method was, however, mostly dependent on its capacity for optimization in many dimensions and the capacity to avoid local minimas, selected to be used in this study.

The evolution method normally works with the same standard deviations for all parts in the parameter vector. In a cab suspension the parameter magnitude is very variable and each parameter has been given an initial standard deviation of its own. This value has then been changed according to the principles described earlier. The technique is equivalent to a type of parameter scaling, and resulted in no further scaling being needed. The programming and the interpretations of the results have therefore been easier to perform.

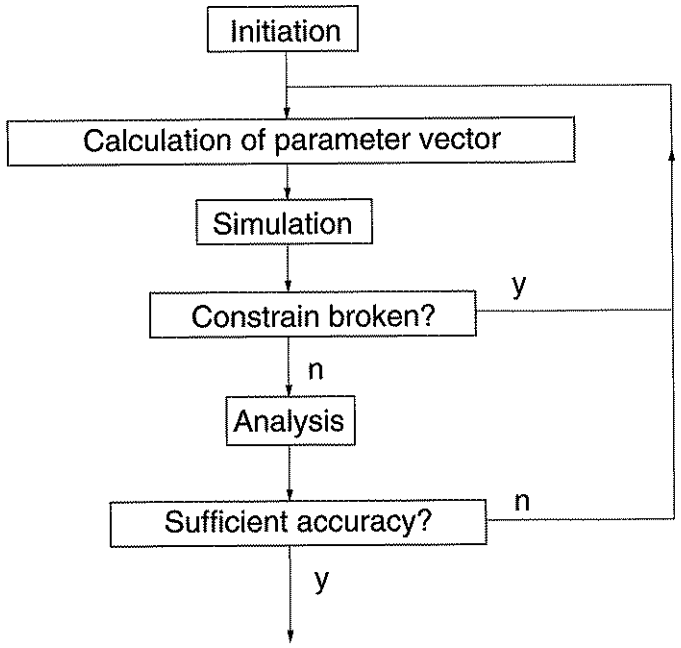

Fig. 82. Schematic description of the program algorithm.

The principle for the developed computer program is very schematically described in Figure 82. The optimization is initiated with a routine defining the initial values for parameters and standard deviations. The first parameter vector used in the simulations is also calculated.

The simulation program then reads the parameter vector and performs the defined simulations. The outputs (normally values for accelerations and suspension travel) are stored simultaneously.

After the simulation, the outputs are analysed and the results stored. Then a new parameter vector can be tested.

Nine parameter guesses have been used in each generation (n=9). When all the vectors were tested it was possible to select the "best" as parent for the next generation.

Normally the evolution has been simulated for 50 generations. In cases when the algorithm failed to converge after 50 generations, another 10-20 generations were simulated.

The general objective function is the driver's vibration load, and the available travel space has been used as constraint. Dahlberg (1979) has discussed and studied the influence of several objective functions and constraints. The standardized ISO 2631 vector sum has been used as the measure of the vibration load in this report but other objective functions, such as unweighted accelerations or jerk can easily be incorporated in the optimizations.

In the reported optimizations, constraints for the maximal allowed travel from the balanced position have been defined in one or more dimensions. When a constraint was exceeded (the travel becomes to large) the simulation was immediately interrupted. The parameter vector was exchanged for a new one, formed with the same standard deviations, and the optimization could continue. Therefore, when the "best" parameter vector is to be selected there were always 9 possibilities and none of them had broken the restriction.

The possibility to penalize the parameter combination breaking the restriction instead of exchanging it was also tried, but problems arose when the optimal solution was close to the restriction. Then, in some cases, 6-7 out of 9 of the parameter guesses were penalized. The best of the remaining 2-3 did not always bring the algorithm closer to the optimum. Therefore the algorithm became unstable and had problems in reaching the optimum.

The great amount of repetitions of the simulation program and the analysis of the result caused the calculation times for the reported optimizations to be 4-8 days depending on the amount of constraints defined. The computer used was an IBM compatible PC with 80386 and 80387 processors working with 33 MHz clock frequency.

8.2 Optimization results

8.2.1 Effects of available travel space

The purpose was to study how the possibilities to work out an effective suspension are affected by the dimensions of the available travel space. The purpose was also to study how the optimum suspension characteristics are affected when the available travel space is changed.

8.2.1.1 Assumptions

The geometry of the suspension was defined according to the geometry of the basic suspension described in Ch. 7.1.

The optimization algorithm was programmed to optimize the vertical and horizontal suspension parameters in a suspension with linear spring and nonlinear damping characteristics. The objective function was defined as the frequency weighted vibration value (ISO 2631 vector sum) measured at the cab's c.o.g. The suspension's vertical and horizontal natural frequencies, together with the nonlinear characteristics of the vertical and horizontal shock absorbers, were optimized (totally 8 parameters: f_{nH}, f_{nH}, R_{0V}, R_{0H}, $PK1_{cV}$ $PK1_{cH}$, $PK2_{cV}$, $PK2_{cH}$).

The lower limit for the horizontal natural frequency was defined to 0.5 Hz and to 0.75 Hz for the vertical direction. The low natural frequencies make it possible to design suspensions with high vibration damping potential. To avoid too large static deviations may it, however, be necessary to add some kind of slowly reacting self levelling system.

As constraint was defined a limit for the cab's deviation from the balanced position, measured at the cab's c.o.g., when driving on track 2 at 6 km/h. The vibration load in that test was estimated as the worst possible, if the driver was still able to control the vehicle. The driver had probably reduced the driving speed before this extreme vibration load appeared. The limit for the maximum deviations was varied between 0.075 and 0.125 m in the x, y and z directions.

The goal for the first study was to find a suspension working well in both normal and extremely rough conditions. The objective function was defined as the mean value of the vibration load when driving on track 1 at 12 km/h and when driving on track 2 at 6 km/h.

8.2.1.2 Results

The large number of optimized parameters resulted in many local minima being found in the objective function. In several cases it was found that repeated optimizations resulted in other optimal parameter vectors. The solutions thus cannot be considered as representing absolute minima. The differences in the objective function were, however, in no case more than 1.5 % for the different solutions.

The optimum suspension characteristics with the defined constraints are reported in Table F. The resulting vibration loads when driving with the optimized suspension on the test tracks are reported in Tables G and H and partly in Figure 83. The vibration levels in the x, y and z directions are weighted values.

Table F. Optimum suspension characteristics for the defined constraints

av. space (m)	f_{nV} (Hz)	f_{nH} (Hz)	R_{0V}	R_{0H}	$PK1_{cV}$ (m)	$PK1_{cH}$ (m)	$PK2_{cV}$	$PK2_{cH}$
0.075	0.75	0.50	0.94	1.08	0.052	0.055	1.47	2.50
0.10	0.75	0.50	0.74	0.82	0.089	0.085	2.40	3.40
0.125	0.75	0.50	0.64	0.67	0.141	0.123	2.78	5.85

Table G. Vibration levels when driving with the optimized suspension on track 1 at 12 km/h

av. space (m)	x (m/s^2)	y (m/s^2)	z (m/s^2)	vector sum (m/s^2)	xr (rad/s^2)	yr (rad/s^2)
0.075	0.56	0.82	0.81	1.60	0.71	0.83
0.10	0.54	0.80	0.64	1.50	0.67	0.72
0.125	0.54	0.81	0.59	1.49	0.68	0.67

Table H. Vibration levels when driving with the optimized suspension on track 2 at 6 km/h

av. space (m)	x (m/s^2)	y (m/s^2)	z (m/s^2)	vector sum (m/s^2)	xr (rad/s^2)	yr (rad/s^2)
0.075	1.43	0.97	2.20	3.27	1.22	1.77
0.10	1.23	0.92	1.95	2.90	1.06	1.65
0.125	1.10	0.88	1.74	2.63	0.87	1.50

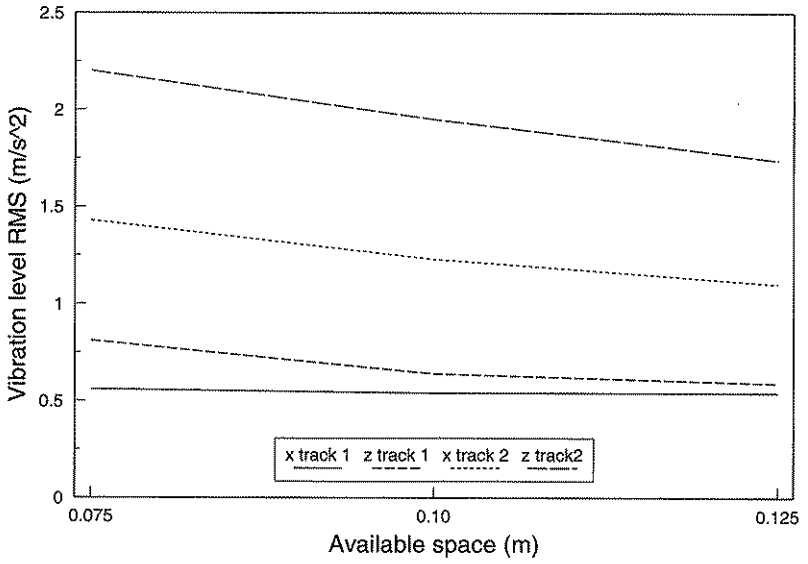

Fig. 83. Vibration levels when driving on the test tracks with the suspensions optimized for different amounts of free available travel space.

8.2.1.3 Conclusions

The results show, as expected, that the possibilities to work out a suspension with good vibration damping capacity increase when the available travel space is increased.

The optimum natural frequencies in both the vertical and horizontal directions are located at the defined lower limits. The optimum damping in the balanced position (R_{OV} and R_{OH}) decreases when more space is available. At the same time, $PK1_{cV}$ and $PK1_{cH}$ are increasing. The results also show that the optimum suspension becomes more progressive (bigger $PK2_{cV}$ and $PK2_{cH}$) when the available space is increased.

The objective function was defined as the average value of the vibration loads when driving on the two tracks. The vibration loads were much higher when driving on the rougher track, and therefore a 5 % decrease of the value on this track influenced the objective function much more than the same relative decrease on the smoother track. The optimized suspension is therefore designed to be more effective on the rougher track, which can be seen in the relative decrease of the vector sum being much higher on that track (19 % and 7 %) when the available space is increased by 0.05 m. For the smoother track there is no vibration load decrease at all for some dimensions, when the suspensions are optimized for more available space.

8.2.2 Suspension optimized for lower average vibration loads

8.2.2.1 Assumptions

In the optimizations described earlier the objective function was defined as the average of the vibration load on the smoother and on the rougher track. For normal driving situations, the smoother test track is probably a better description of the average compared to the very rough test track no. 2. The vibration loads are only exceptionally as large as when driving on track 2 at 6 km/h.

This study was performed to find out the optimum suspension characteristics when the suspension damping capacity on the smoother track was weighted 4 times higher than the capacity on the rougher track. Then it is possible to calculate how the optimum characteristics change when more attention is paid to the damping capacity in more normal driving situations.

All other assumptions are defined in the same way as for the optimizations described earlier. The maximum permitted deviation from the balanced position was constrained to 0.10 m in each direction measured at the cab's c.o.g.

8.2.2.2 Results

The optimum suspension parameters are shown in Table I. The vibration levels for the simulated driving over the two test tracks are shown in Table J.

Table I. Optimum suspension characteristics under defined constraints

f_{nV} (Hz)	f_{nH} (Hz)	R_{0V}	R_{0H}	$PK1_{cV}$ (m)	$PK1_{cH}$ (m)	$PK2_{cV}$	$PK2_{cH}$
0.75	0.5	0.59	0.74	0.078	0.081	3.96	1.48

Table J. Vibration levels when driving with the optimum suspension on the different test tracks

track	velocity (km/h)	x (m/s^2)	y (m/s^2)	z (m/s^2)	vector sum (m/s^2)	xr (rad/s^2)	yr (rad/s^2)
1	12	0.54	0.81	0.59	1.47	0.68	0.68
2	6	1.25	0.92	2.04	2.98	1.27	1.88

8.2.2.3 Conclusions

The suspension optimized in this study has, logically, better damping capacity on the smoother track than the suspension described in Ch. 8.2.1. The suspension's capacity on the rougher surface is, also logically, poorer than the earlier optimized suspension. The changes are, however, rather small in both cases.

The changes are more marked for the suspension parameters. The suspension optimized for lower average vibration load has, in the vertical direction, lower damping around the balanced position, but with a more marked progressiveness. The progressiveness in the vertical directions is, instead, decreasing.

8.2.3 Optimization of linear suspensions

8.2.3.1 Assumptions

The suspensions optimized up to now have had linear spring and nonlinear damping characteristics. Optimizations have also been performed to study the characteristics of a linear suspension meeting the same demands as in the earlier studies. The vibration damping capacity for the two principles can also be compared to get an understanding of the advantages with nonlinear elements.

The optimized parameters in this study were the suspension's vertical and horizontal natural frequency and the vertical and horizontal degree of damping. The other assumptions used were the same as in the study in Ch. 8.2.1, with 0.10 m available space.

8.2.3.2 Results

The optimized suspension is described in Table K. The vibration levels for the simulated driving over the test tracks are shown in Table L.

Table K. The optimum suspension characteristics with the constraints defined above

f_{nV} (Hz)	f_{nH} (Hz)	R_V	R_H
0.75	0.5	1.19	1.23

Table L. Vibration levels when driving with the optimum suspension on the different test tracks

track	velocity (km/h)	x (m/s^2)	y (m/s^2)	z (m/s^2)	vector sum (m/s^2)	xr (rad/s^2)	yr (rad/s^2)
1	12	0.56	0.80	0.81	1.59	0.71	0.82
2	6	1.37	0.96	1.97	3.06	0.96	1.49

8.2.3.3 Conclusions

The linear suspension optimized with the 0.10 m space constraint is very heavily damped. The natural frequencies in both dimensions still become the same as the values defined as lower limits.

The optimized linear suspension gets, as expected, lower vibration damping capacity than the nonlinear suspension optimized for the same amount of available space. The weighted value (vector sum) increases by 6 % on the smoother track and by 5.5 % on the rougher track.

8.2.4 Effects of the lower limits for natural frequencies

8.2.4.1 Assumptions

The results from the optimizations performed earlier showed that the optimal natural frequencies are the same as the ones defined as lower limits. That indicates that the magnitude of the limits influences the possibilities for vibration damping.

A decreased horizontal natural frequency gives rise to larger static suspension travel when driving on side slopes. A decreased vertical natural frequency gives larger static travel when the driver's weight varies or when driving with a passenger in the cab.

The purpose of this optimization was to study the changes for the optimum suspension characteristics when the lower limits for natural frequencies were increased by 0.25 Hz in each direction.

The vibration levels for the two test tracks were equally weighted and the optimization was performed for 0.10 meter available space. The other assumptions and constraints remained unaltered from Ch. 8.2.1.

8.2.4.2 Results

The optimized suspension is described in Table M. The vibration levels when driving on the both tracks are shown in Table N.

Table M. The optimum suspension with the constraints defined above

f_{nV} (Hz)	f_{nH} (Hz)	R_{0V}	R_{0H}	$PK1_{cV}$ (m)	$PK1_{cH}$ (m)	$PK2_{cV}$	$PK2_{cH}$
1.00	0.75	0.67	0.82	0.110	0.155	1.80	3.94

Table N. Vibration loads when driving with the optimum suspension on the different test tracks

track	velocity (km/h)	x (m/s^2)	y (m/s^2)	z (m/s^2)	vector sum (m/s^2)	xr (rad/s^2)	yr (rad/s^2)
1	12	0.65	0.95	0.77	1.79	0.83	0.83
2	6	1.59	1.12	2.23	3.52	1.17	1.74

8.2.4.3 Conclusions

The lower limits defined for the natural frequencies have major effects on the possibilities to work out an effective suspension. Increasing this value by 0.25 Hz in each direction results in an increasing vibration load in all directions. The increase is especially marked when driving on the very rough surface.

It is interesting that the optimum suspension with the increased limits for the natural frequencies, in contrast to the suspensions optimized earlier, did not use the whole available travel space in the x and y directions. When driving with the optimum suspension on track 2 at 6 km/h the maximum travel was only 0.075 m in the x and 0.080 m in the y direction.

9 SUSPENSIONS WITH ACTIVE CHARACTERISTICS

Active suspensions can continuously supply and modulate the flow of energy. Thus, in an active system, forces can be generated which do not depend upon energy previously stored by the suspension. Therefore an active suspension has a very high potential for reducing the driver's vibration load while still maintaining short suspension travel.

Active suspensions consist of actuators such as force or torque generators, measurement and sensing devices, and a feedback controller to provide control commands for the actuators. Active suspensions also require an external power source. The elements are interconnected in such a fashion that some modes of the motion of the vehicle are sensed. These sensed signals are then conditioned through the feedback controller and command signals for the actuators are generated, thus forming a closed loop control system.

The development and analysis of LQG based active cab suspensions is described in this chapter. The vibration damping characteristics of the suspensions are studied. The change in characteristics when the suspension's configuration or design variables are changed is also studied. The discussion is based on the geometry for the basic suspension described in Ch. 7.1.

Linear quadratic optimal control theory has been used to solve the optimization problem. This method provides a compact analytical solution with relatively low design and computing time and the stability of the system is guaranteed. Since the results of an optimization process is a controller which considers and feedbacks all the system states, it offers advantages beyond those of any classical controller structure. Among the disadvantages of this approach are the necessity to measure or to estimate all state variables and the limited choice of performance index, which must be a quadratic function of state and control variables.

9.1 Discrete system description

The active controller can be described both in continuous and discrete automatic control theory. The progress for the digital computer technique has resulted in discrete controllers becoming cheaper, easier to program and more reliable. Most of the more advanced automatic controls are therefore now based on discrete theory and controllers.

The theory for the adaptive time variant controllers described in the next chapter are directly developed in discrete theory. Also the time invariant controllers described in this chapter are most likely to be implemented in discrete technique. Consequently, all the controllers described in this study are based on discrete theory.

The discrete state space model structure used when designing linear quadratic regulators and estimators can be described:

$$\mathbf{x}^s(t+1) = \mathbf{F}\mathbf{x}^s(t) + \mathbf{G}^u\mathbf{u}(t) + \mathbf{G}^w\mathbf{w}(t) \tag{155}$$

where
$\mathbf{w}(t)$ = white noise vector with the covariance matrix $\mathbf{R}_1$.

The objective for the following part is to convert the continuous time description of the the system to the discrete form, usable for the controller gain calculations.

The cab suspension system with weighted outputs, which is a continuous time system, can be described as in Ch. 5.2.3.2:

$$\dot{\mathbf{x}}_w^s = \mathbf{A}_w \mathbf{x}_w^s + \mathbf{B}_w^u \mathbf{u}_w + \mathbf{B}_w^v \mathbf{v}_w \tag{156}$$

with

$$(\mathbf{v}_w)^T = (\ddot{x}_b^d \quad \ddot{y}_b^d \quad \ddot{z}_b^d \quad \dot{xr}_b^d \quad \dot{yr}_b^d) \tag{157}$$

The model can be converted from continuous to discrete time assuming a zero order hold on the inputs, which means that they are assumed to be piecewise constant during the sample time T_s:

$$\mathbf{x}_w^s(t+1) = \mathbf{F}_w \mathbf{x}_w^s(t) + \mathbf{G}_w^u \mathbf{u}_w(t) + \mathbf{G}_w^v \mathbf{v}_w(t) \tag{158}$$

where

$$\mathbf{F}_w = e^{\mathbf{A}_w T_s} \tag{159}$$

$$\mathbf{G}_w^u = \int_0^{T_s} e^{\mathbf{A}_w t} \mathbf{B}_w^u dt \tag{160}$$

$$\mathbf{G}_w^v = \int_0^{T_s} e^{\mathbf{A}_w t} \mathbf{B}_w^v dt \tag{161}$$

The zero order hold assumption for the disturbance inputs is a simplification but the high sample frequency in relation to the disturbance's frequency content makes the errors very small.

In the calculations of feedback and observer gains, the disturbance vector ($\mathbf{v}_w$) can be approximated as the outputs from five ARMA models driven by five white noise sources. The ARMA structure can be described by:

$$A(q^{-1})y(t) = C(q^{-1})e(t) \tag{162}$$

where A and C are polynomials in the delay operator q^{-1}:

$$A(q^{-1}) = 1 + a_1 q^{-1} + \ldots + a_{na} q^{-na} \tag{163}$$

$$C(q^{-1}) = 1 + c_1 q^{-1} + \ldots + c_{nc} q^{-nc} \tag{164}$$

e = white noise with the variance σ_e^2

na and nc are the orders of the relevant polynomials.

Explicity, (165)

$$y(t)+a_1y(t-1)+\ldots+a_{na}y(t-na)=e(t)+c_1e(t-1)+\ldots+c_{nc}e(t-nc)$$

A first order model can only give a rough approximation of the characteristics of the signals, while a higher order model can give a more detailed description, including, for example, the positions of resonance peaks, etc. Models of higher orders results, however, in more complicated controllers, not always offering higher vibration damping potential.

In this study the disturbance signal for each dimension is described by an independent ARMA model, not including any cross correlation with the disturbances in the other dimensions. This is a simplification, while the acceleration in the x direction normally is correlated to the angular movements around the y axis, etc. Controllers based on more complicated disturbance models, also including the cross correlation and directly identified in state space form, have also been tested, but the vibration damping characteristics were not at all improved. The identification algorithms then necessary are rather complicated, and very difficult to implement in the recursive adaptive controller gain calculation described in Ch. 10.

The ARMA model can easily be converted to discrete state space observable canonical form:

$$\mathbf{x}^s(t+1)=\begin{pmatrix}-a_1 & 1 & \ldots & 0\\ -a_2 & 0 & \ldots & 0\\ \ldots & \ldots & \ldots & \ldots\\ -a_{na} & 0 & \ldots & 0\end{pmatrix}\mathbf{x}^s(t)+\begin{pmatrix}c_1-a_1\\ c_2-a_2\\ \ldots\\ c_{nc}-a_{na}\end{pmatrix}e(t) \tag{166}$$

$$y(t)=(1\quad 0\quad \ldots\quad 0)\mathbf{x}^s(t)+e(t) \tag{167}$$

If first order models are used to describe the disturbances then:

$$\mathbf{x}^s(t+1)=\mathbf{F}_e\mathbf{x}^s(t)+\mathbf{G}_e^e\mathbf{e}(t) \tag{168}$$

$$\mathbf{v}_w(t)=\mathbf{I}^{5*5}\mathbf{x}^s(t)+\mathbf{I}^{5*5}\mathbf{e}(t) \tag{169}$$

where

$\mathbf{I}^{n*n}$ = an identity matrix of order n

$\mathbf{e}(t)$ = a vector with discrete white noise with the covariance matrix:

$$\mathbf{R}_e = \begin{pmatrix} \sigma^2_{e\dot{x}} & 0 & 0 & 0 & 0 \\ 0 & \sigma^2_{e\dot{y}} & 0 & 0 & 0 \\ 0 & 0 & \sigma^2_{e\dot{z}} & 0 & 0 \\ 0 & 0 & 0 & \sigma^2_{ex\dot{r}} & 0 \\ 0 & 0 & 0 & 0 & \sigma^2_{ey\dot{r}} \end{pmatrix} \tag{170}$$

$$\mathbf{F}_e = \begin{pmatrix} -a_{1\dot{x}} & 0 & 0 & 0 & 0 \\ 0 & -a_{1\dot{y}} & 0 & 0 & 0 \\ 0 & 0 & -a_{1\dot{z}} & 0 & 0 \\ 0 & 0 & 0 & -a_{1x\dot{r}} & 0 \\ 0 & 0 & 0 & 0 & -a_{1y\dot{r}} \end{pmatrix} \tag{171}$$

$$\mathbf{G}^e_e = \begin{pmatrix} c_{1\dot{x}} - a_{1\dot{x}} & 0 & 0 & 0 & 0 \\ 0 & c_{1\dot{y}} - a_{1\dot{y}} & 0 & 0 & 0 \\ 0 & 0 & c_{1\dot{z}} - a_{1\dot{z}} & 0 & 0 \\ 0 & 0 & 0 & c_{1x\dot{r}} - a_{1x\dot{r}} & 0 \\ 0 & 0 & 0 & 0 & c_{1y\dot{r}} - a_{1y\dot{r}} \end{pmatrix} \tag{172}$$

With second order models becomes:

$$\mathbf{F}_e = \begin{pmatrix} -a_{1\dot{x}} & 1 & 0 & 0 & 0 & 0 & 0 & 0 & 0 & 0 \\ -a_{2\dot{x}} & 0 & 0 & 0 & 0 & 0 & 0 & 0 & 0 & 0 \\ 0 & 0 & -a_{1\dot{y}} & 1 & 0 & 0 & 0 & 0 & 0 & 0 \\ 0 & 0 & -a_{2\dot{y}} & 0 & 0 & 0 & 0 & 0 & 0 & 0 \\ 0 & 0 & 0 & 0 & -a_{1\dot{z}} & 1 & 0 & 0 & 0 & 0 \\ 0 & 0 & 0 & 0 & -a_{2\dot{z}} & 0 & 0 & 0 & 0 & 0 \\ 0 & 0 & 0 & 0 & 0 & 0 & -a_{1\dot{r}x} & 1 & 0 & 0 \\ 0 & 0 & 0 & 0 & 0 & 0 & -a_{2\dot{r}x} & 0 & 0 & 0 \\ 0 & 0 & 0 & 0 & 0 & 0 & 0 & 0 & -a_{1\dot{r}y} & 1 \\ 0 & 0 & 0 & 0 & 0 & 0 & 0 & 0 & -a_{2\dot{r}y} & 0 \end{pmatrix} \tag{173}$$

$$\mathbf{G}_e^e = \begin{pmatrix} c_{1\bar{x}} - a_{1\bar{x}} & 0 & 0 & 0 & 0 \\ c_{2\bar{x}} - a_{2\bar{x}} & 0 & 0 & 0 & 0 \\ 0 & c_{1\bar{y}} - a_{1\bar{y}} & 0 & 0 & 0 \\ 0 & c_{2\bar{y}} - a_{2\bar{y}} & 0 & 0 & 0 \\ 0 & 0 & c_{1\bar{z}} - a_{1\bar{z}} & 0 & 0 \\ 0 & 0 & c_{2\bar{z}} - a_{2\bar{z}} & 0 & 0 \\ 0 & 0 & 0 & c_{1\bar{x}r} - a_{1\bar{x}r} & 0 \\ 0 & 0 & 0 & c_{2\bar{x}r} - a_{2\bar{x}r} & 0 \\ 0 & 0 & 0 & 0 & c_{1\bar{y}r} - a_{1\bar{y}r} \\ 0 & 0 & 0 & 0 & c_{2\bar{y}r} - a_{2\bar{y}r} \end{pmatrix} \tag{174}$$

$$\mathbf{v}_w(t) = \begin{pmatrix} 1 & 0 & 0 & 0 & 0 & 0 & 0 & 0 & 0 & 0 \\ 0 & 0 & 1 & 0 & 0 & 0 & 0 & 0 & 0 & 0 \\ 0 & 0 & 0 & 0 & 1 & 0 & 0 & 0 & 0 & 0 \\ 0 & 0 & 0 & 0 & 0 & 0 & 1 & 0 & 0 & 0 \\ 0 & 0 & 0 & 0 & 0 & 0 & 0 & 0 & 1 & 0 \end{pmatrix} \mathbf{x}^s(t) + \mathbf{I}^{5*5}\mathbf{e}(t) \tag{175}$$

The formulas for third order models are just extensions of the second order formulas.

To get the form first described in this chapter, used when calculating the feedback and observer gains, we have to combine the discrete dynamic system model with the disturbance models. For first order disturbance models:

$$\mathbf{x}^s(t+1) = \begin{pmatrix} \mathbf{F}_w & \mathbf{G}_w^v \\ \mathbf{0}^{5*21} & \mathbf{F}_e \end{pmatrix} \mathbf{x}^s(t) + \begin{pmatrix} \mathbf{G}_w^u \\ \mathbf{0}^{5*6} \end{pmatrix} \mathbf{u}_w(t) + \begin{pmatrix} \mathbf{G}_w^v \\ \mathbf{G}_e^e \end{pmatrix} \mathbf{e}(t) \tag{176}$$

where

$$(\mathbf{x}^s)^T(1{:}13) = (x_c^d - x_b^d \quad y_c^d - y_b^d \quad z_c^d - z_b^d \quad \dot{x}_c^d \quad \dot{y}_c^d \quad z_c^d \quad xr_c^d \quad \dot{x}r_c^d \quad yr_c^d \quad \dot{y}r_c^d \quad \dot{x}_b^d \quad \dot{y}_b^d \quad \dot{z}_b^d) \tag{177}$$

$$(\mathbf{x}^s)^T(14{:}26) = (xr_b^d \quad yr_b^d \quad x_{H1}^s \quad x_{H2}^s \quad y_{H1}^s \quad y_{H2}^s \quad z_{H1}^s \quad z_{H2}^s \quad \dot{x}_b^d \quad \dot{y}_b^d \quad \dot{z}_b^d \quad \dot{x}r_b^d \quad \dot{y}r_b^d) \tag{178}$$

if each variable's time dependency is not written out.

For second order disturbance models:

$$\mathbf{x}^s(t+1) = \begin{pmatrix} \mathbf{F}_w & \mathbf{G}_w^v(:,1) & \mathbf{0}^{21*1} & \mathbf{G}_w^v(:,2) & \mathbf{0}^{21*1} & \mathbf{G}_w^v(:,3) & \mathbf{0}^{21*1} & \mathbf{G}_w^v(:,4) & \mathbf{0}^{21*1} & \mathbf{G}_w^v(:,5) & \mathbf{0}^{21*1} \\ \mathbf{0}^{10*21} & \mathbf{F}_e \end{pmatrix} \mathbf{x}^s(t) + \begin{pmatrix} \mathbf{G}_w^u \\ \mathbf{0}^{10*6} \end{pmatrix} \mathbf{u}_w(t) + \begin{pmatrix} \mathbf{G}_w^v \\ \mathbf{G}_e^e \end{pmatrix} \mathbf{e}(t) \tag{179}$$

9.2 Linear quadratic regulator design

9.2.1 Theory

Assume again the system:

$$\mathbf{x}^s(t+1) = \mathbf{F}\mathbf{x}^s(t) + \mathbf{G}^u\mathbf{u}(t) + \mathbf{G}^w\mathbf{w}(t) \tag{180}$$

Assume also that the system matrices are time invariant and that $\mathbf{w}(t)$is a vector with uncorrelated zero mean stochastic (white) noise.

Let $\mathbf{y}^c(t)$ be the vector with controlled variables:

$$\mathbf{y}^c(t) = \mathbf{H}^c\mathbf{x}^s(t) \tag{181}$$

To minimize the function:

$$J = E\left((\mathbf{y}^c)^T(t)\mathbf{Q}_3\mathbf{y}^c(t)\right) + E(\mathbf{u}^T(t)\mathbf{Q}_2\mathbf{u}(t)) \tag{182}$$

choose the input according to the control law:

$$\mathbf{u}(t) = -\mathbf{K}(t)\mathbf{x}^s(t) \tag{183}$$

where

$$\mathbf{K}(t) = \left[(\mathbf{G}^u)^T\mathbf{S}(t+1)\mathbf{G}^u + \mathbf{Q}_2\right]^{-1}(\mathbf{G}^u)^T\mathbf{S}(t+1)\mathbf{F} \tag{184}$$

and $\mathbf{S}(t+1)$ is the symmetrical positive semidefinite solution of the difference equation:

$$\mathbf{S}(t-1) = \mathbf{F}^T\mathbf{S}(t)\mathbf{F} + \mathbf{Q}_1 - \mathbf{F}^T\mathbf{S}(t)\mathbf{G}^u\left[(\mathbf{G}^u)^T\mathbf{S}(t)\mathbf{G}^u + \mathbf{Q}_2\right]^{-1}(\mathbf{G}^u)^T\mathbf{S}(t)\mathbf{F} \tag{185}$$

with the terminal value = $\mathbf{Q}_1$

$$\mathbf{Q}_1 = (\mathbf{H}^c)^T\mathbf{Q}_3\mathbf{H}^c \tag{186}$$

If the system is either uniformly completely controllable and uniformly completely reconstructible or exponentially stable, $\mathbf{S}(t)$ converges to a matrix $\overline{\mathbf{S}}$. $\overline{\mathbf{S}}$ is the solution of the equation:

$$\overline{\mathbf{S}} = \mathbf{F}^T\overline{\mathbf{S}}\mathbf{F} + \mathbf{Q}_1 - \mathbf{F}^T\overline{\mathbf{S}}\mathbf{G}^u\left[(\mathbf{G}^u)^T\overline{\mathbf{S}}\mathbf{G}^u + \mathbf{Q}_2\right]^{-1}(\mathbf{G}^u)^T\overline{\mathbf{S}}\mathbf{F} \tag{187}$$

Normally, in the time invariant case, $\overline{\mathbf{S}}$ is used to calculate $\mathbf{K}$ which then also becomes time invariant (Kwakernaak & Sivan, 1972; Andersson & Moore, 1989).

9.2.2 Application at the suspension model

The linear quadratic regulator design theory is directly applicable on the cab suspension model, to calculate optimum feedback gains for the controller. The system is not completely controllable, depending on the states describing the frame movements, but all the uncontrollable modes are stable.

The controlled variables $\mathbf{y}^c$ have to be chosen as linear combinations of the states. The weighted acceleration values in the x, y and z directions (x_{16}^s, x_{18}^s and x_{20}^s) have to be limited to control the vibration load in the cab. The suspension travel in the linear directions (x_1^s, x_2^s and x_3^s) must also be limited, just as the angular deviations between the cab and the frame ($x_7^s - x_{14}^s$ and $x_9^s - x_{15}^s$). The cab's angular accelerations are not described by any model states. Instead, the angular velocities (x_8^s and x_{10}^s) can be penalized to limit the angular movements. In order to get a controller striving to keep the cab horizontal, the cab's inclinations in relation to the x and y axis can be penalized.

For a controller, not striving to keep the cab horizontal, $\mathbf{y}^c(t)$ can then be chosen as:

$$(\mathbf{y}^c(t))^T = (x_c^d(t) - x_b^d(t) \quad y_c^d(t) - y_b^d(t) \quad z_c^d(t) - z_b^d(t) \quad xr_c^d(t) - xr_b^d(t) \quad yr_c^d(t) - yr_b^d(t) \quad \dot{x}_w^d(t) \quad \dot{y}_w^d(t) \quad \dot{z}_w^d(t) \quad \dot{xr}_c^d(t) \quad \dot{yr}_c^d(t)) \tag{188}$$

which gives for the system with first order disturbance models:

$$\mathbf{H}^c = \begin{pmatrix}
1 & 0 & 0 & 0 & 0 & 0 & 0 & 0 & 0 & 0 & 0 & 0 & 0 & 0 & 0 & 0 & 0 & 0 & 0 & 0 & 0 & 0 & 0 & 0 & 0 \\
0 & 1 & 0 & 0 & 0 & 0 & 0 & 0 & 0 & 0 & 0 & 0 & 0 & 0 & 0 & 0 & 0 & 0 & 0 & 0 & 0 & 0 & 0 & 0 & 0 \\
0 & 0 & 1 & 0 & 0 & 0 & 0 & 0 & 0 & 0 & 0 & 0 & 0 & 0 & 0 & 0 & 0 & 0 & 0 & 0 & 0 & 0 & 0 & 0 & 0 \\
0 & 0 & 0 & 0 & 0 & 0 & 1 & 0 & 0 & 0 & 0 & 0 & 0 & -1 & 0 & 0 & 0 & 0 & 0 & 0 & 0 & 0 & 0 & 0 & 0 \\
0 & 0 & 0 & 0 & 0 & 0 & 0 & 0 & 1 & 0 & 0 & 0 & 0 & 0 & -1 & 0 & 0 & 0 & 0 & 0 & 0 & 0 & 0 & 0 & 0 \\
0 & 0 & 0 & 0 & 0 & 0 & 0 & 0 & 0 & 0 & 0 & 0 & 0 & 0 & 0 & 1 & 0 & 0 & 0 & 0 & 0 & 0 & 0 & 0 & 0 \\
0 & 0 & 0 & 0 & 0 & 0 & 0 & 0 & 0 & 0 & 0 & 0 & 0 & 0 & 0 & 0 & 1 & 0 & 0 & 0 & 0 & 0 & 0 & 0 & 0 \\
0 & 0 & 0 & 0 & 0 & 0 & 0 & 0 & 0 & 0 & 0 & 0 & 0 & 0 & 0 & 0 & 0 & 1 & 0 & 0 & 0 & 0 & 0 & 0 & 0 \\
0 & 0 & 0 & 0 & 0 & 0 & 0 & 1 & 0 & 0 & 0 & 0 & 0 & 0 & 0 & 0 & 0 & 0 & 0 & 0 & 0 & 0 & 0 & 0 & 0 \\
0 & 0 & 0 & 0 & 0 & 0 & 0 & 0 & 0 & 1 & 0 & 0 & 0 & 0 & 0 & 0 & 0 & 0 & 0 & 0 & 0 & 0 & 0 & 0 & 0
\end{pmatrix} \tag{189}$$

The main design variables are then the penalty matrices $\mathbf{Q}_3$ and $\mathbf{Q}_2$. The values in these matrices can be varied to reach different suspension characteristics, with controller stability always guaranteed. It is very difficult to get a feeling for the size of the variables in the penalty matrices without iterative simulations with different penalties defined.

One way of getting physically more understandable dimensions for the penalties is to define the maximum permitted value for each of the controlled variables ($y_1^{cmax} - y_n^{cmax}$). These values are then inverted to get the values used in the penalty matrices:

$$\mathbf{Q}_3 = \begin{pmatrix}
\left(\frac{1}{y_1^{cmax}}\right)^2 & 0 & \dots & 0 \\
0 & \left(\frac{1}{y_2^{cmax}}\right)^2 & \dots & 0 \\
\dots & \dots & \dots & \dots \\
0 & 0 & \dots & \left(\frac{1}{y_n^{cmax}}\right)^2
\end{pmatrix} \tag{190}$$

where n = the number of controlled variables.

The input penalty matrix $\mathbf{Q}_2$ is normally a diagonal matrix. High input penalties can be used to decrease the need for high power inputs and to create a smoother controller in a system with limited power supply. $\mathbf{Q}_2$ can be calculated from:

$$\mathbf{Q}_2 = \begin{pmatrix} \left(\frac{1}{u_1^{\max}}\right)^2 & 0 & \dots & 0 \\ 0 & \left(\frac{1}{u_2^{\max}}\right)^2 & \dots & 0 \\ \dots & \dots & \dots & \dots \\ 0 & 0 & \dots & \left(\frac{1}{u_n^{\max}}\right)^2 \end{pmatrix} \tag{191}$$

where n = the number of inputs.

The theory shows that the feedback gain calculation can be divided into one part dependent on the basic system and one part dependent on the disturbances (Kwakernaak & Sivan, 1972). In the studied system the feedback gains of states 1-21 are therefore not affected by the variations of the parameters in the ARMA model describing the properties of the disturbances.

9.3 Linear quadratic estimator design

Implementation of the feedback control laws described in the previous chapter requires that the state vector $\mathbf{x}^s$ is available at time t for construction of the control signal. As the states are normally not perfectly measurable, an alternative control law can be used. The feedback can be calculated from the state estimates produced by an observer. The observer uses the signals that can be measured to estimate the total state vector. The certainty equivalence principle then states that it is the optimum to use the estimated parameters when calculating the feedback.

9.3.1 Theory

Assume once again the system:

$$\mathbf{x}^s(t+1) = \mathbf{F}\mathbf{x}^s(t) + \mathbf{G}^u\mathbf{u}(t) + \mathbf{G}^w\mathbf{w}(t) \tag{192}$$

Assume also a vector $\mathbf{y}^m$ with measurable linear combinations of the states:

$$\mathbf{y}^m(t) = \mathbf{H}^m\mathbf{x}^s(t) + \mathbf{j}(t) \tag{193}$$

where $\mathbf{j}(t)$ is the measurement noise vector.

The measurement noise is assumed to be white with the covariance matrix $\mathbf{R}_2$.

Assume the observer configuration:

$$\hat{\mathbf{x}}^s(t+1) = \mathbf{F}\hat{\mathbf{x}}^s(t) + \mathbf{G}^u\mathbf{u}(t) + \mathbf{L}(t)\left(\mathbf{y}^m(t) - \mathbf{H}^m\hat{\mathbf{x}}^s(t)\right) \tag{194}$$

where

$\hat{\mathbf{x}}^s$ = the estimated state vector

$\mathbf{L}(t)$ = the observer gain matrix

The feedback is then decided by:

$$\mathbf{u}(t) = -\mathbf{K}(t)\hat{\mathbf{x}}^s(t) \tag{195}$$

To minimize the covariance matrix for the estimation error:

$$\tilde{\mathbf{x}}^s(t+1) = \mathbf{x}^s(t+1) - \hat{\mathbf{x}}^s(t+1) \tag{196}$$

choose $\mathbf{L}(t)$ as:

$$\mathbf{L}(t) = \mathbf{F}\mathbf{P}(t)(\mathbf{H}^m)^T\left[\mathbf{H}^m\mathbf{P}(t)(\mathbf{H}^m)^T + \mathbf{R}_2\right]^{-1} \tag{197}$$

where $\mathbf{P}(t)$ is iterated from the Riccatti equation:

$$\mathbf{P}(t+1) = \mathbf{F}\mathbf{P}(t)\mathbf{F}^T + \mathbf{R}_1 - \mathbf{F}\mathbf{P}(t)(\mathbf{H}^m)^T\left[\mathbf{H}^m\mathbf{P}(t)(\mathbf{H}^m)^T + \mathbf{R}_2\right]^{-1}\mathbf{H}^m\mathbf{P}(t)(\mathbf{F})^T \tag{198}$$

with

$$\mathbf{R}_1 = (\mathbf{G}^w)^T\mathbf{R}_e\mathbf{G}^w \tag{199}$$

If the system is stabilizable, all states are detectable from the measured variables and all matrices in the Riccatti equation are time invariant $\mathbf{P}(t)$ converge to the constant matrix $\overline{\mathbf{P}}$ when t tends towards infinity. $\overline{\mathbf{P}}$ then becomes the solution of the matrix equation:

$$\overline{\mathbf{P}} = \mathbf{F}\overline{\mathbf{P}}\mathbf{F}^T + \mathbf{R}_1 - \mathbf{F}\overline{\mathbf{P}}(\mathbf{H}^m)^T\left[\mathbf{H}^m\overline{\mathbf{P}}(\mathbf{H}^m)^T + \mathbf{R}_2\right]^{-1}\mathbf{H}^m\overline{\mathbf{P}}(\mathbf{F})^T \tag{200}$$

Then $\mathbf{L}(t)$ becomes time invariant and constant: $\mathbf{L}$.

The observer above, often described as the Kalman Predictor, produces the best estimate in a least square sense with the measured variables known up to $\mathbf{y}^m(t)$. If also $\mathbf{y}^m(t+1)$ is known when estimating $\hat{\mathbf{x}}^s(t+1)$, the Kalman Filter theory can be used. The observer structure becomes the same but with $\mathbf{L}$ calculated from:

$$\mathbf{L} = \overline{\mathbf{P}}(\mathbf{H}^m)^T\left[\mathbf{H}^m\overline{\mathbf{P}}(\mathbf{H}^m)^T + \mathbf{R}_2\right]^{-1} \tag{201}$$

The calculation to obtain the optimum observer has a lot in common with the calculations of the optimal controller feedback gains. The so-called duality between the problems in described in numerous references (see for example Kwakernaak and Sivan, 1972). The duality makes it also possible to use the same computer algorithms to solve the problems.

9.3.2 Application at the suspension model

Some of the states in the cab suspension model can be expensive or difficult to measure. It is then better to use the observer technique described above to estimate the state vector from measurements of some of the most easily measured variables. The choice of measured variables must, however, be done so that all the states are detectable from these

variables. To get an observer working well also in the real, not perfectly linear, suspension system is it also important to study, by simulation, the accuracy of observers with different choices of measured variables and other parameter values.

The variables easiest to measure are probably the lengths of the suspension elements, which can be measured with potentiometer transducers. The cab's and the frame's angular displacements can be measured with inclinometers or gyro transducers. The best way to measure the velocities of the cab and the frame in the x, y and z directions is probably to integrate accelerometer signals. The weighted acceleration values in the cab can be measured with accelerometer transducers connected to the relevant filters.

For an observer based on measurements of the lengths of the suspension elements (deviations from the balanced lengths $l_{e1}^d - l_{e6}^d$), the cab's angular displacements ($xr_c^d \quad yr_c^d$) and the cab's velocities in the x, y and z directions ($\dot{x}_c^d \quad \dot{y}_c^d \quad \dot{z}_c^d$) are, for a system with first order disturbance models:

$$(\mathbf{y}^m(t))^T = (l_{e1}^d(t) \quad l_{e2}^d(t) \quad l_{e3}^d(t) \quad l_{e4}^d(t) \quad l_{e5}^d(t) \quad l_{e6}^d(t) \quad \dot{x}_c^d(t) \quad \dot{y}_c^d(t) \quad \dot{y}_c^d(t) \quad xr_c^d(t) \quad yr_c^d(t)) \tag{202}$$

$$\mathbf{H}^m = \begin{pmatrix}
1 & 0 & 0 & 0 & 0 & 0 & 0 & 0 & 0 & 0 & 0 & 0 & 0 & 0 & 0 & 0 & 0 & 0 & 0 & 0 & 0 & 0 & 0 & 0 & 0 \\
0 & 1 & 0 & 0 & 0 & 0 & 0 & 0 & 0 & 0 & 0 & 0 & 0 & 0 & 0 & 0 & 0 & 0 & 0 & 0 & 0 & 0 & 0 & 0 & 0 \\
0 & 0 & 1 & 0 & 0 & 0 & -l_y & 0 & -l_x & 0 & 0 & 0 & 0 & l_y & l_x & 0 & 0 & 0 & 0 & 0 & 0 & 0 & 0 & 0 & 0 \\
0 & 0 & 1 & 0 & 0 & 0 & -l_y & 0 & l_x & 0 & 0 & 0 & 0 & l_y & -l_x & 0 & 0 & 0 & 0 & 0 & 0 & 0 & 0 & 0 & 0 \\
0 & 0 & 1 & 0 & 0 & 0 & l_y & 0 & l_x & 0 & 0 & 0 & 0 & -l_y & -l_x & 0 & 0 & 0 & 0 & 0 & 0 & 0 & 0 & 0 & 0 \\
0 & 0 & 1 & 0 & 0 & 0 & l_y & 0 & -l_x & 0 & 0 & 0 & 0 & -l_y & l_x & 0 & 0 & 0 & 0 & 0 & 0 & 0 & 0 & 0 & 0 \\
0 & 0 & 0 & 1 & 0 & 0 & 0 & 0 & 0 & 0 & 0 & 0 & 0 & 0 & 0 & 0 & 0 & 0 & 0 & 0 & 0 & 0 & 0 & 0 & 0 \\
0 & 0 & 0 & 0 & 1 & 0 & 0 & 0 & 0 & 0 & 0 & 0 & 0 & 0 & 0 & 0 & 0 & 0 & 0 & 0 & 0 & 0 & 0 & 0 & 0 \\
0 & 0 & 0 & 0 & 0 & 1 & 0 & 0 & 0 & 0 & 0 & 0 & 0 & 0 & 0 & 0 & 0 & 0 & 0 & 0 & 0 & 0 & 0 & 0 & 0 \\
0 & 0 & 0 & 0 & 0 & 0 & 1 & 0 & 0 & 0 & 0 & 0 & 0 & 0 & 0 & 0 & 0 & 0 & 0 & 0 & 0 & 0 & 0 & 0 & 0 \\
0 & 0 & 0 & 0 & 0 & 0 & 0 & 0 & 1 & 0 & 0 & 0 & 0 & 0 & 0 & 0 & 0 & 0 & 0 & 0 & 0 & 0 & 0 & 0 & 0
\end{pmatrix} \tag{203}$$

The matrix $\mathbf{R}_2$ defines the measurement noise covariance. Normally, the errors for a transducer are defined in relation to the transducer's measuring range. It seems reasonable to use this technique also when defining the estimated covariance values. If the standard deviations for the measurement errors in relation to the measuring range are defined for each transducer (σ_i^{max}), together with the measuring ranges (r_i^{max}), where i=1 to n and n are the number of transducers, and the errors are assumed to be uncorrelated to each other, the covariance matrix can be calculated from:

$$\mathbf{R}_2 = \begin{pmatrix}
(r_1^{max} \cdot \sigma_1^{max})^2 & 0 & \dots & 0 \\
0 & (r_2^{max} \cdot \sigma_2^{max})^2 & \dots & 0 \\
\dots & \dots & \dots & \dots \\
0 & 0 & \dots & (r_n^{max} \cdot \sigma_n^{max})^2
\end{pmatrix} \tag{204}$$

A suspension controller including an observer of the type described above is rather complicated and calculation intensive and the whole sample time is probably needed for the calculations. Consequently all the tested observers have been based on the Kalman predictor theory and not the filter theory.

9.4 Nonlinear simulation model with discrete controller

The nonlinear model is, as mentioned above, programmed in the simulation program Simnon. This simulation model has also been used to study the effects of different actively controlled active suspensions. The controller with the observer and regulator has been described as a discrete system with inputs from, and outputs to, the basic continuous time suspension simulation model.

The inputs to the discrete controller, consisting of the vector with measured variables ($\mathbf{y}^m$), has been delayed one time step with regard to the calculation time used in a real controller and to the use of the Kalman Predictor observer.

White measurement noise has been added to the measured signals to imitate the real conditions as closely as possible. That noise corresponds to the measurement noise vector described in the discrete observer calculations.

The outputs from the controller consist of signals making the force actuators produce the calculated optimal forces.

When studying controllers with different feedback and observer gains, it was possible to read the variables automatically from a file. These files were produced in Matlab, where the gains were calculated.

The linear model, and thereby also the controller, includes only one horizontal element working in the x dimension (element 1) and one working in the y dimension (element 2), while the real system includes two horizontal elements working in each of these dimensions. The force F_1 defined by the controller has therefore been divided into equal parts between elements 1a and 1b, and F_2 between elements 2a and 2b. The average length of elements 1a and 1b has been used to get a measurement of x_1^s $(x_c^d - x_b^d)$ and the average length of elements 2a and 2b to get a measurement of x_2^s $(y_c^d - y_b^d)$.

9.5 Linear simulation model with discrete controller

The linear discrete model described earlier can also be used to simulate the system. The linear model is, of course, a simplified description of the real nonlinear frame-suspension-cab system. The comparison between the models has, however, shown that the results from the linear model differ relatively little from those of the nonlinear model (Ch. 6.3).

The linear model was found easier to work with, and was also much faster when the approximate effects of a specified parameter change are to be studied. The linear model has, therefore, been used for most of the prestudies, e.g. to find out which penalty matrices and controller structures can be used.

The linear model also makes it possible to use some of the vast amount of developed theory describing characteristics for linear time invariant state space systems, for example to calculate transfer functions. Most of that theory is not described in this study

since the basic suspension model is nonlinear and best studied by time domain simulation. Neither is this theory applicable to the time variant systems described in the chapter with adaptive controllers.

The structure used for the linear discrete simulation model is:

$$\mathbf{x}^s(t+1) = \mathbf{F}^s\mathbf{x}^s(t) + \mathbf{G}^s\mathbf{u}(t) \tag{205}$$

$$\mathbf{y}^s = \mathbf{H}^s\mathbf{x}^s(t) \tag{206}$$

For the cab suspension system with perfectly measurable states and the feedback gain matrix **K**:

$$\mathbf{F}^s = \begin{pmatrix} \mathbf{F}_w & \mathbf{G}_w^v \\ \mathbf{0}^{5*21} & \mathbf{0}^{5*5} \end{pmatrix} - \begin{pmatrix} \mathbf{G}_w^u \\ \mathbf{0}^{5*6} \end{pmatrix}\mathbf{K} \tag{207}$$

$$\mathbf{G}^s = \begin{pmatrix} \mathbf{0}^{21*5} \\ \mathbf{I}^{5*5} \end{pmatrix} \tag{208}$$

$$(\mathbf{u}^s)^T(t) = (\ddot{x}_b^d(t) \quad \ddot{y}_b^d(t) \quad \ddot{z}_b^d(t) \quad \dot{xr}_b^d(t) \quad \dot{yr}_b^d(t)) \tag{209}$$

$\mathbf{H}^s$ can be chosen as $\mathbf{I}^{26*26}$ to get the time history for all states as output.

The states describing the frame movements are defined by the time series for these variables. These time series have to be defined as input to the simulation model.

For a cab system with noisy state measurements and an observer with the gain matrix **L**, the system can be simulated if:

$$\mathbf{F}^s = \begin{pmatrix} \begin{pmatrix} \mathbf{F}_w & \mathbf{G}_w^v \\ \mathbf{0}^{5*21} & \mathbf{0}^{5*5} \end{pmatrix} & -\begin{pmatrix} \mathbf{G}_w^u \\ \mathbf{0}^{5*6} \end{pmatrix}\mathbf{K} \\ (\mathbf{LH}^m) & \left(\begin{pmatrix} \mathbf{F}_w & \mathbf{G}_w^v \\ \mathbf{0}^{5*21} & \mathbf{I}^{5*5} \end{pmatrix} - \begin{pmatrix} \mathbf{G}_w^u \\ \mathbf{0}^{5*6} \end{pmatrix}\mathbf{K} - \mathbf{LH}^m\right) \end{pmatrix} \tag{210}$$

$$\mathbf{G}^s = \begin{pmatrix} \mathbf{0}^{21*5} \\ \mathbf{I}^{5*5} \\ \mathbf{0}^{26*5} \end{pmatrix} \tag{211}$$

$$(\mathbf{u}^s)^T(t) = (\ddot{x}_b^d(t) \quad \ddot{y}_b^d(t) \quad \ddot{z}_b^d(t) \quad \dot{xr}_b^d(t) \quad \dot{yr}_b^d(t)) \tag{212}$$

Where states 1-26 are the same as in Ch. 9.1 and states 27-52 are the observer's estimated values of the first 26.

In this case, $\mathbf{H}^s$ can be chosen as $\mathbf{I}^{52*52}$ to get the time history for all states as output.

9.6 The simulated suspension's geometry and basic characteristics

The same suspension geometry is used for all simulations with actively controlled suspension elements. This geometry is the same as for the basic suspension described in Ch. 7.1 which is used for the simulations and optimizations with passive elements. The cab and frame end points of the suspension elements are described in Table B.

The same cab characteristics and cab position in relation to the vehicle as given in Ch. 7.1 are also used.

The vertical active force actuators (elements 3-6) are assumed to work in parallel with passive spring elements. The springs support the cab when the engine not is running, reduce the active controller forces, and work as an extra insurance against component errors. The spring constants for the vertical elements are defined to give a basic natural frequency = 0.5 Hz in the z direction. The elastic mountings to the frame are, for these elements, worked out to reach natural frequencies of 0.5 Hz also in the x and y directions. The horizontally working elements (elements 1a, 1b, 2a and 2b in Figure 50) are assumed to be active force actuators without parallel springs. The k_x, k_y and k_z parameters then become:

$$k_x = k_y = k_z = 1431 N/m \tag{213}$$

All other forces from the elements are assumed to be decided by the active controller, and thus no passive damping is present.

The actuators operate with force transducers providing inner loop feedback signals and are imagined to track faithfully a force demand signal determined by the control law. The actuator dynamics can also be included in the model matrices if necessary. This option has not been used in the reported studies. However, in order to study the influence on the vibration damping potential of first order actuator characteristics included in the system matrices, some simulations have been performed with the linear model. The results showed that, as long as the time constants were reasonably short, the vibration damping potential was influenced very little.

9.7 The simulation model inputs

9.7.1 Measurement principle

The input signals used to describe the frame movements in the simulations with active elements are measured according to the technique described in Ch. 5.3.

Measurements were performed when driving on several surfaces with different speeds. In the same way as for the simulations with passive elements, two input signals were used in the simulations with active elements. One signal was measured at track 1 (SS-ISO 5008) when driving at 12 km/h to get an average load. To get an exceptional vibration load, measurements were also performed when driving on track 2 at 6 km/h, as previously.

Trends in tractor design are moving almost exclusively towards 4 WD tractors. To get input signals more characteristic of modern tractors with 4 WD and larger front tyres, a 2-year-old Fendt 306 LSA was used for the measurements, instead of the 15-year-old 2 WD Volvo BM T-650 tractor used for the inputs to the passive elements simulations. Data for the Fendt tractor are shown in Table O.

Table O. Tractor data

Model	Fendt Farmer 306 LSA
Mass	3705 kg
Length	3.990 m
Height	2.625 m
Wheel base	2.280 m
Track width front	1.570 m
Track width rear	1.500 m
Tyres front	13.6-24/8 R
Tyres rear	16.9-34/8 R
Inflation pressure front	0.24 MPa
Inflation pressure rear	0.20 MPa

9.7.2 Input characteristics

The RMS values for the input signals used are described in Table P. The vibrations are calculated for a point located on the tractor's longitudinal symmetry line, 1.50 m above the ground, 0.60 m in front of the tractor's rear axle. Figures 84 and 85 show the frequency content for the same signals.

Table P. The input signals' RMS values calculated for a point located on the tractor's longitudinal symmetry line, 1.50 m above the ground, 0.60 m in front of the tractor's rear axle

Direction	Vibration level RMS (m/s^2 rad/s^2)			
	Track 1		Track 2	
	ISO 2631	Not weighted	ISO 2631	Not weighted
x	1.17	1.84	3.21	3.46
y	0.67	0.98	1.24	1.38
z	2.42	2.77	2.84	4.15
xr	-	1.61	-	3.03
yr	-	2.14	-	3.80
vector sum	3.07	-	5.88	-

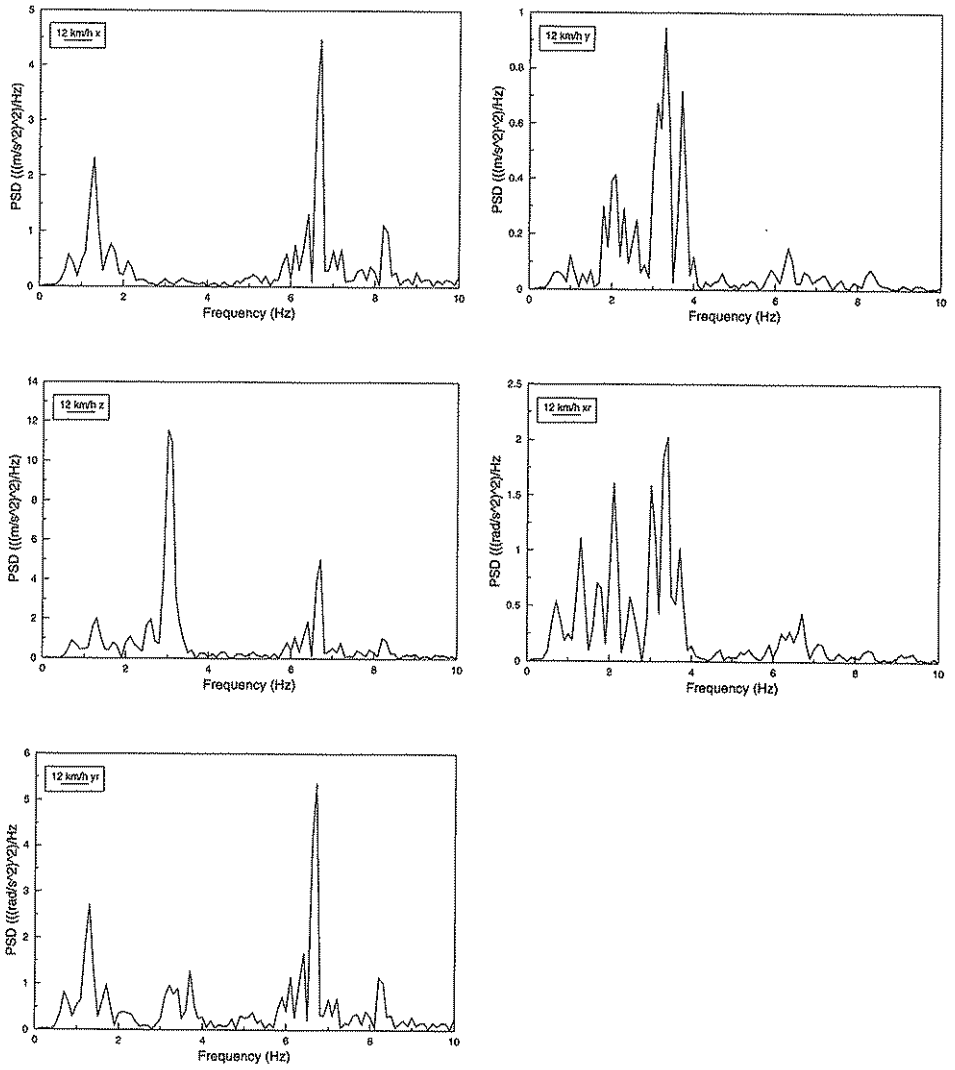

Fig. 84. Power density for the input signals measured on track 1 calculated for a point located on the tractor's longitudinal symmetry line, 1.50 m above the ground, 0.60 m in front of the tractor's rear axle.

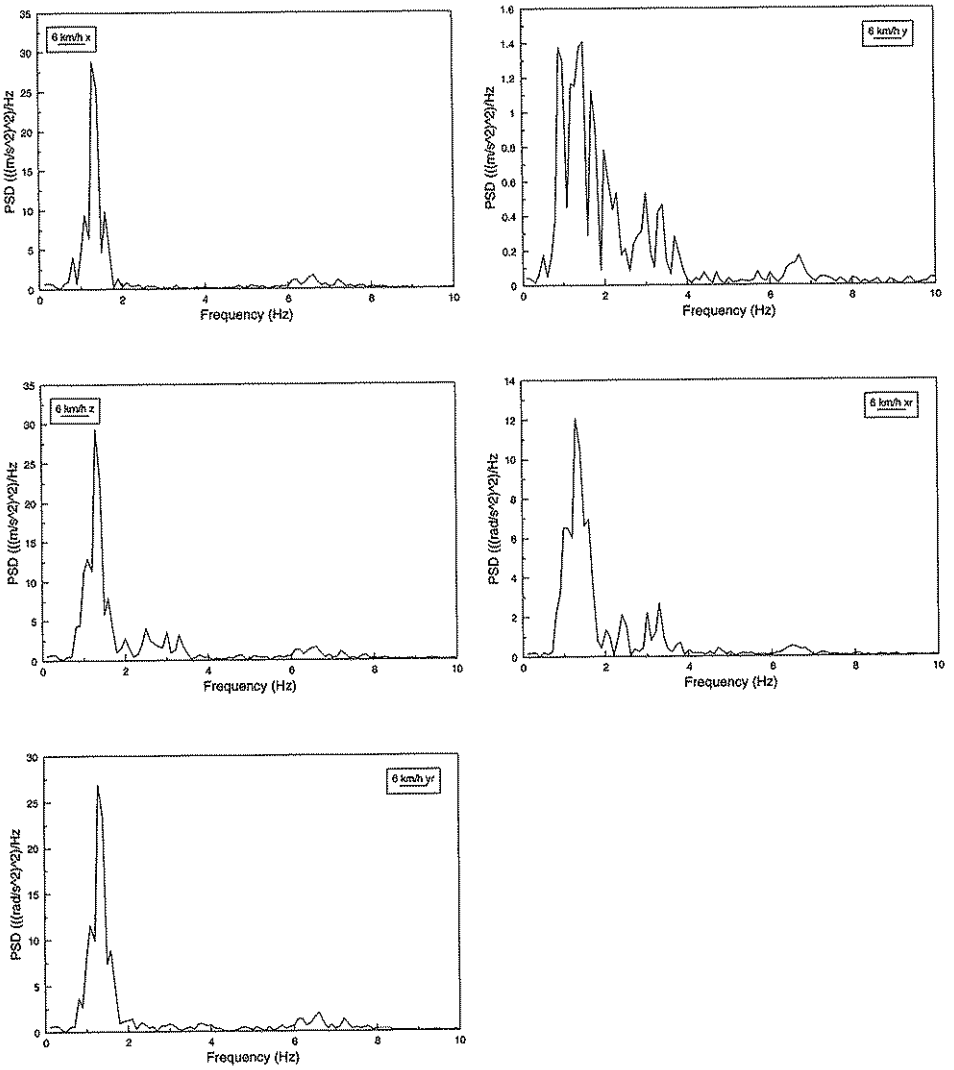

Fig. 85. Power density for the input signals measured on track 2 calculated for a point located on the tractor's longitudinal symmetry line, 1.50 m above the ground, 0.60 m in front of the tractor's rear axle.

9.7.3 Identification of parametric models

The disturbances (frame movements) may be described as parametric models driven by white noise when used in the design of discrete active controllers and observers.

The structure used is the ARMA structure:

$$A(q^{-1})y(t) = C(q^{-1})e(t) \tag{214}$$

or explicitly:

$$y(t)+a_1y(t-1)+\ldots+a_{na}y(t-na)=e(t)+c_1e(t-1)+\ldots+c_{nc}e(t-nc) \quad (215)$$

where e = white noise with the variance $(\sigma^e)^2$.

The signal's frequency content is approximately described by the ARMA model. The approximation normally becomes more exact when the polynomial's order is increased. The size of the so-called "loss function" ($(\sigma^e)^2$) is a measure of the accuracy.

The parameters in the models have to be estimated with an identification algorithm. Matlab's ARMAX procedure has been used for the identification of models of orders 1-3 for the acceleration time series described in the previous chapter (Tables Q and R). The procedure is based on a prediction error algorithm. The time series are assumed to have time invariant characteristics. A recursive least square algorithm usable when the signals have time variant characteristics is described and used in the part handling adaptively controlled active suspensions. The signals were measured with a sampling frequency of 200 Hz.

Table Q. ARMA models of orders 1-2 for the acceleration time series used as simulation model inputs

Track	Dim	na=nc =1			na=nc =2				
		a_1	c_1	$(\sigma^e)^2$	a_1	a_2	c_1	c_2	$(\sigma^e)^2$
1	x	-0.984	0.9718	0.0280	-1.948	0.9789	0.9269	0.7449	5.8e-4
	y	-0.988	0.9231	0.0051	-1.927	0.9474	0.8470	0.5753	3.0e-4
	z	-0.988	0.9570	0.0433	-1.956	0.9773	0.7987	0.6790	1.2e-3
	xr	-0.992	0.8961	0.0128	-1.936	0.9525	0.7035	0.6063	7.5e-4
	yr	-0.986	0.9733	0.0350	-1.947	0.9763	0.8082	0.6733	9.3e-4
2	x	-0.996	0.9687	0.0290	-1.967	0.9764	1.0431	0.6948	7.1e-4
	y	-0.994	0.9217	0.0057	-1.923	0.9337	0.2853	0.7702	6.5e-4
	z	-0.995	0.9539	0.0441	-1.966	0.9751	0.7815	0.6685	1.5e-3
	xr	-0.996	0.9139	0.0181	-1.953	0.9600	0.3250	0.7361	1.2e-3
	yr	-0.994	0.9695	0.0377	-1.965	0.9744	0.8289	0.6809	1.1e-3

Table R. ARMA models of order 3 for the acceleration time series used as simulation model inputs

Track	Dim	na=nc =3						
		a_1	a_2	a_3	c_1	c_2	c_3	$(\sigma^e)^2$
1	x	-2.844	2.752	-0.905	0.127	0.536	0.122	1.8e-4
	y	-2.675	2.434	-0.754	0.116	0.314	0.124	2.2e-4
	z	-2.830	2.717	-0.884	-0.791	0.492	0.160	4.9e-4
	xr	-2.733	2.539	-0.802	-0.097	0.398	0.0436	5.0e-4
	yr	-2.823	2.708	-0.882	-0.060	0.464	0.136	3.6e-4
2	x	-2.915	2.874	-0.959	-0.140	0.514	0.196	1.4e-4
	y	-2.152	1.425	-0.264	0.491	0.666	0.608	4.3e-4
	z	-2.869	2.787	-0.916	-0.179	0.484	0.134	5.9e-4
	xr	-2.462	1.989	-0.524	0.153	0.612	0.344	7.9e-4
	yr	-2.892	2.830	-0.937	-0.225	0.488	0.129	3.3e-4

The identification loss functions for the track 1 signals, with the polynomial orders 1-4, are shown in Figure 86. The figure shows that the loss functions decrease very little when increasing the polynomial order over 3.

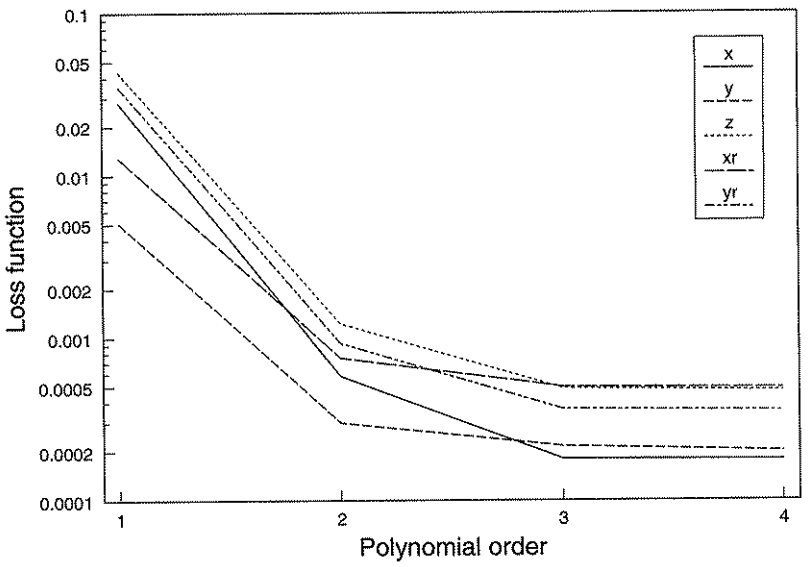

Fig 86. Identification loss functions for the signals measured on track 1.

9.8 Effects of disturbance model orders

The calculation of feedback and observer gains is based on the disturbances being described as the output from ARMA models. The controller structure is dependent on the order of the ARMA models.

The purpose of this study was to show in what way the order of the ARMA models influences the vibration damping potentials of the suspension.

9.8.1 Assumptions

The comparison between the linear and nonlinear simulation models shows that also the linear model describes the real system rather accurately. In order to simplify the computer programming and the result analysis, the linear model was used for the study.

The linear model can be divided into five smaller models, each describing the cab movements in one direction. The results in Ch. 9.14 show that the suspension parameters influencing one of the dimensions have very small effects on the suspension's characteristics in the other dimensions. The five models are relatively similar and there is no reason to believe that the effect of a model structure change in one of the models is not approximately the same as for a change in one of the others. To make the computer times shorter and to simplify the programming, the effects of different disturbance model orders were studied for the linear model describing the z dimension movements.

The suspension geometry and cab characteristics are described in Ch. 9.6. The force actuators were assumed to use inner loop feedback with perfect tracking of the force demand signal determined by the control law.

The continuous time model describing the z dimension movements is:

$$\dot{\mathbf{x}}^s_{zp} = \begin{pmatrix} 0 & 1 & -1 & 0 & 0 \\ \frac{-4k_z}{m} & 0 & 0 & 0 & 0 \\ 0 & 0 & 0 & 0 & 0 \\ \frac{-4k_z \cdot 49.42}{m} & 0 & 0 & -48.93 & 1 \\ \frac{-4k_z \cdot 465.8}{m} & 0 & 0 & -1108 & 0 \end{pmatrix} \mathbf{x}^s_{zp} + \begin{pmatrix} 0 \\ \frac{1}{m} \\ 0 \\ \frac{49.42}{m} \\ \frac{465.8}{m} \end{pmatrix} F_{zp} + \begin{pmatrix} 0 \\ 0 \\ 1 \\ 0 \\ 0 \end{pmatrix} \ddot{z}^d_b \tag{216}$$

where

$$(\mathbf{x}^s_{zp})^T = (z^d_c - z^d_b \quad \dot{z}^d_c \quad \dot{z}^d_b \quad z^s_{H1} \quad z^s_{H2}) \tag{217}$$

$$F_{zp} = F_3 + F_4 + F_5 + F_6 \tag{218}$$

$$\ddot{z}^d_w = (0 \quad 0 \quad 0 \quad 1 \quad 0)\mathbf{x}^s_{zp} \tag{219}$$

This model was sampled as described in Ch. 9.1 and 1-3 states (dependent on the disturbance model order) were added. The sixth state then describes the frame's acceleration in the z dimension.

Matlab was used for the calculation of feedback and observer gains and for the analysis of the simulation results.

The controlled variables were the suspension travel (state 1) and the weighted accelerations in the z dimension (state 4). The measured variables in this study were the suspension travel (state 1) and the frame velocity and acceleration in the z dimension (state 3 and state 6). It was assumed that the lengths of the four vertical elements were measured and the average length used to get a measurement of state 1. The length transducers were assumed to have a measuring range = 0.10 m, the velocity transducer 1.0 m/s and the acceleration transducer a measuring range = 10 m/s^2. The transducers were assumed to have σ^{max} = 2.0 % of the measuring ranges.

It is also interesting to compare the active suspension potential with the potential for passive suspensions in the same environment. By using the feedback gain:

$$\mathbf{K} = (0 \quad c \quad -c \quad 0 \quad 0 \quad 0) \tag{220}$$

where

$$c = 4\pi R f_n m \tag{221}$$

the characteristics for passive linear suspensions with varying natural frequencies and degrees of damping can be calculated with the same formulas as for the active suspensions. The linear suspensions are, of course, simulated without observers.

9.8.2 Results

By varying the penalty on the suspension travel state when keeping the penalty on the weighted acceleration constant ($y_2^{cmax} = 0.010$), the suspension's vibration damping potential for different available travel spaces can be studied. In Figure 87 the suspension travel vs vibration level curves are shown for a controller based on a first order disturbance model. The curves are shown for different values for the penalty on the input (u^{max}).

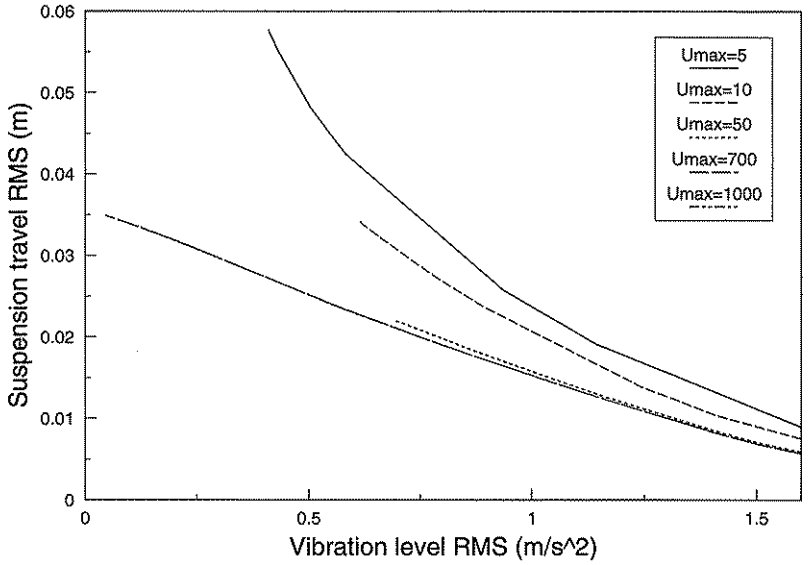

Fig. 87. Suspension travel vs vibration level curves in the z dimension when driving on track 1 at 12 km/h. The controller is based on a first order disturbance model.

The curves in Figure 87 show that the vibration damping potential is increased when the penalty on the force input is decreased. The curves also show that there is a limit when a decreased penalty on the input does not increase the vibration damping potential any more. This optimum curve is the best to use when different active suspensions are compared.

Figure 88 shows the optimal characteristics for z dimension vibration damping for controllers based on disturbance models of orders 1, 2 and 3. The corresponding curves when using passive linear suspensions with natural frequencies of 0.75, 1.00 and 1.25 Hz are also shown in the figure.

The size of the parameters in the feedback gain matrix **K** can show interesting characteristics for the resulting active controllers. Figure 89 shows the connection between the suspension travel RMS and the size of the parameters in the **K** matrix. The values are obtained from the simulations with u^{max} = 1.0 e3 shown in Figure 87.

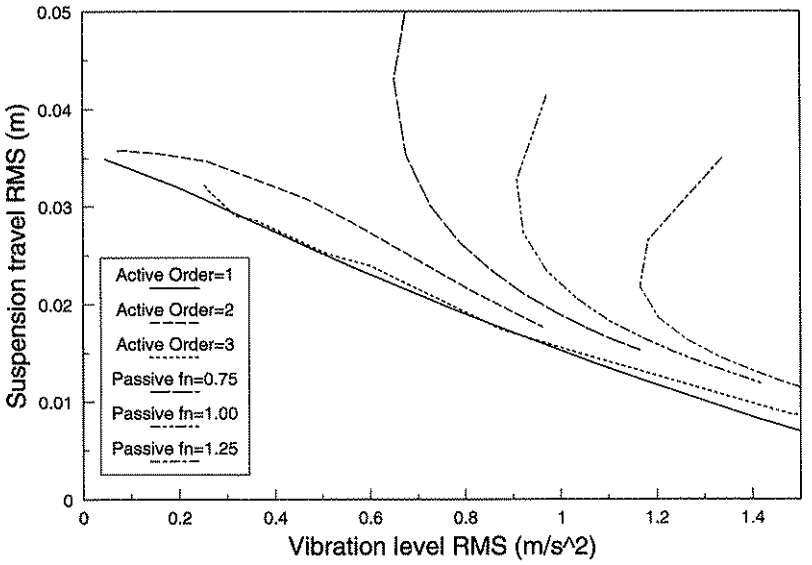

Fig. 88. Suspension travel vs vibration level curves in the z dimension when driving on track 1 at 12 km/h with active suspensions based on disturbance models of different order and with passive suspensions with varying vertical natural frequency and degree of damping.

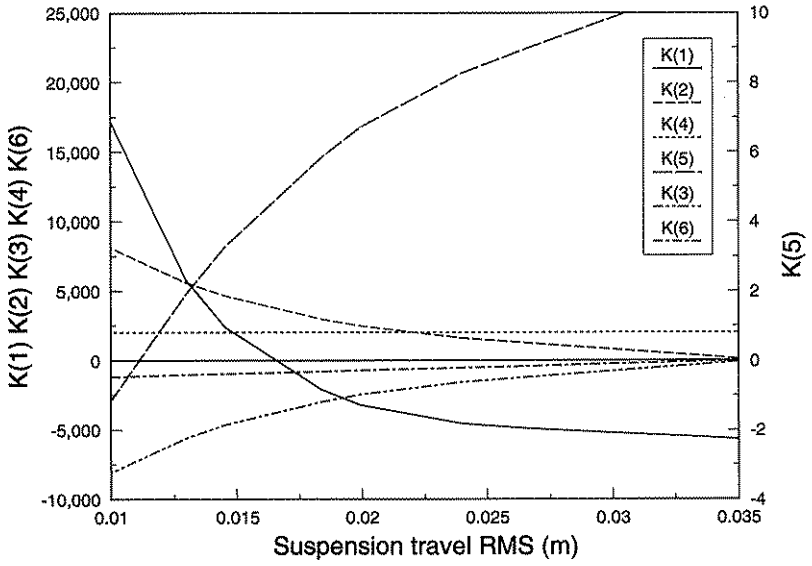

Fig. 89. Feedback gain parameters vs suspension travel RMS in the z dimension when driving on track 1 at 12 km/h. The observer and the controller are based on a first order disturbance model and calculated with $u^{max} = 1.0\ e3$.

9.8.3 Conclusions

The figures show that the vibration damping potential is not increased when the controller is based on disturbance models of higher order than one. Very little further information appears to be included in the added states and the observer's approximations when estimating these added, not measurable states, appear instead to decrease the suspension's vibration damping potential.

The active suspensions show much better vibration damping potential than the passive ones when the available travel space is not so limited. In a very limited travel space the passive suspensions, however, offer almost the same possibilities as the active ones.

Figure 89 shows some very interesting facts. The **K**(1) variable can be described as the spring constant for a spring working in parallel with the permanent spring in the basic construction used to support the cab when the power supply is disconnected. For suspensions resulting in high suspension travel, **K**(1) is negative, which means that the function of the permanent spring is counteracted and that the suspension's natural frequency becomes very small. For suspensions with more decreased travel levels **K**(1), and thereby the natural frequency, is increased.

The feedback gains for states 2 and 3 (the cab's and the frame's velocities) have the same value for all suspensions but with opposite signs. This corresponds to a passive damper with variable damping constant (compare with the **K** matrix used for the simulations of passive suspensions). For a suspension resulting in very small suspension travel, the damping is very high which results in a suspension with almost passive characteristics.

9.9 Controllers based on reduced model

The frame-suspension-cab system can also be described with a linear model with fewer states. The disturbance input vector can, for linear directions, describe the frame velocities instead of accelerations. For the rotational directions, the input vector can describe the angular positions in relation to the coordinate axes instead of the angular velocities. The order of the regulator and the observer then decreases with one state for each dimension and becomes easier to implement in practice. The amount of information available for the controller to use for the vibration damping is, however, also decreased and thus it may be assumed that the vibration damping potential is not as good as for controllers based on the bigger linear model.

The reduced continuous time linear model with frequency weighted outputs becomes:

$$\dot{\mathbf{x}}_r^s = \mathbf{A}_r \mathbf{x}_r^s + \mathbf{B}_r^u \mathbf{u}_r + \mathbf{B}_r^v \mathbf{v}_r \tag{222}$$

where

$$(\mathbf{x}_r^s)^T = (x_c^d - x_b^d \quad y_c^d - y_b^d \quad z_c^d - z_b^d \quad \dot{x}_c^d \quad \dot{y}_c^d \quad \dot{z}_c^d \quad xr_c^d \quad \dot{x}r_c^d \quad yr_c^d \quad \dot{y}r_c^d \quad x_{H1}^s \quad x_{H2}^s \quad y_{H1}^s \quad y_{H2}^s \quad z_{H1}^s \quad z_{H2}^s \;) \tag{223}$$

$$\mathbf{A}_r = \tag{224}$$

$$\begin{pmatrix}
0 & 0 & 0 & 1 & 0 & 0 & 0 & 0 & 0 & 0 & 0 & 0 & 0 & 0 & 0 & 0 \\
0 & 0 & 0 & 0 & 1 & 0 & 0 & 0 & 0 & 0 & 0 & 0 & 0 & 0 & 0 & 0 \\
0 & 0 & 0 & 0 & 0 & 1 & 0 & 0 & 0 & 0 & 0 & 0 & 0 & 0 & 0 & 0 \\
\frac{-4k_x}{m} & 0 & 0 & 0 & 0 & 0 & 0 & 0 & \frac{4k_x h}{m} & 0 & 0 & 0 & 0 & 0 & 0 & 0 \\
0 & \frac{-4k_y}{m} & 0 & 0 & 0 & 0 & \frac{-4k_y h}{m} & 0 & 0 & 0 & 0 & 0 & 0 & 0 & 0 & 0 \\
0 & 0 & \frac{-4k_z}{m} & 0 & 0 & 0 & 0 & 0 & 0 & 0 & 0 & 0 & 0 & 0 & 0 & 0 \\
0 & 0 & 0 & 0 & 0 & 0 & 0 & 1 & 0 & 0 & 0 & 0 & 0 & 0 & 0 & 0 \\
0 & \frac{-4k_y h}{I_{xx}} & 0 & 0 & 0 & 0 & \frac{-4k_z l_y^2}{I_{xx}} - \frac{4k_y h^2}{I_{xx}} & 0 & 0 & 0 & 0 & 0 & 0 & 0 & 0 & 0 & 0 \\
0 & 0 & 0 & 0 & 0 & 0 & 0 & 0 & 0 & 1 & 0 & 0 & 0 & 0 & 0 & 0 \\
\frac{4k_x h}{I_{yy}} & 0 & 0 & 0 & 0 & 0 & 0 & 0 & \frac{-4k_z l_x^2}{I_{yy}} - \frac{4k_x h^2}{I_{yy}} & 0 & 0 & 0 & 0 & 0 & 0 & 0 \\
\frac{-4k_x \cdot 12.57}{m} & 0 & 0 & 0 & 0 & 0 & 0 & 0 & \frac{4k_x h \cdot 12.57}{m} & 0 & -19.90 & 1 & 0 & 0 & 0 & 0 \\
\frac{-4k_x \cdot 157.9}{m} & 0 & 0 & 0 & 0 & 0 & 0 & 0 & \frac{4k_x h \cdot 157.9}{m} & 0 & -157.9 & 0 & 0 & 0 & 0 & 0 \\
0 & \frac{-4k_y \cdot 12.57}{m} & 0 & 0 & 0 & 0 & \frac{-4k_y h \cdot 12.57}{m} & 0 & 0 & 0 & 0 & 0 & -19.90 & 1 & 0 & 0 \\
0 & \frac{-4k_y \cdot 157.9}{m} & 0 & 0 & 0 & 0 & \frac{-4k_y h \cdot 157.9}{m} & 0 & 0 & 0 & 0 & 0 & -157.9 & 0 & 0 & 0 \\
0 & 0 & \frac{-4k_z \cdot 49.42}{m} & 0 & 0 & 0 & 0 & 0 & 0 & 0 & 0 & 0 & 0 & 0 & -48.93 & 1 \\
0 & 0 & \frac{-4k_z \cdot 465.8}{m} & 0 & 0 & 0 & 0 & 0 & 0 & 0 & 0 & 0 & 0 & 0 & -1108 & 0
\end{pmatrix}$$

$$\mathbf{B}_r^u = \begin{pmatrix} 0 & 0 & 0 & 0 & 0 & 0 \\ 0 & 0 & 0 & 0 & 0 & 0 \\ 0 & 0 & 0 & 0 & 0 & 0 \\ \frac{1}{m} & 0 & 0 & 0 & 0 & 0 \\ 0 & \frac{1}{m} & 0 & 0 & 0 & 0 \\ 0 & 0 & \frac{1}{m} & \frac{1}{m} & \frac{1}{m} & \frac{1}{m} \\ 0 & 0 & 0 & 0 & 0 & 0 \\ 0 & \frac{h}{I_{xx}} & -\frac{l_y}{I_{xx}} & -\frac{l_y}{I_{xx}} & \frac{l_y}{I_{xx}} & \frac{l_y}{I_{xx}} \\ 0 & 0 & 0 & 0 & 0 & 0 \\ -\frac{h}{I_{yy}} & 0 & -\frac{l_x}{I_{yy}} & \frac{l_x}{I_{yy}} & \frac{l_x}{I_{yy}} & -\frac{l_x}{I_{yy}} \\ \frac{12.57}{m} & 0 & 0 & 0 & 0 & 0 \\ \frac{157.9}{m} & 0 & 0 & 0 & 0 & 0 \\ 0 & \frac{12.57}{m} & 0 & 0 & 0 & 0 \\ 0 & \frac{157.9}{m} & 0 & 0 & 0 & 0 \\ 0 & 0 & \frac{49.42}{m} & \frac{49.42}{m} & \frac{49.42}{m} & \frac{49.42}{m} \\ 0 & 0 & \frac{465.8}{m} & \frac{465.8}{m} & \frac{465.8}{m} & \frac{465.8}{m} \end{pmatrix} \tag{225}$$

$$\mathbf{u}_r = \mathbf{u}_w \tag{226}$$

$$\mathbf{B}_r^v = \begin{pmatrix} -1 & 0 & 0 & 0 & 0 \\ 0 & -1 & 0 & 0 & 0 \\ 0 & 0 & -1 & 0 & 0 \\ 0 & 0 & 0 & 0 & g - \frac{4k_x h}{m} \\ 0 & 0 & 0 & -g + \frac{4k_y h}{m} & 0 \\ 0 & 0 & 0 & 0 & 0 \\ 0 & 0 & 0 & 0 & 0 \\ 0 & 0 & 0 & \frac{4k_z l_y^2}{I_{xx}} + \frac{4k_y h^2}{I_{xx}} & 0 \\ 0 & 0 & 0 & 0 & 0 \\ 0 & 0 & 0 & 0 & \frac{4k_x l_x^2}{I_{yy}} + \frac{4k_x h^2}{I_{yy}} \\ 0 & 0 & 0 & 0 & 12.57 \cdot \left(g - \frac{4k_x h}{m} \right) \\ 0 & 0 & 0 & 0 & 157.9 \cdot \left(g - \frac{4k_x h}{m} \right) \\ 0 & 0 & 0 & 12.57 \cdot \left(-g + \frac{4k_y h}{m} \right) & 0 \\ 0 & 0 & 0 & 157.9 \cdot \left(-g + \frac{4k_y h}{m} \right) & 0 \\ 0 & 0 & 0 & 0 & 0 \\ 0 & 0 & 0 & 0 & 0 \end{pmatrix} \tag{227}$$

$$(\mathbf{v}_r)^T = (\dot{x}_b^d \quad \dot{y}_b^d \quad \dot{z}_b^d \quad \dot{x}r_b^d \quad \dot{y}r_b^d) \tag{228}$$

The vector with weighted vibrations $\ddot{\mathbf{x}}_w^d$ can be calculated from:

$$\ddot{\mathbf{x}}_w^d = \mathbf{C}_w \mathbf{x}_r^s \tag{229}$$

$$(\ddot{\mathbf{x}}_w^d)^T = (\ddot{x}_w^d \quad \ddot{y}_w^d \quad \ddot{z}_w^d) \tag{230}$$

$$\mathbf{C}_w = \begin{pmatrix} 0 & 0 & 0 & 0 & 0 & 0 & 0 & 0 & 0 & 0 & 1 & 0 & 0 & 0 & 0 & 0 \\ 0 & 0 & 0 & 0 & 0 & 0 & 0 & 0 & 0 & 0 & 0 & 0 & 1 & 0 & 0 & 0 \\ 0 & 0 & 0 & 0 & 0 & 0 & 0 & 0 & 0 & 0 & 0 & 0 & 0 & 0 & 1 & 0 \end{pmatrix} \tag{231}$$

The purpose of this study is to show the characteristics of a suspension with an active controller based on the reduced model. The purpose is also to compare the characteristics with the other suspension types tested.

9.9.1 Assumptions

Controllers based on the reduced model describing the cab movements in five d.o.f. have been tested in rather great detail both in the linear and nonlinear model. To show the

principle and the vibration damping characteristics for controllers based on the reduced model, the results from a simple study using the linear z dimension are shown here. The linear z dimension model becomes:

$$\dot{\mathbf{x}}_{zp}^{s} = \begin{pmatrix} 0 & 1 & 0 & 0 \\ \frac{-4k_z}{m} & 0 & 0 & 0 \\ \frac{-4k_z \cdot 49.42}{m} & 0 & -48.93 & 1 \\ \frac{-4k_z \cdot 465.8}{m} & 0 & -1108 & 0 \end{pmatrix} \mathbf{x}_{zp}^{s} + \begin{pmatrix} 0 \\ \frac{1}{m} \\ \frac{49.42}{m} \\ \frac{465.8}{m} \end{pmatrix} F_{zp} + \begin{pmatrix} -1 \\ 0 \\ 0 \\ 0 \end{pmatrix} \dot{z}_b^d \tag{232}$$

where

$$(\mathbf{x}_{zp}^{s})^T = (z_c^d - z_b^d \quad \dot{z}_c^d \quad z_{H1}^s \quad z_{H2}^s) \tag{233}$$

$$F_{zp} = F_3 + F_4 + F_5 + F_6 \tag{234}$$

$$\dot{z}_w^d = (0 \quad 0 \quad 1 \quad 0)\mathbf{x}_{zp}^{s} \tag{235}$$

This model was sampled as described in Ch. 9.1 and a fifth state was added. This state describes the frame's velocity in the z dimension.

The controlled variables were, as before, the suspension travel (state 1) and the weighted accelerations in the z dimension (state 3). The measured variables in this study were the suspension travel (state 1) and the frame velocity in the z dimension (state 5). The length transducers were assumed to have a measuring range = 0.10 m and the velocity transducer a measuring range = 1.0 m/s. The transducers were assumed to have σ^{max} = 2.0 % of the measuring ranges.

To study the suspension characteristics with the observer's negative effects excluded, the system was also simulated without observer assuming perfectly measurable states.

9.9.2 Results

In Figure 90 the optimum characteristics for z dimension vibration damping for controllers based on the reduced model with and without observer are compared to the characteristics for controllers based on the model including the frame acceleration state. The corresponding curves when using passive linear suspensions with natural frequencies of 0.75, 1.00 and 1.25 Hz are also shown in the figure.

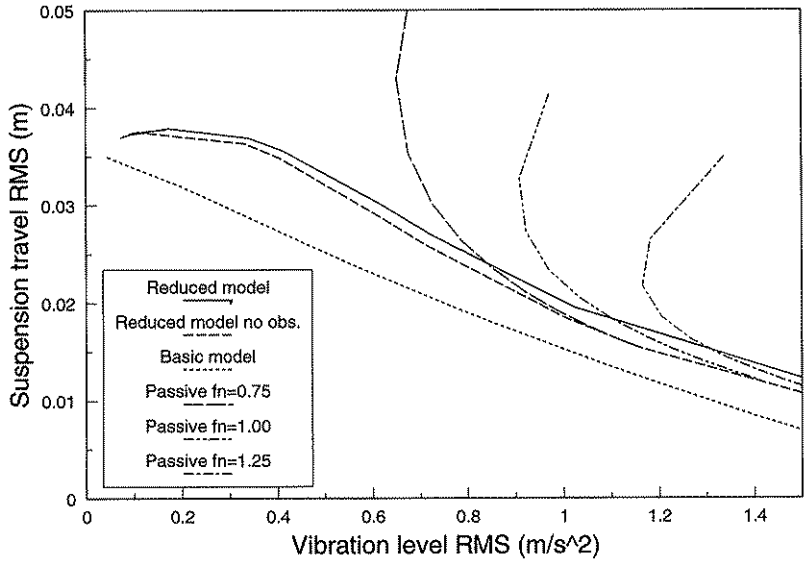

Fig. 90. Suspension travel vs vibration level curves in the z dimension when driving on track 1 at 12 km/h with active controllers based on the basic and the reduced linear model and with passive suspensions with varying vertical natural frequency and degree of damping.

9.9.3 Conclusions

The vibration damping potential using a controller based on the reduced model is not as good as for the controllers studied in the previous chapters. The frame acceleration value is not available for feedback and thus the feedback principle has great similarity with the passive suspension principle.

9.10 Controllers based on model not including absolute velocities

There is another possibility to decrease the number of states in the model describing the frame-suspension-cab interplay. The velocity differences between the cab and the frame ($\dot{x}_c^d - \dot{x}_b^d$, $\dot{y}_c^d - \dot{y}_b^d$ and $\dot{z}_c^d - \dot{z}_b^d$) are then defined as states instead of three states ($\dot{x}_c^d$, $\dot{y}_c^d$ and $\dot{z}_c^d$) being used for the cab's linear velocities and three ($\dot{x}_b^d$, $\dot{y}_b^d$ and $\dot{z}_b^d$) for the frame's linear velocities. The order of the system matrices is then decreased by 3.

The results in Figure 89, where the feedback gains for the cab's and the frame's absolute velocities have the same value but with opposite signs, shows that it is enough to know the differences between these states in each dimension when the feedback should be calculated. Observe that, in contrast to controllers based on the reduced model described in the previous chapter, the information used in the calculation of the feedback in the controller structure described in this chapter are the same as in the standard model used in the main part of this work.

The system can then be described (without frequency weighting of the linear cab accelerations):

$$\dot{\mathbf{x}}_m^s = \mathbf{A}_m \mathbf{x}_m^s + \mathbf{B}_m^u \mathbf{u}_m + \mathbf{B}_m^v \mathbf{v}_m \text{ with:} \tag{236}$$

$$(\mathbf{x}_m^s)^T = (x_c^d - x_b^d \quad y_c^d - y_b^d \quad z_c^d - z_b^d \quad \dot{x}_c^d - \dot{x}_b^d \quad \dot{y}_c^d - \dot{y}_b^d \quad \dot{z}_c^d - \dot{z}_b^d \quad xr_c^d \quad \dot{xr}_c^d \quad yr_c^d \quad \dot{yr}_c^d \quad xr_b^d \quad yr_b^d) \tag{237}$$

$$\mathbf{A}_m = \tag{238}$$

$$\begin{pmatrix}
0 & 0 & 0 & 1 & 0 & 0 & 0 & 0 & 0 & 0 & 0 & 0 \\
0 & 0 & 0 & 0 & 1 & 0 & 0 & 0 & 0 & 0 & 0 & 0 \\
0 & 0 & 0 & 0 & 0 & 1 & 0 & 0 & 0 & 0 & 0 & 0 \\
\frac{-4k_x}{m} & 0 & 0 & 0 & 0 & 0 & 0 & 0 & \frac{4k_x h}{m} & 0 & 0 & g - \frac{4k_x h}{m} \\
0 & \frac{-4k_y}{m} & 0 & 0 & 0 & 0 & \frac{-4k_y h}{m} & 0 & 0 & 0 & -g + \frac{4k_y h}{m} & 0 \\
0 & 0 & \frac{-4k_c}{m} & 0 & 0 & 0 & 0 & 0 & 0 & 0 & 0 & 0 \\
0 & 0 & 0 & 0 & 0 & 0 & 0 & 1 & 0 & 0 & 0 & 0 \\
0 & \frac{-4k_y h}{I_{xx}} & 0 & 0 & 0 & 0 & \frac{-4k_z l_y^2}{I_{xx}} - \frac{4k_y h^2}{I_{xx}} & 0 & 0 & 0 & \frac{4k_z l_y^2}{I_{xx}} + \frac{4k_y h^2}{I_{xx}} & 0 \\
0 & 0 & 0 & 0 & 0 & 0 & 0 & 0 & 0 & 1 & 0 & 0 \\
\frac{4k_x h}{I_{yy}} & 0 & 0 & 0 & 0 & 0 & 0 & 0 & \frac{-4k_z l_x^2}{I_{yy}} - \frac{4k_x h^2}{I_{yy}} & 0 & 0 & \frac{4k_z l_x^2}{I_{yy}} + \frac{4k_x h^2}{I_{yy}} \\
0 & 0 & 0 & 0 & 0 & 0 & 0 & 0 & 0 & 0 & 0 & 0 \\
0 & 0 & 0 & 0 & 0 & 0 & 0 & 0 & 0 & 0 & 0 & 0
\end{pmatrix}$$

$$\mathbf{B}_m^u = \begin{pmatrix}
0 & 0 & 0 & 0 & 0 & 0 \\
0 & 0 & 0 & 0 & 0 & 0 \\
0 & 0 & 0 & 0 & 0 & 0 \\
\frac{1}{m} & 0 & 0 & 0 & 0 & 0 \\
0 & \frac{1}{m} & 0 & 0 & 0 & 0 \\
0 & 0 & \frac{1}{m} & \frac{1}{m} & \frac{1}{m} & \frac{1}{m} \\
0 & 0 & 0 & 0 & 0 & 0 \\
0 & \frac{h}{I_{xx}} & -\frac{l_y}{I_{xx}} & -\frac{l_y}{I_{xx}} & \frac{l_y}{I_{xx}} & \frac{l_y}{I_{xx}} \\
0 & 0 & 0 & 0 & 0 & 0 \\
-\frac{h}{I_{yy}} & 0 & -\frac{l_x}{I_{yy}} & \frac{l_x}{I_{yy}} & \frac{l_x}{I_{yy}} & -\frac{l_x}{I_{yy}} \\
0 & 0 & 0 & 0 & 0 & 0 \\
0 & 0 & 0 & 0 & 0 & 0
\end{pmatrix} \tag{239}$$

$$(\mathbf{u}_m)^T = (F_1 \quad F_2 \quad F_3 \quad F_4 \quad F_5 \quad F_6) \tag{240}$$

$$\mathbf{B}_m^v =$$

$$\begin{pmatrix} 0 & 0 & 0 & 0 & 0 \\ 0 & 0 & 0 & 0 & 0 \\ 0 & 0 & 0 & 0 & 0 \\ -1 & 0 & 0 & 0 & 0 \\ 0 & -1 & 0 & 0 & 0 \\ 0 & 0 & -1 & 0 & 0 \\ 0 & 0 & 0 & 0 & 0 \\ 0 & 0 & 0 & 0 & 0 \\ 0 & 0 & 0 & 0 & 0 \\ 0 & 0 & 0 & 0 & 0 \\ 0 & 0 & 0 & 1 & 0 \\ 0 & 0 & 0 & 0 & 1 \end{pmatrix} \tag{241}$$

$$(\mathbf{v}_m)^T = (\ddot{x}_b^d \quad \ddot{y}_b^d \quad \ddot{z}_b^d \quad \dot{xr}_b^d \quad \dot{yr}_b^d) \tag{242}$$

The states for weighting of the cab accelerations can then easily be added as states 13-18. The total model including discrete disturbance models and used in the digital controller then gets 23 states.

Controllers based on the described model structure have been studied with simulations both in the linear and nonlinear simulation model. If it is possible to measure or calculate (see Ch. 9.11.3) all states and avoid the use of an observer, the vibration damping potential is identical both for controllers based on the model structure described in this chapter and for controllers based on the model structure described earlier. The model structure including fewer states is, in that case, preferable. The reason for the identical damping capacity is, as mentioned before, that the same information is used when the feedback is calculated. The results for suspensions without observers in Figures 93-97 are valid also for this controller structure.

Simulations with observers in the linear simulation model have also shown comparable results between the two controller structures. Simulations using the nonlinear simulation model indicated, however, that the observers seemed to be more sensitive to unmodelled nonlinearities than observers based on the other model structures, and in same cases the suspension became unstable. The reason for these rather unexpected results is not clear, and it is possible that the problems could be avoided if further simulation studies were performed. The instability problems contributed, however, to the original model structure (described in Ch. 9.1) being used for the more comprehensive studies of the actively controlled suspension's characteristics (Chs. 9.12-9.16).

9.11 Effects of different observer inputs

The controller's vibration damping capacity depends to a great extent on how accurately the observer can estimate the states. This accuracy is highly dependent on which combination of states that can be directly measured.

The purpose of this study is to show how different combinations of measured variables affect the vibration damping capacity of the suspension. The purpose is also to show the effects of different levels of transducer measurement error.

9.11.1 Assumptions

The linear z dimension model is used to study the effects of different combinations of measured variables.

The solution of the observer Riccatti equation ($\overline{\mathbf{P}}$) shows the approximate covariance matrix for the estimation errors. The values in the diagonal show the variance for each estimation error and are the most interesting to analyse.

The simplest variables to measure are the length deviations of the suspension elements from the balanced position. The value for state 1 can then be calculated from the average length deviation. This signal has been used in all the tested transducer combinations.

The cab's and/or the frame's acceleration can be measured relatively accurately with accelerometer transducers. The cab's weighted acceleration (state 4) can be filtered from a normal accelerometer output.

The cab's and/or the frame's velocity are very important inputs for the observer. One way to get this signal is to integrate accelerometer signals. One accelerometer can be used both to measure acceleration and velocity at the cab or at the frame.

The measuring ranges for the transducers are assumed to be 0.10 m for the length transducers, 1.0 m/s for the velocity transducers and 10 m/s^2 for the accelerometers. When comparing different transducer combinations, σ^{max} is placed at 2.0 %. It is assumed that the transducer errors not are correlated to each other.

The influence of the transducer and measurement system errors (σ^{max}) is also studied. It is then assumed that state 1, state 3 and state 6 are measured. The same maximum measuring ranges as before are assumed.

9.11.2 Results

The diagonal elements in the $\overline{\mathbf{P}}$ matrix are shown in Table S for four different transducer combinations:

1. state 1 and state 2

2. state 1 and state 3

3. state 1, state 2 and state 4

4. state 1, state 3 and state 6.

Combinations with only length and accelerometer measurement were also studied. Theoretically, all states are observable also from these measurements, but the controllers' vibration damping potentials were very poor and are not shown in the figures.

Table S. The observer's estimation error covariance for different transducer combinations when driving on track 1 at 12 km/h

transducer comb.	$\bar{\mathbf{P}}(1,1)$	$\bar{\mathbf{P}}(2,2)$	$\bar{\mathbf{P}}(3,3)$	$\bar{\mathbf{P}}(4,4)$	$\bar{\mathbf{P}}(5,5)$	$\bar{\mathbf{P}}(6,6)$
1	1.6e-6	2.0e-6	2.5e-3	5.5e-5	1.8e-2	1.75
2	2.1e-7	2.0e-6	2.2e-4	7.6e-6	9.3e-3	0.77
3	1.5e-6	7.4e-7	2.1e-3	4.9e-5	6.1e-3	1.65
4	1.7e-7	2.0e-6	2.0e-5	5.5e-6	8.1e-3	0.19

The optimum suspension travel vs acceleration curves for the four transducer combinations are shown in Figure 91. The results of a simulation of the system assuming that all states are perfectly measurable (no observer used) are also shown.

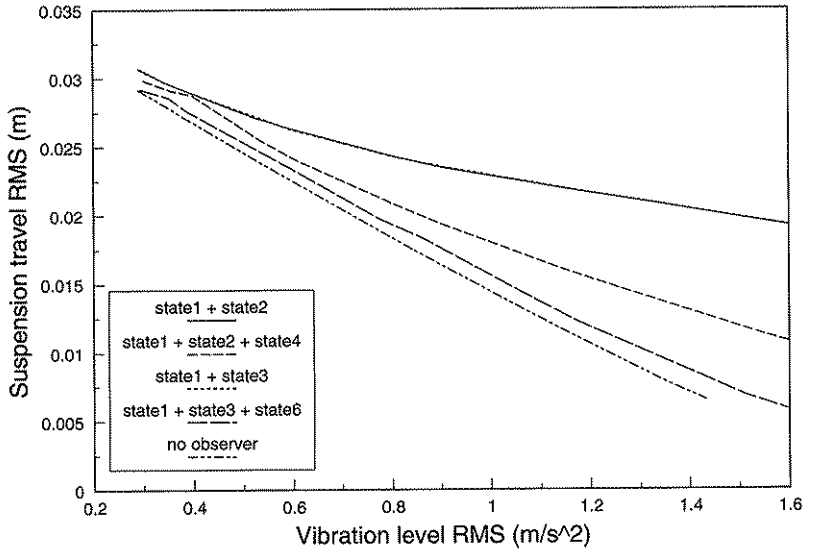

Fig. 91. Suspension travel vs vibration level curves in the z dimension when driving on track 1 at 12 km/h. The observer uses different combinations of measured variables as inputs.

The optimum suspension travel vs weighted acceleration levels were also studied for different values of σ^{max} (Figure 92). The same model and parameter values as before are used.

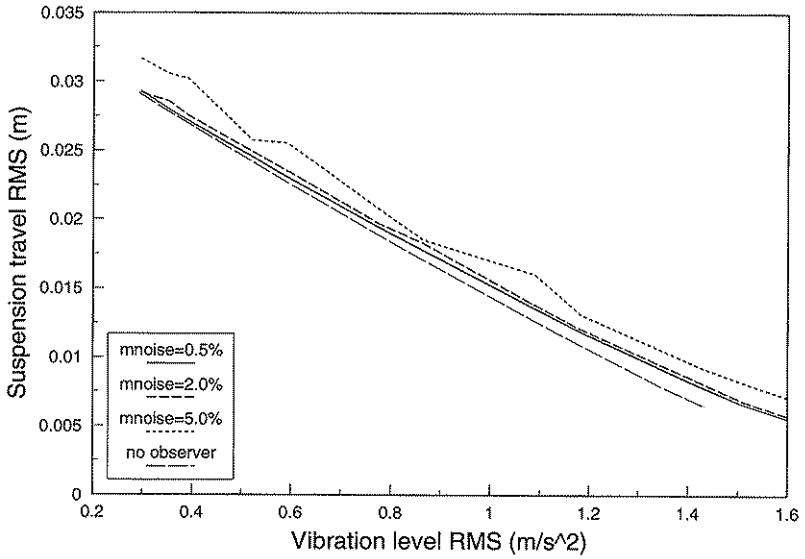

Fig. 92. Suspension travel vs vibration level curves in the z dimension when driving on track 1 at 12 km/h. The observer uses measurements of state 1, state 3 and state 6 as input. The measurement noise values are varied.

9.11.3 Conclusions

The most effective of the studied observers are based on measurements of states 1, 3 and 6. Also an observer based on measurements of states 1, 2 and 4 is very effective. Whereas, if the cab's or the frame's acceleration can not be measured, the suspension's vibration damping potential is decreased.

An increased measurement noise level decreases the vibration damping capacity, which is logical. The decrease is, however, relatively small, and it seems more important to measure the right variables, than to keep the measurement noise levels small.

If the length of the elements and the frame's acceleration are measured it is possible to use a different technique. The length transducer signal can be derived to get the difference between the absolute velocities of the frame and the cab ($x_2^s - x_3^s$). The only further information necessary for calculation of the feedback is then the values for the states describing the weighted acceleration in the cab (x_4^s and x_5^s). These can be calculated if the forces acting on the cab are known. These forces are dependent on the length of the suspension elements (the spring forces) and the controller's signal to the force actuators, which all are known by the controller.

If the described calculations are included in the controller then all information necessary for the calculation of the feedback is known, and the use of an full order observer is avoided. The technique seems to be better than the use of an full order observer but must

of course be studied in extensive simulations before being applied in practise. The technique is probably also applicable to the five d.o.f. cab suspension described in Ch. 9.6.

9.12 Vibration damping potentials for active suspensions

The purpose of this study was to show the vibration damping characteristics for different active suspensions in the different dimensions.

9.12.1 Assumptions

The nonlinear simulation model was used for the simulations. Suspension geometry and cab characteristics are described in Ch. 9.6. An active controller calculated for first order disturbance models was used. The states were estimated with an observer calculated as in Ch. 9.3. Matlab was used for the calculations of feedback and observer gains and for analysis of the simulation results.

The controlled variables were the same as in the example in Ch. 9.2.2:

$$(y^c(t))^T = (x_c^d(t) - x_b^d(t) \quad y_c^d(t) - y_b^d(t) \quad z_c^d(t) - z_b^d(t) \quad xr_c^d(t) - xr_b^d(t) \quad yr_c^d(t) - yr_b^d(t) \quad \dot{x}_w^d(t) \quad \dot{y}_w^d(t) \quad \dot{z}_w^d(t) \quad \dot{xr}_c^d(t) \quad \dot{yr}_c^d(t)) \tag{243}$$

When a run on track 1 at 12 km/h was simulated, the parameters in the penalty matrices, whose effects not were especially studied, were defined by:

$$z_1^{max} = z_2^{max} = z_3^{max} = z_4^{max} = z_5^{max} = 0.010 \tag{244}$$

$$z_6^{max} = z_7^{max} = z_8^{max} = z_9^{max} = z_{10}^{max} = 0.010 \tag{245}$$

$$u_1^{max} = u_2^{max} = u_3^{max} = u_4^{max} = u_5^{max} = u_6^{max} = 1.0\,e3 \tag{246}$$

When simulating a run on track 2 at 6 km/h the parameters were defined by:

$$z_1^{max} = z_2^{max} = z_3^{max} = z_4^{max} = z_5^{max} = 0.010 \tag{247}$$

$$z_6^{max} = z_7^{max} = z_8^{max} = z_9^{max} = z_{10}^{max} = 0.0010 \tag{248}$$

$$u_1^{max} = u_2^{max} = u_3^{max} = u_4^{max} = u_5^{max} = u_6^{max} = 1.0\,e3 \tag{249}$$

It was assumed that the frame's accelerations in the x, y and z directions were measurable and that it was possible to integrate the velocity values from these transducers. It was also assumed that the length of the suspension elements could be used as inputs to the observer.

The observer was assumed to use signals from inclinometers (angle transducers) or gyro transducers for the measurements of the frame's angular positions in relation to the x and y axes. It was also assumed that the frame's angular velocities could be derived from these transducers. The transducers were defined to have σ^{max} = 2.0 % of the measuring range.

9.12.2 Results

In the simulations with the nonlinear model and with an observer there was, in some cases, a tendency for the cab to drift away from the balanced position and oscillate around another middle point. This tendency was not noticed in the linear simulations and neither when the states were assumed to be perfectly measurable.

The reason was found to depend on even small errors in the observer's estimates of the cab's linear velocities (states 4-6), for suspensions with extreme feedback of this parameters, being enough to counteract the feedback from the suspension's deviations (states 1-3), which normally keeps the cab around the balanced position.

By assuming that the observer could use the derivative of the signals from the suspension elements' length transducers to calculate the cab's linear velocities more correctly and use these values for the feedback, the drift tendencies disappeared and the suspension became totally stable.

In Figures 93-95 the suspension travel RMS vs weighted acceleration RMS curves are shown for the x, y and z directions when driving on track 1 at 12 km/h. Only the optimum curves obtained with controllers calculated with very small penalties on the actuator forces are shown: ($u_1^{max} = u_2^{max} = u_3^{max} = u_4^{max} = u_5^{max} = u_6^{max} = 1.0\, e3$).

The curves reached when passive linear suspensions with varying natural frequencies and degrees of damping were used in the same circumstances are also shown in the diagrams. The simulations were also performed assuming that all states were measurable (no observer) to study the effects of the use of the observer. The curves calculated without an observer are also shown in the figures.

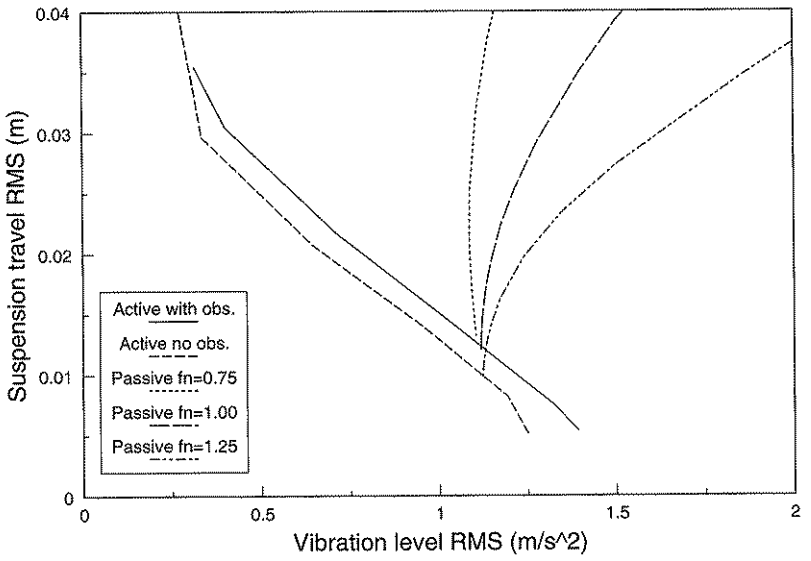

Fig. 93. Suspension travel vs vibration level curves in the x dimension when driving on track 1 at 12 km/h with active suspensions and passive suspensions with varying natural frequencies and degrees of damping.

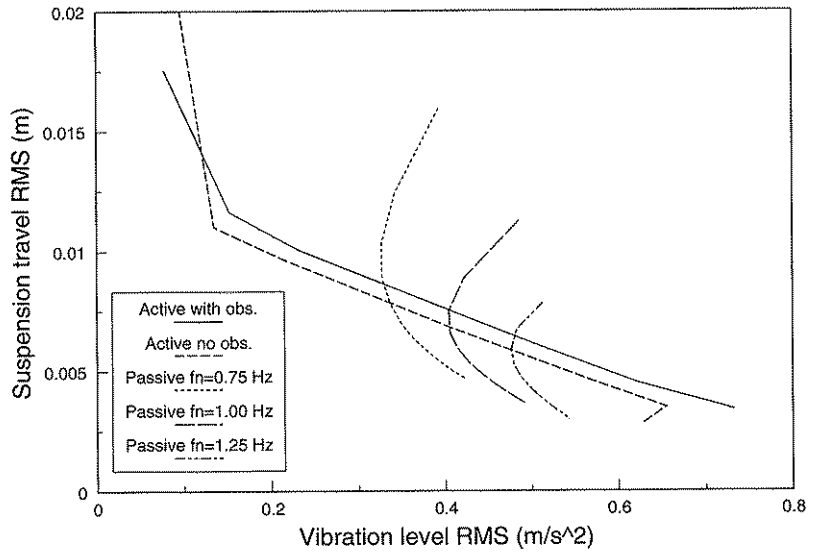

Fig. 94. Suspension travel vs vibration level curves in the y dimension when driving on track 1 at 12 km/h with active suspensions and passive suspensions with varying natural frequencies and degrees of damping.

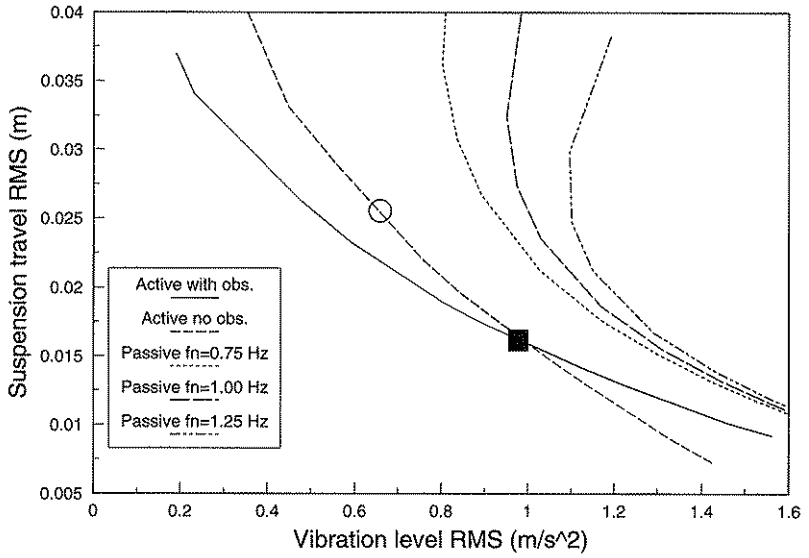

Fig. 95. Suspension travel vs vibration level curves in the z dimension when driving on track 1 at 12 km/h with active suspensions and passive suspensions with varying natural frequencies and degrees of damping.

Curves of the same type as above are also calculated for the angular accelerations around the x and y axes. No states in the model correspond to the angular accelerations. Therefore, in order to restrict the angular vibrations, the states describing angular velocities (state 8 for the xr dimension and state 10 for the yr dimension) have been penalized. Both the angular accelerations and the angular velocities are shown in Figure 96 as a function of the RMS value for the angular deviations between the cab and the frame for the different suspensions.

Simulations as above were also performed with the frame's movements measured on track 2 when driving at 6 km/h. The controllers were based on the ARMA models identified for the acceleration time series used as inputs. Figure 97 shows the results for the z dimension.

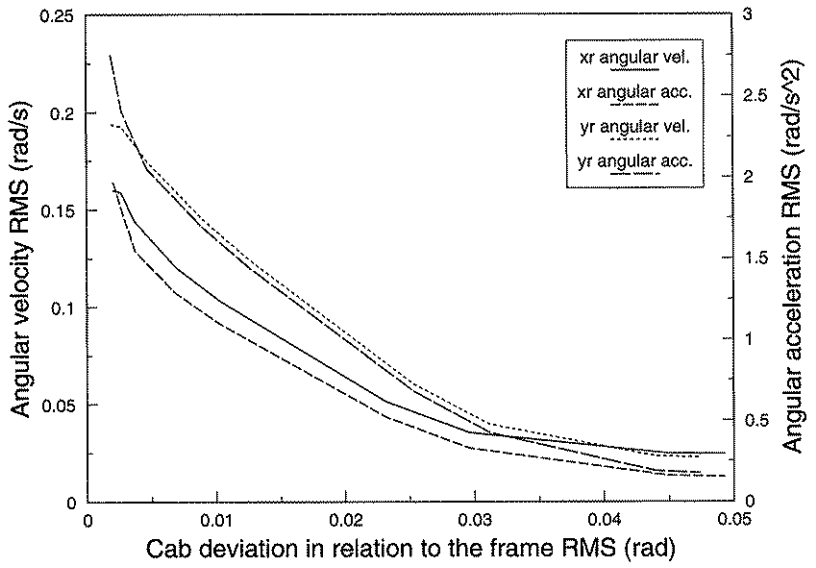

Fig. 96. Angular accelerations and angular velocities vs the angular deviations between the cab and the frame for movements around the x and y axes when driving on track 1 at 12 km/h with different active suspensions.

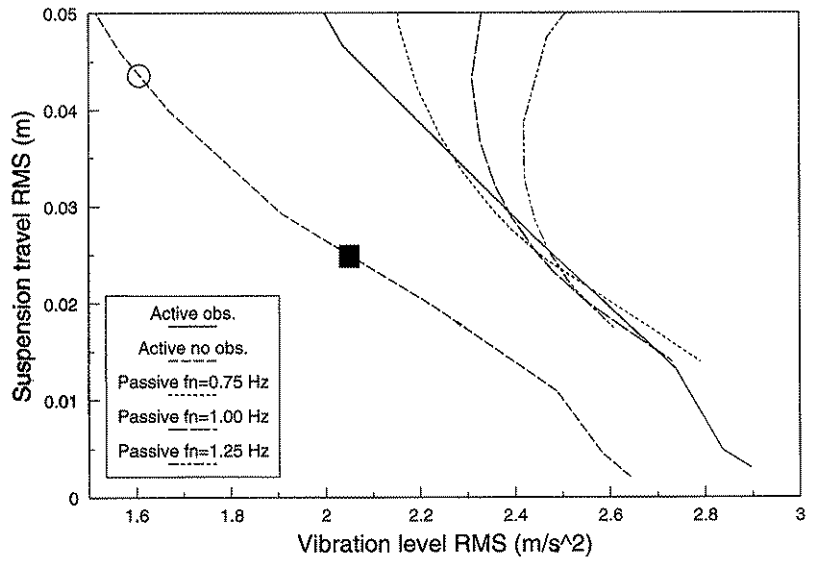

Fig. 97. Suspension travel vs vibration level curves in the z dimension when driving on track 2 at 6 km/h with active suspensions and passive suspensions with varying vertical natural frequencies and degrees of damping.

9.12.3 Conclusions

The figures show that it is possible to design an active suspension with good vibration damping potential in all the studied dimensions.

If an observer must be used to estimate the states when the feedback is calculated, the vibration damping potential is decreased. It is of course favourable to, if possible, avoid the use of observers.

Probably the most important result of this study can be seen if Figures 95 and 97 are compared. One point in each diagram is marked with a square. These suspension characteristics are reached with approximately the same set of feedback gains. The controller optimized to reach a normal RMS travel value of approximately 2.5 cm on the rough track becomes much too heavily damped to be optimal on the smoother track and the vibration damping potential on this track is, therefore, very bad. On the other hand, a suspension designed for normal travel on the smoother track (marked with circles in the figures) results in a travel that is much too large, and probably over-travel, when used on the rougher track. The conclusion is that the controller must be able to adjust the feedback gains depending on the characteristics of the frame movements in order to get a favourable average vibration damping potential, i.e., the controller must be adaptive.

9.13 Power consumption for the active suspensions.

Active suspensions are dependent on a continuous supply of power. The size of the power source can be a limitation for the suspension's vibration damping potential.

The purpose of this study was to show the power consumption for some of the studied active suspensions with different adjustments when driving on different surfaces.

9.13.1 Assumptions

The same assumptions as for the simulations in Ch. 9.12 are used. The power consumption is analysed for the simulations with the nonlinear model shown in Figures 95 and 97. The z dimension curves were chosen because the vibration levels at the frame are highest in that dimension.

It is important to differentiate between negative and positive power values. A positive value means that power must be added from the supply, while a negative value means that power can be converted to heat in the force actuators and that the supply is not loaded.

Note that controllers based on LQG optimization minimize $E(\mathbf{u}^T(t)\mathbf{Q}_2\mathbf{u}(\mathbf{t}))$ and that the sign of $\mathbf{u}(t)$ not is considered.

9.13.2 Results

Figures 98 and 99 show some characteristic values for power consumption for differently adjusted suspensions in the z dimension when driving on the two test tracks. The values

are calculated from the total power consumption in each time step of the four elements working in the z dimension. The values are shown as a function of the RMS z dimension suspension travel values.

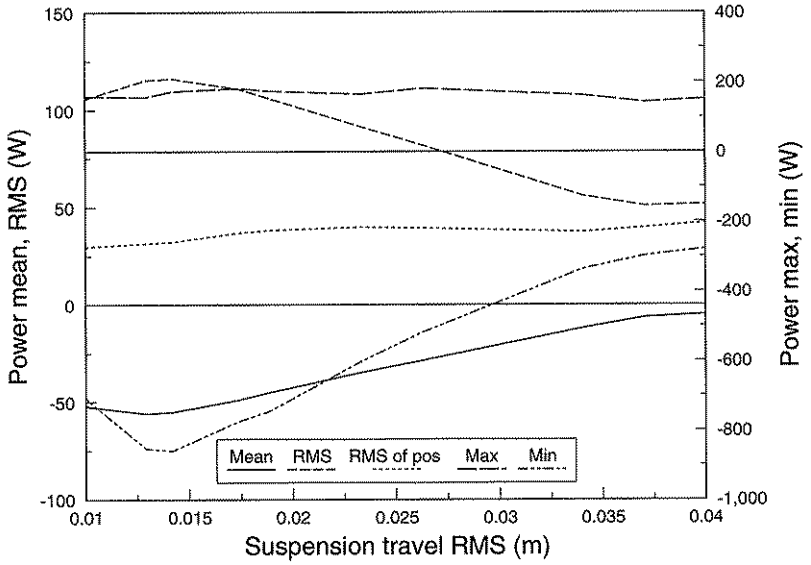

Fig. 98. Power consumption for differently adjusted active suspensions in the z dimension as a function of suspension travel when driving on track 1 at 12 km/h.

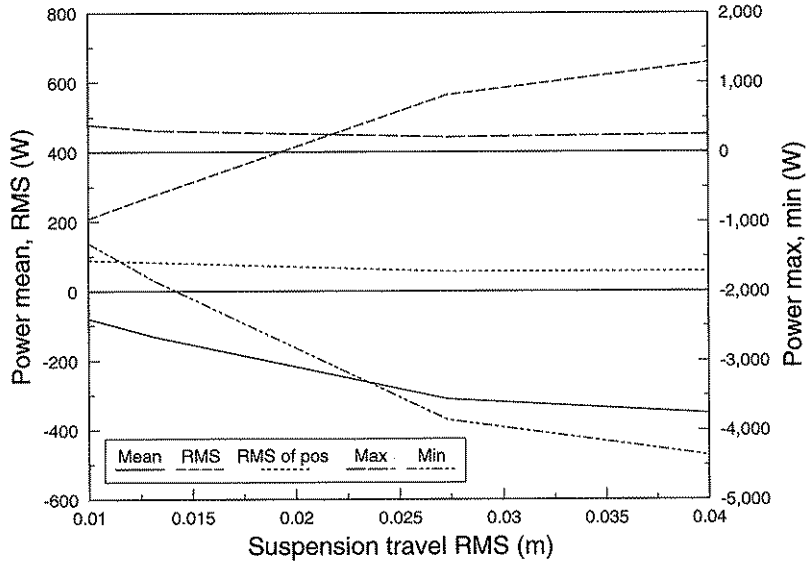

Fig. 99. Power consumption for differently adjusted active suspensions in the z dimension as a function of suspension travel when driving on track 2 at 6 km/h.

9.13.3 Conclusions

Figure 98 shows that the power values are related to suspension travel in a very interesting way when driving on the smoother test track. A suspension adjusted for a very restricted travel space gets a mean power value that is more negative than suspensions adjusted to allow more travel. This depends on the main work in the actuators being performed to restrict travel and thereby absorb energy.

For suspensions allowing more travel the mean power values get closer to zero. In that case, the cab's absolute movements may be very small and the main power is probably needed to counteract for the forces from the springs mounted in parallel with the force actuators.

The maximum power needed for the suspension force actuators in the z dimension when driving on track 1 are relatively small (not over 200 Watt). The absolute values of the minimum values become larger. In that case, however, energy is dissipated and the power source is not loaded.

Note that the values are theoretical values with no respect taken to power losses in the actuators, hydraulic degree of efficiency, etc.

When driving on the extreme track 2 at 6 km/h the suspension is highly adjusted to restrict travel and the power values are also mainly negative. The absolute values of the minimum power values, in contrast to the case when driving on the smoother track, increase when the travel increases, possibly because the suspension movements are very jerky on the very rough surface and become even jerkier when more travel space is used.

9.14 Co-operation between partitioned models

As earlier described, the linear model can be partitioned into five smaller models where each model describes the cab's movements in one dimension. A change of a parameter only included in one of the smaller models then only influences the vibration transmission in that direction. This study was performed to study whether this was approximately valid also when the system was simulated with the nonlinear model. The nonlinear model takes into consideration small angular deviations, etc., which are neglected in the linear model.

9.14.1 Assumptions

The same assumptions as for the simulations in the previous chapter are used. The results are simply a more complete acount of two of the simulations performed in Ch. 9.12. The input measured when driving on track 1 at 12 km/h is used and the active suspension controller uses an observer, as described earlier.

9.14.2 Results

Table T shows the more complete results of the simulations studying the effects of parameter changes in the x dimension, and Table U the results when the suspension characteristics in the z dimension are changed.

Table T. Results from simulations with active controllers calculated with different penalties on suspension travel in the x dimension. The input is measured on track 1 when driving at 12 km/h

y_1^{cmax}	Vibration level (ISO 2631) at the cab's c.o.g (m/s^2 rad/s^2)					Suspension travel RMS (cm)		
	x	y	z	xr	yr	x	y	z
3.2e-4	1.39	0.44	0.81	1.07	1.41	0.53	0.73	1.89
1.0e-3	1.32	0.44	0.81	1.07	1.41	0.76	0.72	1.89
3.2e-3	1.04	0.44	0.81	1.07	1.41	1.39	0.71	1.89
1.0e-2	0.71	0.44	0.80	1.07	1.40	2.16	0.70	1.88
3.2e-2	0.31	0.44	0.81	1.06	1.40	3.54	0.74	1.82

Table U. Results from simulations with active controllers calculated with different penalties on suspension travel in the z dimension. The input is measured on track 1 when driving at 12 km/h

y_3^{cmax}	Vibration level (ISO 2631) at the cab's c.o.g (m/s^2 rad/s^2)					Suspension travel RMS (cm)		
	x	y	z	xr	yr	x	y	z
1.0e-3	0.72	0.44	1.46	1.08	1.40	2.11	0.81	1.01
3.2e-3	0.71	0.44	1.12	1.08	1.40	2.13	0.75	1.42
1.0e-2	0.72	0.44	0.80	1.07	1.40	2.16	0.69	1.89
3.2e-2	0.72	0.44	0.48	1.07	1.40	2.15	0.70	2.63
1.0e-1	0.72	0.44	0.19	1.07	1.40	2.10	0.79	3.70

9.14.3 Conclusions

The results show that a change of the characteristics in one dimension has very small effects on the characteristics in other dimensions. Even a change in the z dimension characteristics does not change the figures for the rotational directions despite the same suspension elements deciding the characteristics in these directions.

An active suspension with five degrees of freedom, as the one studied, is a very complex and expensive construction. The results shows that the partition into five smaller uncoupled models is a good approximation. This is very important because it demonstrates that results from the simulations are applicable also to active suspensions with fewer degrees of freedom, which are perhaps more likely to be implemented in practise.

9.15 Suspensions striving to keep the cab horizontal

Some working operations with agricultural tractors, for example ploughing, cause the vehicle to be inclined relative to the horizontal plane for most of the working time. This imposes a difficult working posture on the driver and may in the long-term be assumed to cause physiological problems.

This study was performed to demonstrate the possibilities of an active suspension to keep the cab horizontal even when the ground and the vehicle's frame are sloping.

9.15.1 Assumptions

When calculating the controllers for the suspensions studied earlier, the cab's angular velocity relative to the x and y axes were penalized (states 8 and 10). To restrict the strokes of the elements, also the angular deviations between the cab and the frame were penalized. If the cab's angular deviations relative to the horizontal plane (states 7 and 9) are penalized instead of the angular velocities, the calculations made by the controller will strive to adjust the suspension in order to keep the cab horizontal. To avoid over-travel the angular deviations between the cab and the frame must still be penalized.

In this study, the cab's angle relative to the y axis has been restricted in order to demonstrate the principle. If a suspension striving to keep the cab horizontal also relative to the x axis is required, then the same technique can be used.

The same assumptions as for the simulations in Ch. 9.12 are used, with the difference that state 9 is penalized instead of state 10. Only the penalty on state 9 is varied and the other penalties are kept constant. The nonlinear simulation model is used and simulations are performed with input from track 1 and a driving speed of 12 km/h.

9.15.2 Results

Figure 100 shows the cab's RMS deviation from the horizontal position vs the angular deviation RMS between the cab and the frame for suspensions with controllers calculated with different penalty matrices.

The cab's and frame's deviations from the horizontal position are shown also in the time domain in Figure 101. The cab's deviations are shown for suspensions calculated with two different penalties on state 9.

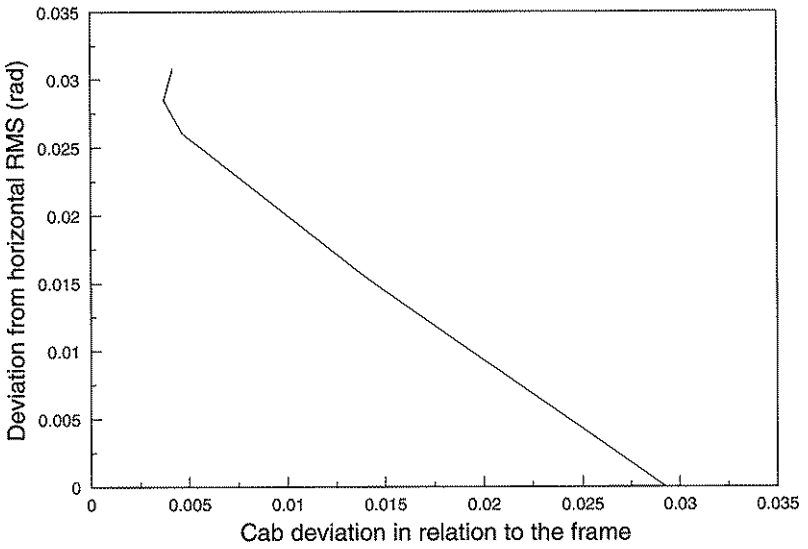

Fig. 100. The cab's deviations from the horizontal plane vs angular deviations between the frame and the cab measured in relation to the y axis for active suspensions with controllers calculated with different penalties on state 9 when driving on track 1 at 12 km/h.

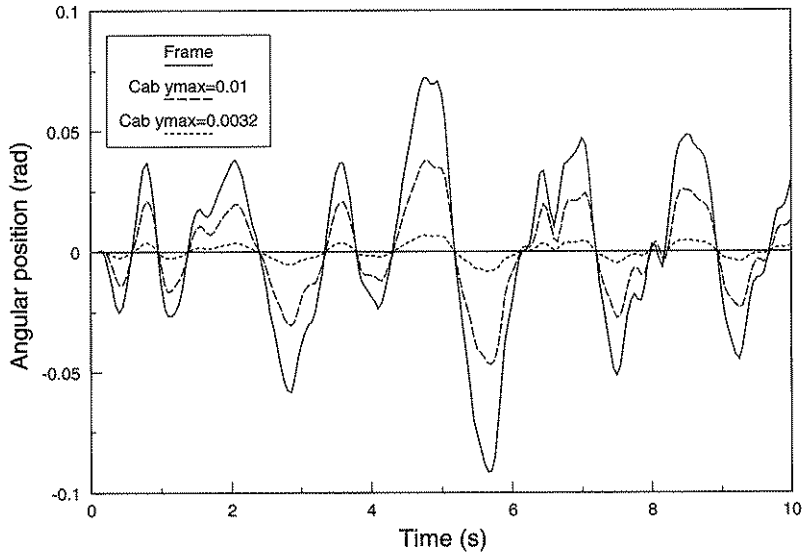

Fig. 101. The cab's and the frame's deviations from the horizontal plane measured relative to the y axis with active suspensions with controllers calculated with two different penalties on state 9 when driving on track 1 at 12 km/h.

9.15.3 Conclusions

The results show that it is possible to design an active suspension striving to keep the cab horizontal even when the vehicle's frame is inclined. There is, however, a risk that the driver experiences a feeling of decreased control of the vehicle when the slope of the cab does not follow that of the rest of the vehicle.

9.16 Comparison between linear and nonlinear simulation model

The purpose of this study was to compare the results from the linear and the nonlinear simulation models when the same active suspension controller was simulated.

9.16.1 Assumptions

The same discrete active suspension controller was simulated both with the linear and the nonlinear model and the same frame movements, measured on track 1 when driving at 12 km/h, were defined. The assumptions were the same as for the simulations described in Ch. 9.12. The penalty matrices were also decided by the values in Ch. 9.12.

Matlab was, again, used to simulate the linear model in discrete form. The nonlinear model was simulated with Simnon. The algorithm used for the integration of the differential equations was a Runge Kutta algorithm of order 4-5.

9.16.2 Results

Figure 102 shows the weighted acceleration values in the x, y and z directions, calculated for the same active controller with the linear and the nonlinear models. The suspensions are studied both when the states are assumed to be directly measurable (no observer) and when the states are estimated with an observer.

Figure 103 shows suspension travel for the same simulations.

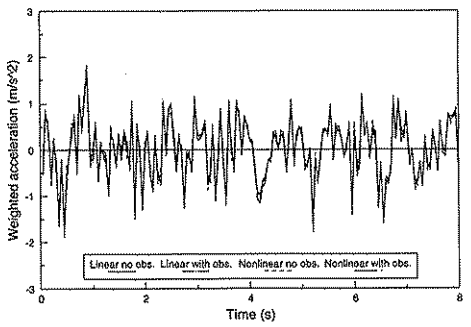

a

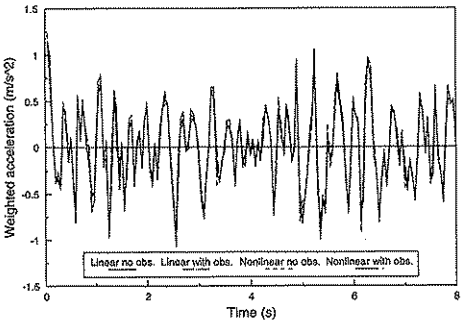

b

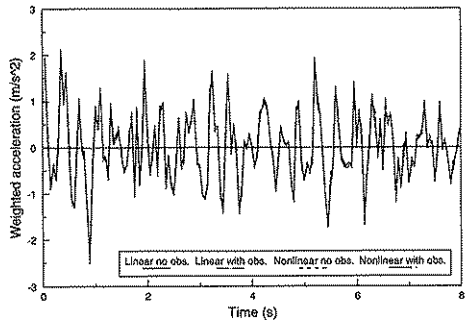

c

Fig. 102. Weighted accelerations in the x (Fig. a), y (Fig. b) and z (Fig. c) dimensions using the same active suspension calculated with the linear and the nonlinear simulation models.

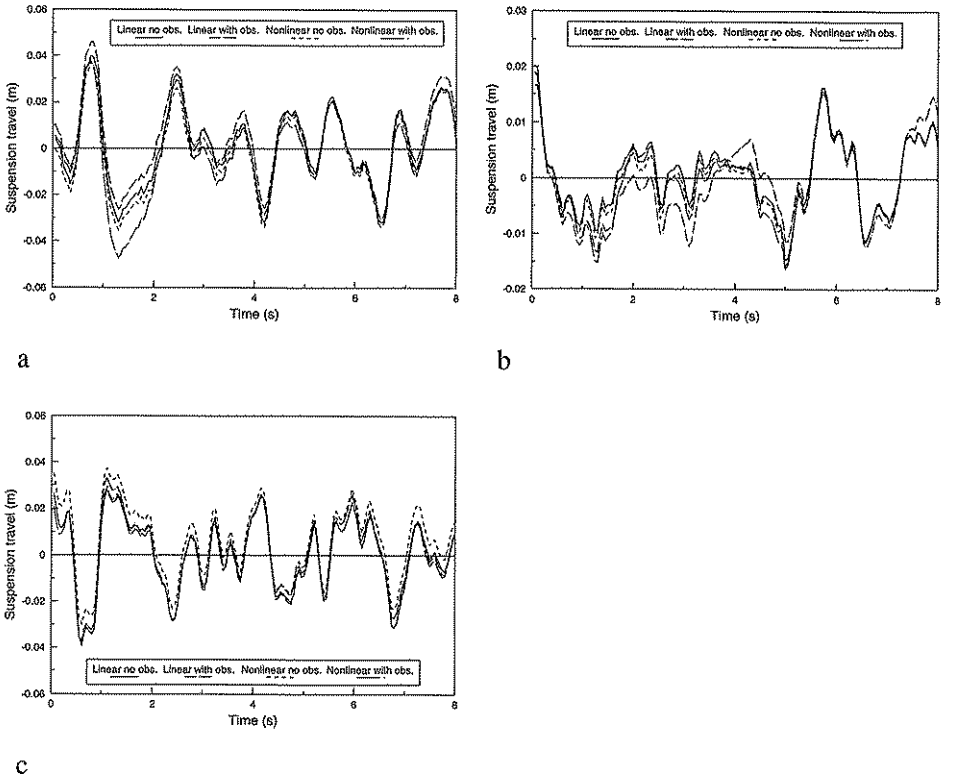

Fig. 103. Suspension travel in the x (Fig. a), y (Fig. b) and z (Fig. c) dimensions using the same active suspension calculated with the linear and the nonlinear simulation models.

9.16.3 Conclusions

The cab acceleration and suspension travel curves, calculated with the linear model, are surprisingly similar to those calculated with the nonlinear model.

Especially the curves calculated without observers have small differences and show that the linear model is a good approximation of the nonlinear one. The suspension controller simulated with an observer shows in some cases slightly larger differences, which is the same trend observed in the earlier simulations, but the differences in that case were also relatively small.

10 ACTIVE SUSPENSIONS WITH ADAPTIVE CONTROLLERS

In the studies in Ch. 9, the frame accelerations were assumed to have time invariant characteristics and thus the controllers also became time invariant. With constant feedback gains, the suspension must be tuned to avoid over-travel at the highest possible acceleration levels, which decreases the vibration damping potential during more normal driving at lower levels.

If controller characteristics can be made dependent on the characteristics of the frame movements and change when the characteristics change, the suspension can be almost optimal for most working conditions, and the average vibration damping potential can be increased.

The suspension controller of the type described earlier can be designed to be time variant with characteristics striving to be optimal for the frame accelerations sensed. The calculations of the observer and the controller gains are then based on an identified model of the input disturbances (frame movements). The disturbance model can be identified with a recursive algorithm striving to change the parameters in the model when the characteristics of the frame movements change.

The parameters in the penalty matrices are used to control the travel in the suspension. If the travel becomes too large the penalty on this state must be increased. If the travel is sensed to become unnecessarily small, the penalty instead can be decreased to get a controller with better vibration damping capacity. The control strategy used is the same as for a standard feedback system.

If the system model, frame acceleration characteristics and penalty matrices are known, then the Riccatti equations necessary to calculate the controller and observer gains can be solved. Depending on the restricted calculation capacity, it is not possible to solve the equations completely in each time step. The iteration formulas described in Ch. 9 can instead be used to get gains always striving towards correct values. The design of the adaptive controller is further described later in this chapter.

Another way to get a controller with time variant characteristics is to precalculate observer and feedback gains for different frame acceleration levels and store them in the controller. The controller can then sense the disturbance characteristics and choose the best of the stored gain matrices. This type of controller is normally named Gain Scheduling (GS) controllers.

The use of GS controllers involves certain difficulties. The system uses no feedback and therefore is very sensitive to changes in the model. It may also be difficult to find a representative auxilary variable to be used for the choice of controller gains. Active suspensions with GS controllers are discussed more in Ch. 10.4.

The tuning of adaptive algorithms must be a compromise and may cause problems. The controller must not be so fast that it overreacts for a single high disturbance value, but must compensate rapidly enough when the average disturbance characteristics really are changed.

10.1 The studied system

The results in Ch. 9.14 show that the partitioning of the studied system in five smaller models is a good approximation and that the interactions between the models are small.

In order to reduce computer times and to simplify the explanations of the results, the studies in this chapter are performed only for one of the five models. An adaptive controller of the studied type also becomes rather complex and is probably only built for one dimension at a time. The z dimension model was chosen because it is the dimension with highest vibration levels and therefore also needs the best vibration protection.

The earlier results also show that the differences between the linear and nonlinear model are small. The studies of different adaptive suspensions are mainly studies of parameter dynamics when the frame acceleration characteristics are varied. Small differences in the results are therefore of no interest. The studies of adaptive suspensions have, thus, been performed using the linear model to reduce the programming and computer times. The use of the linear model also makes the results more general and in no way connected to the special cab suspension.

The continuous time model studied can then be described by:

$$\dot{\mathbf{x}}_{zp}^{s} = \begin{pmatrix} 0 & 1 & -1 & 0 & 0 \\ \frac{-4k_z}{m} & 0 & 0 & 0 & 0 \\ 0 & 0 & 0 & 0 & 0 \\ \frac{-4k_z \cdot 49.42}{m} & 0 & 0 & -48.93 & 1 \\ \frac{-4k_z \cdot 465.8}{m} & 0 & 0 & -1108 & 0 \end{pmatrix} \mathbf{x}_{zp}^{s} + \begin{pmatrix} 0 \\ \frac{1}{m} \\ 0 \\ \frac{49.42}{m} \\ \frac{465.8}{m} \end{pmatrix} F_{zp} + \begin{pmatrix} 0 \\ 0 \\ 1 \\ 0 \\ 0 \end{pmatrix} \ddot{z}_b^d \tag{250}$$

where

$$(\mathbf{x}_{zp}^{s})^T = (z_c^d - z_b^d \quad \dot{z}_c^d \quad \dot{z}_b^d \quad z_{H1}^s \quad z_{H2}^s) \tag{251}$$

$$F_{zp} = F_3 + F_4 + F_5 + F_6 \tag{252}$$

$$\ddot{z}_w^d = (0 \quad 0 \quad 0 \quad 1 \quad 0)\mathbf{x}_{zp}^{s} \tag{253}$$

The model was sampled as described in Ch. 9.1 with a sample time of 0.005 s and a sixth state describing the frame's accelerations in the z dimension was then added.

With m=580 kg and k_z=1431 N/m the model becomes :

$$\mathbf{x}'(t+1)=\begin{pmatrix} 0.9999 & 0.0050 & -.0050 & 0 & 0 & -1.25e-5 \\ -0.0493 & 0.9999 & 1.23e-4 & 0 & 0 & 2.06e-7 \\ 0 & 0 & 1.0000 & 0 & 0 & 0.0050 \\ -2.2053 & -5.70e-3 & 5.70e-3 & 0.7713 & 4.41e-3 & 9.67e-6 \\ -16.66 & -0.0467 & 0.0467 & -4.8920 & 0.9872 & 8.22e-5 \\ 0 & 0 & 0 & 0 & 0 & -a_1 \end{pmatrix}\mathbf{x}'(t)+\begin{pmatrix} 2.15e-8 \\ 8.62e-6 \\ 0 \\ 3.85e-4 \\ 2.91e-3 \\ 0 \end{pmatrix}u(t)+\begin{pmatrix} -1.25e-5 \\ 2.06e-7 \\ 0.0050 \\ 9.67e-6 \\ 8.22e-5 \\ c_1-a_1 \end{pmatrix}e(t) \tag{254}$$

where

$$(\mathbf{x}^s(t))^T=(z_c^d(t)-z_b^d(t)\quad \dot{z}_c^d(t)\quad \dot{z}_b^d(t)\quad z_{H1}^s(t)\quad z_{H2}^s(t)\quad \dot{z}_b^d(t)) \tag{255}$$

The variables that are easiest to measure in the system are the length of the suspension elements (x_1^s) and the acceleration at the frame (x_6^s). The suspension velocity ($x_3^s-x_2^s$) can be calculated by derivation of the length transducer signals. The states describing the weighted acceleration in the cab (x_4^s and x_5^s) can be calculated if the forces acting on the cab in the z dimension are known. These forces depend on the length of the suspension elements (the spring forces) and the controller's signals to the force actuators, both of which are known by the controller.

If the described calculations are included in the controller, all information necessary for the calculation of the feedback is known, and the use of an full order observer is avoided. Neither is it necessary to perform measurements of absolute velocities. Even though the described technique probably is preferable to the use of an full order observer, an observer is used in the described adaptive active suspension controller. The purpose is to show the principles for the observer gain update and that the theory is also usable for other system structures where an full order observer is required.

The results shown in Figures 117-123 are almost identical to those obtained if no observer was used.

10.2 The adaptive controller

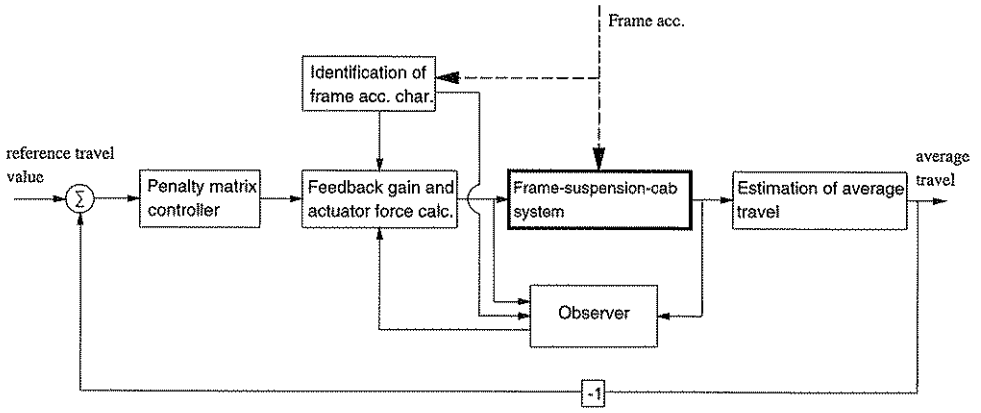

Fig. 104. The structure of the adaptive controller.

Figure 104 shows the structure of the adaptive controller with the dynamic system included.

The frame's acceleration is denoted as disturbance signal. A recursive identification algorithm uses the signals from an accelerometer on the frame to identify the parameters in an ARMA model describing the characteristics of the accelerations.

The observer uses the identified ARMA parameters and the signals from the transducers at the dynamic system to estimate the state vector. The observer gains are updated by an iteration of the Riccatti equation using the latest parameters from the recursive identification.

The regulator uses the estimated state values from the observer to calculate the input to the real system (the actuator forces). The feedback gains are updated by iterating the Riccatti equation using the latest values for the disturbance model and the penalty matrices.

The parameters in the penalty matrices depend on the average travel in the system. If the travel is bigger than a defined reference value, the penalty on the travel state must increase. If the travel is to small the penalty can decrease. The dynamics of the penalty matrix has been studied using traditional automatic control tools in order to get good characteristics for the system and is discussed in a later chapter.

The value used to decide the penalty matrix changes must be a time weighted average of the travel in the suspension.

Lam (1982a and 1982b), Clarke et al. (1985a and 1985b), Åström & Wittenmark (1989) and Bitmead et al. (1990) have discussed adaptive LQG controllers based on state space theory, including feedback gain update in each time step. In these studies, the penalty matrices were assumed to be time invariant. The use of time variant penalty matrices to reach optimal performance, as in this study, is not dealt with.

Each part of the controller is more completely described and tested in the following chapters.

10.2.1 The recursive identification algorithm

A recursive extended-least-square (RELS) algorithm has been used to estimate the parameters in the ARMA model describing the frame acceleration characteristics.

10.2.1.1 Constant forgetting factor

With the degree of the polynomials na and nc standardized to n, the output y(t) from the disturbance model can be written in terms of parameters and signals as:

$$y(t) = \Phi^T(t)\Theta(t) + e(t) \tag{256}$$

where

$$\Theta^T(t) = (a1 \quad \dots \quad an \quad c1 \quad \dots \quad cn) \tag{257}$$

$$\Phi^T(t) = (-y(t-1) \quad \dots \quad -y(t-n) \quad \varepsilon(t-1) \quad \dots \quad \varepsilon(t-n)) \tag{258}$$

and $\varepsilon(t)$ is a proxy to $e(t)$:

$$\varepsilon(t) = y(t) - \Phi^T(t)\Theta(t) \tag{259}$$

Θ is the vector of estimated parameters.

The RELS algorithm can be summarized by:

$$\Omega(t) = \frac{1}{\lambda(t)}\left(\Omega(t-1) - \frac{\Omega(t-1)\Phi(t)\Phi(t)^T\Omega(t-1)}{\lambda(t) + \Phi(t)^T\Omega(t-1)\Phi(t)}\right) \tag{260}$$

$$\varepsilon(t) = y(t) - \Phi(t)^T\Theta(t-1) \tag{261}$$

$$\Theta(t) = \Theta(t-1) + \Omega(t)\Phi(t)\varepsilon(t) \tag{262}$$

where $\Omega(t)$ is a covariance matrix.

The forgetting factor $\lambda(t)$ (where $0 < \lambda(t) \leq 1$) weights the measurements, whereby a measurement received n samples ago will have a weighting proportional to λ^n (assuming a constant forgetting factor) (Hunt & Grimble, 1988).

The constant forgetting factor technique for parameter tracking has been used frequently in adaptive control algorithms. The algorithm, however, encounters problems when little

new information is being brought in by the observations. Ω then increases as λ^{-1} (so-called estimator wind-up). If Ω becomes large in this way then observation noise, or a sudden increase in information, may induce large spurious variations in Θ.

A lot of different changes of the algorithms to avoid the difficulties have been reported (Shah & Cluett, 1988). One way is to suspend the parameter tracking when the input signals are too low, another is to maximize the values for the parameters in Ω.

The RELS algorithm with constant λ has been tested on an acceleration time series (Figure 106) measured on the tractor described in Ch. 9.7. The measurements were performed with the tractor first driving on one surface. The tractor was then stopped for some seconds before the driving was continued on another surface, introducing accelerations with more power in the lower frequency area.

The identified models are of second order (n=2). Several λ values have been tested, but the results shown in the diagrams are calculated with $\lambda = 0.98$. The original algorithm has been used without any restrictions on the covariance matrix.

Figure 105 shows the identified values for the ARMA parameters. To show the tendency for estimator wind-up, the trace (sum of the diagonal elements) for the Ω matrix is also shown in Figure 106.

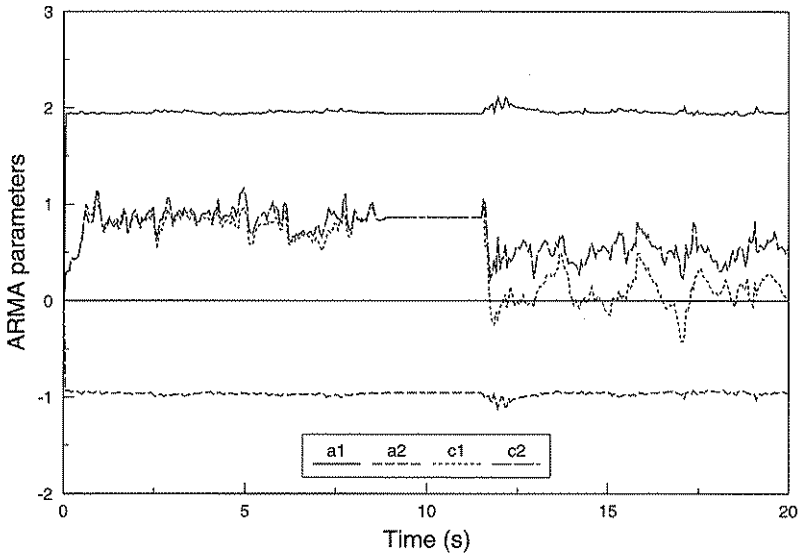

Fig. 105. ARMA model parameters identified with $\lambda = 0.98$.

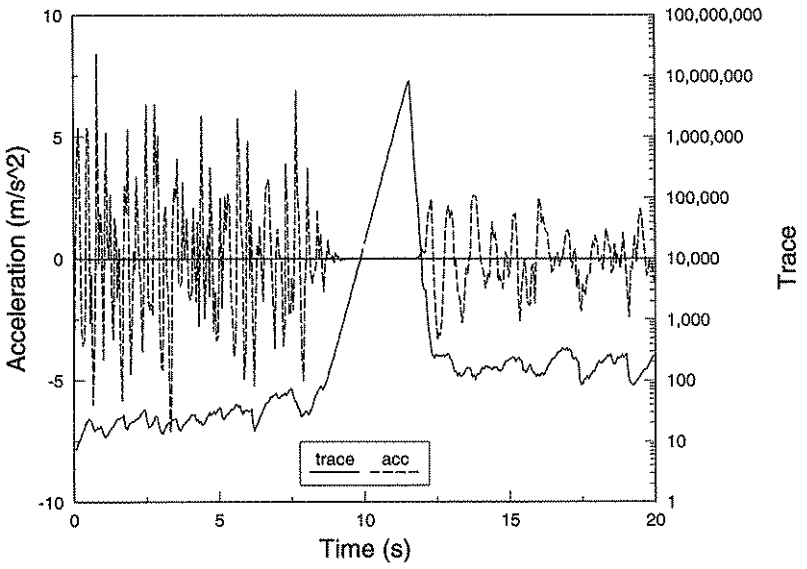

Fig. 106. The trace for the Ω matrix in the described identification together with the acceleration time series used as input.

The results shows that the algorithm can be used to identify the disturbance model parameters. When the input is very low, the values in the covariance matrix increase and must then be limited to avoid stability problems. The very high values in the covariance matrix also explain why the model parameters became very nervous directly after the stop.

10.2.1.2 Variable forgetting factor

When the tractor is driven on different surfaces, periods with relatively constant disturbance characteristics are often interrupted by periods including quick changes. During an identification run is it therefore useful if the forgetting factor can be decreased when a change in the system is sensed. In the absence of prior knowledge of change times, one way of detecting change is through the prediction error $\varepsilon(t)$. If this error grows it may mean that the identified model is incorrect and needs adjustment. At such times, the forgetting factor can be decreased to allow the model to adapt.

As variable forgetting factor (Wellstead & Zarrop, 1991) the following can be used:

$$\lambda(t) = \frac{\tau_\lambda}{\tau_\lambda - 1}\left(1 - \frac{\varepsilon^2(t)}{\tau_\lambda \kappa(t)}\right) \tag{263}$$

where τ_λ determines the rate of adaptation and $\kappa(t)$ is a weighted average of the past values of $\varepsilon^2(t)$. If $\kappa(t)$ is calculated according to:

$$\kappa(t) = \frac{\tau_\lambda - 1}{\tau_\lambda}\kappa(t-1) + \frac{\varepsilon^2(t)}{\tau_\lambda} \tag{264}$$

can $\lambda(t)$ be calculated from:

$$\lambda(t) = \frac{\kappa(t-1)}{\kappa(t)} \tag{265}$$

RELS algorithms offering higher precision or fewer calculations are also developed. To reach higher precision, the algorithms can be based on matrix factorization theory (Wellstead & Zarrop, 1991, Mohtadi, 1988). Faster algorithms can be reached if only the diagonal elements in the Ω matrix are considered. The off-diagonal elements usually have very small effects on the parameters and adaptive controllers including a simplified RELS algorithm have shown almost the same characteristics as normal ones. The number of calculations, however, decreases significantly, especially for higher order models (Warwick, 1988).

The acceleration time series shown in the previous chapter has also been used to study the characteristics for the algorithms with variable forgetting factor.

The algorithm controls the forgetting factor and decreases it when the weighted values of the estimation errors are increasing. The τ_λ parameter decides the speed of the algorithm. In Figure 107, $\lambda(t)$ is shown for identification with $\tau_\lambda = 40$ and 100. The scales of the left and right axes differ in order to make the differences in the curve easier to recognize. Also the c2 parameter is shown for the different τ_λ values (Figure 108).

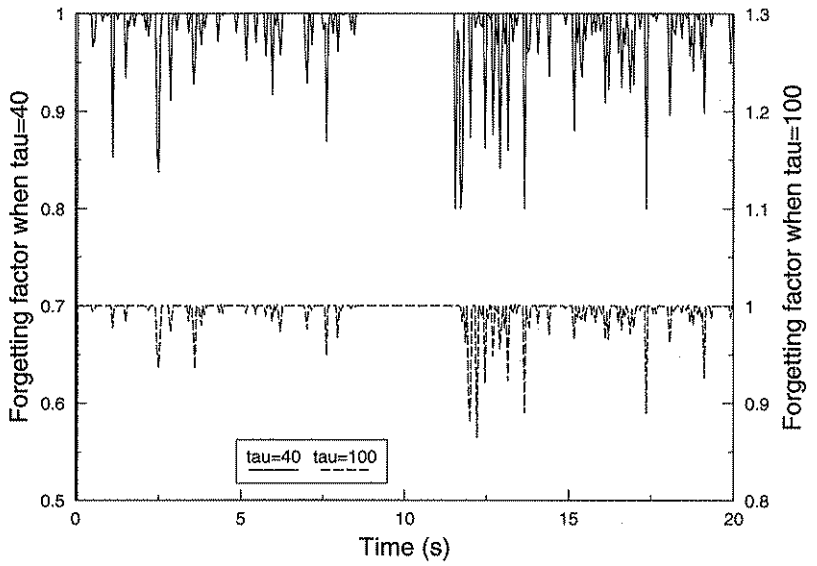

Fig. 107. The forgetting factor in the described identifications with τ_λ = 40 and 100.

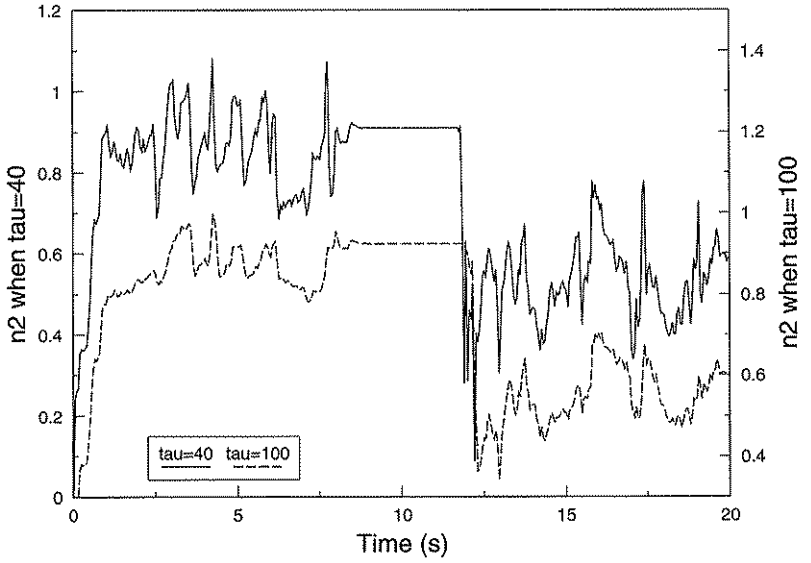

Fig. 108. c2 in the described identifications with τ_λ = 40 and 100.

The algorithm with the variable forgetting factor shows logical characteristics with a decreasing $\lambda(t)$ when the characteristics of the input change. $\lambda(t)$ becomes approximately 1.0 when no information is added, and thereby the estimator wind-up tendencies are eliminated.

With a small τ_λ the algorithm reacts faster when the input characteristics change. If τ_λ is too small the algorithm may, however, become too nervous, with large variations in the estimated parameters.

10.2.2 Recursive feedback gain calculation

The feedback gain's dynamics are decided by the change in disturbance characteristics and the changes for the penalty matrices. It is then assumed that the parameters in the basic continuous time system are time invariant. It is possible to also include variations of these parameters in the adaptive scheme, but this possibility has not been studied.

The studies in Ch. 9.8 have shown that the controller's vibration damping potential was not increased when the disturbance model order was increased over one. The controllers studied have therefore been based on disturbance models of first order.

The **F** and **G** matrices are shown in Ch. 10.1. The disturbance model parameters are calculated with the RELS algorithm.

The state penalty matrix included penalties on the two controlled states, namely state 1 (the suspension travel) and state 4 (the weighted acceleration in the cab). It is the relation

between the two penalties that decides the controller's characteristics. The penalty on state 4 has therefore been kept constant when the state 1 penalty has been varied to reach desired characteristics.

In systems with a limited amount of power available it is, of course, also possible to adjust the penalty on the control ($\mathbf{Q}_2$) to reach less power consuming controllers. The simulations in Ch. 9.13 have shown that the power demands are relatively limited in normal situations. In the studies of adaptive controllers in this chapter, the penalty on the control input has thus been defined so low that the suspension performance is not affected.

The penalty matrices are decided by:

$$(\mathbf{y}^c(t))^T = (z_c^d(t) - z_b^d(t) \quad \ddot{z}_w^d(t)) \tag{266}$$

$$\mathbf{Q}_1 = \begin{pmatrix} \left(\frac{1}{y_1^{cmax}}\right)^2 & 0 & 0 & 0 & 0 & 0 \\ 0 & 0 & 0 & 0 & 0 & 0 \\ 0 & 0 & 0 & 0 & 0 & 0 \\ 0 & 0 & 0 & \left(\frac{1}{y_2^{cmax}}\right)^2 & 0 & 0 \\ 0 & 0 & 0 & 0 & 0 & 0 \\ 0 & 0 & 0 & 0 & 0 & 0 \end{pmatrix} \tag{267}$$

$$\mathbf{Q}_2 = \left(\frac{1}{u^{\max}}\right)^2 \tag{268}$$

where y_2^{cmax} is defined to 0.010, $u^{\max}$ is defined to 1.0 e3 and y_1^{cmax} is made time variant.

The input is then chosen according to the control law:

$$u(t) = -\mathbf{K}(t)\mathbf{x}^r(t) \tag{269}$$

where

$$\mathbf{K}(t) = \left[(\mathbf{G}^u)^T\mathbf{S}(t+1)\mathbf{G}^u + \mathbf{Q}_2\right]^{-1}(\mathbf{G}^u)^T\mathbf{S}(t+1)\mathbf{F} \tag{270}$$

The time dependency for the system description matrices and penalty matrices is not written out in order to make the formulas easier to read.

It is not possible to solve the complete Riccatti equation (to get $\mathbf{S}(t+1)$) in each time step but a controller always striving towards the optimum parameters is reached if the iterative formula for $\mathbf{S}$ is updated once in each time step:

$$\mathbf{S}(t+1) = \mathbf{F}^T\mathbf{S}(t)\mathbf{F} + \mathbf{Q}_1 - \mathbf{F}^T\mathbf{S}(t)\mathbf{G}^u\left[(\mathbf{G}^u)^T\mathbf{S}(t)\mathbf{G}^u + \mathbf{Q}_2\right]^{-1}(\mathbf{G}^u)^T\mathbf{S}(t)\mathbf{F} \tag{271}$$

If a controller with very high calculation capacity is available, the formula can be iterated more than once in each time step in order to get a faster controller. In this study, is it assumed that only one iteration is performed in each time step.

The progress for the feedback gains when a change is defined in the penalty matrices or in the disturbance parameters is studied. The gain dynamics is also an important factor when the feedback mechanism for the penalty matrix changes should be designed.

In Figure 109 the progress for some of the feedback parameters is shown for some parameter changes. At t=1 y_1^{cmax} was decreased from 0.05 to 0.01. At t=3.5 the parameter was further decreased to 0.005 and at t=6 to 0.001. At t=8.5, the parameters describing the disturbance characteristics were suddenly changed to describe an input including more low frequency signals.

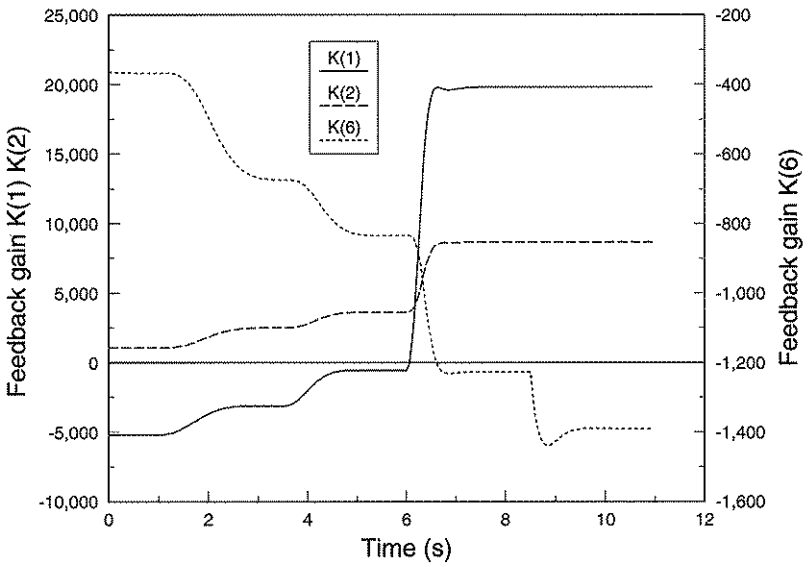

Fig. 109. The feedback gain's time dependency for the parameter changes described above.

The curves shows that the feedback gain changes relatively fast when the penalty matrix is changed. The time constants for the step responses are not really constant but decrease when y_1^{cmax} decreases.

When the disturbance model parameters are changed, only **K**(6) changes, as expected. Even the change for this parameter is relatively small.

10.2.3 Recursive observer gain calculation

If an observer is used to estimate the states in the adaptive active suspension controller, is it reasonable that also the observer gains should be recursively calculated.

If the parameters in the continuous time model are assumed to be time invariant it is the change of the disturbance characteristics that decides the observer gain variations.

The model description used when calculating the observer gains is the one described in Ch. 10.1. The average disturbance input noise variance is not directly calculated by the ordinary RELS algorithm. The $\kappa(t)$ parameter used in the identification algorithm with the variable forgetting factor is, however, a weighted average of the noise variances and seems to be the best available noise variance value.

It is assumed that measurements of the suspension travel (state 1) and the frame accelerations (state 6) are available. It is also assumed that the frame velocity (state 3) can be calculated from the accelerometer signal and used as input to the observer. The transducer measurement ranges and measurement noise levels described in Ch. 9.11 are used in the calculations and assumed to be time invariant.

The observer structure is:

$$\hat{\mathbf{x}}^s(t+1) = \mathbf{F}\hat{\mathbf{x}}^s(t) + \mathbf{G}^u\mathbf{u}(t) + \mathbf{L}(t)\left(\mathbf{y}^m(t) - \mathbf{H}^m\hat{\mathbf{x}}^s(t)\right) \tag{272}$$

The feedback is then decided by:

$$u(t) = -\mathbf{K}(t)\hat{\mathbf{x}}^s(t) \tag{273}$$

The $\mathbf{L}(t)$ matrix is then time variant and calculated from:

$$\mathbf{L}(t) = \mathbf{F}\mathbf{P}(t)\left(\mathbf{H}^m\right)^T\left[\mathbf{H}^m\mathbf{P}(t)\left(\mathbf{H}^m\right)^T + \mathbf{R}_2\right]^{-1} \tag{274}$$

Just as for the Riccatti equation in the feedback gain calculations, it is assumed that the observer's Riccatti equation is iterated once in each time step to get an observer always striving towards the optimum performance.

The iterative formula for $\mathbf{P}(t)$ then becomes:

$$\mathbf{P}(t+1) = \mathbf{F}\mathbf{P}(t)\mathbf{F}^T + \mathbf{R}_1 - \mathbf{F}\mathbf{P}(t)\left(\mathbf{H}^m\right)^T\left[\mathbf{H}^m\mathbf{P}(t)\left(\mathbf{H}^m\right)^T + \mathbf{R}_2\right]^{-1}\mathbf{H}^m\mathbf{P}(t)\left(\mathbf{F}\right)^T \tag{275}$$

where

$$\left(\mathbf{y}^m(t)\right)^T = \left(z_c^d(t) - z_b^d(t) \quad \dot{z}_b^d(t) \quad \ddot{z}_b^d(t)\right) \tag{276}$$

$$\mathbf{R}_1 = \kappa(t) \tag{277}$$

$$\mathbf{R}_2 = \begin{pmatrix} \left(r_1^{\max}\cdot\sigma_1^{\max}\right)^2 & 0 & 0 \\ 0 & \left(r_2^{\max}\cdot\sigma_2^{\max}\right)^2 & 0 \\ 0 & 0 & \left(r_3^{\max}\cdot\sigma_3^{\max}\right)^2 \end{pmatrix} \tag{278}$$

The time dependency for the system description matrices is not written out.

The dynamics for the observer gains are studied when sudden disturbance parameter changes are defined. The observer is first calculated to be optimal for a disturbance signal measured on a small road when driving at 25 km/h. At t=1, the disturbance model was suddenly changed to the one identified for the measurements performed when driving on the very rough test track 2 at 6 km/h. At t=2, the $\mathbf{R}_1$ parameter was changed to be twice as high as before.

Most of the parameter changes were very small when the disturbance models were changed. Figure 110 shows the parameters $\mathbf{L}(4,3)$, $\mathbf{L}(5,3)$ and $\mathbf{L}(6,3)$ for the studied period.

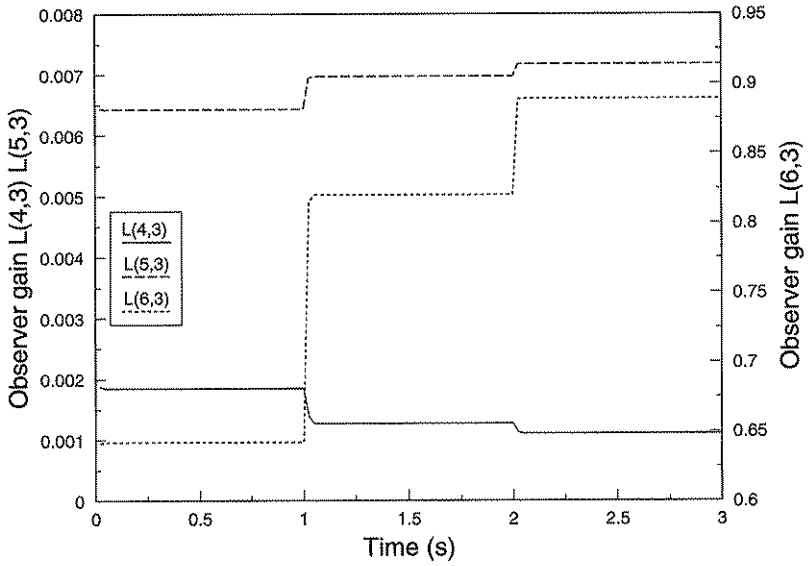

Fig. 110. The observer gain parameters $\mathbf{L}(4,3)$, $\mathbf{L}(5,3)$ *and* $\mathbf{L}(6,3)$ *calculated for the disturbance model changes described above.*

The results of the study show that most of the observer parameters are very insensitive to disturbance model changes. The parameters in the figure were chosen from those showing the highest sensitivity. The parameters change very rapidly (faster than the feedback gains) when the assumptions change.

10.2.4 Recursive calculation of mean travel

The principle for the adaptation in the described controller is based on the parameters in the penalty matrices being varied so that the resulting controller makes optimum use of the available travel space. A recursively calculated mean suspension travel value is compared to a defined reference value and the penalty matrix is changed depending on the result.

The mean suspension travel is normally zero, so it is the mean of the absolute travel values that is interesting. The algorithm becomes more sensitive to extreme travel values if the mean of the squared travel is calculated instead, which may have positive effects on the possibilities to avoid excessive travel.

The technique used for the recursive calculation of the variance for the prediction errors can also be used for the recursive mean travel calculations. The algorithm has the same structure as a first order digital filter:

$$\zeta(t) = \frac{\tau_\zeta - 1}{\tau_\zeta}\zeta(t-1) + \frac{|z_c^d(t) - z_b^d(t)|}{\tau_\zeta} \tag{279}$$

or with squared values:

$$\zeta'(t) = \frac{\tau_\zeta - 1}{\tau_\zeta}\zeta'(t-1) + \frac{(z_c^d(t) - z_b^d(t))^2}{\tau_\zeta} \tag{280}$$

$$\zeta(t) = (\zeta'(t))^{0.5} \tag{281}$$

where $\zeta(t)$ is the weighted average and τ_ζ is the rate of adaptation.

The algorithm has been tested on a time series with travel values from one of the validation studies in Ch. 6.3 (Figure 111). The algorithm using the squared values has been used with τ_ζ = 100 and 300.

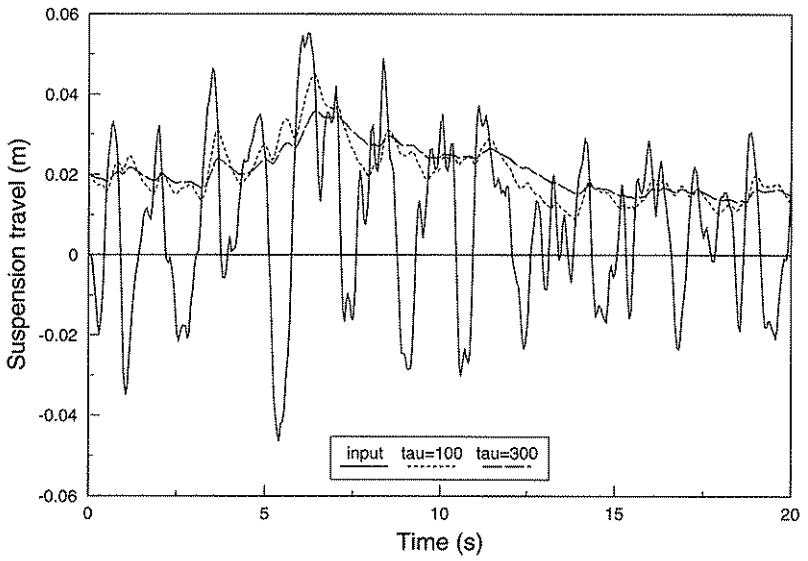

Fig. 111. The input to and the output from the recursive algorithm for calculation of mean suspension travel with τ_ζ = 100 and 300.

The figure shows that the algorithm can be used to recursively calculate average suspension travel values. A smaller τ_ζ results in a faster algorithm, but also more controller parameter changes.

10.2.5 The penalty matrix dynamics

The structure of the adaptive controller is described in Figure 104. The system parts mainly influencing the penalty matrix dynamics are shown in Figure 112.

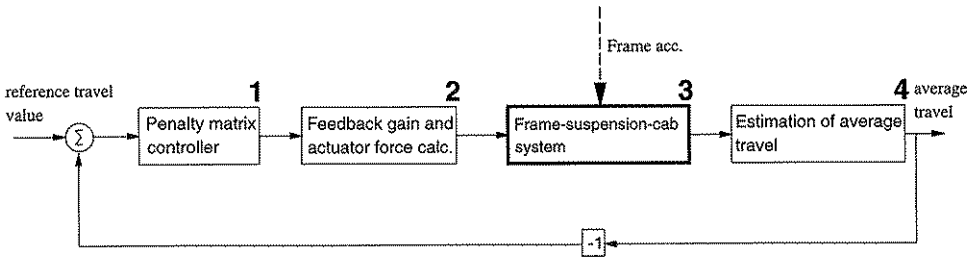

Fig. 112. System influencing the penalty matrix dynamics.

When the frame is moving, the feedback gain vector and the frame acceleration characteristics decide the suspension travel. The travel is measured and the algorithm described in Ch. 10.2.4 is used to recursively calculate the average travel value $\zeta(t)$ (block 4).

The $\zeta(t)$ value is compared with the defined reference value and the difference is used by the penalty matrix controller (block 1) to calculate the penalty matrix changes. The penalty matrix is then used by the recursive algorithm (block 2) described in Ch. 10.2.2 to calculate the feedback gains and the actuator forces.

The observer gain calculation affects the system only indirectly and is not included in the system used for the penalty matrix dynamics analysis.

To decide the structure of the penalty matrix controller, the system is analysed with traditional automatic control tools for feedback systems. The system is not perfectly linear, and thus the linear description of the characteristics for some of the parts must be approximations. The controller is discrete but the involved time constants are so big compared to the sampling time that continuous time theory can be used to make the analysis more understandable.

If the disturbance load variance suddenly is increased, the expected travel variance is also immediately increased. The output from the recursive mean travel calculator (block 4 in Figure 112) then begins to increase. The algorithm for block 4 is a first order digital filter. The continuous transfer function is then approximately:

$$G_4(s) \approx \frac{1}{(sT_4+1)} \tag{282}$$

$$Y_4(s) = G_4(s)U_4(s) \tag{283}$$

where

s = the derivation operator

$Y_i(s)$ = the Laplace transform of the output from block i

$G_i(s)$ = The transfer function for block i

$U_i(s)$ = the Laplace transform of the input to block i

and

$$T_4 \approx T_s\tau_\zeta \tag{284}$$

The average travel value is compared to the defined reference value. The controller with the transfer function G_1 uses the result to calculate the changes for the penalty on the travel state. G_1 decides the system's characteristics and is analysed in the next chapter.

The changed penalty matrix results in changed feedback gains. The changes are dependent on the iterations of the Riccatti equation and therefore involve a time constant. If the system characteristic is assumed to be of first order, the transfer function for block 2 can be described:

$$G_2(s) = \frac{1}{(sT_2 + 1)} \tag{285}$$

Figure 109 can be used when estimating T_2. The figure shows that T_2 is dependent on the working point of the Riccatti equation and thus an average value must be used, if the transfer function described above is to be used.

The expected variance for the travel is immediately changed when the feedback gains are changed and the suspension system therefore involves no time delay. Block 2 and Block 3, however, convert penalty matrix values to suspension travel values and thus G_2 or G_3 must include a constant, which for simplicity is called K_3:

$$G_3(s) = K_3 \tag{286}$$

K_3 defines the relation between the penalty matrix change and the suspension travel change. The varied parameter in the penalty matrix is the parameter defined as the maximum allowed suspension travel (y_1^{cmax}). The value $\mathbf{Q}_1(1,1)$ is then $= \left(\frac{1}{y_1^{cmax}}\right)^2$. The other parameters in the penalty matrices are kept constant.

An increased value for y_1^{cmax} decreases the penalty on the travel state and thereby increases the travel if the frame acceleration characteristics are not changed. K_3 therefore is positive.

The connection between y_1^{cmax} and suspension travel (RMS) is simulated for different z dimension frame acceleration time series with approximately time invariant characteristics. The results are shown in Figure 113.

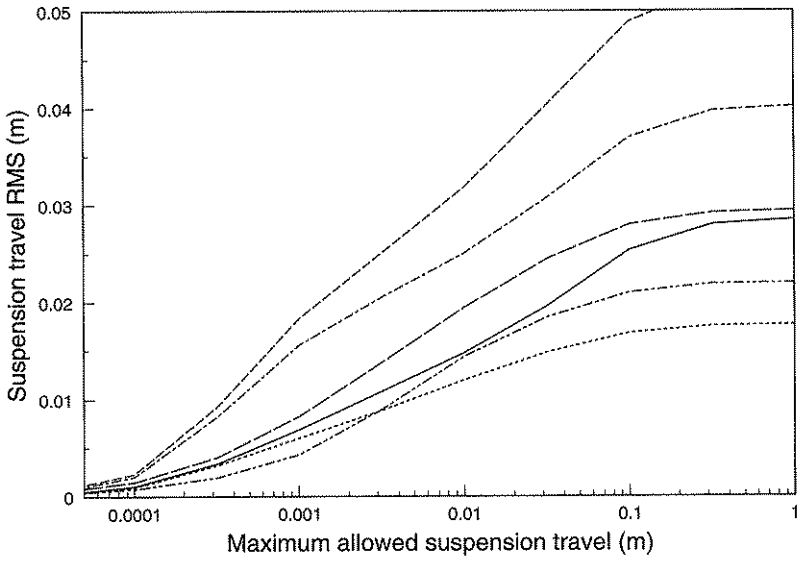

Fig. 113. Suspension travel (RMS) vs y_1^{cmax} for different z dimension frame acceleration time series.

The curve with highest travel values in Figure 113 is from simulations using the extreme input measured when driving on track 2 at 6 km/h. Even for this extreme signal, the RMS travel is very low for y_1^{cmax} = 1.0 e-4. The figure shows also that travel does not increase much when y_1^{cmax} is increased above 0.1. To make the algorithm more robust, y_1^{cmax} can be limited by 1.0 e-4$\leq y_1^{cmax} \leq$ 0.1.

In the interesting area the travel RMS is relatively linearly dependent on $\log(y_1^{cmax})$. To make the system more linear, is it preferable to define K_3 as the relation between the change in suspension travel RMS and the change in $\log(y_1^{cmax})$. The output from the penalty matrix controller then defines $\log(y_1^{cmax})$ instead of y_1^{cmax}.

Figure 113 also shows that K_3 is not exactly the same for all frame acceleration characteristics, but relatively contant. An average value for K_3 can be calculated from the figure.

10.2.6 The penalty matrix controller

The transfer function for the penalty matrix controller ($G_1(s)$) decides the possibilities to keep the mean suspension travel (RMS) close to a defined reference value.

The estimations of the other transfer functions in the system include some approximations. Controllers of PID type are robust to nonlinearities and varying system parameters. They are also easy to implement and have therefore been used in the studied system.

Figure 113 shows that the value for $\log(y_1^{cmax})$ in the penalty matrix which corresponds to a defined travel value is dependent on the frame acceleration characteristics. One way to avoid problems with varying working points is to let the controller define the time derivative of $\log(y_1^{cmax})$ instead of the direct level for the variable. The transfer function for a PD-controller defining the time derivatives becomes:

$$G_1(s) = \frac{K_P + K_D s}{s} \tag{287}$$

This transfer function is the same as for a PI-controller defining the direct level for $\log(y_1^{cmax})$. If the PD-controller is used the total transfer function ($G_T(s)$) for the system becomes:

$$G_T(s) = \frac{G_1(s)G_2(s)G_3(s)G_4(s)}{1 + G_1(s)G_2(s)G_3(s)G_4(s)} \tag{288}$$

$$= \frac{(K_P + K_D s)K_3}{s(sT_2 + 1)(sT_4 + 1) + (K_P + K_D s)K_3} \tag{289}$$

with the characteristic polynomial:

$$s^3 + \frac{T_2 + T_4}{T_2 T_4} s^2 + \frac{K_D K_3 + 1}{T_2 T_4} s + \frac{K_P K_3}{T_2 T_4} \tag{290}$$

The position of the poles can easily be calculated for different values of K_P and K_D by solution of cubic equations.

The step response for the system is studied for different values of K_P and K_D in Figure 114. The other parameters of influence are defined by $T_2 = 0.5$, $T_4 = 1.5$ and $K_3 = 0.010$.

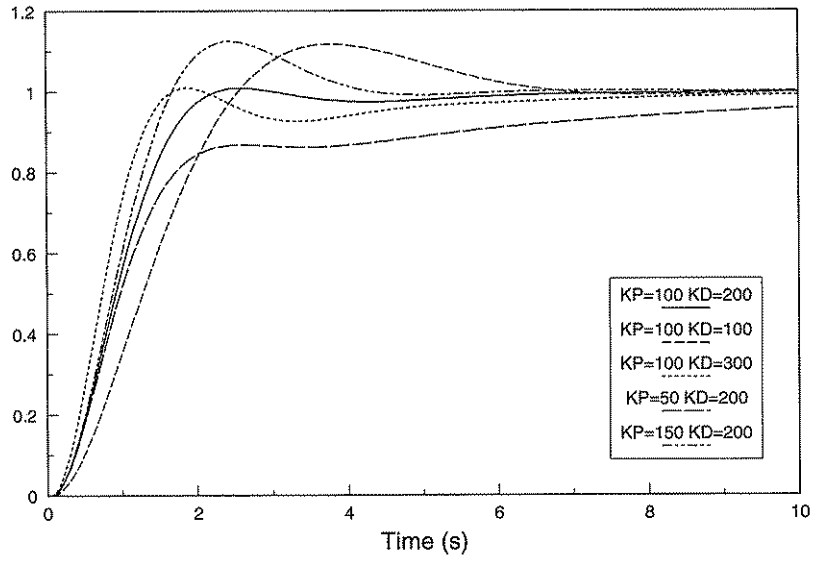

Fig. 114. Step response for the system described above for different values of K_P and K_D.

Figure 114 shows that it is possible to define values for K_P and K_D which make the system stable and relatively fast. Rise times around 1.0 s can be reached without too high overshoots.

It is seldom possible to prove the stability of a system including parameter approximations and relations that are not perfectly linear. The sensitivity to parameter changes is then an important factor to study when examining stability.

Figure 115 shows step responses for the system with $K_P = 100$ and $K_D = 200$. The parameters T_2, T_4 and K_3 have been halved or doubled to study the sensitivity to changed system characteristics.

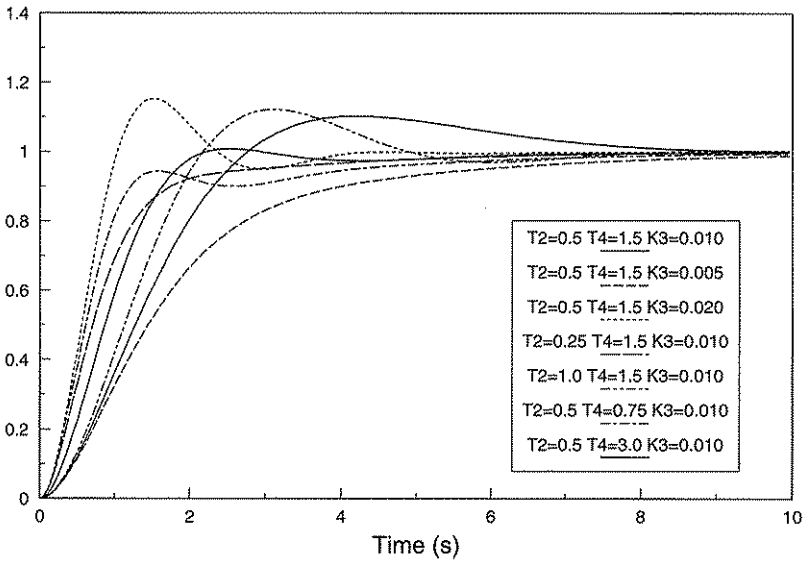

Fig. 115. Step response for the system described above when some parameters are varied.

The system shows satisfactory characteristics and stability even when the parameters are varied as much as in Figure 115.

10.2.7 Implementation of the algorithm

The complete adaptive controller performs numerous calculations in each time step. The processor therefore probably needs the whole sample time to calculate the signal to the force actuator. The calculation order for the algorithm used in the simulations in the next chapter can then be described as in Figure 116.

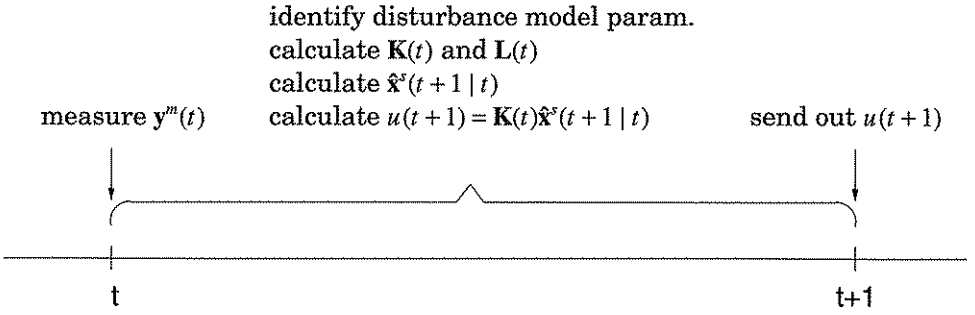

Fig. 116. Schematic description of the adaptive controller's calculation order.

Another possibility is to use $\mathbf{y}^m(t)$ to calculate $\hat{\mathbf{x}}^s(t \mid t)$ with a Kalman filter. $u(t+1)$ is then calculated from $u(t+1) = \mathbf{K}(t)\hat{\mathbf{x}}^s(t \mid t)$. In this case, the system matrices must include a time delay which increases the matrix orders, and the algorithm has therefore not been studied further.

With an extremely fast processor, the calculation time could be neglected and $u(t)$ calculated from $u(t) = \mathbf{K}(t)\hat{\mathbf{x}}^s(t \mid t)$. The effects of this algorithm have been studied in some simulations, but the improvements compared to the algorithm described in Figure 116 were very small.

The controller needs some kind of start-up procedure. This should probably not cause any problems if good initial values for the parameters are precalculated and stored in the controller's memory.

When the vehicle is not moving the weighted travel value cannot be allowed to fall to zero. If the vehicle then begins to move on a relatively coarse surface the adaptive function may be too slow if the penalty on the travel state is too low when the movement begins. Some prestudies showed that, in order to avoid over-travelling, it was preferable to lock the weighted travel value to the defined reference value and the penalty on the travel state to a relatively high value ($\log(y_1^{cmax}) = -3$) when the vehicle not was moving.

Even a very effective adaptive suspension algorithm may encounter problems when very high frame acceleration values suddenly arise on an otherwise relatively smooth surface. To avoid over-travel in such circumstances, some kind of safety function is needed. Some kind of safety function is normally needed also for passive suspensions. One possibility is to build in this function in the controller, whereby very high travel values, for example, can be compensated by very quickly increasing the damping or increasing the spring constant, and thereby avoiding the over-travel. A probably safer technique is to use mechanical shock absorbers or nonlinear dampers which only work at very high suspension element strokes.

10.3 Simulations with adaptively controlled suspensions

The characteristics for the adaptively controlled active suspension have been studied fairly extensively with different parameter values and frame acceleration signals.

The parameter values used in the simulations are:
$\tau_\lambda = 100 \quad \tau_\varsigma = 300 \quad K_3 = 0.010 \quad T_2 = 0.5 \quad T_4 = 1.5 \quad K_P = 100 \quad K_D = 200$

10.3.1 Ordinary varying surface

The input frame acceleration time series used in this simulation is measured when driving on an surface which is relatively rough until the middle of the recorded period and then becomes smoother towards the end of the period (Figure 117).

The weighted acceleration in the cab is also shown in Figure 117. Figure 118 shows the suspension travel and the weighted average travel for the simulated time period. The output from the block calculating the penalty on the travel state ($\log(y_1^{cmax})$) and one of the feedback gains are shown in Figure 119.

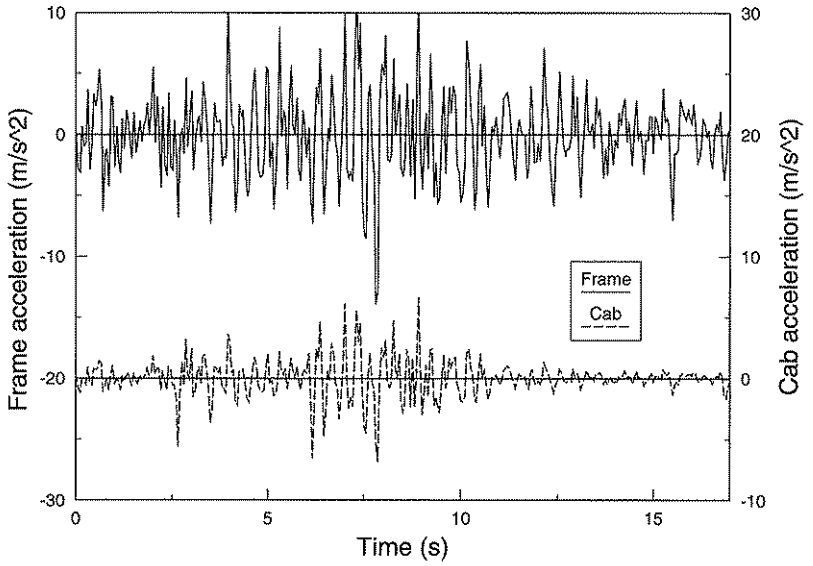

Fig. 117. The frame z dimension accelerations used as input to the simulation described above together with the resulting ISO weighted accelerations in the cab.

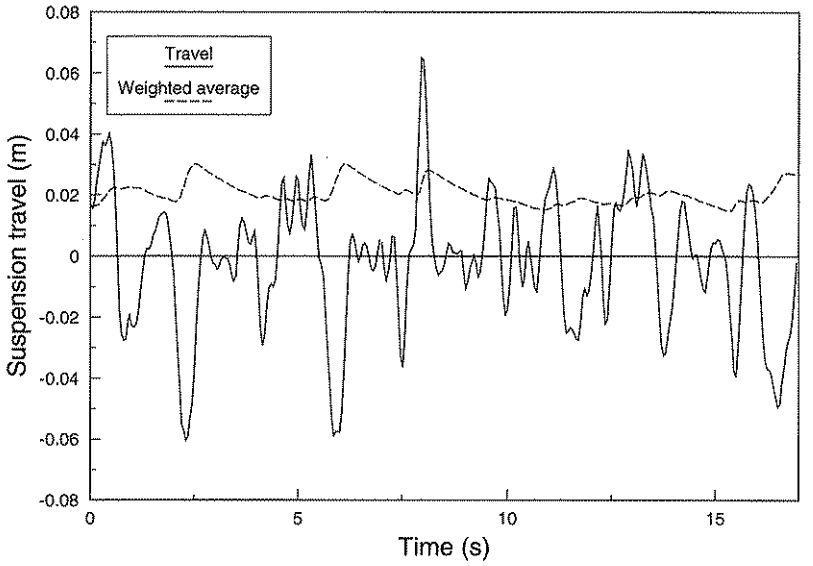

Fig. 118. The suspension travel and the weighted average travel for the simulation described above.

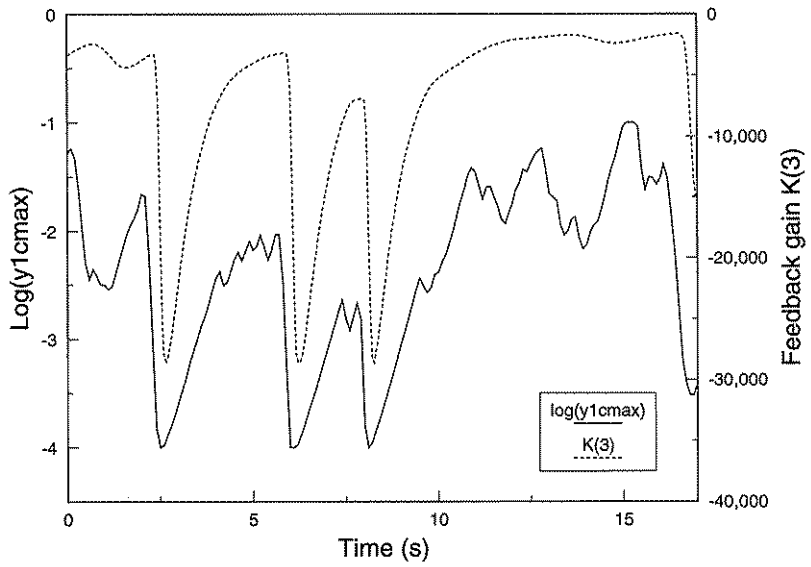

Fig. 119. Log(y_1^{cmax}) *and the feedback gain for state 3 for the simulation described above.*

Figure 118 shows that the controller is able to keep the average travel value relatively close to the defined reference value (0.020 m).

The penalty on the travel state (state 1) is relatively high in the beginning to reduce the travel. From about t=10 s, the input vibration level is lower and the penalty can be decreased to get a suspension with very high vibration damping capacity.

10.3.2 Driving with stops

The input signal used for this simulation is the same as the one used to study the performance for different recursive identification algorithms in Ch. 10.2.1. The measurements were performed with the tractor first driving on one surface. The tractor was then stopped for some seconds before the driving was continued on another surface, introducing accelerations with more power in the lower frequency area.

The weighted acceleration in the cab is shown in Figure 120 together with the frame acceleration input. Figure 121 shows the suspension travel and the weighted average travel values for the simulated time period.

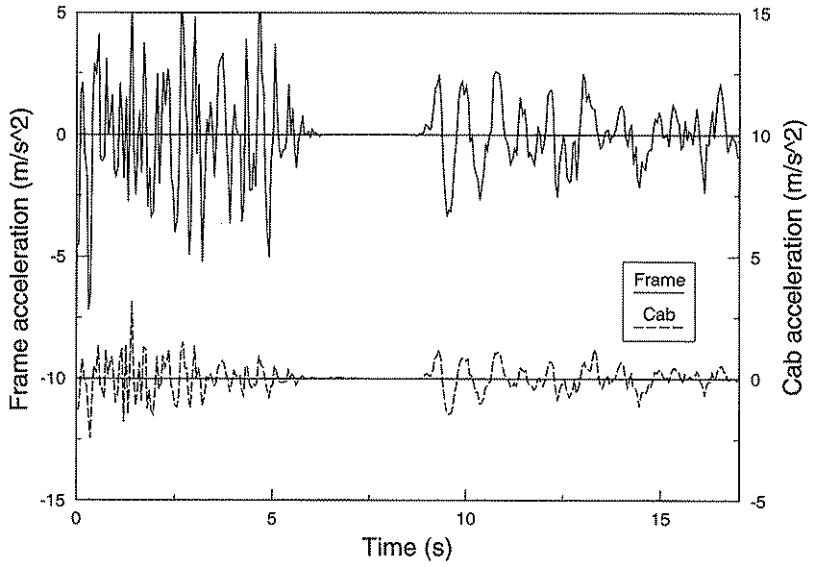

Fig. 120. The frame z dimension accelerations used as input to the simulation described above, together with the resulting ISO weighted accelerations in the cab.

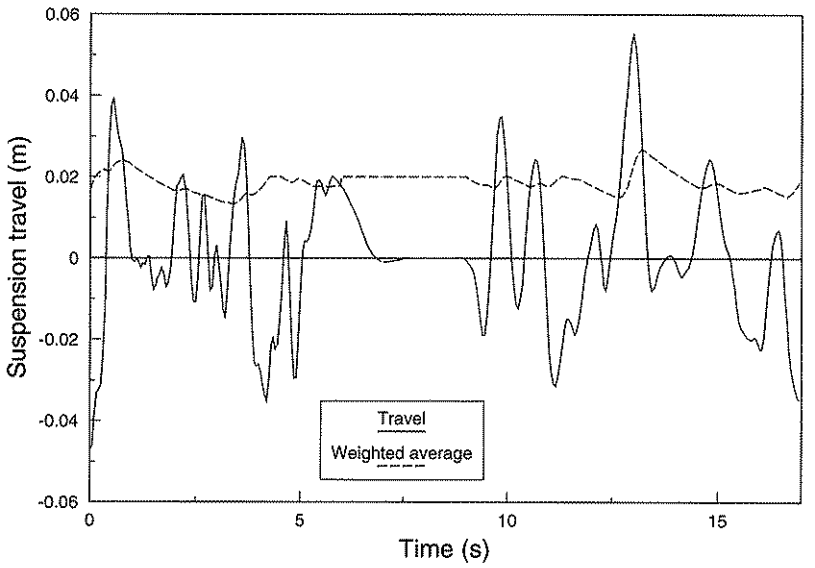

Fig. 121. Suspension travel and the weighted average travel for the simulation described above.

Also in this study the controller keeps the average travel value close to the defined reference value. Between t≈6 and t≈9 the vehicle's velocity is ≈ 0. The average travel

value and the penalty on state 1 are then kept constant and relatively high by the controller. When the vehicle begins to move again, the lock on this parameter is released and the adaptive algorithm is allowed to change the penalty values.

10.3.3 Smooth surface with potholes.

The input used for this simulation is measured when driving on a relatively smooth surface. After some seconds, the vehicle drives over some potholes which induces extreme acceleration values in the frame.

The weighted acceleration in the cab is shown in Figure 122 together with the frame acceleration input. Figure 123 shows suspension travel and the weighted average travel value for the simulated time period.

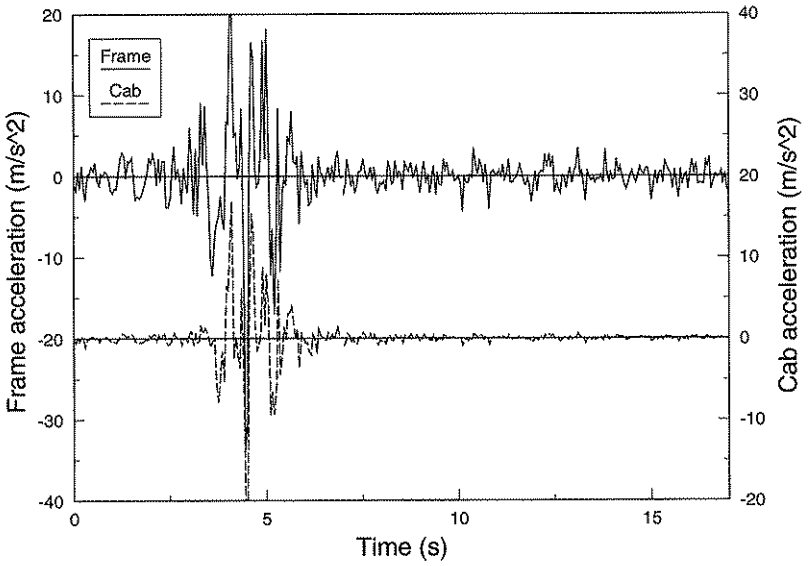

Fig. 122. The frame z dimension accelerations used as input to the simulation described above, together with the resulting ISO weighted accelerations in the cab.

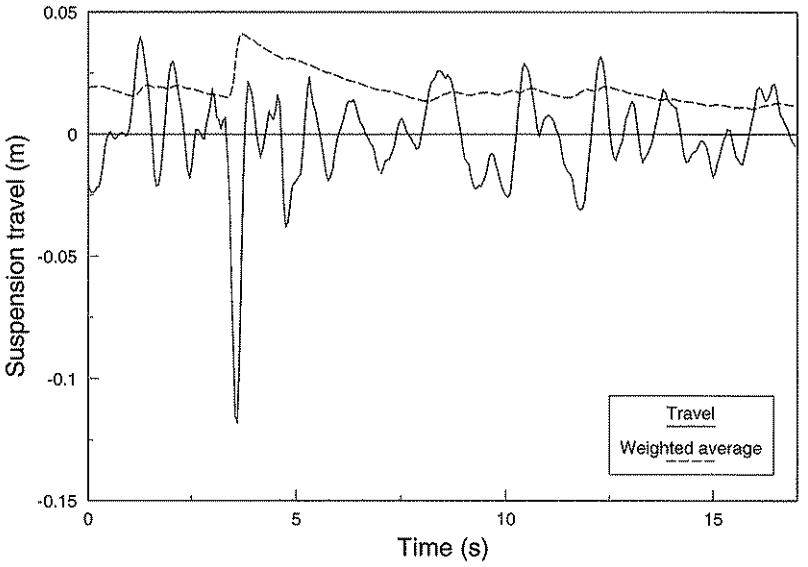

Fig. 123. Suspension travel and the weighted average travel for the simulation described above.

On the relatively smooth surface before the potholes the penalty on the travel state is low, which results in a soft suspension with a good vibration damping potential.

When the first extreme frame acceleration peak occurs, the algorithm is unable to adjust the feedback gains fast enough, and a very high travel value occurs. When the second acceleration peak occurs the gains are adjusted and the travel decreased to a normal level.

The results of these simulations demonstrate the need of some kind of security function to avoid over-travel in extreme situations.

10.4 Controllers based on Gain Scheduling

Gain Scheduling is a nonlinear feedback of special type. It has a linear regulator where parameters are changed as a function of the operating conditions in a preprogrammed way.

Two types of controllers based on Gain Scheduling (GS) theory are discussed. The first type is a traditional GS controller which uses auxilary variables to describe the characteristics of the frame movements. The choice of precalculated and stored feedback and observer gains is then decided by the values of the auxilary variables.

The second type is a simplified, but probably very competitive, version of the adaptive controller described in the earlier parts of Chapter 10. The fact that a change in the ARMA parameters has relatively little effect on the observer and feedback gains is used to design an adaptive controller without any Riccatti equation iteration.

10.4.1 Traditional Gain Scheduling controller

The operating conditions for the cab suspension are decided by the characteristics of the accelerations at the frame. The optimum controller would be obtained if the optimum feedback and observer gains were precalculated and stored for any possible frame acceleration characteristics. When a change in the characteristics is sensed, the controller gains should immediately be modified.

The optimum GS controller cannot be attained in practice. The possibilities to save different feedback and observer gains may be limited by the memory's storage capacity. It may also be very difficult to find auxilary variables that correspond to changes in the dynamic process. The tuning of GS systems is a problem just as in all types of adaptive controllers. The controller must not be so fast that it overreacts for a single unexpected disturbance but must be fast enough when the frame acceleration characteristics really are changed. The major drawback for the GS controllers is, however, normally the lack of feedback to compensate for an incorrect schedule.

The use of GS controllers obviously involves some disadvantages but results in very usable controllers for many applications (Åström & Wittenmark, 1989).

The characteristics were studied for suspensions with active GS controlled suspensions based on some different auxilary variables.

The choice of feedback and observer gains have to be a function of one, or no more than two, auxilary variables to limit the amount of stored gains. It was found that the parameters in the first order ARMA model describing the frame acceleration characteristics did not contain enough information to decide the choice of gains.

Another possibility tested was to use a frequency weighted RMS-value of the accelerations at the frame for the decision of the gains. The frequency weighting filter was designed to correspond to the average transfer function between the frame acceleration input and the travel. This controller was usable, but not perfect, and it was necessary to include large safety margins when chosing feedback gain matrices.

The study showed that it was possible to construct a usable controller based on GS technique. The problems to find usable auxilary variables and variable transformations, together with the impossibility to use feedback correction, resulted however in the gains having to be chosen with large safety margins. The large margins decreased the average vibration damping potential for the suspensions. The results indicated, however, that it is much better to use a GS controller even with few gain levels than a totally time invariant controller.

10.4.2 Simplified adaptive controller

The adaptive controller described earlier in the chapter recalculates the observer and feedback gains depending on the result of a recursive identification algorithm. The results shown in Figure 110 show that the observer gain changes are very small when the

identified ARMA parameters are changed. A relatively small change in the relation between the error level of the transducers change the observer gains more than a disturbance characteristics change from one extreme to the other.

To simplify the controller, the observer gains can then be calculated for an "average" disturbance model and defined as time invariant. Another possibility to simplify the controller would, of course, be to measure all states and not use any observer. If this could be done the robustness of the controller would be increased considerably.

When the disturbance model changes, the feedback gain vector is not changed except for **K**(6). Use of an average disturbance model also in the feedback gain calculations removes the need for the identification algorithm and the controller can be even more simplified. **K**(6) does not become "optimal" any more when it is calculated for an average disturbance model but, for example, Figure 109 shows that the difference is relatively small.

If the disturbance model is defined to be constant it is only the changes in the penalty matrices that decide the changes for the feedback gains **K**. Normally, the only varied parameter in the penalty matrices is the penalty on the travel state $\left(\frac{1}{y_1^{cmax}}\right)^2$. The study in Ch. 10.2.5 showed that y_1^{cmax} can be limited by $1.0e-4 \le y_1^{cmax} \le 0.1$. If the **K** vector is precalculated and stored in the memory for $\log(y_1^{cmax}) = -1.0,\ -1.1\ \ldots\ -4.0$, **K** can be stored in 31 memory cells with 6 parameters, (**K**(1) – **K**(6)) in each cell, totally 186 parameters.

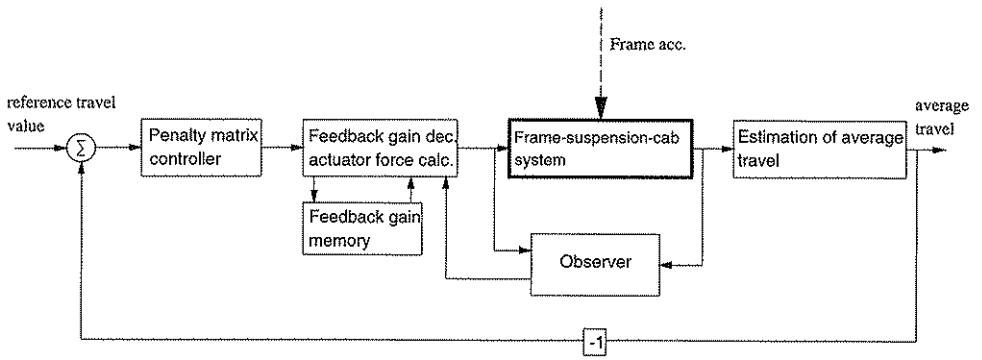

Fig. 124. The structure for the simplified adaptive controller.

An algorithm including the simplifications described above includes no iteration of any kind of covariance matrices and must be relatively simple to design in practise.

The use of GS technique for the choice of the feedback gains results in the T_2 parameter that describes the time constant in the Riccatti iterations and is used in the calculations of the controller gains K_P and K_D, decreases to zero. This enables us to make the system react faster when the average travel value differs from the reference value, with retained stability.

The main advantages reached with the simplified controller are the shorter and easier applications of the algorithm together with the possibilities to obtain a controller with faster reactions. Disadvantages are that the observer and feedback gains no longer are really optimal because no consideration is taken to the changes in the disturbance models. Extra care must also be taken when studying the algorithm's stability because of the many simplifications involved.

The described GS based controller with 31 possible feedback gain vectors is studied in a simulation with the same input as in the simulations with the non-simplified algorithm used in Ch. 10.3.1. The purpose was to compare the two controllers' possibilities to keep the average travel value close to the defined reference value (Figure 125). The same controller parameters as in Ch. 10.3.1 were used. The figure also shows the number (1-31) of the feedback gain used during the simulation.

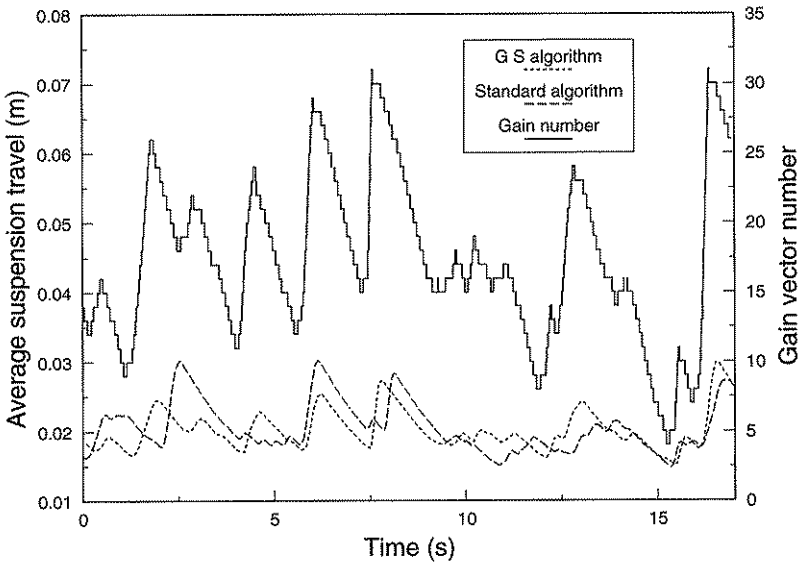

Fig. 125. Weighted average suspension travel using the simplified GS controller and the standard adaptive controller.

The results in Figure 125 show that the controller based on GS theory keeps the average suspension travel value as close to, or perhaps even closer to the defined reference value when compared to the nonsimplified algorithm.

The simplified algorithm has been studied in other simulations with different inputs and parameter values. No stability problems at all have occurred. As mentioned above, K_P and K_D can be adjusted to obtain a faster reacting algorithm and the vibration damping potential can be increased compared to the one for the nonsimplified algorithm. Controllers including the simplified adaptive algorithm have shown very good characteristics in the simulations, and if no problems are found in the necessary full-scale experiments, that algorithm is perhaps the best to use in a practical application.

11 DISCUSSION

11.1 Cab suspension effects on the driver's working environment

The use of a cab suspension results in several positive effects on the driver's working environment. The most important effects are correlated to the possibilities to decrease the vibration load on the driver.

The ISO 2631 exposure time estimation is designed, as mentioned earlier, so that the relative exposure time change between two loads can be examined without the uncertain estimation of absolute exposure times. Also the relative value is somewhat uncertain but gives a good indication of the positive effects.

A measure of the vibration damping potential in general for a passive cab suspension is obtained if the vibration levels using the optimized passive suspension in Ch. 8.2.2 are compared to the levels valid for a rigid cab mounting, presented in Ch. 7.2. When driving on track 1 at 12 km/h the weighted vector sum value is decreased from 2.52 m/s^2 to 1.47 m/s^2, which results in the driver being able to stay in the cab 2.9 times longer if the cab suspension is used. When driving on the rougher track at 6 km/h the vector sum decreases from the very high 4.44 m/s^2 to 2.92 m/s^2, which corresponds to a 2.2 times longer stay.

If the vibration levels for particular dimensions are compared, the results show that the cab suspension gives substantial advantages in all dimensions that are examined in the standard. The dimension with highest benefits when driving on the smooth track is the z dimension. Part of this benefit should also be possible to reach with a conventional seat suspension, and thus benefits in the other dimensions where the seat suspension has insignificant effects are just as important. The reduced angular vibration levels, especially on the smooth surface, are also very positive.

The results of the studies show that active suspensions offer even better possibilities to get an effective vibration protection. Especially adaptively controlled active suspensions have very advantageous characteristics on surfaces with normal roughness without an increased risk of over-travel on rougher surfaces.

The possibilities to design an actively controlled suspension always striving to keep the cab horizontal independent of the frame's slope further increase the positive effects on the driver's working environment.

11.2 The practical use of the models

The simulation models developed are very useful when studying the influence of different parameters on the vibration damping characteristics of different cab suspensions.

The nonlinear model is designed so that the limitations on the studied suspension geometry and element characteristics are very small. A lot of simulations in addition to those discussed in the report were performed. The model structure proved to be adequate for the study of any parameter which was found to be of interest.

The linear model was initially developed only for the design of active suspension controllers. The agreement with the nonlinear model is, however, so large that a lot of the development work, including simulations and analysis, could be done with sufficient accuracy and less programming work in the linear model.

The basic suspension configuration used in the simulations makes it possible to define approximate natural frequencies and degrees of damping in the free moving directions. This makes the results easier to understand and to apply on a suspension based on other types of working elements, but with the same possibility to calculate natural frequencies and damping degrees.

The study is primarily concentrated on the combination agricultural tractor - cab suspension, but the models are general and applicable also to other types of vehicles. Because of the high costs involved, especially the theory including active and adaptively controlled active suspensions are probably even more interesting for applications outside the agricultural area.

11.3 The validation

The nonlinear simulation model is validated against measurements made on a full-scale suspended cab. The agreement was good between the results measured on the full-scale cab and the results calculated with the simulation model. The simulation model is based on classical mechanic theory with only small simplifications needed so the good agreement was not unexpected. Technical and practical problems involved in the relatively complicated validation measurements resulted, however, in the accuracy of the results not being so good that a small error in the simulation model might be possible to detect.

The linear simulation model is exactly defined by the system matrices shown in earlier chapters. The good agreement between results from the linear and the nonlinear model gives another indication to that the errors included in the simulation algorithms are small.

One of the purposes of this work was to optimize the cab suspension to provide the best possible working environment in the cab. In order to validate this and to validate the standard evaluating the vibration's effects on the human body, the validations could be based on another principle. Test drivers should then be asked to drive tractors partly with suspensions optimized according to the ISO 2631 standard and partly with nonoptimal suspensions. The test drivers' subjective opinions of the different working places could then be used to evaluate if the cab suspension designed to be optimal really was optimal.

The described validation technique would have given very interesting results but the funds available for the realization were insufficient. To decrease the effects of the variations between different drivers, it might also be necessary to use a relatively large number of test drivers. Since numerous different factors influence the driver's subjective opinion, it should also be very difficult to find out the reasons for any poor agreement that might appear in the results.

11.4 Choice of dimensioning conditions

The size of the available travel space has been found to be of vital importance for the possibility to construct a cab suspension with high vibration damping potential. Other studies have shown that direct over-travel results in very high instantaneous vibration levels and are experienced as extremely unpleasant by the driver.

Many types of design are based upon the use of safety factors against malfunction, breaking loads, etc. Safety factors must also be used when designing a cab suspension. One of the factors must then define the security against over-travel. The problem in that case is that the maximum vibration load is not defined as it is for most other constructions.

The maximum load must be defined. In the optimizations of passive suspensions performed, this load is defined as the load arising on the tractor frame when the tractor is driving over a specified very rough surface at a defined velocity. It is then assumed that the driver, when he observes that such an extreme vibration load is coming up, reduces the driving speed or changes the vehicle's setting in some way to reduce the unpleasant vibrations he and the vehicle will be subjected to.

The tuning of an adaptive active suspension controller so that it uses the available travel space optimally includes no need for a definition of the highest possible vibration load. The reason is that the adaptive controller adjusts the feedback gains to the optimum values also for extremely high loads. The setting of the reference value for the RMS suspension travel is mainly influenced by the size of the available travel space. The best tactic is probably to have a tuning knob on the controller so that the security margin can be adjusted.

11.5 Choice of suspension principle

The total design problem involves consideration of capital cost, space requirements, component weight, energy consumption, maintainability, reliability and failure modes, noise transmission and generating and advertising potential in addition to more easily quantified performance parameters such as vibration damping potential and space requirements (Sharp and Crolla, 1987).

Passive suspensions with nonlinear damping characteristics have shown very promising characteristics in this study, especially if combined with a slow acting load levelling function to exclude static deviations. In the present reality, where the cost is a very important factor, this type of technique is probably the most likely to be used on a commercial agricultural cab suspension.

Adaptive active suspensions offer possibilities to further improve the vibration protection. The costs involved are, however, at present, probably too high. The development of cheaper components, together with an increased awareness regarding the working environment, may improve the possibilities for use of more advanced suspension damping technology also in the agricultural area.

11.6 Need of further research and development

The results of the study show that an active cab suspension based on linear state feedback probably must have time variant adaptive characteristics to be useful. A method including LQG technique and time variant penalty matrices is developed and used to reach optimal suspension performance. The adaptive controllers become rather complex, especially in the multi-dimensional case. Some simplifications of the algorithms are also described.

The best way to further improve the algorithms and also study the effects of the proposed simplifications is to combine further simulation studies with implementation of the controller in practise. An analytical study of the stability properties for the described controller type should also be valuable, but probably very difficult to perform.

Instead of adaptive LQG controllers it may be possible to use active suspensions with nonlinear state feedback to reach good average performance for the suspension (Gordon et al., 1990 and 1991). The few studies discussing this technique have reported good vibration damping characteristics, but the method in general, and especially the stability properties, when applied to a terrain vehicle cab suspension, must be analysed more thoroughly.

As in all automatic control is it important to develop robust algorithms for the suspension controller, usable also in practical applications and not just in theoretical perfectly linear systems.

The design of a fast and effective force actuator to be used in active suspensions is a complicated task where it is very important to consider production costs. The actuators can be electrically or hydraulically operated. Electrical actuators can be made very fast, but hydraulic ones have the advantage that the vehicle already includes a relatively powerful hydraulic system.

The computer in the controller must also be very fast and reliable. The progress in this area, both referring to capacity and price, is very rapid and thus the mechanical area probably includes the most important restrictions.

Active suspensions can also be simplified to varying degrees to provide suspensions containing most of the advantages of fully active suspensions but with reduced complexity and production costs. By only dissipating energy, semi-active suspensions can be based on relatively simple technique, but still include most of the advantages of the fully active suspension. To be effective on an agricultural tractor, is it probably necessary to include adaptive characteristics also in the semi-active controller.

The connection between loading vibrations in different directions and the driver's discomfort when subjected to the load is defined in standardized norms. There have been major difficulties involved in the development of the norms. The effects of vibrations with frequencies below 1.0 Hz and of angular vibrations are still poorly known. In some

cab suspension studies, the drivers have reported a subjective feeling of decreased driving control and interaction with the vehicle. Knowledge of these tendencies and their causes is very incomplete.

In conclusion, the potential for further improvements of the driver's working environment is still large, but the insufficient knowledge of the interaction between technical measurement values and human reactions is often a limiting factor.

12 SUMMARY

Operators of agricultural tractors and other off-road vehicles are subjected to vibration levels and frequencies known to be injurious to health and deleterious to performance.

The use of a cab suspension results in several positive effects on the driver's working environment. The most important effects are correlated to possibilities to decrease the vibration load on the driver.

The main purpose of this work was to study the possibilities of using the cab suspension technique to improve the driver's environment on an agricultural tractor.

Two simulation models describing the frame-suspension-cab system were developed: A nonlinear model for studying suspension characteristics with only small constrictions on the geometry and on the working principles of the elements, and a linear model which is a simplified description of the same system including more constraints, but more applicable when designing and studying performance for particularly active suspensions.

The simulation models were validated against measurements made on a full scale cab suspension. The models were also compared with each other.

Earlier cab suspension studies, together with the results of this study, have shown that it is possible to design a suspension that works well for a well-defined normal vibration load. The possibilities to design a suspension with attractive characteristics in all types of circumstances have been very little studied. Consequently, a major part of this work has been directed towards different possibilities of achieving these favourable characteristics.

This study has mainly concerned the two extreme types of suspension, namely the totally passive suspension without any possibilities to adjust parameters, and the fully active supension with total control of the regulator parameters and the control forces.

The study is primarily concentrated on the combination agricultural tractor - cab suspension but the models are general and applicable also to other types of vehicles.

The influence of different passive suspension parameters on vibration damping capacity and the requirement for free space in the construction were investigated. Particular emphasis was placed on the effects of passive non-linear suspension elements and varying locations of the elements.

A passive cab suspension implemented with linear elements must have low natural frequencies in all dimensions to provide good vibration insulation. The low natural frequencies result in large suspension strokes and the need for a large amount of free space to avoid over-travel under rough conditions.

Non-linear passive damping elements with harder damping at increasing strokes make it possible to use suspensions with low natural frequencies, even with a relatively low

amount of free space. Non-linear hardening spring elements working in horizontal directions also reduce the strokes, but in contrast to nonlinear damping elements, they also cause substantial increases to the vibration load in the cab.

An optimization model, based on an evolution algorithm, was developed and used to optimize suspension parameters with different types of generally defined constraints. The change in optimized suspension parameters and damping capacity with respect to changes in given restrictions were studied.

Active suspensions can continuously supply and modulate the flow of energy. Thus, in an active system, forces can be generated which do not depend upon energy previously stored by the suspension. Therefore an active suspension has a very high potential for reducing the driver's vibration load while still maintaining short suspension travel.

The development and analysis of LQG based active cab suspensions is described. The vibration damping characteristics of the suspensions were studied. The change in characteristics when the suspension's configuration or design variables are changed is also studied.

Linear quadratic optimal control theory has been used to solve the optimization problem. This method provides a compact analytical solution with relatively low design and computing time and the stability of the system is guaranteed. Since the results of an optimization process is a controller which considers and feedbacks all the system states, it offers advantages beyond those of any classical controller structure.

Suspensions with active characteristics further increase the possibilities to decrease the vibration load in the cab. Particularly the performance on relatively smooth surfaces was found to be excellent. The results also showed that it is possible to design a suspension controller that always strives to keep the cab horizontal even when the vehicle's frame is inclined.

The simulations showed, however, that with constant feedback gains, the active suspension must be tuned to avoid over-travel at the highest possible frame acceleration levels, which decreases the vibration damping potential during more normal driving.

An adaptive active suspension controller based on LQG technique has been developed and studied. The principle for the adaptation is based on the parameters in the penalty matrices being varied so that the resulting controller always strives to make optimum use of the available travel space. The feedback and observer gains are also changed depending on the characteristics of the frame movements.

The adaptively controlled active suspension has shown promising characteristics. Some simplifications of the rather complicated algorithm are also described.

13 ACKNOWLEDGEMENTS

I wish to express my sincere gratitude to all those who have supported me and made this work possible. The following persons I want to mention in particular:

Professor Bruno Nilsson, my main supervisor, for skilful and stimulating supervision and for the great freedom I have had when planning my work.

Professor Tomas Nybrandt, my second supervisor, especially for good advice on the more theoretical parts.

Mr Marek Zylberstein for initiating the cab suspension project and for interesting discussions, especially concerning working environment questions.

Asst. Professor Håkan Lanshammar at Uppsala University, for valuable and constructive comments and advice on my Licenciate thesis.

Mr Sven-Erik Thiberg at Luleå University of Technology, for assistance with knowledge and measurement equipment, when performing the validation measurements.

Mr Jan-Erik Rova, ASA-Products AB in Kiruna, for the design and construction of the full-scale suspension used for the validation measurements.

Mr Bengt-Olof Wikström at the National Institute of Occupational Health in Stockholm, for assistance with knowledge and measurement equipment when collecting the input signals used.

Dr Håkan Jönsson for stimulating discussions and for always being ready to answer my more or less carefully prepared questions.

Mr Örjan Bergwall for skilful transforming of manuscripts to computer based documents.

Mr Nigel Rollison for correcting my linguistic misstages.

The electronic and workshop staffs at the Department of Agricultural Engineering, especially Mr Staffan Klensmeden and Mr Sven Andersson for the design of the data acquisition equipment used in the validation measurements.

The "lunch gang", Hasse, Janne, Jonny, Kenneth, Sigge, Stefan and Sven, for stimulating discussions on a wide range of subjects of varying suitability for inclusion in a thesis.

A great number of other colleagues at the Department have contributed to the work and I am most grateful to all of them, even though many of them are not mentioned here by name. However, I would like to make particular mention of the administrative staff, and especially Mr Anders Wesslen, for assistance with all the practical problems that otherwise may be so stressful and time consuming.

14 REFERENCES

Ahlén, A., Solbrand, G. & Sternad, M. 1982. Numerisk lösning av ett optimal-styrproblem med evolutionsmetoden. Unpublished. Department of Technology, Uppsala University, Sweden.

Andersson, B & Moore, J. 1989. Optimal control, linear quadratic methods. Prentice Hall.

Åström, K.J. & Wittenmark, B. 1989. Adaptive control. Addison-Wesley.

Bitmead, R.R., Gevers, M. & Wertz, V. 1990. Adaptive optimal control, the thinking man's GPC. Prentice Hall.

Bjurwald, M., Carlsöö, S., Hansson, J-E. och Sjöflot, L. 1973. Helkroppsvibrationer - en teknisk-fysiologisk studie av arbetsställningar och förarstolar. Arbete och hälsa. The National Institute of Occupational Health, Sweden. 7.

Bottoms, D.J. 1975. An experimental study of tractor drivers' posture using a swivelling seat. Paper presented at the 6th International Congress of Rural Medicine, Cambridge, The United Kingdom.

BS 6841, 1987. British Standard Guide to Measurement and evaluation of human exposure to whole-body mechanical vibration and repeated shock. Brittish Standards Institution.

Byrne, J & Katebi, M. R. 1988. LQG adaptive autopilots. In: Implementation of self-tuning controllers (ed. Warwick, K.). P. Peregrinus Ltd. 260-278.

Claar, P.W. & Sheth, P.N. 1982. Effect of agricultural tractor and trailer combinations on operator ride vibration. American Society of Agricultural Engineers. ASAE 82-1551.

Clarke, D.W., Kanjilal, P.P. & Mohtadi, C. 1985a. A generalized LQG approach to self-tuning control, Part 1, Aspects of design. International Journal of Control. 41:1509-1523.

Clarke, D.W., Kanjilal, P.P. & Mohtadi, C. 1985b. A generalized LQG approach to self-tuning control, Part 2, Implementation and simulation. International Journal of Control. 41:1525-1544.

Crolla, D.A. 1980. A theoretical analysis of the ride vibration of agricultural tractor and trailer combinations. Vehicle System Dynamics. 9:237-260.

Crolla, D.A. 1981. Off-road vehicle dynamics. Vehicle System Dynamics. 10:253-260.

Dahlberg, T. 1979. Optimization criteria for vehicles travelling on a randomly profiled road - a survey. Vehicle System Dynamics. 8:239-252.

Deltenre, A. & Destain, M-F. 1990. Numerical simulation of agricultural tractors ride vibration. Paper presented at AgEng 1990, Berlin, Germany.

El Madany, M.M. 1987. An analytical investigation of isolation systems for cab ride. Computers & Structures. 27:679-688.

Elmqvist, H., Åström, K.J. & Schöntal, T. 1986. Simnon, User's Guide for MS-DOS Computers. Department of Automatic Control, Lund Institute of Technology, Lund, Sweden.

Gordon, T.J., Marsh, C. & Milsted, M.G. 1990. Control law design for active and semi-active automobile suspension systems. VDI-Berichte. 816:537-546.

Gordon, T.J., Marsh, C. & Milsted, M.G. 1991. A comparison of adaptive LQG and nonlinear controllers for vehicle supension systems. Vehicle System Dynamics. 20:321-340.

Gustafsson, L. 1989. Tidsstyrd simulering. Unpublished. Department of Technology, Uppsala University, Sweden.

Göhlich, H. 1984. The development of tractors and other agricultural vehicles. J. agric. Engng Res. 29:3-16.

Hac, A. 1987. Adaptive control of vehicle suspension. Vehicle System Dynamics. 16:57-74.

Hansson, P.A. 1989. Laborationsbänk med möjlighet att simulera olika traktorers hydraulsystem - konstruktion och provning. Report 89:08, Department of Agricultural Engineering, Swedish University of Agricultural Sciences, Uppsala, Sweden.

Harris, C.M. (ed.). 1988. Shock and Vibration Handbook, Third Edition. McGraw-Hill.

't Hart, J. 1977. Suspended driver's cab for off-road vehicles. Leaflet no. 12, Department of Mechanical Engineering, Delft University of Technology, Delft, The Netherlands.

Hilton, D.J. & Moran, P. 1975. Experiments in improving tractor operator ride by means of a cab suspension. J. agric. Engng Res. 20:433-448.

Hunt, K.J. & Grimble, M.J. 1988. LQG based self-tuning controllers. In: Implementation of self-tuning controllers (ed. Warwick, K.). P. Peregrinus Ltd. 41-66.

ISO 2631. 1974. Guide for the evaluation of human exposure to whole-body vibration. International Organization for Standardization.

Karnopp, D. & Margolis, D. 1984. Adaptive suspension concepts for road vehicles. Vehicle System Dynamics. 13:145-160.

Kauss, W. 1981. Aktive, hydraulische Swingungsisolierung des Fahrerplatzes ungefederter, geländegängiger Fahrzeuge. Technischen Universität, Berlin, Germany. Ph.D. Thesis.

Kauss, W. & Weigelt, H. 1980. Die gefederte Traktorkabine - verbesserter Schwingungsschutz und Fahrkomfort. Landtechnik. 8/9:396-401.

Kjellberg, A. & Wikström, B-O. 1985. Whole-body vibration: exposure time and acute effects - a review. Ergonomics. 28:535-543.

Kwakernaak, H. & Sivan, R. 1972. Linear optimal control system. Wiley.

Lam, K.P. 1982a. Design of stochastic discrete time linear optimal regulators, Part 1, Relationships between control laws based on a time series approach and a state space approach. International Journal of System Science. 13:979-1000.

Lam, K.P. 1982b. Design of stochastic discrete time linear optimal regulators, Part 2, Extension and computational procedures. International Journal of System Science. 13:1001-1011.

Lines, J.A., Peachey, R.O. & Collins, T.S. 1992. Predicting the ride vibration of an unsuspended tractor using the dynamic characteristics of rolling tyres. Journal of Terramechanics. 29:307-315.

Lines, J.A., Whyte, R.T. & Stayner, R.H. 1989. Suspension for tractor cabs. Proc. of the 3rd International Symposium of the International Section of the ISSA for Research on Prevention of Occupational Risks, Vienna, Austria. 148-150.

Lizell, M. 1990. Dynamic levelling for ground vehicles. Royal Institute of Technology, Stockholm, Sweden. Ph. D. Thesis.

Matlab. 1989. User's Guide. The MathWorks Inc, South Natick, Massachusetts, USA.

Matthews, J. 1973. The measurement of tractor ride comfort. Society of Automotive Engineers. SAE 730795:2712-2728.

McLeod, R.W. & Griffin, M.J. 1988. Performance of a complex manual control task during exposure to vertical whole-body vibration between 0.5 and 5.0 Hz. Ergonomics. 31:1193-1203.

Mitschke, M. 1969. Nichtlineare Feder- und Dämpferkennungen im Kraftfahrzeug. ATZ. 71:14-21.

Mohtadi, C. 1988. Numerical algorithms in self-tuning control. In: Implementation of self-tuning controllers (ed. Warwick, K.). P. Peregrinus Ltd. 67-95.

Muth, C. 1982. Einführung in die Evolutionsstrategie. Regelungstechnik. 30:297-303.

Rakheja, S. & Sankar, S. 1984. Suspension design to improve tractor ride :II. Passive cab suspension. Society of Automotive Engineers. SAE 841108:4.1105-4.1112.

Rechenberg, I. 1973. Evolutionsstrategie Optimierung technischer Systeme nach Prinzipien der biologischen Evolution. Frommann-Holzboog.

Robert, B. 1988. A new comfort for the farmer : the suspended cab. Paper presented at AgEng 1988, Paris, France.

Roley, D.G. 1975. Tractor cab suspension performance modeling. Univ. of California, Davis, USA. PhD Thesis.

Rosegger, R. & Rosegger, S. 1960. Health effects of tractor driving. J. agric. Engng Res. 5:241-275.

Rova, J-E. 1990. ASA-products AB, Kiruna, Sweden. Personal communication.

Sachs, H.K. 1979. An adaptive control for vehicle suspensions. Vehicle System Dynamics. 8:201-206.

Shah, S.L. & Cluett, W.R. 1988. RLS based estimation schemes for self-tuning control. In: Implementation of self-tuning controllers (ed. Warwick, K.). P. Peregrinus Ltd. 23-40.

Sharp, R.S. & Crolla, D.A. 1987. Road vehicle suspension system design - a review. Vehicle System Dynamics. 16:167-192.

SS-ISO 2631. 1982. Vibration och stöt - Vägledning för bedömning av helkroppsvibrationers inverkan på människan. Standardiseringskommissionen i Sverige. Sweden.

SS-ISO 5008. 1981. Lantbruk - Hjultraktorer och självgående maskiner - Mätning av maskinvibrationer som påverkar föraren. Standardiseringskommissionen i Sverige. Sweden.

Stayner, R.M., Collins, T.S. & Lines, J.A. 1984. Tractor ride vibration simulation as an aid to design. J. agric. Engng Res. 29:345-355.

Suggs, C.W. & Huang, B.K. 1969. Tractor cab suspension design and scale model simulation. Trans. ASAE. 12:283-289.

Symon, K.R. 1971. Mechanics, Third Edition. Addison-Wesley.

Thelin, A. 1980. Work and health among farmers, A study among 191 farmers in Kronoberg county, Sweden. Scand. J. Soc. Med. 22.

Warwick, K. 1988. Simplified algorithms for self-tuning control. In: Implementation of self-tuning controllers (ed. Warwick, K.). P. Peregrinus Ltd. 96-125.

Weigelt, H. & Göhlich, H. 1985. Improvements in tractor dynamics by various means of suspension systems. Proc. of the 8th Joint Ergonomics symp. Silsoe, The United Kingdom.

Wellstead, P.E. & Zarrop, M.B. 1991. Self-tuning systems, control and signal processing. Wiley.

Wuolijoki, E. 1981. Effects of simulated tractor vibration on the psycho-physiological and mechanical functions on the driver: comparison of some excitatory frequencies. Acta Forestalia Fennica.

Zylberstein, M. 1981. Fjädrande-dämpande upphängning av hytt på skogsmaskin : Jämförelse mellan stum upphängning och upphängning typ MTAB och KGA på skogsmaskin. Report, Logging Research Foundation, Stockholm. Sweden.

15 APPENDIX

15.1 Results from the simulations in Chapter 7.3.1

1. Input measured on track 1 (12 km/h)

f_{nv} (Hz)	R_v	Vibration level (ISO 2631) at the cab's c.o.g. (m/s^2 rad/s^2)						Maximum deviation of the cab's c.o.g. from the balanced position (cm)		
		x	y	z	vector sum	xr	yr	x	y	z
0.75	0.2	0.67	1.01	0.50	1.77	1.03	0.70	5.8	7.5	9.1
	0.5	0.65	0.96	0.51	1.70	0.69	0.63	5.2	7.2	5.8
	0.8	0.65	0.95	0.64	1.74	0.66	0.71	4.9	7.2	4.3
	1.0	0.65	0.95	0.73	1.77	0.68	0.77	4.9	7.2	3.7
1.00	0.2	0.65	0.98	0.57	1.74	1.34	0.81	5.2	7.2	8.1
	0.5	0.65	0.96	0.65	1.75	0.88	0.78	4.9	7.0	4.6
	0.8	0.65	0.96	0.81	1.81	0.83	0.85	5.0	7.1	3.3
	1.0	0.65	0.95	0.92	1.86	0.84	0.91	5.0	7.1	2.8
1.25	0.2	0.65	0.96	0.79	1.81	1.35	1.05	4.9	6.9	5.8
	0.5	0.65	0.96	0.82	1.81	1.00	0.92	5.0	7.0	3.6
	0.8	0.65	0.95	0.98	1.89	0.94	0.98	5.0	7.0	2.7
	1.0	0.65	0.95	1.08	1.94	0.95	1.02	5.1	7.0	2.4
1.50	0.2	0.66	0.96	0.99	1.91	1.62	1.32	5.1	7.0	4.2
	0.5	0.65	0.95	0.99	1.91	1.12	1.05	5.1	7.0	2.9
	0.8	0.65	0.95	1.13	1.98	1.05	1.07	5.1	7.0	2.3
	1.0	0.65	0.95	1.23	2.03	1.05	1.11	5.1	7.0	2.0

2. Input measured on track 2 (6 km/h)

f_{nv} (Hz)	R_v	Vibration level (ISO 2631) at the cab's c.o.g. (m/s^2 rad/s^2)						Maximum deviation of the cab's c.o.g. from the balanced position (cm)		
		x	y	z	vector sum	xr	yr	x	y	z
0.75	0.2	1.99	1.54	1.74	3.94	0.91	1.44	12.5	8.8	27.1
	0.5	1.66	1.22	1.60	3.31	0.68	1.36	10.3	7.4	15.4
	0.8	1.59	1.14	1.78	3.27	0.80	1.41	9.0	7.8	12.8
	1.0	1.58	1.12	1.84	3.31	0.88	1.46	8.6	8.1	11.3
1.00	0.2	1.88	1.44	2.62	4.23	1.48	2.54	12.6	9.0	26.3
	0.5	1.61	1.17	2.13	3.51	1.05	1.73	9.3	6.7	16.8
	0.8	1.58	1.12	2.18	3.48	1.09	1.65	8.2	7.9	11.6
	1.0	1.58	1.12	2.23	3.52	1.16	1.66	8.1	8.3	9.6
1.25	0.2	1.81	1.34	3.43	4.66	2.31	3.95	12.0	7.9	23.6
	0.5	1.59	1.12	2.54	3.72	1.41	1.95	8.4	7.0	14.3
	0.8	1.59	1.11	2.45	3.66	1.36	1.80	8.3	8.2	9.9
	1.0	1.59	1.12	2.47	3.68	1.39	1.79	8.4	8.6	8.4
1.50	0.2	1.69	1.21	4.03	4.97	2.43	3.13	9.1	6.0	19.1
	0.5	1.59	1.10	2.84	3.93	1.68	2.07	8.7	7.8	12.2
	0.8	1.59	1.12	2.66	3.80	1.58	1.99	8.6	8.6	8.9
	1.0	1.59	1.12	2.65	3.81	1.59	1.88	8.6	8.9	7.1

15.2 Results from the simulations in Chapter 7.3.2

1. Input measured on track 1 (12 km/h)

$PK1_{cv}$	$PK2_{cv}$	Vibration level (ISO 2631) at the cab's c.o.g. (m/s^2 rad/s^2)						Maximum deviation of the cab's c.o.g. from the balanced position (cm)		
(cm)		x	y	z	vector sum	xr	yr	x	y	z
3	1	0.65	0.96	0.63	1.74	0.68	0.73	4.8	7.2	4.4
	2	0.65	0.96	0.69	1.76	0.72	0.79	4.9	7.1	4.2
	3	0.65	0.96	0.77	1.79	0.76	0.87	4.9	7.1	3.9
6	1	0.65	0.96	0.56	1.72	0.68	0.67	5.0	7.2	5.0
	2	0.65	0.96	0.55	1.72	0.70	0.68	5.0	7.1	5.1
	3	0.65	0.97	0.56	1.72	0.72	0.69	5.0	7.1	5.1
9	1	0.65	0.96	0.53	1.71	0.69	0.65	5.1	7.2	5.3
	2	0.65	0.96	0.51	1.71	0.71	0.64	5.2	7.2	5.7
	3	0.65	0.97	0.51	1.71	0.72	0.64	5.2	7.2	5.8

2. Input measured on track 2 (6 km/h)

$PK1_{cV}$ (cm)	$PK2_{cV}$	Vibration level (ISO 2631) at the cab's c.o.g. (m/s^2 rad/s^2)						Maximum deviation of the cab's c.o.g. from the balanced position (cm)		
		x	y	z	vector sum	xr	yr	x	y	z
3	1	1.58	1.13	1.98	3.37	1.05	1.67	8.5	8.3	10.0
	2	1.58	1.13	2.31	3.56	1.52	2.05	8.2	8.8	7.9
	3	1.57	1.14	2.58	3.75	1.93	2.47	8.0	9.1	6.7
6	1	1.60	1.15	1.81	3.30	0.89	1.55	9.1	7.8	12.1
	2	1.60	1.15	1.97	3.39	1.11	1.76	8.9	8.1	11.3
	3	1.59	1.15	2.14	3.48	1.38	2.00	8.7	8.4	10.5
9	1	1.61	1.17	1.74	3.29	0.81	1.49	9.5	7.6	13.2
	2	1.62	1.17	1.81	3.33	0.92	1.62	9.5	7.7	13.3
	3	1.62	1.17	1.90	3.38	1.07	1.76	9.4	7.8	12.9

15.3 Results from the simulations in Chapter 7.4.1

1. Input measured on track 1 (12 km/h)

f_{nH}	R_V	Vibration level (ISO 2631) at the cab's c.o.g. (m/s^2 rad/s^2)						Maximum deviation of the cab's c.o.g. from the balanced position (cm)		
(Hz)		x	y	z	vector sum	xr	yr	x	y	z
0.5	0.2	0.81	1.21	0.78	2.18	0.95	0.82	18.3	28.6	6.4
	0.5	0.58	0.88	0.72	1.64	0.93	0.80	11.0	16.2	5.2
	0.8	0.54	0.81	0.68	1.52	0.91	0.79	7.6	10.5	4.7
	1.0	0.54	0.80	0.67	1.52	0.91	0.79	6.3	8.8	4.5
0.75	0.2	1.06	1.65	0.86	2.88	0.94	0.81	13.8	21.3	5.8
	0.5	0.69	1.08	0.69	1.92	0.92	0.79	6.7	10.6	4.5
	0.8	0.65	0.96	0.66	1.75	0.91	0.79	4.9	7.0	4.3
	1.0	0.66	0.94	0.66	1.73	0.90	0.79	4.14	5.7	4.2
1.0	0.2	0.97	1.67	0.67	2.79	0.91	0.81	9.6	11.3	4.5
	0.5	0.76	1.17	0.65	2.05	0.90	0.80	5.3	6.6	4.2
	0.8	0.73	1.04	0.65	1.90	0.90	0.79	3.7	4.8	4.1
	1.0	0.74	1.01	0.65	1.87	0.90	0.79	3.1	4.1	4.1
1.25	0.2	1.02	1.71	0.67	2.87	0.90	0.81	5.6	8.1	4.5
	0.5	0.84	1.20	0.65	2.15	0.90	0.80	3.9	4.6	4.2
	0.8	0.80	1.09	0.65	2.00	0.90	0.79	3.0	3.4	4.1
	1.0	0.80	1.06	0.65	1.97	0.90	0.79	2.5	3.0	4.1
1.50	0.2	1.21	1.66	0.67	2.95	0.90	0.80	4.5	5.2	4.2
	0.5	0.92	1.22	0.65	2.24	0.90	0.79	3.0	3.7	4.1
	0.8	0.85	1.11	0.65	2.07	0.90	0.79	2.4	2.8	4.1
	1.0	0.83	1.09	0.65	2.02	0.90	0.79	2.1	2.3	4.0

2. Input measured on track 2 (6 km/h)

f_{nH}	R_H	Vibration level (ISO 2631) at the cab's c.o.g. (m/s^2 rad/s^2)						Maximum deviation of the cab's c.o.g. from the balanced position (cm)		
(Hz)		x	y	z	vector sum	xr	yr	x	y	z
0.5	0.2	1.54	1.26	2.47	3.73	2.22	2.14	24.4	25.6	17.2
	0.5	0.98	0.90	2.32	2.98	1.43	1.88	15.7	15.2	12.7
	0.8	1.16	0.90	2.33	3.11	1.39	1.93	12.7	11.8	11.0
	1.0	1.27	0.93	2.33	3.21	1.39	1.93	11.2	10.2	10.7
0.75	0.2	1.51	1.63	2.38	3.91	1.48	2.08	16.7	24.0	13.6
	0.5	1.51	1.22	2.37	3.61	1.40	1.98	11.5	12.1	12.2
	0.8	1.58	1.13	2.38	3.61	1.39	1.95	8.3	8.1	10.5
	1.0	1.62	1.13	2.39	3.65	1.39	1.95	6.9	6.7	10.2
1.00	0.2	2.52	2.21	2.66	5.41	1.43	2.10	25.7	20.6	12.9
	0.5	1.98	1.43	2.42	4.20	1.40	1.98	10.4	8.1	10.7
	0.8	1.88	1.28	2.41	3.99	1.38	1.96	7.0	5.3	10.1
	1.0	1.86	1.26	2.42	3.97	1.39	1.97	5.7	4.4	10.1
1.25	0.2	3.18	2.19	2.66	6.02	1.44	2.04	15.0	12.1	10.4
	0.5	2.34	1.54	2.43	4.62	1.39	1.98	9.0	5.7	10.1
	0.8	2.08	1.39	2.43	4.26	1.39	1.97	6.0	3.8	10.2
	1.0	2.00	1.35	2.43	4.17	1.39	1.98	4.8	3.2	10.2
1.50	0.2	3.89	2.30	2.62	6.85	1.43	2.03	13.1	8.8	10.8
	0.5	2.57	1.62	2.46	4.91	1.39	1.98	7.8	4.4	10.0
	0.8	2.20	1.45	2.44	4.42	1.39	1.98	5.0	3.0	10.2
	1.0	2.09	1.41	2.44	4.29	1.39	1.97	4.1	2.6	10.3

15.4 Results from the simulations in Chapter 7.4.2

1. Input measured on track 1 (12 km/h)

$PK1_{cH}$ (cm)	$PK2_{cH}$	Vibration level (ISO 2631) at the cab's c.o.g. (m/s^2 rad/s^2)						Maximum deviation of the cab's c.o.g. from the balanced position (cm)		
		x	y	z	vector sum	xr	yr	x	y	z
3	1	0.56	0.83	0.68	1.56	0.91	0.79	7.3	9.2	4.6
	2	0.58	0.88	0.68	1.63	0.91	0.79	6.4	7.6	4.5
	3	0.61	0.93	0.68	1.70	0.91	0.79	5.8	6.6	4.5
6	1	0.56	0.85	0.70	1.59	0.92	0.79	8.9	11.4	4.9
	2	0.58	0.89	0.70	1.64	0.92	0.79	9.0	11.3	4.9
	3	0.60	0.92	0.70	1.69	0.92	0.79	8.9	10.8	4.9
9	1	0.57	0.86	0.71	1.61	0.92	0.79	9.8	12.6	5.0
	2	0.59	0.90	0.71	1.67	0.93	0.80	10.5	13.3	5.2
	3	0.60	0.92	0.72	1.70	0.93	0.80	10.7	13.4	5.2

2. Input measured on track 2 (6 km/h)

$PK1_{cH}$ (cm)	$PK2_{cH}$	Vibration level (ISO 2631) at the cab's c.o.g. (m/s^2 rad/s^2)						Maximum deviation of the cab's c.o.g. from the balanced position (cm)		
		x	y	z	vector sum	xr	yr	x	y	z
3	1	1.20	0.91	2.34	3.15	1.39	1.93	10.5	10.7	10.1
	2	1.30	0.95	2.38	3.28	1.39	1.94	8.5	7.6	10.2
	3	1.41	1.00	2.42	3.42	1.39	1.96	7.6	6.1	10.0
6	1	1.07	0.89	2.32	3.03	1.39	1.93	12.6	12.3	11.1
	2	1.07	0.91	2.32	3.05	1.38	1.93	11.7	11.5	11.0
	3	1.10	0.93	2.34	3.09	1.38	1.92	11.2	10.4	10.7
9	1	1.02	0.88	2.31	2.98	1.39	1.93	13.6	13.4	11.5
	2	0.99	0.89	2.31	2.96	1.39	1.92	13.6	13.4	11.6
	3	0.98	0.90	2.31	2.96	1.39	1.92	13.4	12.9	11.5

15.5 Results from the simulations in Chapter 7.4.3

1. Input measured on track 1 (12 km/h)

$PK1_\alpha$ (rad)	$PK2_\alpha$	Vibration level (ISO 2631) at the cab's c.o.g. (m/s^2 rad/s^2)						Maximum deviation of the cab's c.o.g. from the balanced position (cm)		
		x	y	z	vector sum	xr	yr	x	y	z
0.075	1	0.78	1.25	0.65	2.16	0.90	0.80	4.9	5.6	4.2
	2	0.80	1.28	0.65	2.22	0.90	0.80	4.7	5.5	4.2
	3	0.82	1.33	0.65	2.28	0.90	0.80	4.4	5.3	4.2
0.150	1	0.71	1.15	0.66	2.00	0.91	0.80	5.2	6.4	4.2
	2	0.68	1.14	0.66	1.97	0.91	0.80	5.1	6.6	4.2
	3	0.67	1.14	0.66	1.97	0.91	0.80	5.1	6.5	4.2
0.225	1	0.68	1.09	0.66	1.91	0.91	0.80	5.1	7.3	4.2
	2	0.64	1.04	0.67	1.84	0.91	0.80	5.7	7.7	4.2
	3	0.62	1.01	0.67	1.79	0.91	0.80	5.9	8.0	4.3

2. Input measured on track 2 (6 km/h)

$PK1_\alpha$ (rad)	$PK2_\alpha$	Vibration level (ISO 2631) at the cab's c.o.g. (m/s^2 rad/s^2)						Maximum deviation of the cab's c.o.g. from the balanced position (cm)		
		x	y	z	vector sum	xr	yr	x	y	z
0.075	1	2.85	1.72	2.56	5.31	1.43	2.02	8.7	6.8	10.1
	2	3.15	1.83	2.63	5.73	1.44	2.00	7.4	6.0	10.2
	3	3.26	1.91	2.50	5.85	1.41	1.97	7.0	5.6	10.4
0.150	1	2.20	1.50	2.47	4.47	1.41	2.02	0.3	8.3	10.1
	2	2.29	1.60	2.54	4.66	1.44	2.05	9.9	8.3	10.0
	3	2.33	1.69	2.60	4.80	1.48	2.05	9.4	7.5	9.9
0.225	1	1.89	1.35	2.43	4.06	1.40	2.00	10.2	8.6	10.2
	2	1.77	1.32	2.44	3.94	1.41	2.02	9.8	9.0	10.1
	3	1.69	1.31	2.45	3.87	1.41	2.04	9.5	9.1	10.0

15.6 Results from the simulations in Chapter 7.5

1. Input measured on track 1 (12 km/h)

Element location in relation to the cab's c.o.g. (m)	Vibration level (ISO 2631) at the cab's c.o.g. (m/s^2 rad/s^2)						Maximum deviation of the cab's c.o.g. from the balanced position (cm)		
	x	y	z	vector sum	xr	yr	x	y	z
-1.00	0.67	0.51	0.76	1.40	0.51	0.74	12.2	16.3	3.4
-0.80	0.68	0.60	0.76	1.48	0.59	0.74	10.3	15.4	3.2
-0.60	0.66	0.73	0.77	1.58	0.73	0.74	8.2	14.6	3.2
-0.40	0.65	0.84	0.74	1.66	0.87	0.74	6.5	12.2	3.9
-0.20	0.64	0.91	0.71	1.71	0.92	0.75	5.4	9.5	4.2
0.00	0.65	0.96	0.66	1.75	0.91	0.79	4.9	7.0	4.3
0.20	0.66	0.98	0.64	1.78	0.93	0.86	4.6	6.1	4.4
0.40	0.67	0.96	0.63	1.76	1.07	0.93	4.8	7.3	4.6
0.60	0.67	0.93	0.65	1.73	1.30	1.02	5.3	9.9	4.7
0.80	0.66	0.92	0.67	1.71	1.52	1.12	6.1	13.1	6.7
1.00	0.64	0.94	0.69	1.73	1.72	1.21	7.4	16.7	4.7

2. Input measured on track 2 (6 km/h)

Element location in relation to the cab's c.o.g. (m)	Vibration level (ISO 2631) at the cab's c.o.g. (m/s^2 rad/s^2)						Maximum deviation of the cab's c.o.g. from the balanced position (cm)		
	x	y	z	vector sum	xr	yr	x	y	z
-1.00	1.14	0.72	2.39	3.04	1.07	1.40	12.0	14.6	10.5
-0.80	1.24	0.74	2.39	3.15	1.09	1.48	11.3	12.1	10.4
-0.60	1.38	0.80	2.38	3.26	1.14	1.56	10.5	11.2	10.4
-0.40	1.49	0.91	2.38	3.41	1.22	1.64	9.7	10.6	10.4
-0.20	1.56	1.03	2.38	3.55	1.31	1.76	8.9	9.6	10.2
0.00	1.58	1.13	2.37	3.61	1.39	1.95	8.3	8.1	10.5
0.20	1.53	1.16	2.34	3.56	1.52	2.16	7.8	6.8	10.9
0.40	1.45	1.13	2.30	3.45	1.70	2.34	7.5	6.7	11.2
0.60	1.33	1.06	2.36	3.28	1.89	2.49	7.4	7.0	11.3
0.80	1.20	0.97	2.25	3.12	2.07	2.60	7.6	7.7	11.3
1.00	1.08	0.90	2.24	2.98	2.22	2.67	8.4	8.9	11.3

15.7 Results from the simulations in Chapter 7.6

1. Input measured on track 1 (12 km/h)

Horizontal distance between the suspension elements (m)		Vibration level (ISO 2631) at the cab's c.o.g. (m/s^2 rad/s^2)						Maximum angular deviation between the cab and the frame (rad)	
x	y	x	y	z	vector sum	xr	yr	xr	yr
0.60	1.20	0.65	0.96	0.65	1.75	0.90	0.17	0.088	0.085
0.80	1.20	0.65	0.96	0.66	1.75	0.89	0.35	0.087	0.102
1.00	1.20	0.65	0.96	0.67	1.75	0.89	0.50	0.086	0.098
1.20	1.20	0.65	0.96	0.67	1.76	0.90	0.56	0.088	0.069
1.40	1.20	0.65	0.96	0.67	1.76	0.90	0.60	0.089	0.056
1.60	1.20	0.65	0.96	0.67	1.76	0.91	0.65	0.088	0.042
1.80	1.20	0.65	0.96	0.67	1.76	0.91	0.72	0.089	0.033
2.00	1.20	0.65	0.96	0.67	1.75	0.91	0.79	0.089	0.027
2.20	1.20	0.65	0.96	0.66	1.75	0.91	0.87	0.089	0.023
2.40	1.20	0.65	0.96	0.66	1.75	0.91	0.94	0.089	0.020
2.60	1.20	0.65	0.96	0.66	1.75	0.91	0.99	0.089	0.018
2.80	1.20	0.65	0.96	0.66	1.75	0.91	1.05	0.089	0.016
3.00	1.20	0.65	0.96	0.66	1.75	0.91	1.09	0.089	0.014
2.00	0.60	0.65	0.96	0.65	1.75	0.31	0.80	0.136	0.027
2.00	0.80	0.65	0.96	0.67	1.76	0.66	0.80	0.157	0.027
2.00	1.00	0.65	0.96	0.67	1.76	0.82	0.80	0.126	0.026
2.00	1.20	0.65	0.96	0.67	1.76	0.91	0.79	0.089	0.027
2.00	1.40	0.65	0.96	0.67	1.75	0.96	0.79	0.068	0.027
2.00	1.60	0.65	0.96	0.65	1.75	1.02	0.79	0.052	0.028
2.00	1.80	0.65	0.96	0.65	1.75	1.07	0.79	0.040	0.028
2.00	2.00	0.65	0.96	0.65	1.75	1.12	0.80	0.033	0.028

2. Input measured on track 2 (6 km/h)

Horizontal distance between the suspension elements (m)		Vibration level (ISO 2631) at the cab's c.o.g. (m/s^2 rad/s^2)						Maximum angular deviation between the cab and the frame (rad)	
x	y	x	y	z	vector sum	xr	yr	xr	yr
0.60	1.20	1.58	1.12	2.33	3.58	1.39	0.33	0.081	0.114
0.80	1.20	1.58	1.12	2.33	3.57	1.34	0.56	0.082	0.094
1.00	1.20	1.58	1.12	2.33	3.58	1.34	0.83	0.081	0.083
1.20	1.20	1.58	1.12	2.36	3.60	1.36	1.11	0.081	0.067
1.40	1.20	1.58	1.13	2.39	3.62	1.38	1.39	0.082	0.057
1.60	1.20	1.58	1.12	2.41	3.63	1.39	1.62	0.083	0.047
1.80	1.20	1.58	1.12	2.39	3.62	1.39	1.82	0.083	0.043
2.00	1.20	1.58	1.12	2.37	3.61	1.39	1.97	0.083	0.038
2.20	1.20	1.58	1.12	2.35	3.59	1.38	2.07	0.083	0.034
2.40	1.20	1.58	1.12	2.33	3.58	1.38	2.15	0.083	0.031
2.60	1.20	1.58	1.12	2.32	3.57	1.37	2.20	0.082	0.027
2.80	1.20	1.58	1.12	2.31	3.57	1.37	2.23	0.082	0.025
3.00	1.20	1.58	1.12	2.31	3.57	1.37	2.26	0.082	0.023
2.00	0.60	1.58	1.12	2.38	3.60	0.41	2.00	0.109	0.041
2.00	0.80	1.58	1.12	2.38	3.61	0.70	1.99	0.108	0.041
2.00	1.00	1.58	1.12	2.38	3.61	1.05	1.98	0.088	0.040
2.00	1.20	1.58	1.12	2.37	3.61	1.39	1.97	0.083	0.038
2.00	1.40	1.58	1.13	2.35	3.59	1.64	1.96	0.074	0.038
2.00	1.60	1.58	1.13	2.33	3.58	1.84	1.95	0.062	0.038
2.00	1.80	1.58	1.12	2.32	3.57	1.99	1.95	0.053	0.038
2.00	2.00	1.58	1.12	2.32	3.57	2.12	1.96	0.045	0.038